

https://dspace.org/

The CIS influence of the corrin ring in cobalt corrins

Ghadimi, Nafise

2016

http://hdl.handle.net/10539/21738

Ghadimi, Nafise (2016) The CIS influence of the corrin ring in cobalt corrins, University of the Witwatersrand, Johannesburg, <http://hdl.handle.net/10539/21738>

Downloaded from a DSpace repository. https://dspace.org/

THE *CIS* INFLUENCE OF THE CORRIN RING IN COBALT CORRINS

Nafise Ghadimi

Supervised by H M Marques

A thesis submitted to the Faculty of Science, University of the Witwatersrand, Johannesburg, in fulfilment of the requirements for the degree of Doctor of Philosophy

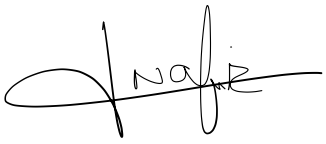
December 2015

DECLARATION

I declare that this is my own unaided work. It is being submitted for the Degree of Doctor of Philosophy at the University of the Witwatersrand, Johannesburg. It has not been submitted before for any degree or examination at any other University.

Nafise Ghadimi

December 2015



PUBLICATIONS

1. N. Ghadimi, C. B. Perry, M. A. Fernandes, P. P. Govender and H. M. Marques, Probing the nature of the Co(III) ion in cobalamins: the reactions of aquacobalamin (vitamin B_{12a}), aqua-10-chlorocobalamin and aqua-10-bromocobalamin with anionic and neutral ligands, *Inorg. Chim. Acta*, 436, 29-38, **2015**

2. N. Ghadimi, C.B. Perry, P.P. Govender, and H.M. Marques, Probing the nature of the Co(III) ion in cobalamins: the ligand substitution reactions of aquacyanocobester, aquacyano(10–nitro)cobester and aquacyano(10–amino)cobester, *Inorg. Chim. Acta*, in press, **2016**

ABSTRACT

It is well-established that there is electronic communication between the equatorial and axial ligands in the cobalt corrins. It can therefore be anticipated that the electronic structure of the corrin ligand will affect the chemistry of the axial coordination sites of Co(III) in these complexes. To probe this *cis*-influence the electronic structure of the corrin was perturbed by substituting the H atom at C10 by Br (which is π electron-donating towards the corrin) in aquacobalamin ($[H_2OCbl]^+$), and by NO_2 (which is strongly electron-withdrawing) and NH_2 (which is strongly electron-donating) in aquacyanocobester ($[ACCbs]^+$). The first part of this study was dedicated to aqua-10-bromocobalamin ($[H_2O\text{-}(10\text{-}Br)Cbl]^+$) and the second part to aquacyano-10-nitrocobester ($[AC\text{-}(10\text{-}NO_2)Cbs]^+$) and aquacyano-10-aminocobester ($[AC\text{-}(10\text{-}NH_2)Cbs]^+$).

The successful synthesis of $[H_2O\text{-}(10\text{-}Br)Cbl]^+$, was verified by ESI-MS, ^1H and ^{13}C NMR, uv-vis spectroscopy and XRD.

The stability constants for the substitution of coordinated H_2O by a series of anionic (N_3^-, NO_2^-, SCN^-, SO_3^{2-}) and neutral N-donor ligands (imidazole, DMAP) were obtained for $[H_2OCbl]^+$, $[H_2O\text{-}(10\text{-}Br)Cbl]^+$ and $[H_2O\text{-}(10\text{-}Cl)Cbl]^+$ under the same conditions. Substitution of the C10 H by Cl or Br favours the coordination of anionic ligands, but discriminates against the binding of neutral N-donor ligands. The anionic ligands bind more strongly to $[H_2O\text{-}(10\text{-}Br)Cbl]^+$ than to $[H_2OCbl]^+$ with log *K* values between 0.05 and 0.62 (average 0.33) larger. Conversely, neutral ligands bind less strongly to $[H_2O\text{-}(10\text{-}Br)Cbl]^+$ than to $[H_2OCbl]^+$ with log *K* values between 0.29 and 0.36 (average 0.33) smaller. DFT (BP83/TZVP) calculations were used to rationalise these observations. When H is changed to Cl or Br, the metal ion becomes less positive. When the *β* ligand changes from a neutral to an anionic ligand, the partial charge on the C10 substituent becomes more negative. Replacing C10 H by Cl or Br discriminates against a neutral ligand because of the greater electron richness of the metal. If the ligand is an anion, however, the charge donation can be accepted by delocalisation onto the C10 substituent.

The reaction kinetics of the substitution of H_2O in $[H_2O\text{-}(10\text{-}Br)Cbl]^+$ were determined for the ligands N_3^- and imidazole and were compared with values available for $[H_2OCbl]^+$ and $[H_2O\text{-}(10\text{-}Cl)Cbl]^+$. The results showed that both N_3^- and imidazole react more slowly with $[H_2O\text{-}(10\text{-}$

Br)Cbl]$^+$ than with [H_2OCbl]$^+$, consonant with the previous observations for [H_2O-(10-Cl)Cbl]$^+$. Although $\Delta H^{\ddagger}$ values are smaller, they do not compensate for significantly more negative values of $\Delta S^{\ddagger}$, indicative of a transition state that occurs earlier along the reaction coordinate in [H_2O-(10-Br)Cbl]$^+$ and [H_2O-(10-Cl)Cbl]$^+$ whereas the transition state occurs later along the reaction coordinate with [H_2OCbl]$^+$. It is argued that this is a consequence of the lower charge density on the metal, making it a better electrophile both towards the incoming and the departing ligand.

Dicyano-10-nitrocobester ([DC-(10-NO_2)Cbs]) and dicyano-10-aminocobester ([DC-(10-NH_2)Cbs]) were synthesised from dicyanocobester [DCCbs] by established methods and converted to the aquacyano form so that the thermodynamics and kinetics of the substitution of coordinated H_2O by a variety of ligands could be investigated.

The stability constants for the substitution of coordinated H_2O by a number of neutral (imidazole, DMAP, methylamine) and anionic (N_3^-, NO_2^-, SCN^-, SO_3^{2-}, CN^-) ligands were determined for [ACCbs]$^+$, [AC-(10-NO_2)Cbs]$^+$ and [AC-(10-NH_2)Cbs]$^+$ in 50% isopropanol. The soft anions (SO_3^{2-} and CN^-) bind better to the softer Co(III) metal centre in [AC-(10-NH_2)Cbs]$^+$ and [ACCbs]$^+$ than in [AC-(10-NO_2)Cbs]$^+$ and the converse is true for the hard anions (N_3^-, NO_2^- and SCN^-). The case is less clear for the N-donor ligands; DMAP clearly has a higher affinity for [AC-(10-NH_2)Cbs]$^+$ and [ACCbs]$^+$ than for [AC-(10-NO_2)Cbs]$^+$, but there is little discrimination in the case of imidazole and methylamine.

This implies that the affinity of the metal for an exogenous ligand depends on the electron density at the metal centre. DFT calculations showed that as the C10 substituent is changed from NH_2 to H to NO_2, the charge density on the metal centre decreases and the metal becomes harder.

The kinetics of the substitution of H_2O by CN^- in [ACCbs]$^+$, [AC-(10-NO_2)Cbs]$^+$ and[AC-(10-NH_2)Cbs]$^+$ in 50% isopropanol were determined. The results showed that the substitution of coordinated H_2O proceeded with biphasic kinetics and through a dissociative interchange (I_d) mechanism where there is nucleophilic participation of the entering ligand in the transition state. The slower phase corresponds to the substitution of coordinated H_2O *trans* to OH^- in the aqua hydroxo species, which, together with the dicyano species, is inevitably present in solutions of [ACCbs]$^+$, and the faster phase corresponds to the substitution of the coordinated H_2O *trans* to CN^- in the aquacyano species. The difference in rate of the reaction of the [AC-(10-Z)Cbs] (Z = H, NH_2 and NO_2) was not very large, the ratio between the largest (for Z = H) and the smallest

(for Z = NO_2) is just over 40, and does not follow the electron donor properties of Z. This is misleading, however, because of a compensation effect between $\Delta H^{\ddagger}$ and $\Delta S^{\ddagger}$. As values of $\Delta H^{\ddagger}$ become smaller, which causes an increase in the reaction rate, $\Delta S^{\ddagger}$ becomes less positive (or more negative), which causes a decrease in the reaction rate. Hence, comparing rate constants at any particular temperature is not very informative and the compensation effect masks the *very significant* differences in the reactivity of the metal ion towards the entering CN^- ligand. The compensation effect is attributed to the position of the transition state along the reaction coordinate, which depends on the charge density on the metal ion. Indeed, if all three reactions had the same value of $\Delta S^{\ddagger}$ then the values of the rate constant would be in the approximate ratio 10^9:10^6:1 for Z = NH_2, H and NO_2, respectively.

This study shows that how profoundly the perturbation of the electronic structure of the corrin affects the thermodynamic and kinetic properties of the Co(III) ion, and provides further evidence that the unusual chemistry of Co(III) in the cobalt corrins is a consequence of the *cis*-influence of the equatorial macrocyclic ligand.

To the Chemical Society

ACKNOWLEDGEMENTS

I would like to express my gratitude to my supervisor, Professor Helder Marques, for his endless help and guidance.

I also want to thank

- Dr. Christopher Perry for teaching me the fundamentals of bioinorganic research, running the DFT calculations and helping to assign NMR spectra.
- My friends and colleagues in lab 328 for their help and their consultations, in particular, Sadhna Mathura.
- Dr. Richard Mampa and Dr. Myron Johnson for collecting NMR data.
- Dr. Marietjie Stander for collecting mass spectra data.
- Dr. Penny Govender and Dr. Christopher Perry for the DFT calculations.
- Kim Wiid for her assistance in the use of the stopped-flow spectrometer.
- The School of Chemistry for being awesome and supportive.
- The University of the Witwatersrand and the NRF for financial support.
- My parents for their support and encouragement throughout these years as well as my sisters.
- My beloved husband for his patience and his support; he always cheered me up when I was desperate and hopeless.

Contents

	Page
Declaration	ii
Publication	iii
Abstract	iv
Dedication	vii
Acknowledgment	viii
List of Figures	xviii
List of Tables	xxiii
List of Abbreviation	xxv
Symbols	xxvii
Chapter 1	
Introduction	
1.1 An Introduction to Vitamin B_{12}	1
1.1.1 Roles of Vitamin B_{12} in the Human Body	3
1.2 Structural Details of Vitamin B_{12} and its Derivatives	4
1.3 Cleavage of the Co–C Bond	6
1.3.1 Co–C Bond Homolysis	6
1.3.2 Co–C Bond Heterolysis	7
1.4 Corrin and Porphyrins Macrocycles	9
1.4.1 Aspects of the Corrin Ring	9
1.4.2 A Note on Porphyrins	9
1.4.3 A Comparison of Porphyrin and Corrin	11
1.5 Cis- and Trans- Influences/Effects	12
1.6 Electronic Spectra of Vitamin B_{12} and Its Derivatives	20

1.7 Ligand Substitution Reaction 27

1.7.1 Stability Constant (log *K*) 27

1.7.2 Reaction Kinetics 28

1.8 Density Functional Theory (DFT) Calculations 31

1.9 Aims of This Project 33

1.10 Organisation of This Work 36

1.11 References 37

Chapter 2

Materials, Methods and Instrumentation

2.1 Reagents, Solvents and Buffers Used in This Project 42

2.2 General Methods 44

2.2.1 pH Measurements 44

2.2.2 Buffers 44

2.2.2.1 Phosphate Buffer 45

2.2.3 Sep-Pak Cartridges 45

2.2.4 Column Chromatography 45

2.2.5 Auto-column Chromatography 46

2.2.6 Stopped-Flow Spectrophotometry 46

2.3 Characterisation Techniques 47

2.3.1 High Performance Liquid Chromatography (HPLC) 47

2.3.2 uv-vis Spectroscopy 48

2.3.3 Electrospray Ionisation (ESI) Mass Spectroscopy 48

2.3.4 Nuclear Magnetic Resonance (NMR) Spectra 48

2.3.5 X-ray Diffraction Crystallography 49

2.3.6 Molecular Modelling 50

2.4 Synthesis and Characterisation of the Modified C10 Cobalt Corrins 50

2.4.1 Synthesis and Characterisation of [H2O-(10-Br)Cbl]$^+$ 50

2.4.1.1 uv-vis Spectroscopy of [H2O-(10-Br)Cbl]$^+$ 52

2.4.1.2 ESI-MS of [H2O-(10-Br)Cbl]$^+$ 53

2.4.1.3 NMR Spectroscopy of [H2O-(10-Br)Cbl]$^+$ 53

2.4.2 Synthesis of [H2O-(10-Cl)Cbl]$^+$ 54

2.4.3 Synthesis of Coα,Coβ-dicyano(10-nitro)cobyrinic Acid Heptamethyl Ester (dicyano-10-nitrocobester, [DC(10-NO_2)Cbs]) 54

2.4.3.1 uv-vis Spectroscopy of [DC-(10-NO_2)Cbs] 55

2.4.3.2 ESI-MS of [DC-(10-NO_2)Cbs] 56

2.4.3.3 NMR Spectroscopy of [DC-(10-NO_2)Cbs] 56

2.4.4 Conversion of [DC-(10-NO_2)Cbs] into [AC-(10-NO_2)Cbs]$^+$ 57

2.4.5 Synthesis of Coα,Coβ-dicyano(10-amino)cobyrinic Acid Heptamethyl Ester (dicyano-10-aminocobester, [DC-(10-NH_2)Cbs]) 59

2.4.5.1 uv-vis Spectroscopy of [DC-(10-NH_2)Cbs] 60

2.4.5.2 ESI-MS of [DC-(10-NH_2)Cbs] 60

2.4.5.3 NMR Spectroscopy of [DC-(10-NH_2)Cbs] 61

2.4.6 Conversion of [DC-(10-NH_2)Cbs] to [AC-(10-NH_2)Cbs]$^+$ 61

2.5 A Probe into the Solution Chemistry of C10-Modified Cobalt Corrinoids 62

2.5.1 Data analysis 62

2.5.2 Spectroscopic pK_a Inevstigations as a Function of pH 62

2.5.2.1 The effect of pH on the acid dissociation constant (pK_a) of [H_2O-(10-Br)Cbl]$^+$, [H2OCbl]$^+$ and [H_2O-(10-Cl)Cbl]$^+$ 62

2.5.2.2 Effect of pH on the Acid Dissociation Constant (pK_a) of [AC-(10-NO_2)Cbs]$^+$, [AC-(10-NH_2)Cbs]$^+$ and [ACCbs]$^+$ 63

2.5.3 Stability Constants (log *K*) 64

2.5.3.1 Stability Constants (log *K*) for Substitution of H_2O by Exogenous Ligands in $[H2O\text{-}(10\text{-}Br)Cbl]^+$, $[H2O\text{-}(10\text{-}Cl)Cbl]^+$ and $[H2OCbl]^+$ 64

2.5.3.2 Stability Constants (log *K*) for Substitution of H_2O by Exogenous Ligands in $[AC\text{-}(10\text{-}NO_2)Cbs]^+$, $[AC\text{-}(10\text{-}NH_2)Cbs]^+$, and $[ACCbs]^+$ 66

2.5.4 Kinetic Investigations of Ligand Substitution Reactions 68

2.5.4.1 Kinetic Investigations of Ligand Substitution Reactions of $[H_2O\text{-}(10\text{-}Br)Cbl]^+$ 68

2.5.4.2 Kinetic Investigations of Ligand Substitution Reactions of $[AC\text{-}(10\text{-}NO_2)Cbs]^+$, $[AC\text{-}(10\text{-}NH_2)Cbs]^+$ and $[ACCbs]^+$ Using Stopped-flow Spectrophotometry 69

2.6 Determination of Crystal Structure 71

2.6.1 Crystal Structural Determination of $[H_2O\text{-}(10\text{-}Br)Cbl]^+$ and $[N_3\text{-}(10\text{-}Br)Cbl]$ 71

2.6.2 Crystal Structure Determination of $[DC\text{-}(10\text{-}NO_2)Cbs]$ 74

2.7 References 75

Chapter 3

The Thermodynamics of The Reactions of Aquacobalamin (vitamin B_{12a}), Aqua-10-chlorocobalamin and Aqua-10-bromocobalamin with Anionic and Neutral Ligands

3.1 Introduction 77

3.2 pK_a Determination of $[H_2OCbl]^+$, $[H_2O\text{-}(10\text{-}Br)Cbl]^+$ and $[H_2O\text{-}(10\text{-}Cl)Cbl]^+$ 78

3.2.1 Introduction

3.2.2 Results and Discussion 79

3.2.2.1 Determination of the pK_a of $[H_2OCbl]^+$ 79

3.2.2.2 Determination of the pK_a of $[H_2O\text{-}(10\text{-}Cl)Cbl]^+$ 81

3.2.2.3 Determination of the pK_a of $[H_2O\text{-}(10\text{-}Br)Cbl]^+$ 83

3.2.2.4 DFT Calculations 86

3.2.2.5 Conclusion 87

3.3 Determination of the Stability Constants of $[H_2O\text{-}(10\text{-}Br)Cbl]^+$, $[H_2OCbl]^+$ and $[H_2O\text{-}(10\text{-}Cl)Cbl]^+$ with Various Anionic and Neutral Ligands 88

3.3.1 Introduction 88

3.3.2 Results and Discussion 90

3.3.2.1 The uv-vis Spectroscopic Changes of $[H_2O\text{-}(10\text{-}Br)Cbl]^+$ Toward Ligand Binding (Qualitative Investigation) 91

3.3.2.2 The uv-vis Spectroscopic Changes of $[H_2O\text{-}(10\text{-}Cl)Cbl]^+$ and $[H_2OCbl]^+$ Toward Ligand Binding (Qualitative Investigation) 98

3.3.2.3 Conclusion 100

3.3.2.4 Determination of Stability Constants (Quantitative Examination) 102

3.3.2.5 Conclusion 107

3.4 QTAIM Calculations 107

3.4.1 Conclusion 111

3.5 X-ray Crystallography of $[H_2O\text{-}(10\text{-}Br)Cbl]^+$ and $[N_3\text{-}(10\text{-}Br)Cbl]$ 112

3.5.1 Conclusion 116

3.6 Summary of the Chapter 116

3.7 References 126

Chapter 4

The Kinetics of the Reaction of Aqua-10-bromocobalamin with Azide and Imidazole

4.1 Introduction 128

4.2 Results and Discussion 130

4.3 Conclusion 136

4.4 References 137

Chapter 5

The Thermodynamics of the Reactions of Aquacyanocobester, Aquacyano-10-nitrocobester and Aquacyano-10-aminocobester with Anionic and Neutral Ligands

5.1 Introduction 138

5.2 pK_a Determination of $[ACCbs]^+$, $[AC\text{-}(10\text{-}NO_2)Cbs]^+$ and $[AC\text{-}(10\text{-}NH_2)Cbs]^+$ 140

5.2.1 Introduction 140

5.2.2 Results and Discussion 141

5.2.2.1 Determination of the pK_a of $[ACCbs]^+$ 141

5.2.2.2 Determination of the pK_a of $[AC\text{-}(10\text{-}NO_2)Cbs]^+$ 146

5.2.2.3 Determination of the pK_a of $[AC\text{-}(10\text{-}NH_2)Cbs]^+$ 150

5.2.2.4 Summary of pK_a values 156

5.2.3 Conclusions 157

5.3 Determination of the Stability Constants of $[ACCbs]^+$, $[AC\text{-}(10\text{-}NO_2)Cbs]^+$ and $[AC\text{-}(10\text{-}NH_2)Cbs]^+$, with Various Anionic and Neutral Ligands 157

5.3.1 Introduction 157

5.3.2 Results and Discussion 161

5.3.2.1 Ligand Binding Studies with Nitrite 161

5.3.2.2 Ligand Binding Studies with Azide 163

5.3.2.3 Ligand Binding Studies with Thiocyanate 165

5.3.2.4 Ligand Binding Studies with Sulfite 167

5.3.2.5 Ligand Binding Studies with Cyanide 169

5.3.2.6 Ligand Binding Studies with Imidazole 171

5.3.2.7 Ligand Binding Studies with Methylamine 173

5.3.2.8 Ligand Binding Studies with DMAP 175

5.3.3 Summary of Results and Conclusions 177

5.4 QTAIM Analysis 179

5.4.1 Conclusions 187

5.5 Summary of This Chapter 188

5.6 References 189

Chapter 6

The Kinetics of the Reaction of Aquacyano-10-nitrocobester, Aquacyano-10-aminocobester and Aquacyanocobester with Cyanide

6.1 Introduction 190

6.2 Results and Discussion 191

6.3 Conclusions 198

6.4 References 200

Chapter 7

Conclusions and Future Work

7.1 Conclusions 201

7.2 Future work 204

7.3 References 206

Appendices

Appendices for Chapter 2

2.1 Calculation For Multi-Component Buffer 207

2.2 ESI-MS Data for $[H_2O\text{-}(10\text{-}Br)Cbl]^+$ 209

2.3 ESI-MS Data for [DC-(10-NO_2)Cbs] 212

2.4 ESI-MS Data for [AC-(10-NO_2)Cbs]$^+$ 215

2.5 NMR Spectra and Assignments for [H_2O-(10-Br)Cbl]$^+$ in CD_3OD 216

2.6 NMR Spectra and Assignments for [DC-(10-NO_2)Cbs] in $CDCl_3$ 225

2.7 Crystallographic Data 232

2.8 Derivation of Equations for the Determination of Stability Constants 247

2.9 Derivation of Equations for the Correction of *K* Taking Free Ligand and Metal into Account 250

Appendices for Chapter 3

3.1 Spectroscopic Changes for Binding of Anionic and Neutral Ligands to [H_2O-(10-Z)Cbl]$^+$ 253

Appendices for Chapter 4

4.1 Primary Kinetic Data for the Reaction of N_3^- and Imidazole with [H_2O-(10-Br)Cbl]$^+$ 260

Appendices for Chapter 6

6.1 Primary kinetic data for the reaction of CN^- with [AC-(10-NO_2)Cbs]$^+$, [AC-(10-NH_2)Cbs]$^+$ and [ACCbs]$^+$ in 50% isoprpanol 263

LIST OF FIGURES

Figure		Page
1.1	The structure, numbering scheme, and standard view of the most important cobalamins.	2
1.2	Alternative conformations of cobalamins differing with respect to the lower or α axial ligation site.	5
1.3	Heterolytic and homolytic Co–C bond formation and cleavage for the reaction catalyzed by methyl-tetrahydrofolate and the reaction of interconversion of (R) methylmalonyl-CoA into succinyl-CoA, from left to right.	8
1.4	The cobalt corrin structure, red dots indicate the delocalised π electron system.	10
1.5	The backbone of all porphyrins. The indicated blue pathway shows the delocalised 18-π electron system. This structure was created by Küster in 1912. However, Hans Fischer is often credited with identifying this structure in 1929.	11
1.6	The *cis*- and *trans*- influences	13
1.7	Correlation of the β band with the C10 proton chemical shift ((R^2= 0.97). The data were obtained from **Table 1.4**.	19
1.8	Energy levels of the ų electron system and their corresponding bands in the absorption spectrum of aquacobalamin.	22
1.9	Molecular orbital diagram for $[CH_3Co^{III}(CR)Br]PF_6$.	23
1.10	The "atypical" spectrum of sulfitocobalamin	26
1.11	The "typical" spectrum of $[H_2OCbl]^+$.	26
1.12	Simulated electronic absorption spectra of C10-substituted corrins. (a) Calculated spectra for electron donating L groups ($\sigma_p < 0$). (b) Calculated spectra for electron withdrawing L groups ($\sigma_p > 0$).	32
2.1	HPLC chromatogram of purified $[H_2O\text{-}(10\text{-}Br)Cbl]^+$ with retention time of 6.48 min using gradient elution programme, 75% phosphate buffer pH 3.0 and 25% acetonitrile	52
2.2	The uv-vis spectrum of $[H_2O\text{-}(10\text{-}Br)Cbl]^+$.	53

2.3	HPLC chromatogram of [DC-(10-NO_2)Cbs] with a retention time of 2.56 min using the isocratic elution programme, 3% methanol in ethyl acetate.	55
2.4	The uv-vis spectrum of [DC-(10-NO_2)Cbs].	56
2.5	uv-vis spectra show the full conversion of [DC-(10-NO_2)Cbs] (purple) to [AC-(10-NO_2)Cbs]$^+$ (blue) in 50% isopropanol/water.	58
2.6	HPLC chromatogram of [AC-(10-NO_2)Cbs]$^+$ with retention time of 2.60 min using the isocratic elution programme, 3% methanol in acetic acid.	59
2.7	The uv-vis spectrum of [DC-(10-NH_2)Cbs].	61
2.8	uv-vis spectra illustrate the full conversion of [DC-(10-NH_2)Cbs] (purple) to [AC-(10-NH_2)Cbs]$^+$ (red) in 50% isopropanol/water.	62
2.9	An example of a trace recorded for the reaction of CN^- with [ACCbs]$^+$ at 21 ^oC.	70
2.10	Crystal structure of [H_2O-(10-Br)Cbl]$^+$, (a) ORTEP diagrams with the ellipsoids drawn at the 50% contour level, (b) capped sticks diagram.	72
2.11	Crystal structure of of [N_3-(10-Br)Cbl]$^+$, (a) ORTEP diagram with the ellipsoids drawn at the 50% contour level, (b) capped sticks diagram. Solvate molecules are omitted for clarity.	73
3.1	The effect of pH on the absorbance spectrum of [H_2OCbl]$^+$ at 25 ^oC in an aqueous solution, pH ranging from 5.5 (blue) to 10.6 (red).	80
3.2	A plot of the change in absorbance of aquacobalamin at 352 nm to which **Equation 2.1** has been fitted.	81
3.3	The effect of pH on the uv-vis spectrum of [H_2O-(10-Cl)Cbl]$^+$, varying pH from 4.7 (blue) to 10.4 (red).	82
3.4	A plot of the change in absorbance of [H_2O-(10-Cl)Cbl]$^+$ at 356 nm to which **Equation 2.1** has been fitted.	83
3.5	The effect of pH on the uv-vis spectrum of [H_2O-(10-Br)Cbl]$^+$, on varying pH from 5.21 (green) to 9.9 (red).	84
3.6	A plot of the change in absorbance of [H_2O-(10-Br)Cbl]$^+$ at 355 nm to which **Equation 2.1** has been fitted.	85
3.7	van't Hoff plot for the ionisation of coordinated H_2O in [H_2O-(10-Br)Cbl]$^+$. From the slope and intercept ΔH = 34 ± 2 kJ mol^{-1} and ΔS = –26 ± 6 J K^{-1} mol^{-1} were determined, respectively.	86

3.8 A uv-vis spectrum of $[H_2O\text{-}(10\text{-}Br)Cbl]^+$ in neutral pH at 25 ^oC. 91

3.9 Absorption spectra of $[H_2O\text{-}(10\text{-}Br)Cbl]^+$, (a) in an aqueous solution of unbuffered neutral solution at 25 ^oC, in 1 cm pathlength cell, and in the presence of: (b) NO_2^-, (c) N_3^-, (d) SCN^- and (e) SO_3^{2-}. 92

3.10 The absorbance changes observed for the binding of N_3^- to $[H_2O\text{-}(10\text{-}Br)Cbl]^+$ at pH 6 at 25 ^oC. 94

3.11 Spectroscopic changes associated with the binding of SO_3^{2-} to $[H_2O\text{-}(10\text{-}Br)Cbl]^+$. 95

3.12 The spectral changes of the binding of imidazole to the $[H_2O\text{-}(10\text{-}Br)Cbl]^+$. 96

3.13 Spectroscopic changes associated with the binding of DMAP to $[H_2O\text{-}(10\text{-}Br)Cbl]^+$. 98

3.14 Relationship between the γ bands of both $[LCbl]^{n+}$ and $[L\text{-}(10\text{-}Br)Cbl]^{n+}$ ($R^2 = 0.92$). 102

3.15 Changes in the uv-vis spectrum on substituting coordinated H_2O in $[H_2O\text{-}(10\text{-}Br)Cbl]^+$ by N_3^- at 25 ^oC, pH 6.5. The insert shows a fit of the absorbance change at 355 nm to the binding isotherm given by **Equation 2.4** of the text. 103

3.16 The correlation between the stability constants for $[H_2O\text{-}(10\text{-}Br)Cbl]^+$ and $[H_2OCbl]^+$ complexes with anionic ligands. 105

3.17 The correlation between the stability constants for $[H_2O\text{-}(10\text{-}Br)Cbl]^+$ and $[H_2O\text{-}(10\text{-}Cl)Cbl]^+$ complexes with anionic ligands. 106

3.18 Energy-minimised DFT models of (top) $[H_2O\text{-}(10\text{-}Z)Cbl]^+$ with (left to right) Z = H, Cl, Br; and (bottom) $[N_3\text{-}(10\text{-}Z)Cbl]$ with (left to right) Z = H, Cl, Br 109

3.19 ORTEP diagrams with the ellipsoids drawn at the 50% contour level (a) $[H_2O\text{-}(10\text{-}Br)Cbl]^+$ and (b) $[N_3\text{-}(10\text{-}Br)Cbl]^+$. Solvate molecules are omitted for clarity. 114

4.1 Absorbance-time traces for the reaction of (left) N_3^- with $[H_2O\text{-}(10\text{-}Br)Cbl]^+$ (66 μM N_3^-, 25.0 ^oC, pH 5.85 MES buffer, μ = 0.50 M, Na_2SO_4) and (right) imidazole with $[H_2O\text{-}(10\text{-}Br)Cbl]^+$ (6.5 mM Im, 25.0 ^oC, pH 6.9, MOPS buffer, μ = 0.50 M, Na_2SO_4). The red line is the best fit of **Equation 2.10** of the text (**Chapter 2**) to the experimental data which gave k_I^{obs} = 3.02(2) × 10^{-2} s^{-1} and 3.88(4) × 10^{-2} s^{-1}, respectively. 131

4.2 Plots of k_I against (top) $[N_3^-]$ (25.0 ^oC) and (bottom) imidazole (20.0 ^oC). The intercept in the first case is significant statistically different from zero, 132

but not in the second case. The gradients give the second order-rate constant, k_{II}.

4.3 Eyring plots for the reaction of N_3^- (top) and imidazole (bottom) with $[H_2O$-(10-Br)Cbl$]^+$. 133

4.4 Eyring plots for the reverse rate constant of the reaction of N_3^- with $[H_2O$-(10-Br)Cbl$]^+$. 134

5.1 The structures of $[ACCbs]^+$ **(1)**, $[ACSYCbs]^+$ **(2)** and [5-seco-ACCbs] **(3)**. 139

5.2 The effect of pH on the uv-vis spectrum of $[ACCbs]^+$, on varying pH from 5.8 (red) to 12.0 (blue). 143

5.3 Plots of the change in absorbance of $[ACCbs]^+$ in 50% isopropanol/buffer solutions at 25 ^oC, (A) at 354 nm fitted to a single pK_a model, (B) at 354 nm fitted to a two pK_a model (C) at 585 nm fitted to a single pK_a mpdel, (D) at 585 nm fitted to a two pK_a model. 144

5.4 Van't Hoff plot for the ionisation of coordinated H_2O in $[ACCbs]^+$. 146

5.5 The effect of pH on the uv-vis spectrum of $[AC$-(10-NO_2)Cbs$]^+$, on varying pH from 6.7 (purple) to 12.3 (blue). 147

5.6 Monitoring the absorbance change with pH (A) an example of a fit to a single pK_a fit at the γ band of $[AC$-(10-NO_2)Cbs$]^+$, (B, D) examples of a fit to a single pK_a model and (C, E) examples of a fit to a two pK_a model. 148

5.7 van't Hoff plot for the ionisation of coordinated H_2O in $[AC$-(10-NO_2)Cbs$]^+$. 150

5.8 The effect of pH on the uv-vis spectrum of $[AC$-(10-NH_2)Cbs$]^+$, varying pH from 6.2 (red) to 12.6 (green). 151

5.9 Monitoring the absorbance change with pH, (A) at the γ band of $[AC$-(10-NH_2)Cbs$]^+$ using a single pK_a model, (B, D, F) examples of a fit of the experimental data to a single pK_a model at 510, 600 and 374 nm, respectively and (C, E,G) examples of a fit to a two pK_a model with one pK_a around 8 and the other > 10. 152

5.10 van't Hoff plot for the ionisation of coordinated H_2O in $[AC$-(10-NH_2)Cbs$]^+$. 154

5.11 Absorbance changes on titrating (top) $[AC$-(10-NH_2)Cbs$]^+$ and (bottom) $[AC$-(10-NO_2)Cbs$]^+$ between pH 8 and pH 1.5. The inserts show fitting of the data at the γ-band maximum to an expression for a single pK_a at 5.1 ± 0.1 for $[AC$-(10-NH_2)Cbs$]^+$ and 3.4 ± 0.3 for $[AC(10$-$NO_2)Cbs]^+$. (The results are average results of three titrations monitored at three and two different wavelengths, respectively). 156

5.12 Changes in the uv-vis spectrum on substituting coordinated H_2O in (top) $[AC\text{-}(10\text{-}NO_2)Cbs]^+$, (middle) $[AC\text{-}(10\text{-}NH_2)Cbs]^+$ (bottom) $[ACCbs]^+$ by NO_2^- at 25 ^oC, pH 7.1. The insert shows a fit of the absorbance change at 347, 360 and 561 nm, (from top to bottom) to the binding isotherm given by **Equation 2.4**. 162

5.13 Changes in the uv-vis spectrum on substituting coordinated H_2O in (top) $[AC\text{-}(10\text{-}NO_2)Cbs]^+$, (middle) $[AC\text{-}(10\text{-}NH_2)Cbs]^+$ and (bottom) $[ACCbs]^+$ by N_3^- at 25 ^oC, pH 6.9. The insert shows a fit of the absorbance change at 348, 607 and 575 nm, (from top to bottom) to the binding isotherm given by **Equation 2.4** and **Equation 2.3** (for $[ACCbs]^+$). 164

5.14 Changes in the uv-vis spectrum on substituting coordinated H_2O in (top) $[AC\text{-}(10\text{-}NO_2)Cbs]^+$, (middle) $[AC\text{-}(10\text{-}NH_2)Cbs]^+$ (bottom) $[ACCbs]^+$ by SCN^- at 25 ^oC, pH 7.2. The insert shows a fit of the absorbance change at 348, 607 and 575 nm, (from top to bottom) to the binding isotherm given by **Equation 2.3**. 166

5.15 Changes in the uv-vis spectrum on substituting coordinated N_3^- in (top) $[N_3CN\text{-}(10\text{-}NO_2)Cbs]$, (middle) $[N_3CN\text{-}(10\text{-}NH_2)Cbs]$ and (bottom) $[N_3CNCbs]$ by SO_3^{2-} at 25 ^oC, pH 8.9. The insert shows a fit of the absorbance change at 346, 570 and 365 nm, (from top to bottom) to the binding isotherm given by **Equation 2.4**. 168

5.16 Changes in the uv-vis spectrum on substituting coordinated N_3^- in (top) $[N_3CN\text{-}(10\text{-}NO_2)Cbs]$, (middle) $[N_3CN\text{-}(10\text{-}NH_2)Cbs]$ and (bottom) $[N_3CNCbs]$ by CN^- at 25 ^oC, pH 10.1. The insert shows a fit of the absorbance change at 362, 595 and 370 nm, (from top to bottom) to the binding isotherm given by **Equation 2.4**. 170

5.17 Changes in the uv-vis spectrum on substituting coordinated H_2O in (top) $[AC\text{-}(10\text{-}NO_2)Cbs]^+$, (middle) $[AC\text{-}(10\text{-}NH_2)Cbs]^+$ (bottom) $[ACCbs]^+$ by imidazole at 25 ^oC, pH 6.9. The insert shows a fit of the absorbance change at 355, 330 and 363 nm, (from top to bottom) to the binding isotherm given by **Equation 2.4.** 172

5.18 Changes in the uv-vis spectrum on substituting coordinated H_2O in (top) $[AC\text{-}(10\text{-}NO_2)Cbs]^+$, (middle) $[AC\text{-}(10\text{-}NH_2)Cbs]^+$ (bottom) $[ACCbs]^+$ by $MeNH_2$ at 25 ^oC, pH 10.3. The insert shows a fit of the absorbance change at 355, 367 and 555 nm, (from top to bottom) to the binding isotherm given by **Equation 2.3.** 174

5.19 Changes in the uv-vis spectrum on substituting coordinated H_2O in (top) $[AC\text{-}(10\text{-}NO_2)Cbs]^+$, (middle) $[AC\text{-}(10\text{-}NH_2)Cbs]^+$ and (bottom) $[ACCbs]^+$ by DMAP at 25 ^oC, pH 8.5. The insert shows a fit of the absorbance change at 450, 565 and 362 nm, (from top to bottom) to the binding isotherm given by **Equation 2.4 and Equation 2.3** (for $[AC\text{-}(10\text{-}NO_2)Cbs]^+$). 176

5.20 BP86/TVZP models of (from top) $[(H_2O)(CN)Cbs]^+$, $[(H_2O)(CN)(10\text{-}NO_2)Cbs]^+$ and $[(H_2O)(CN)(10\text{-}NH_2)Cbs]^+$. 183

5.21 The normal *trans* influence is reproduced in BP86/TZVP models of $[(L)(CN)Cbs]^{n+}$. The bond length between Co and the β ligand, L = H_2O, Im, NO_2^-, CN^-, is plotted against the *trans* Co–CN bond length. 185

5.22 The dependence of (A) the Co–OH_2 bond length, (B) the ratio of the potential and kinetic energy densities at the bond critical point (bcp) of the Co–OH_2 bond, (C) the charge density at the bcp of the Co–OH_2 bond, and (D) the Bader charge on Co in BP86/TZVP models of $[(H_2O)(CN)Cbs]^+$ on the Hammett para constant, σ_p, of the C10 substituent. 186

6.1 Fits of **Equation 6.4** to the absorbance-time trace of the reaction at 25 °C of CN^- with (A) [ACCbs[$^+$, 370 nm, $[CN^-]$ = 0.386 mM, pH 8.9; (B) $[AC\text{-}(10\text{-}NO_2)Cbs]^+$, 361 nm, $[CN^-]$ = 6.17 mM, pH 9.4; and (C) $[AC\text{-}(10\text{-}NH_2)Cbs]^+$, 372 nm, $[CN^-]$ = 0.204 mM, pH 9.1. 193

6.2 Eyring plots for the reaction of (A) (top) $[ACCbs]^+$, (middle) $[AC\text{-}(10\text{-}NO_2)Cbs]^+$ and (bottom) $[AC\text{-}(10\text{-}NH_2)Cbs]^+$ with CN^-. 196

6.3 There is a compensation effect between values of $\Delta H^{\ddagger}$ and $\Delta S^{\ddagger}$ for the ligand substitution of coordinated H_2O in $[AC\text{-}(10\text{-}Z)Cbs]^+$ (Z = H, NH_2, NO_2). 197

LIST OF TABLES

Table		page
1.1	Details on the structural differences between corrins and porphyrins.	12
1.2	Co-axial ligand bond length (in Å).	16
1.3	Second-order rate constants for ligand substitution of X by L in various $Co^{III}(N_4)$ complexes.	17
1.4	Correlation between absorption and NMR of cobalamins and cobinamide (data from Ref 73).	18
1.5	Effect of the β axial ligand nature on the γ band position in cobalamins.	25
2.1	Summary of chemicals used in this study.	42
2.2	Summary of buffers used.	44
2.3	Multi-step gradient elution programme.	47
3.1	Stability constants for the displacement of coordinated H_2O, in $[H_2OCbl]^+$ and $[H_2O\text{-}(10\text{-}Cl)Cbl]^+$.	89
3.2	Shift in wavelength of the γ, *D*, β and α bands and isosbestic points on binding of anionic ligands to $[H_2O\text{-}(10\text{-}Br)Cbl]^+$.	93
3.3	Shifts in γ, *D*, β and α bands and isosbestic points on ligand binding of neutral ligands to $[H_2O\text{-}(10\text{-}Br)Cbl]^+$.	97
3.4	Shift in wavelength of γ, *D*, β and α bands and isosbestic points on binding of anionic and neutral ligands to $[H_2O\text{-}(10\text{-}Cl)Cbl]^+$.	99
3.5	Shift in wavelength of γ, *D*, β and α bands and isobestic points on binding of anionic ligands to $[H_2OCbl]^+$.	100
3.6	Summary on the position of the principal bands in the uv-vis spectrum of complexes of $[H_2OCbl]^+$ and the 10-Cl and 10-Br analogues.	101
3.7	Stability constants (as log *K* values) for the substitution of coordinated H_2O in $[H_2O\text{–}(10\text{-}Z)Cbl]^+$ (Z = H, Cl, Br) by an exogenous ligand $L^{a,b}$.	104
3.8	Axial bond lengths and QTAIM properties at the bond critical point in DFT models of $[L\text{-}(10\text{-}Z)Cbl]^{n+}$, X = H_2O or N_3^-, *n* = 1 or 0, Z = H, Cl or Br $^{a.}$.	110

3.9	A comparison of structural metrics in the crystal structures of $[H_2OCbl]^+$, $[H_2O\text{-}(10\text{-}Cl)Cbl]^+$ and $[H_2O\text{-}(10\text{-}Br)Cbl]^+$ and of $[N_3Cbl]$ and $[N_3\text{-}(10\text{-}Br)Cbl]$.	115
4.1	Second-order rate constants for ligand substitution of X by L in various $Co^{III}(N_4)$ complexes.	129
4.2	Rate constants and activation parameters for the reaction of N_3^- and imidazole with $[H_2O\text{-}(10\text{-}Br)Cbl]^+$, $[H_2O\text{-}(10\text{-}Cl)Cbl]^+$ and $[H_2OCbl]^+$.	135
5.1	The acid dissociation constants of $[ACCbs]^+$, in 50% isopropanol/buffer Solutions.	145
5.2	The acid dissociation constants of $[AC\text{-}(10\text{-}NO_2)Cbs]^+$, in 50% isopropanol/buffer Solutions.	149
5.3	The acid dissociation constants of $[AC\text{-}(10\text{-}NH_2)Cbs]^+$ in 50% isopropanol/buffer solutions.	153
5.4	The Acid Dissociation Constants of the Cobesters $[AC\text{-}(10\text{-}Z)Cbs]^+$, Z = H, NO_2, NH_2, in 50% Aqueous Isopropanol Solutions.	156
5.5	Stability constants for the substitution of water by anionic ligands in $[ACCbs]^+$, $[ACSYCbs]^+$ and [5-seco-ACCbs] at 25 ^oC.	159
5.6	Stability constants for the substitution of water by neutral ligands in $[ACCbs]^+$ and $[ACSYCbs]^+$ at 25 ^oC.	160
5.7	Values of log *K* for replacement of coordinated H_2O in the cobesters $[AC\text{-}(10\text{-}Z)Cbs]^+$, Z = H, NO_2, NH_2, in 50% aqueous isopropanol solutions by exogenous ligands L at 25.0 ^oC.	178
5.8	Structural and electronic properties of $[L(CN)(10\text{-}Z)Cbs]^{n+}$; L = H_2O, imidazole, CN^- and NO_2^-; Z = H, NO_2, NH_2; from BP86/TZVP models.	180
6.1	Kinetic data for the substitution of coordinated H_2O in $[ACCbs]^+$, $[AC\text{-}(10\text{-}NO_2)Cbs]^+$ and $[AC\text{-}(10\text{-}NH_2)Cbs]^+$ with CN^-.	195

LIST OF ABBREVIATIONS

$[ACCbs]^+$	Aquacyanocobester
$[AC\text{-}(10\text{-}NH_2)Cbs]^+$	Aquacyano-10-aminocobester
$[AC\text{-}(10\text{-}NO_2)Cbs]^+$	Aquacyano-10-nitrocobester
$[ACSYCbs]^+$	Aquacyano-stable yellow cobester
[5-seco-ACCbs]	5-seco aquacyanocobester
[AdoCbl]	Adenosylcobalamin
B_{12a}	Vitamin B_{12a} (aquacobalamin)
[CNCbl]	Vitamin B_{12} (cyanocobalamin)
[CN-(10-Cl)Cbl]	Cyano-10-chlorocobalamin
COSY	Homonuclear 2D shift correlation spectroscopy
[DCCbs]	Dicyanocobester
$[DC\text{-}(10\text{-}NO_2)Cbs]$	Dicyano-10-nitrocobester
$[DC\text{-}(10\text{-}NH_2)Cbs]$	Dicyano-10-aminocobester
DMB	5,6-Dimethylbenzimidazole
DMAP	*N*,*N*-dimethylaminopyridine
[EtCbl]	Ethylcobalamin
[Et-(10-Br)Cbl]	Ethyl-10-bromocobalamin
ESI-MS	Electrospray ionisation-mass spectrometry
$[H_2OCbl]^+$	Aquacobalamin
$[H_2O\text{-}(10\text{-}Br)Cbl]^+$	Aqua-10-bromocobalamin
$[H_2O\text{-}(10\text{-}Cl)Cbl]^+$	Aqua-10-chlorocobalamin
HMBC	Homonuclear multiple bond correlation
HSQC	Heteronuclear single quantum coherence
HOMO	Highest occupied molecular orbital

HPLC	High pressure liquid chromatography
LUMO	Lowest unoccupied molecular orbital
[MeCbl]	Methylcobalamin
[Me-(10-Cl)Cbl]	Methyl-10-chlorocobalamin
NMR	Nuclear magnetic resonance
pK_a	Acid dissociation constant
pK_{co}	Acid dissociation constant of coordinated H_2O in corrin complexes
ppm	Parts per million
ROSEY	Rotating frame Overhauser effect spectroscopy
[SeCNCbl]	Selenocyanatocobalamin
TOCSY	Total correlation spectroscopy
uv-vis	Ultraviolet-visible
α-ligand	The lower axial ligand coordinated to the Co ion in corrins
β-ligand	The upper axial ligand coordinated to the Co ion in corrins

Buffers

CAPS	3-(Cyclohexylamino)-propanesulfonic acid
CHES	Cyclohexylaminoethanesulfonic acid
MES	3-(N-Morpholino)-ethanesulfonic acid
MOPS	3-(N-Morpholino)-propanesulfonic acid
Tris	Tris(hydroxymethyl)-aminomethane

Symbols

μ	Ionic strength
A_1	Final absorbance
A_0	Initial absorbance
A_λ	Absorbance at monitored wavelength
K	Binding constant
K_a	Ionisation constant
k^1_{obs}	Experimentally determined pseudo first-order rate constant for the substitution of H_2O by exogenous ligand
k_I	pH-corrected pseudo first-order rate constant
k_{II}	Second-order rate constant
K_{obs}	Experimentally determined binding constant for coordination of exogenous ligand
k_s^{II}	Second-order rate constant for the slower reaction
k_f^{II}	Second-order rate constant for the faster reaction
k_r	Reverse rate constant
λ	Wavelength
σ_p	Hammett sigma parameter

CHAPTER 1

Introduction

1.1 An Introduction to Vitamin B_{12}

Vitamin B_{12} or cobalamin is the largest and most structurally complicated vitamin, and one of the eight B vitamins which is water soluble and plays an important role in the human body. Its anti-pernicious anaemia property and also its unusual chemical reactivity given the presence of Co(III), have prompted scientists to undertake many investigations into vitamin B_{12} and its derivatives.

Initially, the anti-pernicious anaemia factor (vitamin B_{12}) was discovered by accident in 1920 by George Whipple. He had been doing experiments which involved inducing anaemia in dogs by bleeding them and then feeding them various types of food to observe which diets resulted in the fastest recovery from the anaemia. He noticed that the quickest recovery was achieved after injection of large amounts of liver extract. This specific treatment was tried by different scientists.[1,2] In 1948, Mary Shaw Shrob *et al*.[3] applied *Lactobacilis lactis Dorner* (LLD) assay to extract the anti-pernicious anaemia factor form the liver extract and isolate the vitamin B_{12}. Following the extraction of the red crystalline compound (vitamin B_{12}), the chemical structure of vitamin B_{12} was determined by Dorothy Crowfoot Hodgkin *et al*.[4] in 1956 based on crystallographic data. Primarily deep red crystalline needles of vitamin B_{12} were given to Hodgkin to analyse. After taking some X-ray photographs of these crystals she reported the approximate molecular weight as 1500.[5] At a later stage, larger crystals were grown from water which had a larger unit cell compared to air-dried crystals. Hodgkin assumed that the crystals had more water molecules of crystallisation, since when these crystals were removed from their mother liquor and exposed to air they shrank, become opaque, and brittle.

In 1951, a detailed chemical structure of vitamin B_{12} became available; one molecule of vitamin B_{12} contained a cobalt atom, 5′, 6′-dimethylbenzimidazole (DMB), 1-α-D-ribofuranoside (2′ or 3′) phosphate, D_g-1-amino-2-propanol, several amide groups, and a cyanide group. The estimated general formula was $C_{63}H_{88}O_{14}N_{14}PCo$.[6] **Figure 1.1** shows the numbering structure of vitamin B_{12} and its most crucial derivatives.

References on page 37

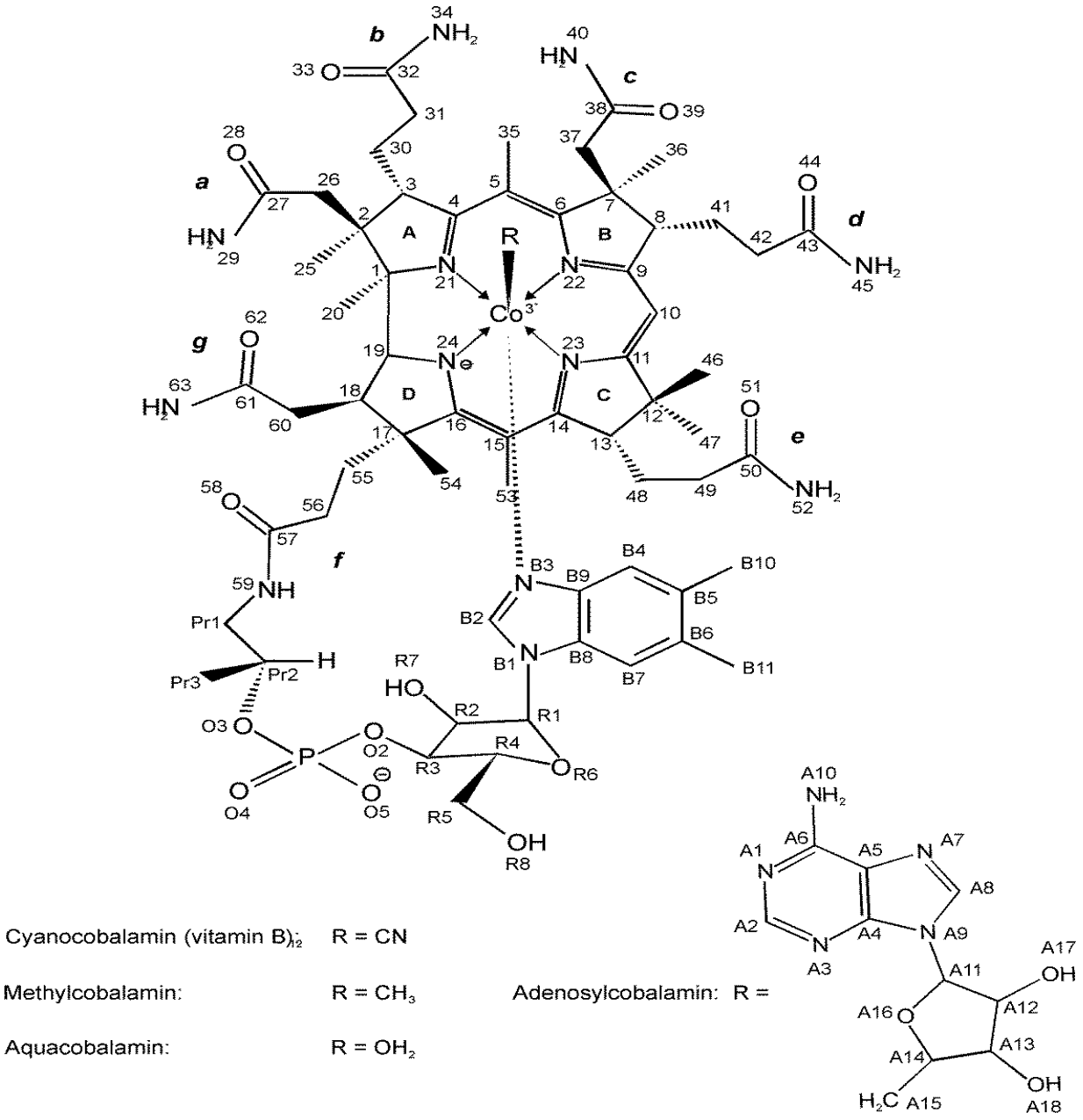


Figure 1.1 The structure, numbering scheme, and standard view of the most important cobalamins.[7]

References on page 37

1.1.1 Roles of Vitamin B_{12} in the Human Body

Vitamin B_{12} is one of the most crucial vitamins in the human body as it is involved in: i) formation of the blood cells; ii) formation of a protective layer on nerve cells; iii) conversion of carbohydrates, fats, proteins from food into energy; iv) DNA synthesis; vi) DNA methylation; and vii) degradation of propionyl coenzyme A (CoA).[8]

Lack of vitamin B_{12} causing pernicious anaemia, loss of balance, numbness or tingling in arms and legs and weakness. Recent studies show that deficiency of vitamin B_{12} can also initiate a high risk of breast cancer,[9] since vitamin B_{12} deficiency can induce inadequate DNA synthesis and abnormal DNA methylation through derangement of one-carbon metabolism; these two mechanisms are most relevant for the carcinogenic effect of vitamin B_{12} deficiency.[10] In general vitamin B_{12} deficiency can occur in the following cases: people over age of 50 who lose the ability to absorb vitamin B_{12} from foods; people who have had gastrointestinal surgery, or who have digestive disorders; and also people who have insufficient uptake of vitamin B_{12} in their diets. Vitamin B_{12} deficiency can be treated by taking animals products, multivitamins, and having adequate intake of vitamin B_{12} or cyanocobalamin ([CNCbl]) in forms of pills, nasal gel or injection.

In the human body, the active form of cobalamin is not vitamin B_{12} itself, but one of two coenzymes which are derived from it and are essential for the functioning of some enzymes. These two coenzymes are adenosylcobalamin ([AdoCbl] or vitamin B_{12} coenzyme) and methylcobalamin ([MeCbl]). In mammals these two cofactors are required for the activity of two enzymes: the mitochondrial methylmalonyl-CoA mutase and cytoplasmic methionine synthase.[11,12] The structure of these coenzymes were determined crystallographically by Galen Lenhert[13,14] and Marzilli and co-workers,[15] respectively. Discovery of a Co–C bond in the structure of [AdoCbl] was serendipitous; hence it was the first naturally occurring organometallic compound to be discovered. Both structures of [AdoCbl] and [MeCbl] resemble each other apart from the upper axial ligand.

References on page 37

1.2 Structural Details of Vitamin B_{12} and its Derivatives

The basic macrocyclic ligand common to all vitamin B_{12} derivatives is the "corrin" ligand, and it is derived from the word "core". The term "corrinoid" is a general term for all the compounds containing a corrin ring. Typically, when the structure of vitamin B_{12} is viewed from the top or *β* face, the molecule is usually drawn from C1-C19, on the left side, with C1 on top of C19, as shown in **Figure 1.1**. From the lower side or *α* position, the methyl group C20 attached to C1 points toward lower or *α* face. Cobalamins have 7 side chains which are categorised into two groups: acetamide chains (*a, c, g*) which occur above the plane and propionamide chains (*b, d, e, f*) which occur below the plane of the corrin macrocycle. Cobalamin is a term used for vitamin B_{12} and its all derivatives where the *f* side chain is linked to propanolamine-phosphate-ribose-dimethylbenzimidazole (DMB) group. These compounds are also referred to as "complete corrinoids". If the DMB base is altered, the compound is a "cobamide". The term "incomplete corrinoids" refers to cases when phosphate, ribosyl and base are removed and water replaces the α-position, but the *f* side chain is retained; these cases are also called "cobinamides". The most well-known of the "cobinamides" is aquacyanocobinamide (known as Factor B). If all the side chains are hydrolysed including the *f* side chain, the compound is called a "cobyric acid"; the most well-known is dicyanocobyric acid heptamethyl ester (also known as dicyanocobester ([DCCbs])). If all other side chains except the *f* side chain of the vitamin B_{12} are hydrolysed, the compound is termed a "hexacarboxylic acid".

In the cobalt corrinoids in their most stable oxidation state the central cobalt atom exists in the +3 oxidation state. It is coordinated by four equatorial nitrogen atoms donated by the tetrapyrrolic corrin ring. A bulky base, 5',6'-dimethylbenzimidazole (DMB), is coordinated to the cobalt atom from the lower face (*α* axial ligand position). From the upper face (*β* axial ligand position) the cobalt atom is coordinated to a ligand such as cyanide, water, methyl or 5′-deoxyadenosyl groups. As these six ligands are not identical, the octahedral complex becomes tetragonally distorted, with a tendency towards the square planar state. The DMB base is attached to the Co (in the lower or *α* position) through B_3 atom and to the ribose by a glycosyl link from B1 N to R1. The upper *β* ligand is H_2O or CN^- in case of aquacobalamin ($[H_2OCbl]^+$) or cyanocobalamin ([CNCbl]), respectively. The oxidation state of Co metal can change in the structure of vitamin B_{12} from +3 to +1. As the oxidation state of Co atom decreases the number

References on page 37

of axial ligands decreases as well. Co(III) has typically two axial ligands, Co(II) one, and Co(I) none. Interestingly, alkylcobalamins stay preferentially in the six-coordinate "base-on" state, which is in contrast to the "base-off/His-on" state (**Figure 1.2**) found in the active site of both mammalian B_{12} enzymes.[16] The base-on confirmation predominates at physiological pH, because the pK_a for the "base-on" to "base-off" transition varies from -2.13 to 3.17 depending on the nature of the upper axial ligand.[17] Change in axial ligand disposition and oxidation state has been shown to have a salient role in the redox reactions involving [MeCbl] and [AdoCbl] containing enzymes.[18,19]

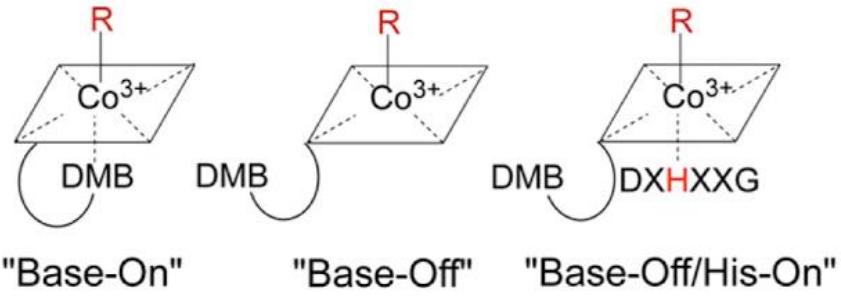


Figure 1.2 Alternative conformations of cobalamins differing with respect to the lower or α axial ligation site.[20]

The upper face (β position) of cobalamins can be occupied by a wide range of atoms and groups. Over the years, many structures of cobalamins and its derivatives have been reported; but the most critical cobalamins are [CNCbl], [MeCbl] and [AdoCbl]. In the first compound the upper face is occupied by a cyanide ligand and with a relatively short (1.86 Å)[21] Co–CN bond. In the latter two biologically-active B_{12} coenzymes, [MeCbl] (where the β axial ligand is methyl) and [AdoCbl] (where the β axial ligand is methylene 5′-deoxyadenosyl) the bond length of Co–C is slightly longer than in [CNCbl] (1.98 Å and 2.00 Å in [MeCbl] and [AdoCbl], respectively). The overall structures of these two alkylcobalamins are similar despite their different upper axial ligands (β axial ligands). The Co–N_{axial} bond length is 2.21 Å in [AdoCbl],[22] and 2.19 Å in [MeCbl].[15] This is in a good agreement with the pK_a for protonation of the DMB base in these

References on page 37

two compounds (3.7 in [AdoCbl] and 2.9 in [MeCbl]).[17] In addition the presence of a Co–C bond in [MeCbl] and [AdoCbl] classifies them as organometallic complexes which play a critical role in enzymatic reactions due to homolytic or heterolytic bond cleavage of this bond in [AdoCbl] and [MeCbl], respectively. For further study of the homolytic and heterolytic cleavage of Co–C, a great number of structural analogues of these compounds have been synthesised and reported.[21,23-27]

1.3 Cleavage of the Co–C Bond

Methylmalonyl-CoA mutase and methionine synthase are two enzymes that require vitamin B_{12} as a cofactor. Two basic reaction modes are essential for the reactions catalysed by vitamin B_{12}-dependent enzymes and are detailed below.

1.3.1 Co–C Bond Homolysis

The homolytic mode of formation and cleavage of the organometallic axial bond at the cobalt centre is an oxidation-reduction reaction resulting in a free alkyl radical R• and Co(II). In 5'-adenosylcobalamin-containing enzymes, the first step is homolytic Co–C bond cleavage to generate a carbon-centred deoxyadenosyl radical and a metal centred cob(II)alamin radical; thus [AdoCbl]-dependent enzymes act as radical generators.[28] In all [AdoCbl]-dependent enzymes (except ribonucleotide reductase), the initial step is followed by a rearrangement in which the adjacent H and X substituents are interchanged as is shown in **Figure 1.3.** Methylmalonyl-CoA mutase catalyses the conversion of (2R)-methylmalonyl-CoA to succinyl-CoA; in this reaction the free adenosyl radical is created and initially reacts with the product group before reacting with anything else while moving towards the substrate.[29,30]

Brown and co-workers[31,32] undertook a study with neopentylcobalamin analogues and neopentylcobalamin analogues complexed to the vitamin B_{12} binding protein, haptocorrin, to investigate the role of the *c* side chain rotational motion on the thermal Co–C homolysis. They found that the activation entropy for thermal Co–C bond homolysis is controlled by a steric restriction of the rotation of the *c* side chain of the analogues. When neopentylcobalamin and its analogues were stabilized 380-fold toward homolysis on being complexed to haptocorrin, this

References on page 37

entropic stabilisation comes from hydrogen-bonding interaction of the acetamide side chains with the protein pocket. They also suggested that 30-40% of the catalytic properties of the [AdoCbl]-dependent enzymes could come from this restricted motion, but concluded that it is not the only mechanism in operation. Perry *et al*.[33] have suggested that transfer of electron density onto the Co(III) centre imparts some Co(II)-like character onto it; along with further modulation of this by binding of the protein, this may activate Co–C bond towards homolysis.

1.3.2 Co–C Bond Heterolysis

The Co–C heterolytic mode of cleavage follows a two electron oxidation-reduction reaction which leads to formation of Co(III) and R^- or Co(I) and R^+. In methyl-transfer reactions, MeCbl-containing enzymes catalyse the Me–Co bond heterolysis to form CH_3^+ (methyl carbocation) and Co(I).[28] Methionine synthase catalyses the transfer of a methyl group from methyl tetrahydrofolate to cob(I)alamin and then to homocysteine to generate H_4folate and methionine, **Figure 1.3**.

Dölker and co-workers[34] studied the effect of axial ligands on the heterolytic Co–C bond cleavage. They found out the distance between the cobalt metal centre and the axial ligands plays a critical role in heterolytic Co–C bond cleavage. They showed that in methyl-transfer reactions, the distance between the cobalt centre and methyl group should not be long for the heterolysis reaction to occur.

References on page 37

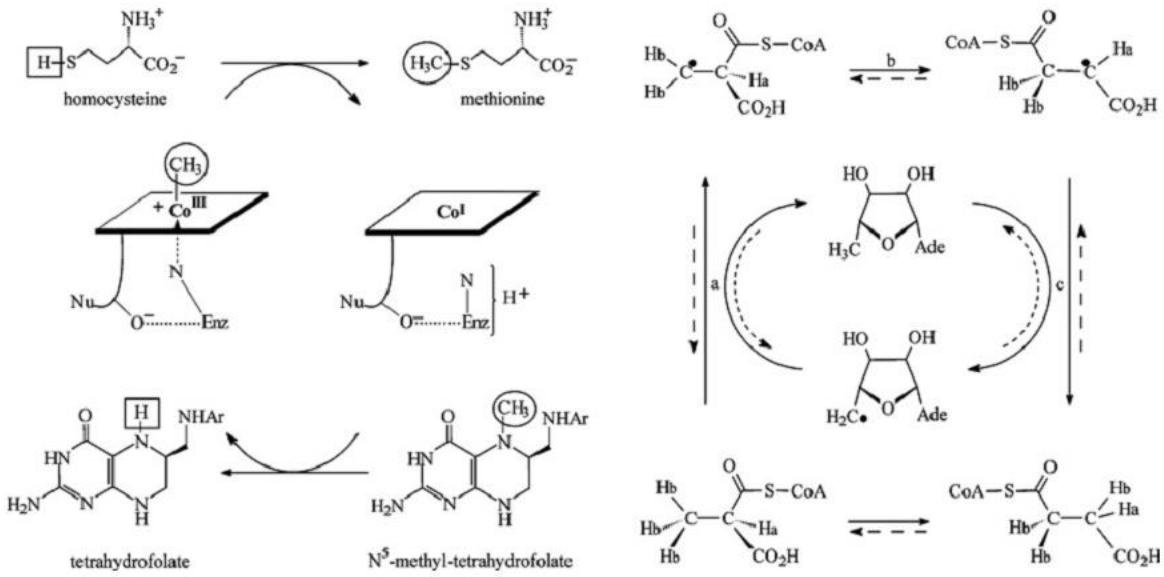


Figure 1.3 Heterolytic and homolytic Co–C bond formation and cleavage for the reaction catalyzed by methyl-tetrahydrofolate and the reaction of interconversion of (R) methylmalonyl-CoA into succinyl-CoA, from left to right.[35]

References on page 37

1.4 Corrin and Porphyrins Macrocycles

1.4.1 Aspects of the Corrin Ring

Corrin has two pyrrole rings attached together, producing a 14 π-electron conjugation system, with C_{2V} symmetry system; the symmetry can be lowered to C_1 due to the partial conjugation system and presence of 10 saturated carbons[36] as shown in **Figure 1.4**. These features with a number of the sp^3 hybridised carbons makes the corrin ring flexible and non-planar and creates a small central cavity; all these features are critical in cobalt corrin chemistry.[37,38]

Corrinoids such as cobalamins are seldom metal-free[39,40] and they have a strong preference to coordinate to cobalt whereas other corrinoids have preference to coordinate to metals such as Zn, Rh, Ni and Pd.[41-44] To rationalise why a rare and inert cobalt metal is preferred by cobalamins, the synthetic pathway of corrins can be considered here. In the early stages of molecular evolution, cobalamins came first form the anaerobic reducing atmosphere, and thus these macrocycles use transition metals for their redox properties.[45] Among the first row transition metals such as Fe or Cr, Co is the only metal in cobalamins which can be reduced to +1 oxidation state for some catalytic functions.

1.4.2 A Note on Porphyrins

The name porphyrin comes from the Greek word porphyros, meaning purple. This macrocycle consists of four pyrrole rings linked together by a methine bridges at their *α*-carbons (according to IUPAC system α-carbons are C1, 4, 6, 9, 11, 16) **Figure 1.5**. These deeply coloured macrocycles exhibit D_{4h} symmetry and maintain a planar conformation. Porphyrins have 26 delocalised π-electrons in total and are aromatic. The fully conjugated (18-π electron) system causes the intense colour of porphyrins with an intense Soret absorbance (ca. 400 nm) and very high extinction coefficient.[46] Porphyrins tend to stay planar, but they have also shown a fair degree of flexibility, for instance when coordination of a metal ion happens. The degree of distortion depends on the size of the metal ion;[47] when the metal ion is smaller than the cavity, a "ruffled" conformation is obtained.[48] Even in a metal-free porphyrin distortion happens as a result of repulsions between protonated nitrogen atoms.[49,50] Deprotonation of the nitrogen atoms

References on page 37

of the pyrrole rings allow the porphyrin to bind to a wide range of transition metal ions for example, Ti,[51-53] V,[54,55] Cr,[55,56] Mn,[57-59] Fe,[60-62] Co,[63-65] Ni,[66-68] Cu[69-71] and Zn,[72-74] from the first row of d-block, and to non-metals such as phosphorous.[75] However, among this wide range of metal porphyrins probably only iron porphyrins have significant biological function, and are essential for the process of respiration, where haemoglobin and myoglobin are responsible for oxygen carrying and storage, respectively. Iron is also involved in biological electron transport, where the cytochromes are the key components.

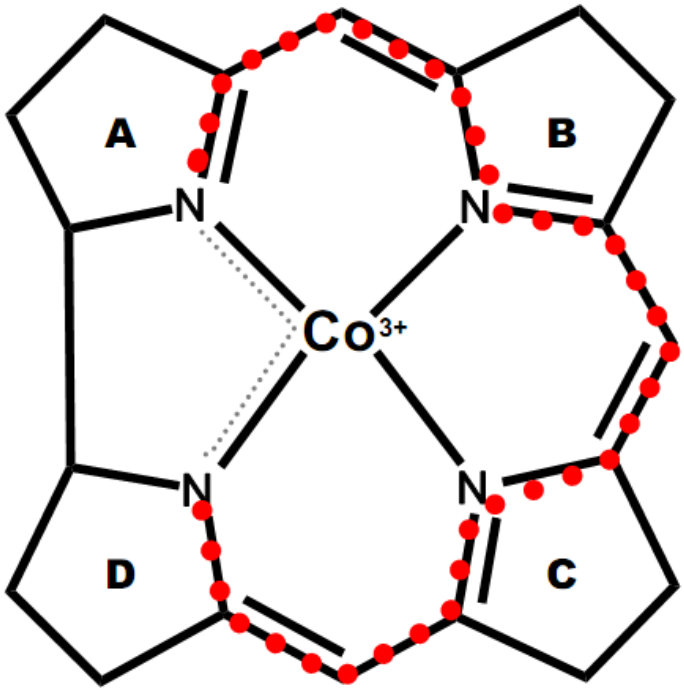


Figure 1.4 The cobalt corrin structure, red dots indicate the delocalised π electron system.[45]

References on page 37

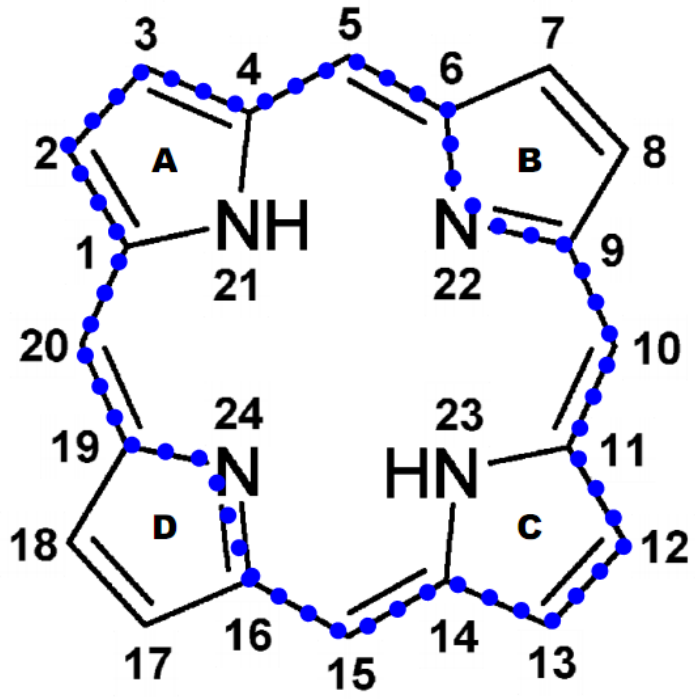


Figure 1.5 The backbone of all porphyrins. The indicated blue pathway shows the delocalised 18-π electron system. This structure was proposed by Küster in 1912. However, Hans Fischer is often credited with identifying this structure in 1929.[76,77]

1.4.3 A Comparison of Porphyrin and Corrin

Some critical structural differences are the cause of the functional differences between corrins and porphyrins; these include cavity size, metal ion preferences and ring flexibility. Geno and Halpern[78] suggested that the porphyrins are not suitable ligands for coenzyme B_{12} due to their inflexibility. They performed a series of experiments on benzylcobaltoctaethylporphyrin complexes and the corresponding benzylcobalt complexes with the flexible equatorial ligand, dimethylglyoxime. They studied the electronic and steric properties of the axial ligands of these two groups on the Co–C bond dissociation energy. Their findings suggested that the porphyrin ligand is not flexible enough in this role. On the other hand, a number of researchers reported on the extreme flexibility of porphyrin ring.[79,80] Eschenmoser[81] stated that the reason for occurrence

References on page 37

of corrin structure, rather than porphyrin, in B_{12} is that corrin preceded porphyrins in the evolutionary time scale. Corrinoids were produced initially under anaerobic conditions.[82,83] **Table 1.1** shows some factors that impact these two macrocycles functionality.

Table 1.1 Details on the structural differences between corrins and porphyrins.

	Porphyrins	Corrins
Symmetry system	D_{4h}	C_{2v}, C_1
Electron conjugation system	18 π	14 π
Number of pyrrole rings	4 (directly linked by a methane bridge)	2 pyrrole ring directly attached
Ring geometry	Planar	Non planar
Choice of metal	Fe	Co
Cavity size	larger	smaller

1.5 Cis- and Trans- Influences/Effects

The *cis*-effect is the effect of L ligand on its neighbouring ligand Y, and the *trans*-effect is the effect of L ligand on its *trans* ligand Y[84] as shown in **Figure 1.6**. The term "kinetic" *cis*- and *trans*- effects are described as the effect of a metal coordinated group on the rates of ligand substitution reactions of groups either *cis* or *trans* to it. The thermodynamic influence is the effect on the stability constant (log *K*) for the substitution of a coordinated L ligand by an incoming ligand. The ground state influence is the effect of ligand L on the physical properties of ligand Y, or on the metal–L bond length and angle.

References on page 37

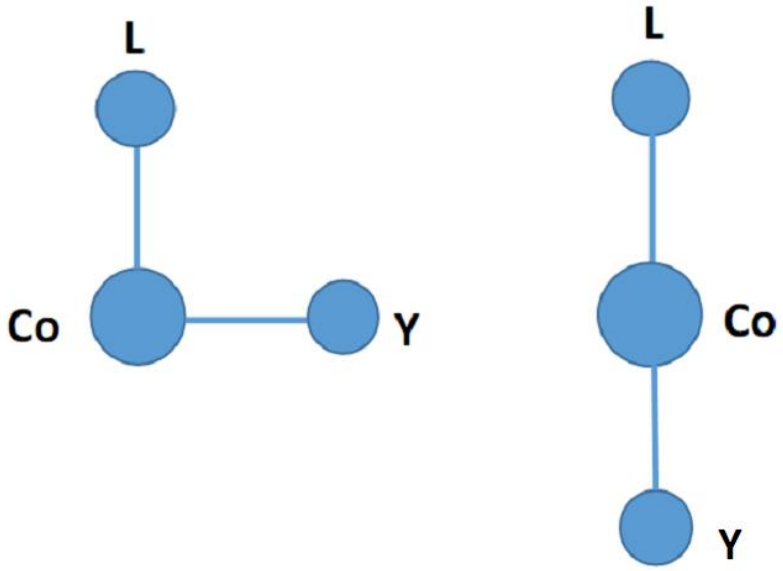


Figure 1.6 The *cis*- and *trans*- influences.

Chernyaev[85] who investigated square-planar platinum(II) complexes, introduced the concept of *cis*- and *trans*- influences. He was also the first to recognise the existence of a specific order for the *trans*-influence amongst the ligands. Pratt and Throp[86] investigated the same effects in cobalt(III) complexes and found out that the order is slightly different compared to platinum(II) complexes. They also divided their studies of *cis*- and *trans*- effects/influences into three phases:[87,88]

i) Ground state influence, which involves the bond lengths of the axial ligands
ii) Chemical equilibria (thermodynamics influences)
iii) Rates of reaction (kinetics effects)

They deduced that there is a correlation between *trans*- and *cis*- influences. The effect of the axial ligand on the electronic spectrum of the ring corrin system (*cis*-influence) and on the equilibrium between water and benzimidazole (*trans*-influence) shows a general similarity with the position of the ligand in the nephelauxetic series, which is based on the amount of negative

References on page 37

charge that the ligand donates to the metal ion through σ-bonding. The general order is as follows: N ~ O ~ Cl ~ Br and C in CN^- < S, Se, I and C in the organo-ligands; and CN^- < ethinyl < vinyl < ethyl for the carbanions.[87-89]

The thermodynamic *trans*-influence was studied by Hayward *et al*.[90] for several ligand substitution reactions of cobalamins and cobinamides. The results show the thermodynamic *trans*-influence of ligand L on the equilibria for the substitution of other possible axial ligands Y by Z. This study also demonstrates that as the ligand changes in the following order: H_2O, NC^-, $HC{\equiv}C^-$, $H_2C{=}CH^-$, CH_3 the *trans* cobalt-cyanide bond becomes less stable relative to the Co–DMB bond which consequently becomes less stable relative to Co–water bond. The following reasons rationalise why corrinoids were chosen for the study of the thermodynamic *trans*-influence:

i) Corrinoids are octahedral which prevents the uncertainty of the binding of further ligands that may occur with square-planar complexes
ii) The corrin ring resists *cis*-*trans* isomerisation
iii) The equilibria are fairly rapidly established in most cases
iv) A wider range of axial ligands can be studied than in simpler Co(III) complexes.

The effect of varying ligand L (in the *β* axial position) on the Co–N bond lengths in both *cis* and *trans* position in three cobalt complexes was studied by Pratt[91] (data are presented in **Table 1.2**). Pratt pointed out that varying the ligand L significantly affects the *trans* position and only dimethylphosphine and methyl exert *cis* lengthening. This result shows the correlation between the σ-donor ability of the ligands and *trans*-lengthening; as the σ-donor ability of a ligand increases more electron density deposits on Co atom and results in more *trans*-lengthening. In addition, the *cis*-lengthening was also observed for strong σ-donor ligands, for example, methyl and dimethylphosphine. From the data in **Table 1.2**, it is noticeable that the order of *trans*-effect is the same for all three complexes: ammonia < sulfite < methyl which correlates with nephelauxetic effect. The structural data for other cobalamins[92] shows the order of *trans*-lengthening of L to be: $H_2O < NH_3 \leq HO^- \sim Cl^- \sim SCN^- \sim NO_2^- < CN^- \sim (SC(NH_2)_2^- < SO_3^{2-} \sim Me^- < P(OMe)^2O^-$. The data show substitution of H and OMe by F in CH_3 and $P(OMe)O^-$ result in a decrease in the *trans* effect. The crystal structure of $[H_2OCbl]^+$[93] is shown to have an

References on page 37

unusually long Co–NB_3 (1.925 Å) bond length which might be due to the interaction of DMB base with corrin ring in the area of C5. In *β*-cyano-imidazolyl-cobamide and *β*-methyl-imidazolyl-cobamide[21,27] where the bulky DMB base in cobalamin has been replaced by a less bulky imidazole moiety, the bond lengths of Co–NB_3 were shorter in both cases compare to the analogous cobalamins (1.97 Å compared with 2.01Å and 2.09 Å compared with 2.19 Å, respectively). The same effect would be observed if the upper axial ligand was water, a Co–NB_3 bond length of no greater than 1.885 Å for the imidazole coordinated base *trans* to water would be expected,[91] therefore the long Co–NB_3 bond length would not be unusual.

An "inverse" *trans*-influence was observed for alkylcobalamins, where both the Co–NB_3 and Co–L bond lengths increase; this increase is due to the σ-donor ability of the L ligand (*β* position) in alkylcobalamin compounds. Initially, the analysis of the crystal structures of several alkylcobalamins revealed that the "inverse" *trans*-influence is related to the electronic properties of L. However, at a later stage, DFT calculations by Randaccio[94] showed that the "inverse" *trans* effect is not a true *trans*-influence, but rather a steric effect. As the bulkiness of the L ligand increases the steric repulsion between the ligand L and corrin ring becomes greater; this results in lengthening of both Co–NB_3 (steric *trans*-influence) and Co–L bonds (steric *cis* influence). These calculations also showed that in the "regular" *trans*-influence the positive charge decreases on Co atom as the σ-donor ability of ligand L increases. Whereas in "inverse" *trans*-influence, the converse is observed due to the lengthening of Co–L bond resulting in decreased σ-donation from the ligand to the metal. Hence it causes a more positively charged Co centre.[94] Related DFT calculations by Ryde, Jensen and recently Kuta have validated these findings.[95,96] A recent study by Perry[97] showed that substitution of the *β* axial ligand by a bulky alkyl group, phenylvinyl, exhibits an "inverse" *trans*-effect where the Co–N bond to DMB increases to 2.217(8) as the Co–C bond to the *β* organic ligand increases to 2.004(8), while the results for vinylcobalamin and chlorovinylcobalamin have shorter Co–C bond length (1.912 and 1.953 Å, respectively). Presumably the longer Co–C bond length in phenylvinylcobalamin is due to the greater steric bulk of phenyl substituent.

References on page 37

Table 1.2 Co-axial ligand bond length (in Å).

	L–Co(NH_3)		L–Co($dmgH)_2NH_3$		L–Co(corrin)(DMB)		Reference
L	Co–N (*cis*)	Co-N (*trans*)	Co–N (*cis*)	Co-N (*trans*)	Co–N (*cis*)	Co–N (*trans*)	
H_2O					1.88-1.90	1.925	98
NH_3	1.966	1.966	1.983	1.960			
HO^-						1.98	98
CN^-					1.88-1.92	2.01	98
CF_3^-					1.87-1.95	2.05	98
SO_3^{2-}	1.966	2.055		2.030		2.17	98
CH_3^-	1.973	2.105		2.053	1.88-1.97	2.19	98
$PF(OMe)O^-$					1.99-1.92	2.09	98
$P(OMe)_2O^-$					1.91-1.96	2.20	98
$SC(NH_2)_2^-$					1.87-1.91	2.03	94
Cl^-					1.89-1.92	1.98	94
SCN^-					1.89-1.92	1.99	99
$SeCN^-$					1.89-1.92	2.02	99
NO_2^-					1.87-1.92	1.99	99

References on page 37

In the cobalamins, the electron rich corrin ring appears to enhance the rate of the ligand substitution reactions of X by L, apparently through a kinetic *cis*-effect, since typical Co(III) complexes are inert. Presumably, this lability is due to the delocalization of extra electron density from the corrin ring onto the metal centre which makes Co(III) behave somewhat like labile Co(II). A series of second-order rate constants for the substitution of water by various ligands in some Co(III) complexes (each containing four N-donor ligands in the equatorial plane) are presented in **Table 1.3**.

Table 1.3 Second-order rate constants for ligand substitution of X by L in various $Co^{III}(N_4)$ complexes.

X	Complex	L	k_2/ M^{-1} s^{-1}	Reference
OH^-	Corrin	N_3^-	1.6×10^5	100
OH^-	Porphyrin[a]	N_3^-	7.2×10^2	101
H_2O	Corrin	I^-	2.2×10^3	102
H_2O	Porphyrin[a]	I^-	1.62	103
I^-	Corrin	SCN^-	1.5×10^2	102
I^-	Corrin	$S_2O_3^{2-}$	6.8	104
I^-	Cobaloxime[b]	SCN^-	1.2×10^{-3}	105
H_2O	Corrin	SCN^-	8.2×10^2	102
H_2O	$(NH_3)_4$	SCN^-	8.6×10^{-7}	106

[a] Tetrakis (4-N-methylpyridyl)porphinato. [b] Bis(dimethylglyoximato).

The results show that the rate constants for the substitution of water in corrin, porphyrin, cobaloxime and amine complexes are in the approximate ratio of $10^9 : 10^6 : 10^4 : 1$.

A study of the proton magnetic resonance spectra of some cobalamins by Hill and co-workers[88] revealed that the chemical shift of the methane hydrogen at C10 position of the corrin ring is dependent on the ligand that is attached to the cobalamin. Further studies

References on page 37

implied that keeping benzimidazole as the fixed ligand while the axial ligand (β position) varied in the order $H_2O < OH^- < C_2H_3^- < CH_3^-$ led the resonance of C10 hydrogen to shift upfield. When the water was the fixed ligand then the order became $CH_3^- \sim C_2H_5^- < CN^-$.[88] Hill pointed out that their results for benzimidazole can be compared with compounds where the cobalt atom experiences an increase in electron density, which results in an increase of electron density at the C10 position. Moreover, they also found a correlation between the energies of the α and β bands (in the uv-vis spectrum) and proton chemical shifts at the C10 position; **Table 1.4** shows the values. From the presented data it is notable that when the charge density increases at the C10 position the shielding of hydrogen at this position also increases and the ^{1}H NMR resonance appears at higher field. **Figure 1.7** shows this correlation (R^2= 0.97), which is a plot of the β band wavelength against the δ value of H10. These findings were also confirmed by Chemaly;[107] she undertook a study on various phosphite ligands such as $P(OCH_2)_3CCH_2CH_3$, $P(OCH_3)_2O^-$, $P(OCH_2CH_3)_2O^-$ and $P[OCH(CH_3)_2]_2O^-$ with vitamin B_{12a} and the data revealed that the β band wavelength and the δ values of H10 for the phosphitocobalamins confirm the same trend as shown in **Figure 1.7**.

Table 1.4 Correlation between absorption and NMR of cobalamins and cobinamide (data from Ref 73).

Compound	α band/ 10^{-3} cm^{-1}	β band/ 10^{-3} cm^{-1}	C10 hydrogen chemical shift/ δ
Dicyanocobinamide	17.2	18.5	4.13
Ethylcobalamin	18.1	19.0	4.12
Methylcobalamin	18.2	19.1	4.12
Vinylcobalamin	18.2	19.2	4.05
Hydroxocobalamin	18.6	19.35	3.92
Aquacobalamin	19.0	20.05	3.72
Methylcobinamide	21.7	21.7	3.20

References on page 37

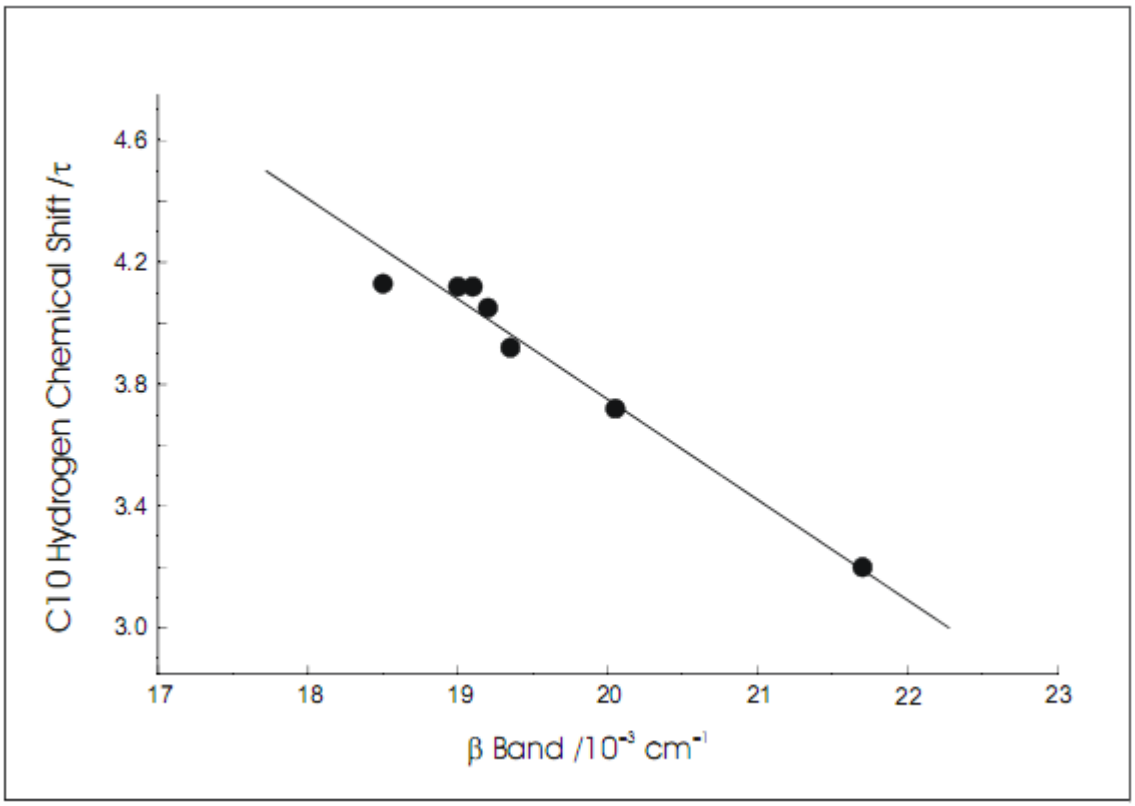


Figure 1.7 Correlation of the *β* band with the C10 proton chemical shift ((R^2= 0.97). The data were obtained from **Table 1.4**.[108]

The *cis*-influence of the corrin ring was further studied by Brown and co-workers.[109] They synthesised a series of L-10-chlorocobalamin compounds (where the proton of C10 is substituted by Cl) and obtained their crystal structures. A number of differences in bond lengths and bond angles were found between L-10-chlorocobalamin and their parent compounds. In cyano-10-chlorocobalamin ([CN-(10-Cl)Cbl]) the Co–C bond is longer and C–N bond of CN^- was shorter compared to [CNCbl]. In aqua-10-chlorocobalamin perchlorate ([H_2O-(10-Cl)Cbl·ClO_4) the Co–O bond length was similar to that found in aquacobalamin perchlorate ([H_2OCbl·ClO_4]), but the Co–NB_3 bond length was longer. In methyl-10-chlorocobalamin ([Me-(10-Cl)Cbl]) and [MeCbl] the bond lengths of Co–C and Co–NB_3 were identical, whereas the bond length of Co and equatorial nitrogen were shorter. In addition, they also noticed the equilibrium constant for the

References on page 37

coordination of DMB to Co is smaller in [CN-(10-Cl)Cbl] and [Me-(10-Cl)Cbl] compared to their parent compounds. These results highlighted the electron donating nature of the axial ligand (L) and the C10 substituent (Cl) onto the corrin ring. NMR studies for $[H_2O\text{-}(10\text{-}Cl)Cbl]^+$ and $[H_2OCbl]^+$ showed that the substitution of Cl at C10 caused the ^{13}C resonance of C10 to move downfield.[109] The NMR studies on aqua-10-nitrosocobalamin $([H_2O\text{-}(10\text{-}NO)Cbl])^+$ and $[H_2OCbl]$ revealed that the substitution of C10 hydrogen by an NO group caused a larger downfield shift for the ^{13}C resonance of C10, which indicates a greater sigma-withdrawing power of the NO group compared to Cl. [108]

1.6 Electronic Spectra of Vitamin B_{12} and Its Derivatives

Absorption spectroscopy is an important experimental technique in cobalamin chemistry. Information can be obtained on, for example, the valence of the cobalt atom, the substituents on the corrin ring, *cis*- and *trans*- influences on the corrin ring, and the nature of the axial ligands. Cobalamins have a wide range of colours from yellow or brown (e.g. [EtCbl]) through red (e.g. [CNCbl]) to green (e.g. 7-de(carbamoylmethyl)-8-dehydrocyanocobalamin) and purple as in selenocyanatocobalamin ([SeCNCbl]). Due to their high extinction coefficients, only a small quantity of sample is needed. The uv-visible spectrum of vitamin B_{12} was first reported in 1949 by Ellis and co-workers[110] and since then, uv-visible spectroscopy has become a central technique in the study of cobalamins.

The main band of the spectra of the Co(III)corrinoids appear above 300 nm due to the spin-allowed $\pi\text{-}\pi^*$ transitions within the corrin ring. $\pi\text{-}\pi^*$ transitions occur when an electron moves from a frontier occupied molecular orbital to a low-lying unoccupied molecular orbital in the corrin complex. This electronic transition is often referred to as a HOMO-LUMO transition, even though the orbitals involved may consist of other frontier orbitals. The energy difference between the HOMO and LUMO is called the HOMO-LUMO gap. One of the earliest, but still useful, descriptions of the spectra of the cobalt corrins was explained by Day.[111] **Figure 1.8** shows a labelled spectrum of $[H_2OCbl]^+$. The most intense band always occurs in the region of 350-370 nm and it is known as γ band. The second most intense bands occur in the region of 420-600 nm and are known as the $\alpha\beta$ bands. Finally, bands *D* and *E* with the lowest intensity

References on page 37

occur in the region of 390-420 nm. In 1966, for the first time absorption bands at longer wavelengths and lower intensities than *αβ* bands of cobalamins were reported by Pratt and Throp.[87]

To rationalise the electronic bands of vitamin B_{12}, Kuhn *et al;*[112] performed studies on the absorption of vitamin B_{12} and their results can be seen in **Figure 1.8**. The lowest energy levels from 1 to 7 of the π electron are filled and transition only occurs from 6 → 9. Transition from 7 → 8 corresponds to the *αβ* bands, transition from 6 → 8 corresponds to the *DE* and lastly transition from 7 → 9 corresponds to *γ* band. No more transition would be expected at energies higher than those of the *γ* band.[89]

Pratt[89] stated that although the charge-transfer bands are expected from transitions between the cobalt and the axial ligands or between the cobalt and the corrin ring, they are difficult to identify. Therefore, only the charge-transfer between cobalt and the phenolato axial ligand has been observed. Following this statement by Pratt, Ochiai *et al.*[113] performed a Hückel molecular orbital calculation, on a model compound *viz*. [RCo^{III}(CR)Br]Y. **Figure 1.9** shows the energy diagram that they produced, where the $2a_1$ level is the σ-bonding orbital of the cobalt centre and the $3a_1$ level is the σ-antibonding orbital of the alkyl carbon atom. Their calculations imply that the charge transfer band is the transition between these two levels and it is also likely that this band is hidden beneath the more intense $\pi \rightarrow \pi^*$ bands in the same region.[114]

References on page 37

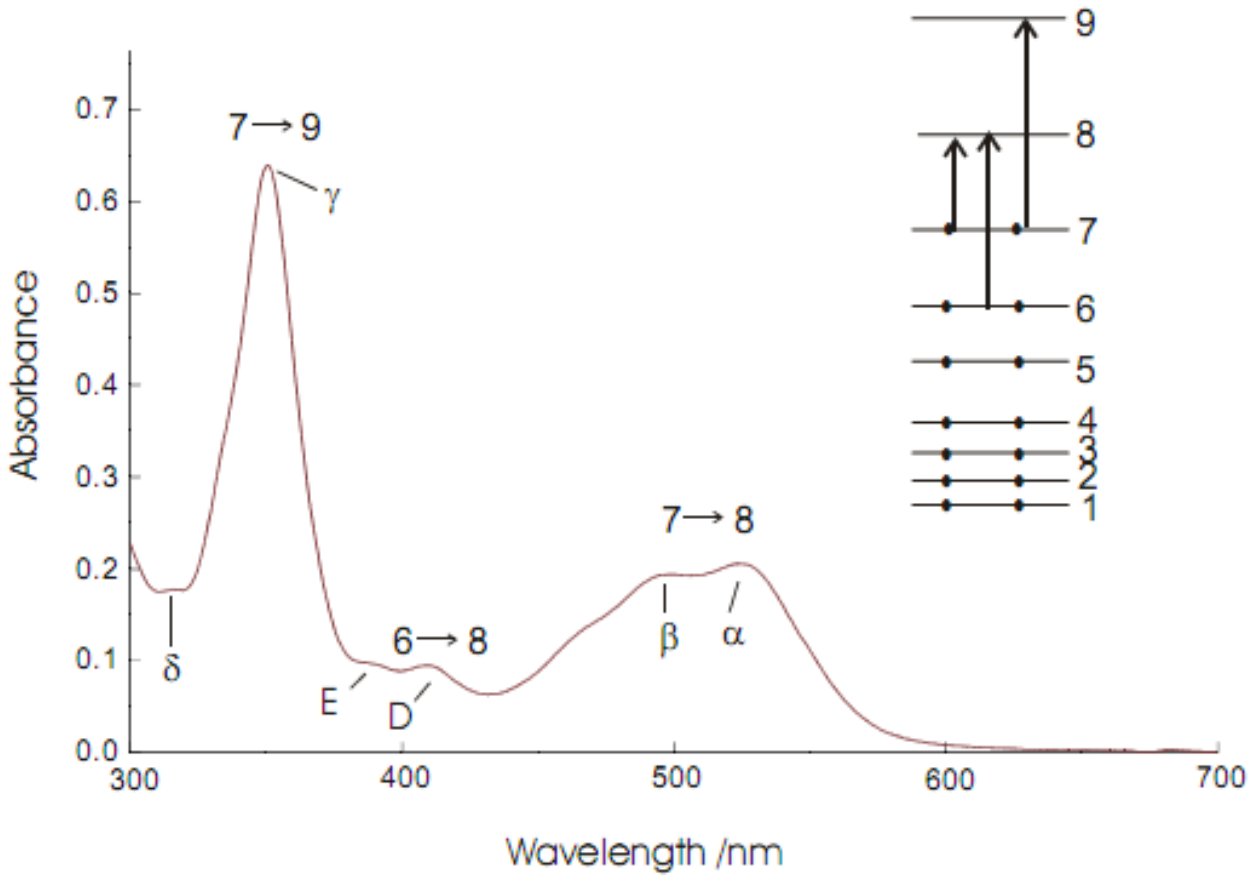


Figure 1.8 Energy levels of the π electron system and their corresponding bands in the absorption spectrum of [H_2OCbl].[112]

References on page 37

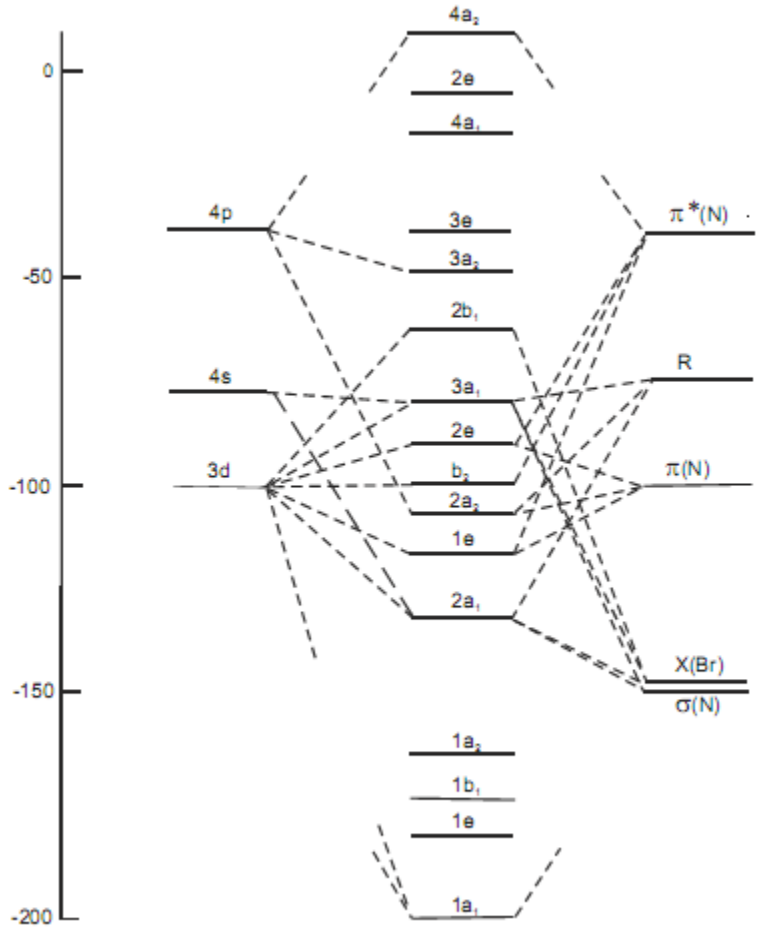


Figure 1.9 Molecular orbital diagram for $[CH_3Co^{III}(CR)Br]PF_6$.[113]

Basically the main bands in the electronic spectrum of cobalamins are very similar to those in the spectrum of the metal porphyrins, with the γ band (called the Soret band in porphyrins) around 400 nm and $\alpha\beta$ bands around 550 nm.

The spectra of the cobalamins are categorised in two groups, "typical" and "atypical". The latter is seen with the alkylcobalamins such as [MeCbl], or cobalamins containing the soft ligands $S_2O_3^{2}$, SO_3^{2-}, I^-. **Figure 1.10** shows the spectrum of sulfitocobalamin ($[SO_3Cbl]^-$). In an "atypical" spectrum the γ band occurs at longer wavelength (~370 nm) and is less intense. **Figure 1.11** shows the "typical" spectrum, that of $[H_2OCbl]^+$. It was assumed that one of the

References on page 37

reason that a wide range of spectra occur in corrinoids is related to the conformational changes of the corrin ring which is induced by changes in the cobalt-nitrogen bonds.[87] Hill *et al.* concluded form circular dichroism studies combined with the absorption spectra that the electronic rather than steric properties of the axial ligands play a critical role in determination of the conformation. They also performed ESR studies on B_{12r}, which showed that changing one axial ligand can cause a large change in the electronic structure of the cobalt ion in the compound.[115]

The position of the γ band shifts in response to the electron donor ability of the axial ligand. Electronegative ligand atoms such as N, O, Br, Cl and C in CN^- shifts the γ band to shorter wavelengths and the opposite is seen for electron donating ligand atoms such as S, Se, and C in organo-ligands.[89] These ligands exert considerable influence on the *cis*- and *trans*- influences of the corrin ring. Gaussian analysis on the electronic spectra of eleven cobalamin complexes was performed by Perry and Marques[116] and they concluded that the model which was proposed by Kuhn[112] (**Figure 1.9**) is over-simplified. Their analysis was in good agreement with DFT calculations performed by Stich *et al.*[117] which implies that the γ band corresponds to at least three electronic transitions. They also believe that "typical" and "atypical" spectra of cobalamins are not fundamentally different and the differences are related to the components of the γ band moving apart with an increase in electron density from the axial ligand field. The role of the axial ligands on the spectra of corrinoids were summarised by Pratt[89] as follows:

i) The axial ligands have a great impact on the intensities of the absorption bands.
ii) The σ-donor ability of the ligand is its most important property.
iii) The intensity of the γ band drops as the difference between the donor strengths of the axial ligands increases.
iv) The γ band moves to longer wavelengths as the sum of the donor strengths of the two axial ligands increases.

The electronic absorption spectra of cobalamins are influenced by the nature of the axial ligands and the oxidation state of the metal. All observed electronic transitions for Co(III) cobalamins have initially been attributed to $\pi \rightarrow \pi^*$ transitions of the corrin ring.[118] The nature of the axial ligands have a noticeable effect on the energy of the highest occupied orbital (7π); consequently this has a great effect on the energies and positions of γ and $\alpha\beta$ absorption bands.[119] For the σ

References on page 37

donating axial ligands, the energy of this orbital (7π) decreases linearly with increasing overlap between the axial ligand orbitals and cobalt $4p_z$ orbital, and causes the cobalt shift to the higher wavelength.[119] More recently, Brown and co-workers showed that the substitution of the H at C10 by Cl causes the bands in the electronic spectrum of L-10-chlorocobalamin (L = H_2O, Me or CN^-) derivatives to shift to lower energies, in line with an increase in the electron density in the corrin ring.[109] In addition the electronic transitions of cobalamin shift to lower energies as the donor power of the axial ligand L increases. All of these observations imply that the axial ligands and the corrin macrocycle are in the electronic communication. **Table 1.5** shows the position of the γ as a function of the β axial ligand.

Table 1.5 Effect of the β axial ligand nature on the γ band position in cobalamins.

Ligand	γ Band	Reference
H_2O	350	[120]
Benzimidazole	354	[120]
α-picoline	356	[120]
Azide	358	89
Imidazole	358	[120]
Pyridine	360	[120]
γ -picoline	361	[120]
β-picoline	361	[120]
Sulphite	364	89
Cysteine	370	89

References on page 37

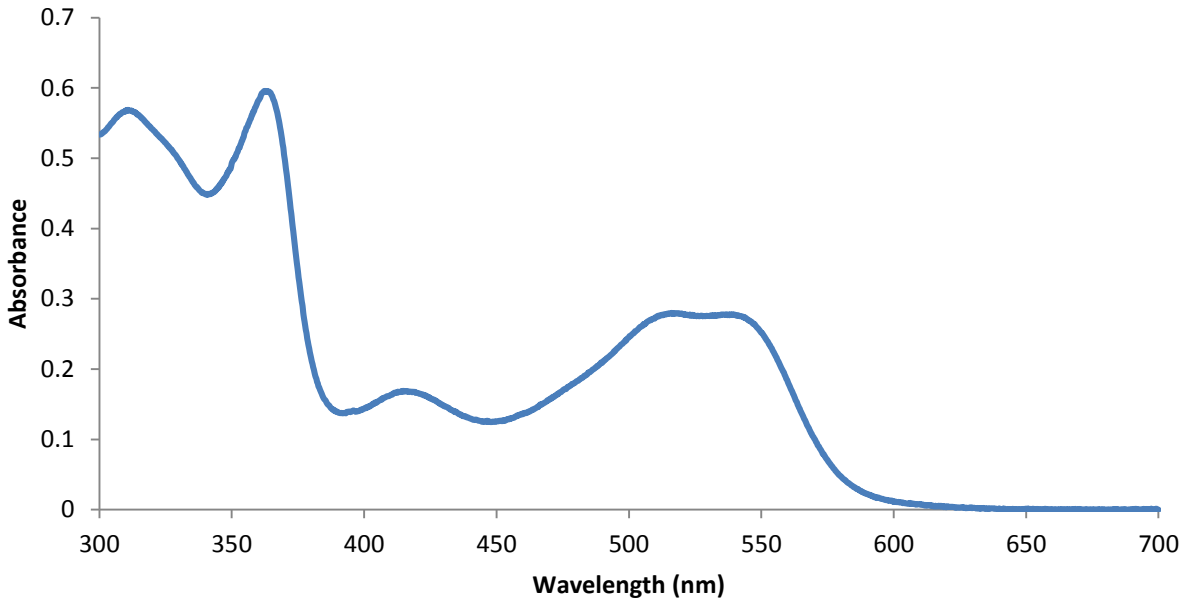


Figure 1.10 The "atypical" spectrum of [SO_3Cbl].

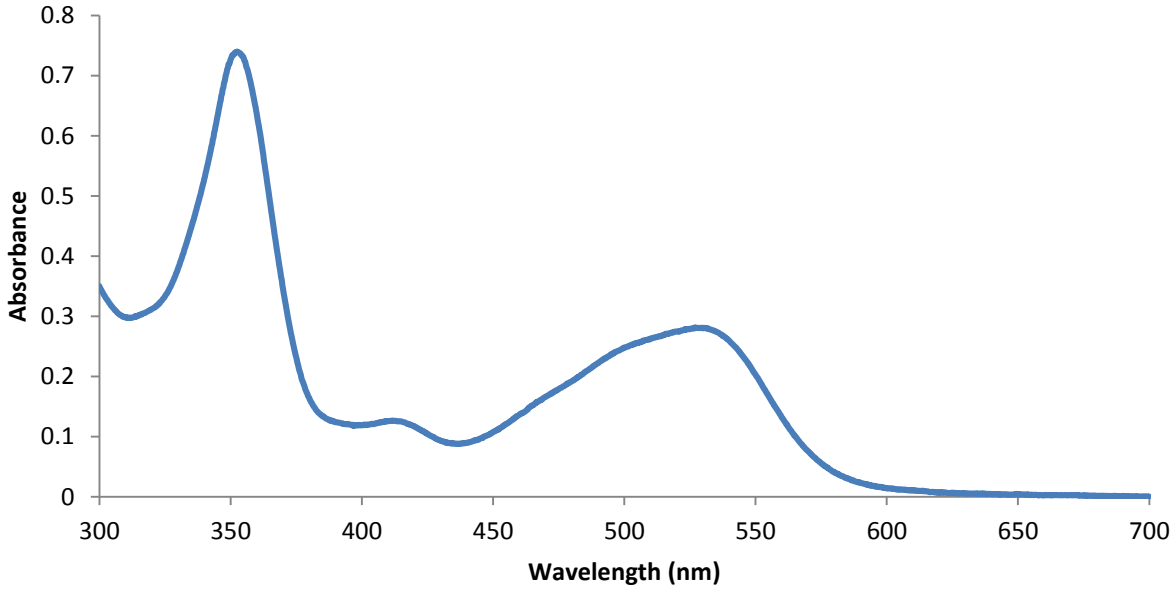


Figure 1.11 The "typical" spectrum of $[H_2OCbl]^+$.

References on page 37

1.7 Ligand Substitution Reactions

1.7.1 Stability Constants (log K)

$[H_2OCbl]^+$ and its derivatives undergo substitution of the axial ligand by a variety of incoming ligands (L), including neutral and anionic ligands. **Equation 1.1** symbolises a typical substitution reaction.

$$DMB–Co–H_2O + L \overset{K}{\rightleftharpoons} DMB–Co–L + H_2O \qquad (\mathbf{1.1})$$

To date many stability constants have been determined for vitamin B_{12} derivatives.[90,100,102,121-130] The determination of stability constants was initially used to study the *trans*-influence in cobalt corrinoid chemistry. Pratt[98] investigated the *trans*-influence in cobalamins by replacement of water axial ligand by various incoming ligands such as cyanide. He noticed that the stability constant decreased for cyanide ligand as the donor power of the incoming ligand increased and resulted in decrease of the Lewis acidity of the Co(III) ion.[98]

All studies to date deduced that the *trans*-influence of the ligand in the *α*-position and the nature of the incoming ligand play significant roles in determining the value of a stability constant.[89,98] For instance the bulkiness of the incoming ligand causes steric repulsion between the substituent and the corrin ring and results in a lower value of the stability constant.[123,131]

As the ligand in the *trans*-position becomes a stronger σ-donor the equilibrium constants decrease in value. The general order of the thermodynamic *trans*-influence is as follow:[89] H_2O, Cl^-, $CH_3CN < CN^- <$ organo-ligands, thiourea, NCS^-, HS^-, RS^-, $S_2O_3^{2-}$, I^-. This order is in good agreement with the order of the ligands in the nephelauxetic series.

Recent studies have been committed to the *cis*-influence of the corrin ring on equilibrium constant (log *K*). Knapton *et al*.[132] undertook a study on the ligand substitution reactions of aqua-10-chlorocobalamin, where the H of the C10 position is substituted by Cl, with neutral and anionic ligands to determine the *cis*-influence of the Cl substituent on the corrin ring toward ligand substitution. Their findings suggest that the Cl at the C10 position donates more electron density to the corrin ring and consequently increases the charge density on the Co atom; hence anionic ligands bind more strongly to cobalt in $[H_2O\text{-}(10\text{-}Cl)Cbl]^+$ compared to $[H_2OCbl]^+$ itself

References on page 37

and the converse is true for neutral ligands (further discussion of this can be found in **Chapter 3**). A similar study was performed by Knapton,[104] but this time the H of C10 position in $[H_2OCbl]^+$ was substituted by a NO group. The data showed that the NO group deactivates the cobalt atom toward any ligand binding reaction. Chemaly *et al.*[133] investigated the *cis*-influence of the corrin ring in a vitamin B_{12} derivative called stable yellow aquacyanocobyrinic acid heptamethyl ester ($[ACSYCbs]^+$), where oxidation at C5 leads to a less extensive conjugated system and results in a harder Co(III) character. The data for the ligand binding reactions of $[ACCbs]^+$ with anionic ligands revealed that the trend in log *K* for substitution of H_2O in $[ACCbs]^+$ parallels that in aquacyano-stable yellow cobester ($[ACSYCbs]^+$) as well as other corrins. In $[ACSYCbs]^+$, the log *K* values for substitution of H_2O *trans* to CN^- with CN^- and SO_3^{2-} are smaller compared to $[ACCbs]^+$, which implies that soft donor atom ligands bind more strongly to the softer Co(III) in $[ACCbs]^+$, and the converse is true for hard donor ligands (further details can be found in **Chapter 5**).

1.7.2 Reaction Kinetics

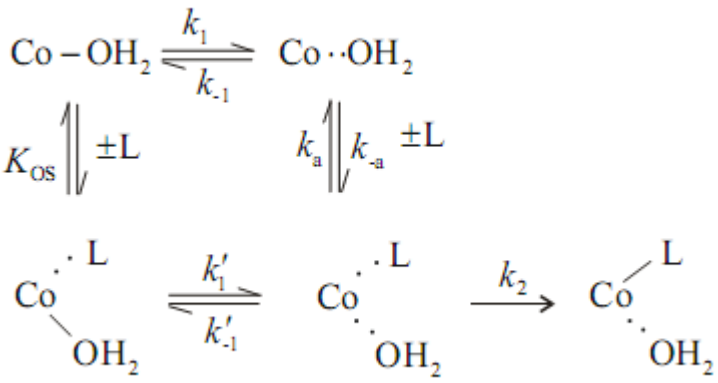
The study of reaction rate constants and activation parameters provide a good understanding of *cis*- and *trans*-effects of the cobalt corrinoids. It is essential to know what type of mechanism is involved in the ligand substitution reactions of vitamin B_{12} and its derivatives. In general three simple pathways can be recognized:

i) A dissociative path (D), where the leaving ligand is lost in the first step.
ii) An associative path (A), where the entering ligand adds first, forming an intermediate of increased coordination number.
iii) An interchange path (I), when the leaving ligand relocates from the inner to the outer coordination sphere as the incoming ligand relocates from the outer to the inner coordination sphere.[134]

There was some debate about the mechanism of the substitution reactions of the cobalamins. Several studies were performed to conclude that cobalamins undergo a dissociative mechanism.[135,136] Subsequently, Reenstra and Jencks carried out an extensive investigation on the reaction of cyanide with cobalamins and also considered the results others. Thusius[136] and

References on page 37

Poon;[137] argued that the rate and stability constants for a wide range of ligands vary over ranges of 10^2 and 10^{11} respectively. So they concluded that these results were consistent with a dissociative interchange mechanism. **Equation 1.2** describes their theory.



(1.2)

The above equation shows a D mechanism when the Co–OH_2 bond is broken and the product is formed on addition of the ligand (k_a) through the k_2 process. If the addition of water to the intermediate is slow compared with k_{-a}, a D mechanism is favoured over an I_d mechanism, but in order to be a second-order reaction this addition of water should occur rapidly relative to that of ligand. Since water is not particularly reactive towards metals, an I_d mechanism is more likely to occur.

Since 1988 Marques and co-workers have performed a series of studies on vitamin B_{12} with a wide range of ligands, to determine the mechanism by which the substitution reaction operates.[131,138-141] In their studies various ligands including imidazole and a number of its derivatives as well as histidine and histamine were used. The rate of substitution of water by these ligands was found to depend linearly on the base strength of the ligand. This finding suggested that for these ligands there is a nucleophilic participation of the incoming ligand in the transition state. Further studies were performed on SCN^-, $S_2O_3^{2-}$, NO_2^-, SO_3^{2-} and HSO_3^{2-} "which supports this theory".[139] The experimentally determined activation parameters for these ligands and the previously studied ligand CN^- indicated that significant differences exist between the activation parameters. The activation parameters for CN^- ($\Delta H^{\ddagger}$ = 51.7 kJ mol^{-1} and $\Delta S^{\ddagger}$= -25

References on page 37

J K^{-1} mol^{-1}) and SO_3^{2-} ($\Delta H^{\ddagger}$ = 79.9 kJ mol^{-1} and $\Delta S^{\ddagger}$= 33 J K^{-1} mol^{-1}) can be compared with $\Delta H^{\ddagger}$ = 63-67 kJ mol^{-1} and $\Delta S^{\ddagger}$ = 20-26 J K^{-1} mol^{-1} for $S_2O_3^{2-}$, NO_2^- and HSO_2^{3-}. The low $\Delta H^{\ddagger}$ and very negative $\Delta S^{\ddagger}$ for the reaction with CN^- might be due to the bond formation of Co and CN^- in the transition state compensating for the Co–O bond breaking.[139] The activation parameters for SO_3^{2-} can be related to its strong *trans*-labilising effect in cobalamins.[89,142] This suggests that the large $\Delta H^{\ddagger}$ value arises from a weakening of the Co–N bond of the axial benzimidazole group as the Co–SO_3^{2-} bond is formed in the transition state.[139]

Marques[143] also undertook a study on a series of primary amines and found that $\Delta H^{\ddagger}$ varies between 80 and 50 kJ mol^{-1} whereas $\Delta S^{\ddagger}$ varies between 50 and -50 J K^{-1} mol^{-1}. The rate of substitution of the amines also varied linearly with their donor power. All these findings provide evidence for axial ligand substitution in cobalamins proceeding via an I_d mechanism.

Conclusive evidence was provide when Stochel and Eldik[144] found that a plot of k_{obs} versus [pyridine] produced a saturation curve. Since this not observed for other ligands, the limiting rate constant cannot be the unimolecular loss of H_2O from Co(III); hence the reaction must proceed through an interchange mechanism.

Marques and co-workers[141] studied a range of ligands which exhibited saturation kinetics including hydroxylamine, methyl glycinate, pyridine, 4-methylpyridine, imidazole and histamine in order to determine which mechanism is in operation for the substitution of the aqua ligand in $[H_2OCbl]^+$ by the incoming ligand. The results showed that the saturating rate constants and the activation parameters ($\Delta H^{\ddagger}$ and $\Delta S^{\ddagger}$) values differ for each of the ligands. These findings confirmed that for these ligands an I_d mechanism is in operation since the activation parameters are dependent on the nature of L, whereas for a D mechanism the saturating rate constant corresponds to the unimolecular release of water from the molecule. Thus it is now well-established that the substitution reaction of $[H_2OCbl]^+$ with any incoming ligand involves an I_d mechanism.

Marques and Knapton[104] investigated the ligand substitution reactions of imidazole, N_3^- and $S_2O_3^{2-}$ with iodocobalamin ([ICbl]) in order to probe the mechanism when a bulkier ligand such

References on page 37

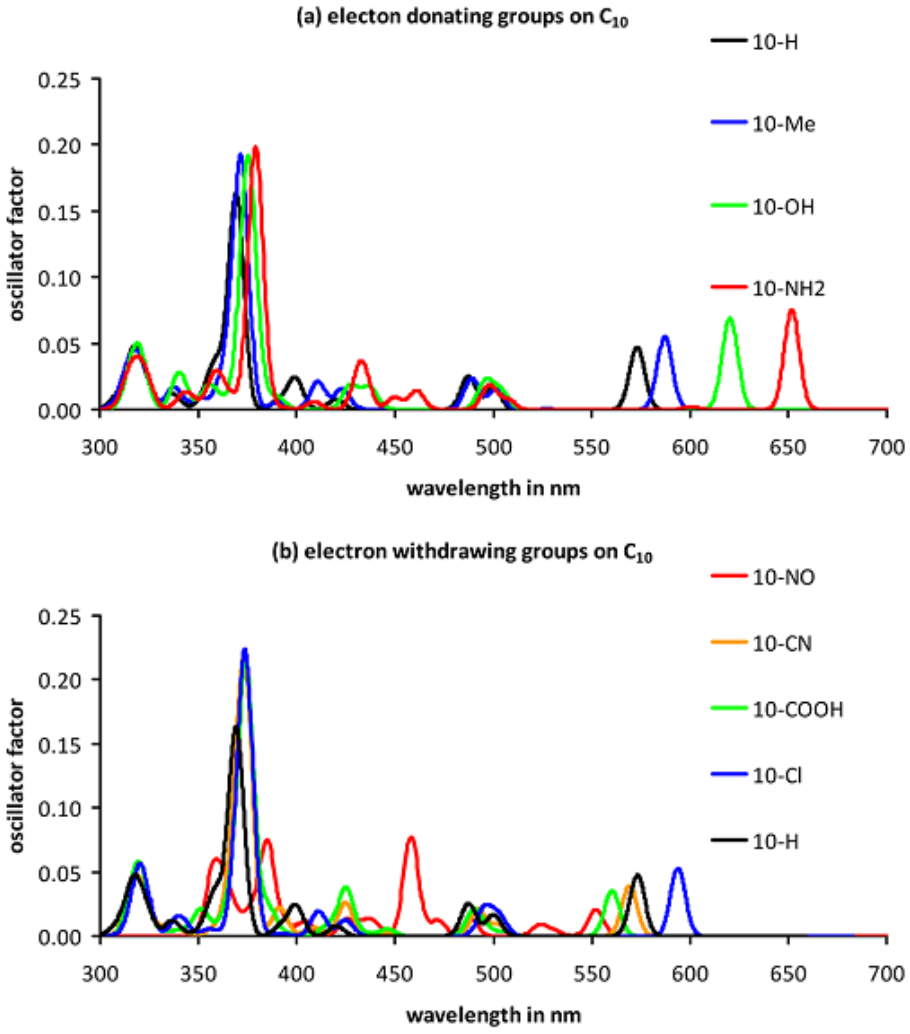
as I^- replaces the axial water ligand. Would the mechanism remain I_d or would the bulky ligand prevent the incoming ligand from forming an outer-sphere complex with the metal centre? The obtained results demonstrated that the ligand substitution reactions of [ICbl] also proceed through an interchange (I_d) mechanism with nucleophilic participation of the incoming ligand in the transition state. They also investigated the *cis*-effect of the corrin ring on the kinetic reactions $[H_2O\text{-}(10\text{-}Cl)Cbl]^+$.[132] The kinetics of the replacement of H_2O with two probe ligands, pyridine and N_3^- were investigated. The rate constants for reaction with pyridine showed saturation whereas those for substitution by N_3^- did not. These data suggested that the reaction proceeded through an interchange mechanism. They also obtained more positive values for the activation parameters for the reaction between these ligands and $[H_2OCbl]^+$, which implied that the transition state occurred earlier along the reaction coordinate in $[H_2O\text{-}(10\text{-}Cl)Cbl]^+$ and it also reacts more slowly with these probe ligands than $[H_2OCbl]^+$.

1.8 Density Functional Theory (DFT) Calculations

DFT is a useful technique which has been used for several decades to interpret the electronic properties of the cobalamins.[25,145] Recently, Perry and co-workers[146] studied the *cis*-influence of substitution at C10 of the corrin in a series of dicyanocobalt corrinoids using DFT and Time Dependent Density Functional Theory (TD-DFT) methods. The *cis*-influence on the uv-vis absorption spectra, the CN stretching frequencies of the axial ligands and the topological properties of the electron density, were studied. The electron-donating or electron-withdrawing ability of the C10 substituent was quantised by its Hammett parameters (σ_p) which affects the position of the prominent bands in uv-vis spectra of various derivatives (see **Figure 1.12**) and the ionicity of the Co–CN bond. The results suggested that as the withdrawing power of the C10 substituent decreases, the bond becomes stronger and more ionic, and as a consequence the CN^- stretching frequency increases. They also reported a further examination of the *cis*-influence of the corrin ring by examining the ground state structural and thermodynamic effects that altering the electron density of the equatorial corrin ring has on the bonds to the axial ligands (α and β positions). This study was performed by replacing H at C10 by a wide range of electron-donating and electron-withdrawing groups. The results showed that the position of the α band correlates with the Hammett constant (σ_p) of the C10 substituent; for example, as electron donation at C10 increases the spectrum shifts to longer wavelength (red-shifted) because the HOMO–LUMO gap

References on page 37

decreases; in addition the CN^- ligand becomes more constrained (there is an increase in the CN^- stretching frequency). Partial charges were also calculated on the complexes from the Quantum Theory of Atoms in Molecules (QTAIM) approach. The data suggested that as the electron donation from the substituent increase, the charge on C and Co becomes more positive whereas that on N atoms (equatorial ligands) becomes more negative; this implies that the ionic character of the NC–Co–CN system increases. More details are described in **Chapter 3**, **Section 3.4**.



References on page 37

Figure 1.12 Simulated electronic absorption spectra of C10-substituted corrins. (a) Calculated spectra for electron donating L groups ($\sigma_p < 0$). (b) Calculated spectra for electron withdrawing L groups ($\sigma_p > 0$).[146]

1.9 Aims of This Project

The main aim of this study was to further investigate the *cis*-labilising effect of the C10 substituent on the corrin ring. Previous studies in our research group have shown that perturbing the electronic structure of $[H_2OCbl]^+$ by substituting the C10-H by chloro, nitroso and amino groups influence the thermodynamics and kinetics of the ligand substitution reactions of the central Co(III) of the cobalt corrins.[108] However, a full investigation on $[H_2O\text{-}(10\text{-}NO)Cbl]^+$ and $[H_2O\text{-}(10\text{-}NH_2)Cbl]^+$ was not feasible because the former was deactivated toward ligand substitution and the latter was not stable in aqueous media. In pursuit of our goal, three different compounds were investigated: $[H_2O\text{-}(10\text{-}Br)Cbl]^+$, aquacyano-10-nitrocobester ($[AC\text{-}(10\text{-}NO_2)Cbs]^+$) and aquacyano-10-aminocobester ($[AC\text{-}(10\text{-}NH_2)Cbs]^+$) for specific reasons as mentioned below. This study was divided into two parts.

a) The first part of this study was dedicated to the modification of the C10 position of the corrin ring in $[H_2OCbl]^+$, and the H of the C10 position was replaced by Br. This study provided enough data to compare the results with a previous study performed by Knapton[108] on $[H_2OCbl]^+$ which was modified by three different groups at C10, $[H_2O\text{-}(10\text{-}Cl)Cbl]^+$, $[H_2O\text{-}(10\text{-}NO)Cbl]^+$ and $[H_2O\text{-}(10\text{-}NH_2)Cbl]^+$. In that study three different groups with different σ-donor power were chosen, ranging from strongly electron-donating $–NH_2$ to strongly electron-withdrawing NO in order to provide further insight into the *cis*-labilising effect of the corrin. In this study Br was chosen for two main reasons:

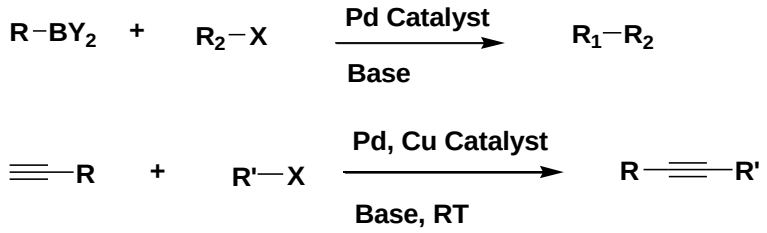
    i) Firstly, to confirm the trend observed by Knapton[108] on substituting the C10 H by Cl. It is well known that Br is more electronegative, softer and hence more polarisable than Cl. Hence, Br can be expected to act as a stronger σ-donor compared to Cl. This hypothesis was tested by comparing the thermodynamics and kinetics of the ligand substitution reactions of $[H_2O\text{-}(10\text{-}Cl)Cbl]^+$and $[H_2O\text{-}$

References on page 37

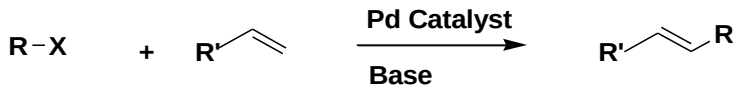
(10-Br)Cbl]$^+$ with [H_2OCbl]$^+$. Towards this end the following objectives were pursued:

- Synthesis of [H_2O-(10-Br)Cbl]$^+$, following a similar method as Wagner reported.[147]
- Purification of [H_2O-(10-Br)Cbl]$^+$ by reverse phase column chromatography.
- The characterisation of aqua-10-bromocobalamin using MS, uv-vis and NMR.
- Measurement of the acid dissociation constant (pK_a) of coordinated H_2O in order to correct stability and rate constants for the effect of pH.
- Measurement of the stability constants (log K) for the replacement of H_2O in [H_2O-(10-Br)Cbl]$^+$ with a variety of neutral ligands (imidazole, 4-N,N-dimethylaminopyridine and methylamine) and anionic ligands (N_3^-, NO_2^-, SO_3^{2-}, SCN^-), and comparison of the results with [H_2OCbl]$^+$ and [H_2O-(10-Cl)Cbl]$^+$ for the same ligands, in order to determine what effect the nature of C10 substituent has on the ligand binding properties of Co(III).
- Measurement of the kinetics of ligand substitution of H_2O in [H_2O-(10-Br)Cbl]$^+$ with N_3^- and imidazole for comparison with equivalent data for [H_2OCbl]$^+$.
- Interpretation of QTAIM and DFT calculations, which were performed by Govender and Perry, to rationalise the thermodynamic and kinetics findings.

ii) Br was chosen as the C10 substituent because it was envisaged that Br can be replaced by a wide range of alkyl groups by a cross-coupling reaction (Suzuki-Miyura, Sonogoshira, Heck), as illustrated below.



References on page 37



Exploring this, however, fell outside the scope of this project and forms the foundation for future work.

b) The second phase of this project was dedicated to the modification of the C10-H in [DCCbs] in which the C10-H has been substituted by NO_2 and NH_2 groups. Knapton[108] reported that $[H_2O\text{-}(10\text{-}NH_2)Cbl]^+$ was unstable in solution and further investigations were not feasible; thus, [DCCbs] was explored because it is structurally simpler and chemically more robust that cobalamin itself. A significant disadvantage of this compound is the presence of CN^- ligand at the α position which has a stronger *trans* effect than the nitrogenous base, DMB of cobalamin. The results therefore cannot be directly compared to those obtained with $[H_2OCbl]^+$ and a different reference compound is required; $[ACCbs]^+$ was chosen as the reference compound. The following was pursued for this part of the project,

- Synthesis of $[DC\text{-}(10\text{-}NO_2)Cbs]$ and $[DC\text{-}(10\text{-}NH_2)Cbs]$, as reported by Gryko and co-workers.[148]
- Purification of $[DC\text{-}(10\text{-}NO_2)Cbs]$ and $[DC\text{-}(10\text{-}NH_2)Cbs]$, using column chromatography.
- Characterisation of $[DC\text{-}(10\text{-}NO_2)Cbs]$ and $[DC\text{-}(10\text{-}NH_2)Cbs]$ using NMR, MS, and uv-vis spectroscopy.
- Conversion of $[DC\text{-}(10\text{-}NO_2)Cbs]$ and $[DC\text{-}(10\text{-}NH_2)Cbs]$ to $[AC\text{-}(10\text{-}NO_2)Cbs]^+$ and $[AC\text{-}(10\text{-}NH_2)Cbs]^+$ to provide a ligand, H_2O, that is readily replaced by exogenous ligands in order to study the ligand substitution reactions of these compounds.
- Measurement of the acid dissociation constant (pK_a) as function of temperature for $[AC\text{-}(10\text{-}NO_2)Cbs]^+$ and $[AC\text{-}(10\text{-}NH_2)Cbs]^+$, in order to enable correction for the effect of pH to be made on the stability and rate constants.

References on page 37

- Measurement of the stability constants (log *K*) for the replacement of H_2O in $[AC\text{-}(10\text{-}NO_2)Cbs]^+$ and $[AC\text{-}(10\text{-}NH_2)Cbs]^+$ with a range of neutral ligands (methylamine, imidazole, 4-N,N-dimethylaminopyridine) and anionic ligands (N_3^-, NO_2^-, SO_3^{2-}, SCN^-, CN^-) and compare the results with those available for $[ACCbs]^+$ (also re-measured in this study) in order to determine what effect the C10 substituent has on the ligand binding properties of Co(III).
- Measurement of the kinetics of ligand substitution of H_2O in $[AC\text{-}(10\text{-}NO_2)Cbs]^+$ and $[AC\text{-}(10\text{-}NH_2)Cbs]^+$ with CN^- ligand to compare with equivalent data for $[ACCbs]^+$.
- Interpretation of QTAIM and DFT calculations, which were performed by Govender and Perry, to rationalise our thermodynamic and kinetics findings.

1.10 Organisation of This Work

Methods, characterisations and materials are given in **Chapter 2**. Each chapter starts with an introduction containing brief reference to the relevant literature and the specific aims of the work. This is followed by a Results and Discussion section in which results of this study are presented and compared to the results of relevant studies. The last section is a concluding statement in which conclusions are made based on the reported findings. All references are listed at the end of each Chapter and numbering is relevant to that Chapter only. The last Chapter, **Chapter 7,** contains a summary of the general conclusions of this study and its contribution to ongoing research of the *cis*-labilising influence of the corrin ring on the chemistry of Co(III) in the cobalt corrins..

References on page 37

1.11 References

(1) Minot, G. R.; Murphy, W. P. *J. Am. Med. Assoc.* **1926**, *87*, 470.

(2) Mokuuada, K. *Gastroenterol. Hepatol.* **1999**, *14*, 301.

(3) Rickes, E. L.; Brink, N. G.; Koniiuszy, F. R.; Wood, T. R.; Folkers, K. *Science.* **1948**, *107*, 397.

(4) Brink, C.; Crowfoot, D. H.; June, L.; Pickworth, J.; Robertson, J.; White, J. *Nature.* **1954**, *174*, 1169.

(5) Hodgkin, D. C.; Porter, M. W.; Spiller, R. C. *Proc. Roy. Soc. Lond. B.* **1950**, *136*, 609.

(6) Alicino, J. F. *J. Am. Chem. Soc.* **1951**, *73*, 4051.

(7) Perry, C. B. PhD, University of the Witwatersrand, 2004.

(8) Beck, W. S.; Flavin, M.; Ochoa, S. *J. Biol. Chem.* **1957**, *229*, 997.

(9) Zhang, S. M.; Willet, W. C.; Selhub, J.; Hunter, D. J.; Giovannucci, E. L.; Holmes, M. D.; Colditz, G. A.; Hankinson, S. E. *JNCI.* **2003**, *95*, 373.

(10) Choi, S. W. *Nutr Rev.* **1999**, *57*, 250.

(11) Kolhouse, J. F.; Allen, R. H. *proc. Natl Acad. Sci. USA* **1977**, *74*, 921.

(12) Mellman, I. S.; Youngdahi-Turner, P.; Huntington, F. W.; Rosenberg, L. E. *Proc. Natl. Acad. Sci. USA* **1977**, *74*, 916.

(13) Lenhert, P. G. *Proc. Roy. Soc. Lond. A.* **1968**, *303*, 45.

(14) Lenhert, P. G.; Hodgkin, D. C. *Nature.* **1961**, 937.

(15) Rossi, M.; Glusker, J. P.; Randaccio, L.; Summers, M. F.; Toscano, P. J.; Marzilli, L. G. *J. Am. Chem. Soc.* **1985**, *107*, 1729.

(16) Drennan, C. L.; Huang, S.; Drummond, J. T.; Matthews, R. G.; Lidwig, M. L. *Science.* **1994**, *266*, 1669.

(17) Brown, K. L.; M.;, H. J. *J. Am. Chem. Soc.* **1984**, *106*, 7894.

(18) Guest, J. R.; Friedman, S.; Woods, D. D.; Smith, E. L. *Nature.* **1962**, *195*, 340.

(19) Mancia, F.; Keep, N. H.; Nakagawa, A.; Leadly, P. F.; McSweeney, S.; Rasmussen, B.; Bösecke, P.; Diat, O.; Evan, P. R. *Structure.* **1996**, *4*, 339.

(20) Gherasim, C.; Lofgren, M.; Banerjee, R. *J. Biol. Chem.* **2013**, *288*, 13186.

(21) Kräutler, B.; Kornat, R.; Stupperich, E.; Färber, G.; Gruber, K. *Inorg. Chem.* **1994**, *33*, 4128.

(22) Bouqquiere, J. P.; Finney, J. L.; Lehmann, M. S.; Lindley, P. F.; Savage, H. F. J. *Acta. Crystallogr.* **1993**, *B49*, 79.

(23) Pagano, T. G.; Marzilli, L. G.; Flocco, M. M.; Tsai, C.; Carrell, H. L.; Glusker, J. P. *J. Am. Chem. Soc.* **1991**, *113*, 531.

(24) Alcock, N. W.; Waters, M. *Proc. Indian Acad. Sci. (Chem. Sci.)* **1984**, *93*, 219.

(25) Zou, X.; Brown, K. L. *Inorg. Chim. Acta.* **1998**, *267*, 305.

(26) Wagner, F.; Afshar, C. E.; Carrell, H. L.; Glusker, J. P. *Inorg. Chem.* **1999**, *38*, 1785.

(27) Fasching, M.; Schmidt, W.; Kräutler, B.; Stupperich, E.; Schmidt, A.; Kratky, C. *J. Chim. Acta.* **2000**, *83*, 2295.

(28) Ludwig, M. L.; Drennan, C. L.; Matthews, R. G. *Structure.* **1996**, *4*, 505.

(29) Banerjee, R. *Chem. Biol.* **1999**, *4*, 175.

(30) Rossi, M.; Glusker, J. P. In *Molecular structure and energentics*; VCH: Weinheim, 1988.

(31) Brown, K. L.; Chang, C. K.; Marques, H. M. *Inorg. Chem.* **1995**, *34*, 3038.

(32) Brown, K. L.; Evans, D. R.; Cheng, S.; Jacobsen, W. D. *Inorg. Chem.* **1996**, *35*, 217.

(33) Perry, C. B.; Fernandes, M. A.; Brown, K. L.; Zou, X.; Valente, E. J.; Marques, H. M. *Eur. J. Inorg. Chem.* **2003**, 2095.

(34) Dölker, N.; Maseras, F.; Liedós, A. *J. Phys. chem. B.* **2003**, *107*, 306.
(35) Kraütler, B. *Biochem. Soc. Trans.* **2005**, *33*, 806-810.
(36) Jensen, K. P.; Ryde, U. *Chem. BioChem.* **2003**, *4*, 413.
(37) Geno, M. K.; Halpern, J. *J. Am. Chem. Soc.* **1987**, *109*, 1238.
(38) Halpern, J. *Science.* **1985**, *227*, 869.
(39) Toohey, J. I. *Proc. Nat. Acad. Sci.* **1965**, *54*, 934.
(40) Muller, P. M.; Farooq, S.; Hardegger, B.; Salmon, W. S.; Eschenmoser, A. *Angew. Chem. Int. Ed. Engl.* **1973**, *12*, 914.
(41) Schiebel, H. M.; Schulten, H. R. *Tetrahedron.* **1979**, *35*, 1191.
(42) Yamada, Y.; Miljkovic, E.; Wehrhrli, P.; Golding, B.; Loliger, P.; Keese, R.; Muller, K.; Eschenmoser, A. *Angew. Chem. Int. Ed. Engl.* **1969**, *8*, 343.
(43) Fischli, A.; Eschenmoser, A. *Angew. Chem. Int. Ed. Engl.* **1967**, *6*, 866.
(44) Bormann, D.; Fischli, A.; Keese, R.; Eschenmoser, A. *Angew. Chem. Int. Ed. Engl.* **1967**, *6*, 868.
(45) Mathura, S. PhD, University of the Witwatersrand, 2013.
(46) Smith, K. M. *In Porphyrins and Metallopophyrins*; Elserivier Publishing Co: Amsterdam, 1975.
(47) Huheey, J. E. *Inorganic Chemistry*; Harper and Row: New York, 1983.
(48) Munro, O. Q.; Marques, H. M.; Debrunner, P. G.; Mohanrao, K.; Scheidt, W. R. *J. Am. Chem. Soc.* **1995**, *117*, 935.
(49) Lavalle, D. K. *The chemistry and biochemistry of N-substituted porphyrins*; VCH Publishers, Inc.: New York, 1987.
(50) Dolphin, D.; Academic Press: New York, 1978.
(51) Lecomte, C.; Protas, J.; Marchon, J. C.; Nakajima, M. *Acta Crystallogr., Sect. B.* **1978**, *B34*, 2856.
(52) Guilard, R.; Latour, J.-M.; Lecomte, C.; Marchon, J. C.; Protas, J.; Ripoll, D. *Inorg. Chem.* **1978**, *17*, 1228.
(53) Berreau, L. M.; Young, V. G. J. W., L. K.; *Inorg. Chem.* **1995**, *34*, 527.
(54) Drew, M. G. B.; Mitchell, P. C. H.; Scott, C. E. *Inorg. Chim. Acta.* **1984**, *82*, 63.
(55) Molinaro, F. S.; Ibres, J. A. *Inorg. Chem.* **1976**, *15*, 2278.
(56) Petterson, R. C. *Acta Crystallogr., Sect. B.* **1969**, *B25*, 2527.
(57) Camenzind, M. J.; Hollander, F. J.; Hill, C. L. *Inorg. Chem.* **1982**, *21*, 4301.
(58) Kriner, J. F.; Reed, C. A.; Scheidt, W. R. *J. Am. Chem.* **1977**, *99*, 1093.
(59) Hill, C. L.; Williamson, M. M. *Inorg. Chem.* **1985**, *24*, 2836.
(60) Kriner, J. F.; Scheidt, W. R. *Inorg. Chem.* **1975**, *14*, 2081.
(61) Hoffman, A. B.; Collins, D. M.; Day, V. W.; Fleischer, E. B.; Srivastava, T. S.; Hoard, J. L. *J. Am. Chem.Soc.* **1972**, *94*, 3620.
(62) Scheidt, W. R.; Osvath, S. R.; Lee, Y. J. *J. Am. Chem.Soc.* **1987**, *109*, 1958.
(63) Scheidt, W. R.; Turowska-Tyrk, I. *J. Am. Chem. Soc.* **1994**, *106*, 5188.
(64) Scheidt, W. R. *J. Am. Chem. Soc.* **1974**, *96*, 84.
(65) Doppelt, P.; Fischer, J.; Weiss, R. *J. am. Chem. Soc.* **1984**, *106*, 5188.
(66) Kriner, J. F.; Garofalo, J.; Scheidt, W. R. *Inorg. Nucl. Chem. Letters.* **1975**, *11*, 107.
(67) Cullen, D. L.; Meyers, e. F. *J. Am. Chem. Soc.* **1974**, *96*, 2095.
(68) Meyers, E. F. *Acta. Crystallogr., Sect. B.* **1972**, *28*, 2162.
(69) De Angelis, S.; Solari, E.; Floriani, C.; Chiesi-Villa, A.; Rizzoli, C. *J. Am. Chem. Soc.* **1994**, *116*, 5691.
(70) Moustakali, I.; Tulinsky, A. *J. Am. Chem. Soc.* **1973**, *95*, 6811.

(71) Hatada, M. H.; Tulinsky, A.; Chang, C. K. *J. Am. Chem. Soc.* **1980**, *95*, 6811.
(72) Bag, N.; Chern, S. S.; Peng, S. M.; Chang, C. K. *Inorg. Chem.* **1995**, *34*, 753.
(73) Collins, D. M.; Hoard, J. L. *J. Am. Chem. Soc.* **1970**, *92*, 3761.
(74) Cullen, D. L.; Meyer, E. F. *Acta Crystallogr., Sect. B.* **1976**, *B32*, 2259.
(75) Mangani, S.; Meyer, E. F.; Cullen, D. L.; Tsutsui, M.; Carrano, C. J. *Inorg. Chem.* **1983**, *22*, 400.
(76) Battersby, A. R. *Nat. Prod. Rep.* **2000**, *17*, 507.
(77) Milgrom, L. R. *The colours of Life: An introduction to the chemistry of porphyrins and related compounds*; Oxford University Press: Oxford, 1997.
(78) Geno, M. K.; Halpern, J. *J. Am. Chem.* **1987**, *109*, 1238.
(79) Munro, O. Q.; Bradley, J. C.; Hancock, R. D.; Marques, H. M.; Marsicano, F.; Wade, P. W. *J. Am. Chem.* **1992**, *114*, 7218.
(80) Munro, O. Q.; Marques, H. M.; Debrunner, P. G.; Mohanrao, K.; Scheidt, W. R. *J. Am. Chem.* **1995**, *9*, 138.
(81) Eschenmoser, A. *Angew. Chem. Int. Ed. Engl.* **1988**, *27*, 5.
(82) Decker, K.; Jungermann, K.; Thauer, R. K. *Angew. Chem. Int. Ed. Engl.* **1970**, *9*, 138.
(83) Georgopapadakou, N. H.; Scott, A. I. *J. Theor. Biol.* **1977**, *69*, 381.
(84) Hodgkin, D. C.; Pickworth, J.; Robertson, J. H.; Prosen, R. J.; Sparks, R. A.; Trueblood, K. N.; Vos, A. *Proc. Roy. Soc. Lond. A.* **1959**, *251*, 306-352.
(85) Chernyaev, I. I. *Izvestiia Instituta po Izucheniiu Plotiny i Drugikh Blagorodnykh Metallov* **1926**, *1*, 243.
(86) Pratt, J. M.; Throp, R. G. *Advances in Inorganic Chemistry and Radiochemistry* **1969**, *12*, 375.
(87) Pratt, J. M.; Thorp, R. G. *J. Chem. Soc. A.* **1966**, 187.
(88) Hill, H. A. O.; Mann, B. E.; Pratt, J. M.; Thorp, R. G.; Williams, R. J. P. *J. Chem. Soc. A.* **1968**, 2419.
(89) Pratt, J. M. *The Inorganic Chemistry of Vitamin B_{12}*; Academic Press: London, 1972.
(90) Hayward, G. C.; Hill, H. A. O.; Vanston, N. J.; Pratt, J. M.; Williams, R. J. P. *J. Chem. Soc.* **1965**, 6485.
(91) Pratt, J. M. *in Chemistry and Biochemistry of B_{12}*; Wiley and Sons, Inc: New York, 1999.
(92) Pratt, J. M. In *Chemistry and Biochemistry of B12*; Banerjee, R., Ed.; Wiley and Sons, Inc: New York, 1999, p 73.
(93) Kratky, C.; Färber, G.; Gruber, K.; Wilson, K.; Dauter, Z.; Nolting, H.; Konrat, R.; Kräutler, B. *J. Am. Chem. Soc.* **1995**, *117*, 4654.
(94) Randaccio, L.; Geremia, S.; Stener, M.; Toffoli, D.; Zangrando, E. *Eur. J. Inorg. Chem.* **2002**, 93.
(95) Jensen, K. P.; Ryde, U. *J. Mol. Struct. (Theochem)* **2002**, *585*, 239.
(96) Kuta, J.; Wuerges, J.; Randaccio, L.; Kozlowski, P. M. *J. Phys. Chem. A.* **2009**, *113*, 11604.
(97) Perry, C. B.; Shin, N.; Fernandes, M. A.; Marques, H. M. *Dalton Trans.* **2013**, *42*, 7555.
(98) Pratt, J. M. *Chemistry and Biochemistry of B_{12}*; John Wiley & Sons, Inc: New York, 1999.
(99) Garau, G.; Geremia, S.; Marzilli, L. G.; Nardin, G.; Randaccio, L.; Tauzher, G. *Acta Crystallogr., Sect. B: Struct. Sci* **2003**, *59*, 51.
(100) Marques, H. M.; Bradley, J. C.; Brown, K. L.; Brooks, H. *J. Chem. Soc. Dalton Trans.* **1993**, 3475.
(101) Pasternack, R. F.; Gillies, B. S.; Stromsted, J. P. *Bioinorg. Chem.* **1978**, *8*, 33.
(102) Betterton, E. A. PhD, University of the Witwatersrand, 1982.
(103) Ashley, K. R.; Berggren, M.; Cheng, M. *J. Am. Chem. Soc.* **1975**, *97*, 1422.

(104) Marques, H. M.; Knapton, L.; Zou, X.; Brown, K. L. *J. Chem. Soc. Dalton Trans.* **2002**, 3195.
(105) Hague, D. N.; Halpern, H. *J. Inorg. Chem.* **1967**, *6*, 2059.
(106) Jackson, W. G.; Jurisson, S. S.; McGregor, B. C. *Inorg. Chem.* **1985**, *24*, 1788.
(107) Chemaly, S. M. *J. Inorg. Biochem.* **1991**, *44*, 1.
(108) Knapton, L. PhD, University of the Witwatersrand, 2005.
(109) Brown, K. L.; Cheng, S.; Zou, X.; Zubkowski, J. D.; Valente, E. J.; Knapton, L.; Marques, H. M. *Inorg. Chem.* **1997**, *36*, 3666.
(110) Ellis, B.; Petrow, V.; Snook, G. F. *J. Pharm. Pharmacol.* **1949**, *1*, 60.
(111) Day, P. *Theor. Chim. Acta.* **1967**, *7*, 328.
(112) Kuhn, H.; Drexhage, K. H.; Martin, H. *Proc. Roy. Soc. A.* **1965**, *288*, 348.
(113) Ochiai, E.; Long, K. M.; Sperati, C. R.; Busch, D. H. *J. Am. Chem. Soc.* **1969**, *91*, 3201.
(114) Ochiai, E. *Bioinorganic Chemistry An Introduction*; Ally and Bacon: Boston, 1977.
(115) Hill, H. A. O.; Pratt, J. M.; Williams, R. J. P. *Proc. Roy. Soc, Series A* **1965**, *288*, 352.
(116) Perry, C. B.; Marques, H. M. *S. Afr. J. Chem.* **2005**, *58*, 9.
(117) Stich, T. A.; Brooks, A. J.; Buan, N. R.; Brunold, T. C. *J. Am. Chem. Soc.* **2003**, *125*, 5897.
(118) Brown, K. L. *Chem. Rev.* **2005**, *105*, 2075.
(119) Schrauzer, G. N. *Naturwissenschaften* **1966**, *53*, 459.
(120) Hill, J. A.; Pratt, J. M.; Williams, R. J. P. *J. Theor. Biol.* **1962**, *3*, 423.
(121) Firth, R. A.; Hill, H. A. O.; Pratt, J. M.; Thorp, R. G.; Williams, R. J. P. *J. Chem. Soc. A.* **1969**, 381.
(122) Betterton, E. A.; Chemaly, S. M.; Pratt, J. M. *J. Chem. Soc. Dalton Trans.* **1985**, 1619.
(123) Baldwin, D. A.; Betterton, E. A.; Pratt, J. M. *J. Chem. Soc. Dalton Trans.* **1983**, 2217.
(124) Marques, H. M.; Marsh, J. H.; Mellor, J. R.; Munro, O. Q. *Inorg. Chim. Acta.* **1990**, *170*, 259.
(125) Hanania, G. I. H.; Irvine, D. H.; Irvine, M. V. *J. Chem. Soc. A* **1966**, 269.
(126) Baldwin, D. A.; Betterton, E. A.; Chemaly, S. M.; Pratt, J. M. *J. Chem. Soc. Dalton Trans.* **1983**, 225.
(127) Firth, R. A.; Hill, H. A. O.; Pratt, J. M.; Thorp, R. G.; Williams, R. J. P. *J. chem. Soc. A.* **1986**, 2428.
(128) Baldwin, D. A.; Betterton, E. A.; Chemaly, S. M.; pratt, J. M. *J. Chem. Soc. Dalton Trans.* **1985**, 1613.
(129) Hamza, M. S. A.; Pratt, J. M. *J. Chem. Soc. Dalton Trans.* **1996**, 3721.
(130) Chemaly, S. M.; Brown, K. L.; Fernandes, M. A.; Munro, O. Q.; Grimmer, C.; Marques, H. M. *Inorg. Chem.* **2011**, *50*, 8700.
(131) Marques, H. M.; Egan, T. J.; Marsh, J. H.; Mellor, J. R.; Munro, O. Q. *Inorg. Chim. Acta.* **1989**, *166*, 249.
(132) Knapton, L.; Marques, H. M. *Dalton Trans.* **2005**, 889.
(133) Chemaly, S. M.; Florczak, M.; Dirr, H.; Marques, H. M. *Inorg. Chem.* **2011**, *50*, 8719.
(134) Langford, C. H.; Gray, H. B. *Ligand substitution processes*; Benjamin, W. A. Inc.: New York, 1965.
(135) Basolo, F.; Pearson, R. G. *Mechanisms of Inorganic reactions*; Wiley: New York, 1958.
(136) Thusius, D. *J. Am. Chem. Soc.* **1971**, *93*, 2629.
(137) Poon, C. K. *Coord. Chem. Rev.* **1973**, *10*, 1.
(138) Marques, H. M.; Brown, K. L.; Jacobsen, W. *J. Biol. Chem.* **1988**, *263*, 12378.
(139) Marques, H. M. *J. Chem. Soc. Dalton Trans.* **1991**, 339.
(140) Marques, H. M.; Breet, E. L. J.; Prinsloo, F. F. *J. Chem. Soc. Dalton Trans.* **1991**, 2941.

(141) Marques, H. M.; Bradley, J. C.; Campbell, L. A. *J. Chem. Soc. Dalton Trans.* **1992**, 2019.

(142) Firth, R. A.; Pratt, J. M.; Hill, H. A. O.; Mann, B. E.; Throp, R. G.; Williams, R. J. P. *J. chem. Soc. A.* **1968**, 2419.

(143) Marques, H. M. *J. Chem. Soc. Dalton Trans.* **1991**, 1437.

(144) Stochel, G.; van Eldik, R. *Inorg. Chem.* **1990**, *29*, 2075.

(145) De Ridder, D. J. A.; Zangrando, E.; Bürgi, H. B. *J. Mol. Struct.* **1996**, *374*, 63.

(146) Navizet, I.; Perry, C. B.; Govender, P. P.; Marques, H. M. *J. Phys. Chem. B.* **2012**, *116*, 8836.

(147) Wagner, F.; Berhauer, K. *Ann. N. Y. Acad. Sci.* **1964**, *112*, 580.

(148) Proinsias, K. Ó.; Kurcoń, S.; Gryko, D. *Eur. J. Org. Chem.* **2012**, 154.

CHAPTER 2

Materials, Methods and Instrumentation

2.1 Reagents, Solvents and Buffers Used in This Project

Table 2.1 Summary of chemicals used in this study.

Chemical	**Supplier**
Reagents	
Hydroxocobalamin (vitamin B_{12a})	Roussel
Dicyano cobyrinic acid heptamethyl ester	Sigma-Aldrich
Fine chemicals, ligands	
Sodium hydrogen carbonate	Merck
Sodium sufite	Saarchem
Sodium sulfate	Merck
Sodium chloride	Merck
Sodium dihydrogen phosphate	Merck
Sodium nitrite	Saarchem
Sodium carbonate	Merck
Biological buffers	
3-(N-Morpholino)-propanesulfonic acid (MOPS)	Sigma-Aldrich
Cyclohexylaminoethanesulfonic acid (CHES)	Sigma-Aldrich
3-(N-Morpholino)-ethanesulfonic acid (MES)	Sigma-Aldrich
N-(cyclohexyl-3-amino)-propanesulfonic acid (CAPS)	Sigma-Aldrich
4-(2-Hydroxylrthyl)piperazine-1-ethanesulfonic acid (HEPES)	Sigma-Aldrich
Tris(hydroxylmethyl)-aminoethane (Tris)	Merck

References on page 75

Ligands	
Sodium azide	Riedel-de-Haën
Sodium cyanide	Merck
Sodium thiocyanate	Sigma-Aldrich
Methylamine hydrochloride	Sigma-Aldrich
3,5-Dimethylaminopyridine	Sigma-Aldrich
Solvents	
Acetonitrile	Sigma-Aldrich
Dichloromethane	Sigma-Aldrich
Deuterated chloroform	Sigma-Aldrich
Deuterated methanol	Sigma-Aldrich
Ethanol	Sigma-Aldrich
Ethanol	Sigma-Aldrich
Ethyl acetate	Merck
Hexane	Sigma-Aldrich
Methanol	Sigma-Aldrich
Acid and Bases	
Acetic acid (glacial)	N. T. Laboratory Supplies
Hydrochloric acid	Ace
Nitric acid	Ace
Phosphoric acid	Sigma-Aldrich
Sulfuric acid	Ace
Sodium hydroxide	Sigma-Aldrich
Gases	
Argon	Afrox

References on page 75

2.2 General Methods

2.2.1 pH Measurements

The pH of all solutions were measured using a Metrohm 780 pH meter with Metrohm LL UnitrodePt 1000 glass electrode. Standard Metrohm ready-to-use buffer solutions at pH 4 (potassium hydrogen phthalate), 7 (phosphate) and 9 (borate) were always used to calibrate the electrode using a 3 buffer calibration, 30 min prior to the experiment at a specific temperature in which the experiment was performed using a water circulating bath. This device is accurate enough to record the pH to 3 decimal places.

2.2.2 Buffers

The buffers used throughout this research are presented in **Table 2.2**. To adjust the pH of buffers, NaOH or H_2SO_4 was used. A multi-component buffer system was used for pK_a studies. Ionic strength was adjusted to 0.5 M with Na_2SO_4. A sample calculation can be found in **Appendix 2.1**.

Table 2.2 Summary of buffers used.

Buffer	Concentration/ M	pH range	pK_a/ 25 ^oC
MES	0.1	5.5-6.7	6.1
MOPS	0.1	6.5-7.9	7.2
HEPES	0.1	6.8-8.2	7.5
Tris/HCl	0.1	7.0-9.0	8.1
CHES	0.1	8.6-10.0	9.3
CAPS	0.1	9.7-11.1	10.4

References on page 75

2.2.2.1 Phosphate Buffer

A phosphate buffer (0.025 M, pH 3.0) was made by dissolving sodium dihydrogen phosphate (6.8045 g) in deionised water (2.0 L). The pH was adjusted with concentrated phosphoric acid.

2.2.3 Sep-Pak Cartridges

Sep-Pak reverse phase C18 cartridges were found useful to adsorb analytes from aqueous solutions. Sep-Pak cartridges are pre-packed plugs containing a silica-based bonded phase with strong hydrophobicity (C18 resin) used to adsorb analytes from aqueous solutions.

Initially, one cartridge-volume of a mobile phase (deionised water/acetonitrile (HPLC grade) (50%)) was passed through slowly. Secondly, the cartridge was washed with 10 cartridge-volume of deionised water. Thirdly, the sample was loaded using either a 1 mL syringe or a Pasteur pipette. Then the sample was washed with deionised water exhaustively. Finally, the sample was eluted using the mobile phase (50% acetonitrile in deionised water).

2.2.4 Column Chromatography

Column chromatography is a purification method for the separation of different components from a mixture of compounds. Firstly the compounds to be separated were dissolved in a mobile phase which carried the compound through a stationary phase comprised of silica packed in a column. As the individual components had different functional groups they had different affinities for the stationary phase resulting in varying retention times. Thus, individual components separated while eluting in ascending order of polarity as the most polar compound were adsorbed strongly to the polar silica particles. The compounds were collected in different fractions.

Compounds were dissolved in the minimum amount of a solvent (mobile phase) which was used in packing the column to carry the compounds through the stationary phase (normal silica). Nonpolar compounds bind less strongly than polar compounds on a polar adsorbent (silica) and dislodged more easily with nonpolar solvents. Therefore, the nonpolar compounds in a mixture elute first from the column. The more polar compounds were eluted with more polar solvents.

References on page 75

Eluted compounds were collected in fractions from the column and the purity was checked by HPLC.

2.2.5 Auto-column Chromatography

[L-(10-Z)Cbl] (L = H_2O, ethyl; Z= Br, Cl) was chromatographed on a 230 × 15 mm C18 column using a Büchi Sepacore chromatographic system consisting of two C-605 pump modules, a C-615 pump manager, a C-660 fraction collector, and a C-635 uv photometer.

All buffers were prepared freshly and filtered (0.45 μm filters) under vacuum before use. The acetonitrile used for the eluting solvent was HPLC grade.

The column was flushed with phosphate buffer/acetonitrile (60%) for 20 minutes and then with phosphate buffer for 1 hour at a flow rate of 3 ml min^{-1}. Samples were diluted with deionised water before being injected onto the column using a 10 mL syringe. A gradient of phosphate buffer (25 mM, pH 3) and CH_3CN from 0 to 40% CH_3CN at a flow rate of 3 ml min^{-1} was used to elute the product from the column.

2.2.6 Stopped-Flow Spectrophotometry

The kinetics of the substitution of H_2O by the probe ligand CN^- in aquacyanocobester ($[ACCbs]^+$), aquacyano-10-nitrocobester ($[AC\text{-}(10\text{-}NO_2)Cbs]^+$) and aquacyano-10-aminocobester ($[AC\text{-}(10\text{-}NH_2)Cbs]^+$) were determined by stopped-flow spectrophotometry. Data were collected on an Applied Photophysics stopped flow spectrophotometer with a 2 mm pathlength cell, using an ozone-free xenon ARC lamp and SpectraKinectic 05-109 monochromator set at a slit width of 2 nm. The temperature of the reaction cell was controlled using a LKB Bromma-Multitemp thermostated water circulator.

References on page 75

2.3 Characterisation Techniques

2.3.1 High Performance Liquid Chromatography (HPLC)

HPLC was used to assess the purity of the products. The HPLC system used consisted of a Dionex Ultimate 3000 pump and Ultimate photodiode array detector. Data analysis was performed using the onboard Chromeleon software package. A Supelco Discovery column (25 cm x 4.6 mm, 5 μm, C18 reverse phase) coupled to a guard column (4 x 3.0 mm; C18) was used for the separations.

All solutions were prepared freshly and filtered (0.45 μm filters) under vacuum before use. All solvents were HPLC grade.

The HPLC column was flushed with deionised water for 5 minutes, then with phosphate buffer/acetonitrile (98%) for 10 minutes (**Table 2.3)** or ethyl acetate/methanol (97%). A Hamilton gastight HPLC syringe was used to inject 20 mL of samples onto the column using a Rheodyne valve and a multi-step gradient **Table 2.3** or an isocratic elution system (ethyl acetate/methanol (97%)). The column was flushed with phosphate buffer/acetonitrile (80%) or ethyl acetate/methanol (97%) when it was necessary with the flow rate of 1 mL min^{-1}. At the completion of the run column was flushed with deionised water/acetonitrile (80%) for 30 minutes.

Table 2.3 Multi-step gradient elution programme.

Time/ min	%Phosphate buffer	%Acetonitrile
0.2	98	2
2	85	15
5	75	25
8	65	35
14.5	98	2
15	100	0

References on page 75

2.3.2 uv-vis Spectroscopy

Three different uv-vis spectrophotometers were used for different experiments throughout this project. Spectra during pK_a titrations were recorded on a Cary 300 Bio uv-vis spectrophotometer, spectra; during ligand binding experiments they were recorded on a Cary 100 uv-vis spectrophotometer. Spectra for kinetic studies of $[H_2O\text{-}(10\text{-}Br)Cbl]^+$ were recorded on Agilent uv-vis photodiode array spectrophotometer. Collections of data were facilitated by the scan application of the Cary WinUV software.[1] All samples were run against a background applicable to that experiment system (i.e. against appropriate buffer(s) and ionic strength adjustor). Full spectra were recorded between 300 and 700 nm, with a spectral band width of 2 nm, signal averaging time of 0.5 s, data interval of 1.00 nm and scan rate of 120.00 nm min^{-1}. These spectra were exported as comma-delimited text files so that they could be opened in Microsoft Excel spreadsheets, and analysed statistically using CurveFit or SigmaPlot.[2]

2.3.3 Electrospray Ionisation (ESI) Mass Spectroscopy

All compounds made in this study were characterised by ESI-MS. Low resolution mass spectra were recorded on a Waters Synapt G2 Mass spectrometer equipped with Acquity Binary Solvent Manager Software. The sample was prepared in acetonitrile/chloroform and exposed to an ESI source with a cone voltage of 15 V in both positive and negative mode. Data are reported as mass to charge ratios (m/z).

All data were collected at the Central Analytical Facilities, University of Stellenbosch, and analysed by the author. Mass spectra can be found in **Appendices 2.2**, **2.3 and 2.4**.

2.3.4 Nuclear Magnetic Resonance (NMR) Spectra

NMR was used to characterise all novel compounds synthesised, $[H_2O\text{-}(10\text{-}Br)Cbl]^+$ and dicyano-10-nitrocobester [DC(10-NO_2)Cbs]. One-dimensional ^1H, ^{13}C and DEPT135, two-dimensional proton homonuclear (COSY, TOCSY, NOESY and ROESY) and two-dimensional heteronuclear (^1H-^{13}C) experiments (HSQC and HMBC) NMR spectra were recorded on 15 mg samples dissolved in 700 µL of MeOD/$CDCl_3$ on a Brüker Avance III 500 spectrometer operating at 500.133 MHz (^1H) and 125.770 MHz (^{13}C) using a 5-mm PABBO broad band

References on page 75

probe. All NMR spectra were internally referenced to TMS. NMR spectra were processed using Brüker Topspin 3.0 (Avance III 500) and Topspin 2.1 (Avance III 300) software packages.

All NMR spectra were collected at University of the Witwatersrand and analysed by the author using MestReNova Software.[3] All NMR spectra can be found in **Appendices 2.5** and **2.6**.

2.3.5 X-ray Diffraction Crystallography

Intensity data from crystals of $[H_2O\text{-}(10\text{-}Br)Cbl]^+$ were collected at –100(2) °C on a Bruker X8 Proteum diffractometer equipped with a PLATINUM 135 CCD detector and Montel 200 optics, using Cu K_α radiation (45kV, 60mA) from a Microstar rotating-anode generator. The collection method involved ω-scans of width 0.5° and 1024 × 1024 bit data frames. Details of the crystallographic data are given in **Table 2.7.1, Appendix 2.7**.

For crystals of azido-10-bromocobalamin ($[N_3\text{-}(10\text{-}Br)Cbl]$) intensity data were collected at –100(2) ºC on a Bruker APEX II CCD area detector diffractometer with graphite monochromated Mo K_α radiation (50 kV, 30 mA). The collection method involved ω-scans of width 0.5° and 512 × 512 bit data frames. Data collection was carried out using the APEX 2[4] data collection software followed by data reduction using the program *SAINT+*[5] and multiscan absorption corrections using *SADABS*.[5] The crystal structures were solved by direct methods using *SHELXS-97*.[6] Non-hydrogen atoms were first refined isotropically followed by anisotropic refinement by full matrix least squares calculations based on F^2 using *SHELXL-97*.[6] Hydrogen atoms were first located in the difference map then positioned geometrically and allowed to ride on their respective parent atoms, with isotropic thermal parameters fixed at 1.2 (CH, CH_2 and NH_2) or 1.5 (CH_3 and OH) times those of their corresponding parent atoms. It was not possible to locate the hydrogen atoms on several of the water molecules. The contribution of these hydrogen atoms has, however, been accounted for in the chemical formula and related data such as crystal density and F(000). Figures were prepared using *ORTEP-3*.[7] The structure files for $[H_2O\text{-}(10\text{-}Br)Cbl]^+$ and $[N_3\text{-}(10\text{-}Br)Cbl]$ have been deposited at the Cambridge Structural Database (deposition numbers CCDC-1057492 and CCDC-1057493, respectively). A list of bond length and angles is given in **Table 2.7.2** for $[H_2O\text{-}(10\text{-}Br)Cbl]^+$ and **Table 2.7.3** for $[N_3\text{-}(10\text{-}Br)Cbl]$ in **Appendix 2.7**.

References on page 75

2.3.6 Molecular Modelling

Models of $[H_2O\text{-}(10\text{-}Z)Cbl]^+$, Z = H, Cl or Br, in which all substituents of the corrin ring were truncated to H and with imidazole as the α axial ligand, were explored using density functional theory (DFT) calculations. All calculations were performed with the Gaussian-09 program,[8] the GGA BP86 functional[9,10] and the TZVP basis set.[11,12] Both the density-fitting approximation[13,14] and the density-fitting TZVP basis[15,16] was used so as to minimize calculation time. To explore the topological properties of the electron density, wave function files were generated with Gaussian-09 and analysed using Bader's QTAIM[17] as implemented in AIMALL.[18]

Starting from the crystallographic coordinates of dicyanocobester ([DCCbs]),[19] models of $[L(CN)(10\text{-}Z)Cbs]^{n+}$, with the axial ligands L and CN^-, and C10 substituent Z, L = H_2O, imidazole, CN^- or NO_2^-, Z = H, NO_2 or NH_2, were constructed. All substituents of the corrin ring were truncated to H, and their structures were explored using density functional theory (DFT) calculations. These calculations were performed with the Gaussian-09 program,[8] the GGA BP86 functional[9,10] and the TZVP basis set.[11,12] Both the density-fitting approximation[13,14] and the density-fitting TZVP basis[15,16] was used so as to minimize calculation time. To explore the topological properties of the electron density, wave function files were generated with Gaussian-09 and analysed using Bader's Quantum Theory of Atoms in Molecules (QTAIM)[17] as implemented in AIMALL.[18]

All the DFT calculations were performed by Perry and Govender and the data were interpreted by the author.

2.4 Synthesis and Characterisation of the Modified C10 Cobalt Corrins

2.4.1 Synthesis and Characterisation of $[H_2O\text{-}(10\text{-}Br)Cbl]^+$

$[H_2O\text{-}(10\text{-}Br)Cbl]^+$ was synthesised with a few modifications to the procedure that was reported by Wagner in 1965.[20] Hydroxocobalamin ([OHCbl]) (100 mg, 0.07 mmol) was dissolved in 50 mL of 5% acetic acid/methanol in a round bottom flask and deaerated by Ar. 1.0 g of Zn granules were placed in a beaker half filled with 0.1 M HCl for 30 minutes; afterwards they were washed by deionised water and dried with acetone. Zinc granules were placed in a dry and clean flask through which a steady stream of Ar was passed. After 30 min the solution was cannula-

References on page 75

transferred into the flask containing the zinc metal at room temperature. The solution rapidly turned from red to brown to gray consistent with the reduction to Co(I). After reduction (20 min), ethyl bromide (7 mmol) was added and left to react for 30 min in the dark under an Ar atmosphere. The alkylation reaction was monitored by HPLC. After quantitative conversion of [OHCbl] into ethylcobalamin ([EtCbl]), the reaction mixture was cannula-transferred into a clean round bottom flask and rotary evaporated to dryness (50 ^{o}C) in the dark. After that crude [EtCbl] was dissolved in glacial acetic acid (20 mL) and deaerated by Ar. After 30 min n-bromo =succinamide (NBS, 0.08 mmol) was added and left for an hour in the dark under Ar. The bromination reaction was monitored by HLPC. The solution was cannula-transferred into a clean round bottom flask and rotary evaporated to dryness (50 ^{o}C). Conversion of ethyl-10-bromocobalamin ([Et-(10-Br)Cbl]) into $[H_2O\text{-}(10\text{-}Br)Cbl]^+$ was carried out in an acidic solution (HCl 0.1 M), that was exposed to ambient laboratory light for a few hours. The conversion process was monitored by HPLC. HPLC confirmed that the sample contained impurities. The product was then diluted with deionised water and neutralised with sodium hydrogen carbonate, then chromatographed on C18 phase silica using auto-column. Assessment of the purity of the products was done by HPLC. **Figure 2.1** shows a typical chromatogram of $[H_2O\text{-}(10\text{-}Br)Cbl]^+$. Purified samples were desalted before they were used using a Sep-Pak cartridge to remove the phosphate buffer salt from the sample.

References on page 75

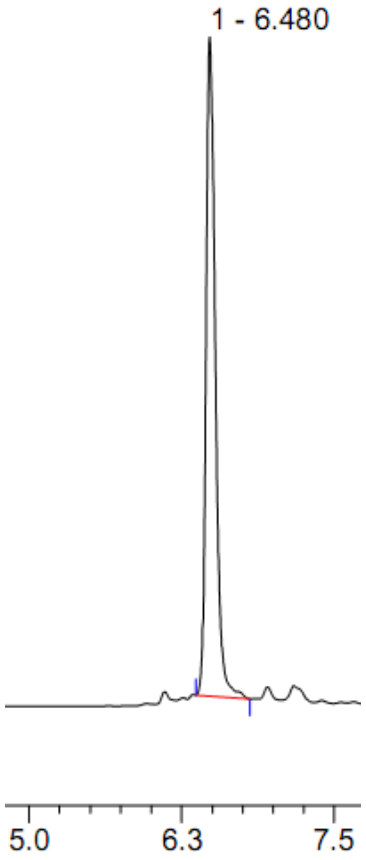


Figure 2.1 HPLC chromatogram of purified $[H_2O\text{-}(10\text{-}Br)Cbl]^+$ with retention time of 6.48 min using gradient elution programme, 75% phosphate buffer pH 3.0 and 25% acetonitrile.

2.4.1.1 uv-vis Spectroscopy of $[H_2O\text{-}(10\text{-}Br)Cbl]^+$

A uv-vis spectrum was recorded as it is shown in **Figure 2.2**. It shows that the principal uv-vis bands in $[H_2O\text{-}(10\text{-}Br)Cbl]^+$ occur at 555, 539 and 356 nm, respectively, which are consistent with the observations recorded by Wagner[20] and as observed for aqua-10-chlorocobalamin $[H_2O\text{-}(10\text{-}Cl)Cbl]^+$ (principal bands occurred at 558, 536 and 355 nm),[21] with very little change to the intensity of the absorbance.[21] The observed red-shifted of the bands in the spectrum (from 534, 504 and 353 nm) are similar to those reported for $[H_2O\text{-}(10\text{-}Br)Cbl]^+$[21] because both bromine and chlorine are resonance donating toward the corrin ring.

References on page 75

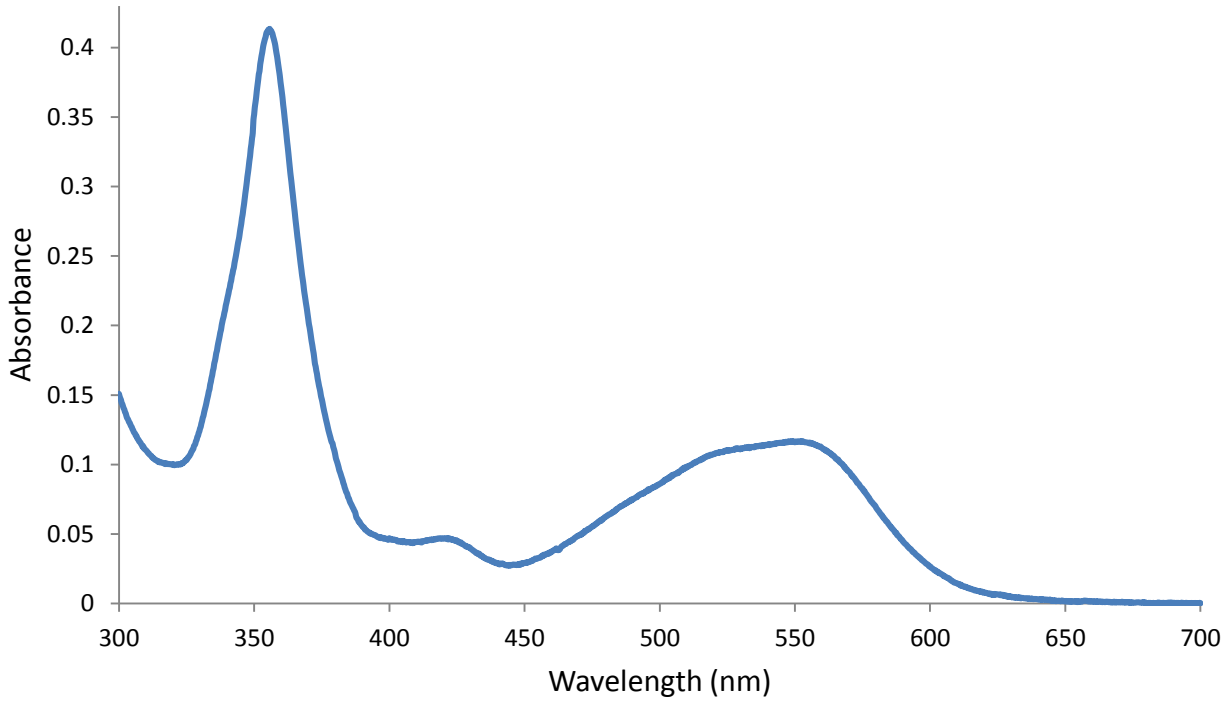


Figure 2.2 The uv-vis spectrum of $[H_2O\text{-}(10\text{-}Br)Cbl]^+$.

2.4.1.2 ESI-MS of $[H_2O\text{-}(10\text{-}Br)Cbl]^+$

ESI-MS was used in both positive and negative mode to confirm the molecular mass of $[H_2O\text{-}(10\text{-}Br)Cbl]^+$. The detected peaks at 715.73 (19.5%), 1408.48 (3.3%) and 1431.47 (1%) correspond to $(M–H_2O+Na)^{2+}$, $(M–H_2O)^+$ and $(M–H_2O+Na)^+$, respectively. These observations confirmed that $[H_2O\text{-}(10\text{-}Br)Cbl]^+$ was synthesised successfully. Full mass spectra of $[H_2O\text{-}(10\text{-}Br)Cbl]^+$ are presented in **Appendix 2.2**.

2.4.1.3 NMR Spectroscopy of $[H_2O\text{-}(10\text{-}Br)Cbl]^+$

The ^1H and ^{13}C NMR spectra of $[H_2O\text{-}(10\text{-}Br)Cbl]^+$ were assigned using the methodology developed by Brown.[22-26] The full assignments and NMR spectra are given in **Appendix 2.5**, and a brief account of the methodology used is given there as well. As expected, because of the substitution of the C10 H by Br, the ^{13}C resonance of C10 shifts downfield

References on page 75

$\Delta\left(\delta_{[H_2O\text{-}(10\text{-}Br)Cbl]^+} - \delta_{[H_2OCbl]^+}\right)$ = 10.49 ppm, as do those of C8, C12 and C47, while there are upfield shifts in the resonances of C9, C11 and C46. These changes are similar to those observed when substituting C10 H by Cl (**Appendix 2.5**).

2.4.2 Synthesis of $[H_2O\text{-}(10\text{-}Cl)Cbl]^+$

This was prepared as described elsewhere.[27]

2.4.3 Synthesis of Coα,Coβ-dicyano(10-nitro)cobyrinic Acid Heptamethyl Ester (dicyano-10-nitrocobester, [DC(10-NO_2)Cbs])

[DC(10-NO_2)Cbs] was prepared by the reaction of [DCCbs] with nitric acid essentially as described by Gryko *et al.*[28] with slight changes to their method; nitric acid 53% was used rather than 65% and the solvent system for purification was changed from 0.5-3.0% ethyl acetate in dichloromethane to 0.5-3.0% methanol in ethyl acetate.

[DCCbs] (20 mg, 0.01 mmol) was dissolved in acetonitrile (6 mL) and treated with nitric acid (10 mL, 53%). The mixture was stirred at ambient temperature in the dark for 1.5 h. The mixture was then diluted with dichloromethane (20 mL) and quenched by pouring into sodium hydrogen carbonate aq. (20 mL). The organic layer was separated and again was washed with sodium hydrogen carbonate aq. and sodium cyanide aq. (25 mL). The organic layer was then dried with sodium sulfate, filtered, and rotary evaporated to dryness (40 ^oC). The crude compound was purified on a normal silica gel column. Cyanide was added to the silica to sustain [DC-(10-NO_2)Cbs] species. A solvent system of 3% methanol in ethyl acetate was used to elute the product. The purity of the product was then checked by HPLC, using an isocratic elution programme of 3% methanol in ethyl acetate. A typical chromatogram of [DC-(10-NO_2)Cbs] is shown in **Figure 2.3**.

References on page 75

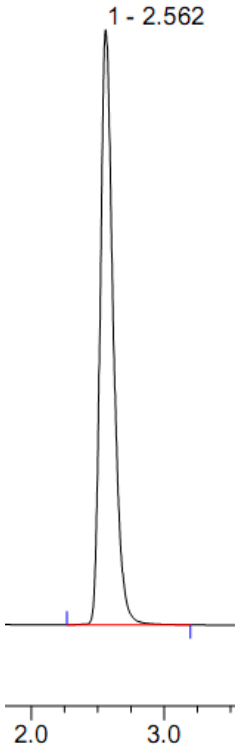


Figure 2.3 HPLC chromatogram of [DC-(10-NO_2)Cbs] with a retention time of 2.56 min using the isocratic elution programme, 3% methanol in ethyl acetate.

2.4.3.1 uv-vis Spectroscopy of [DC-(10-NO_2)Cbs]

The uv-vis spectrum of [DC-(10-NO_2)Cbs] has not been reported in the literature to best of our knowledge. The uv-vis spectrum of [DC-(10-NO_2)Cbs] was recorded in 50% isopropanol/water and, as expected, the principal bands were blue-shifted to 580, 545 and 362 nm, respectively (**Figure 2.4**), because the NO_2 substituent at C10 acts as an electron withdrawing group toward corrin ring and decrease the charge density on the corrin ring.

References on page 75

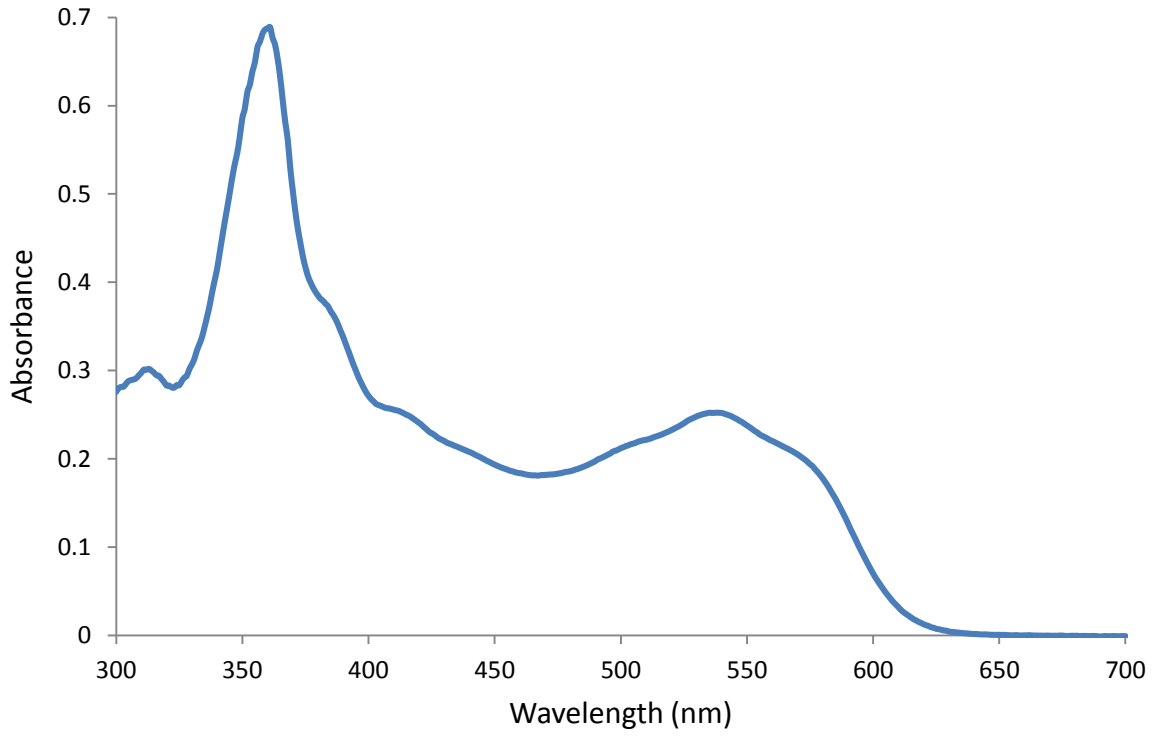


Figure 2.4 The uv-vis spectrum of [DC-(10-NO_2)Cbs].

2.4.3.2 ESI-MS of [DC-(10-NO_2)Cbs]

[DC-(10-NO_2)Cbs] was characterised by MS in both positive and negative mode. Detected signals at 1156.4 and 1107.4 were assigned to $(M + Na)^+$ and $(M - CN)^+$, respectively. This observation confirmed that [DC-(10-NO_2)Cbs] was synthesised successfully as the former value is the same value obtained by Gryko.[28] The [DC-(10-NO_2)Cbs] showed a peak at 1107.4 which is consistent with the loss of one axial cyanide ligand. The loss of one or two axial cyanide ligands has been observed in the mass spectra of many cobesters.[29,30] Selected mass spectra of [DC-(10-NO_2)Cbs] are presented in **Appendix 2.3.**

2.4.3.3 NMR Spectroscopy of [DC-(10-NO_2)Cbs]

The ^1H and ^{13}C NMR spectra of [DC-(10-NO_2)Cbs] in $CDCl_3$ were assigned using the reported assignments for [DCCbs].[31-35] Unfortunately, the C10 resonance was not assigned as H8 did not

References on page 75

show any coupling to C10 in the HMBC spectrum. DFT calculated chemical shifts predict that C10 should be somewhere around 124 ppm; if that is indeed the case then the ^{13}C resonance of C10 shifts downfield by 33 ppm.

Substitution of C10 H by NO_2 also led the C8, C9, C11, C47, C46 and C47 resonances shifted downfield, whereas the resonance of C12 is shifted upfield. The full assignments and NMR spectra are given in **Appendix 2.6.**

2.4.4 Conversion of [DC-(10-NO_2)Cbs] into [AC-(10-NO_2)Cbs]$^+$

Two methods have been investigated for the conversion of dicyano cobalt corrins to the aquacyano form, in which a water molecule replaces one of the axial cyanide groups. The first method was developed by Chemaly[29] for conversion of [DCCbs] to the aquacyano form. [ACCbs]$^+$ was prepared by dissolving [DCCbs] in methanol containing glacial acetic acid (pH 3.0) and left under a slow stream of N_2 for 24 h.[19,36] The conversion reaction was monitored by uv-vis as the colour changed from purple to red.

Another method was developed by Palet *et al.*[37] In this approach, the sample was dissolved in methanol in a round bottom flask and then acetic acid was added to the flask to achieve the 10% (v/v) acetic acid while stirring. Then the solvent was removed using a rotary evaporation. The residue was re-dissolved in the 10% methanol/acetic acid. This procedure was repeated for 4-6 times until the uv-vis spectrum no longer changed.

In this study the second approach was used. [DC-(10-NO_2)Cbs] was dissolved in methanol in a round bottom flask and then acetic acid was added to it to achieve 10% (v/v) acetic acid, then the solvent was removed using rotary evaporating (40 ^oC). Then the residue was re-dissolved in 10% methanol/acetic acid. This procedure was repeated at least for 3 times. As the conversion proceeded the γ band shifted from 363 to 350 nm, as the colour changed from red to orange. **Figure 2.5** shows the complete conversion of [DC-(10-NO_2)Cbs] to [AC-(10-NO_2)Cbs]$^+$. The purity of [AC-(10-NO_2)Cbs]$^+$ was checked by HPLC (**Figure 2.6**); a single peak with retention time of 2.60 min was found, using an isocratic programme (**Table 2.4**). ESI-MS was also employed to assess the product. The peak at m/z = 1107.5 was assigned to $(M - H_2O)^+$ which

References on page 75

confirmed that the conversion reaction was successful; the ESI-MS spectrum is shown in **Appendix 2.4.**

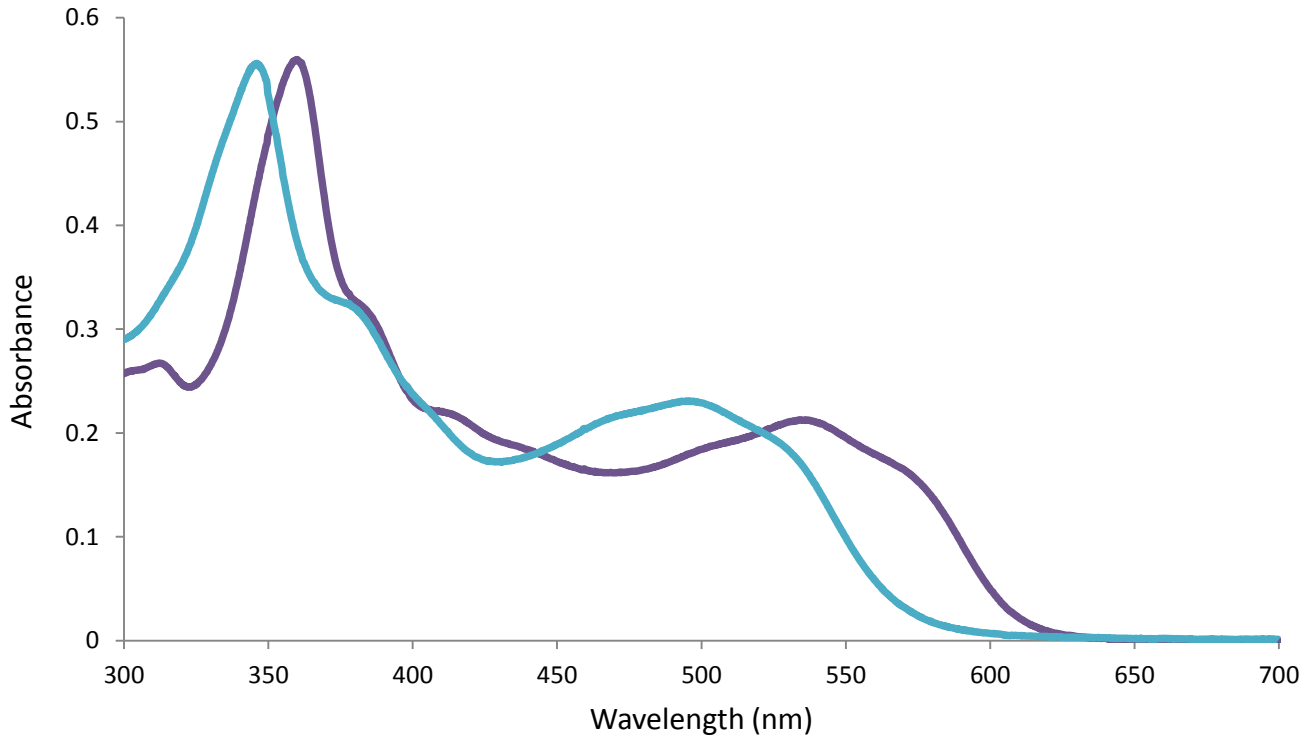


Figure 2.5 uv-vis spectra show the full conversion of [DC-(10-NO_2)Cbs] (purple) to [AC-(10-NO_2)Cbs]$^+$ (blue) in 50% isopropanol/water.

References on page 75

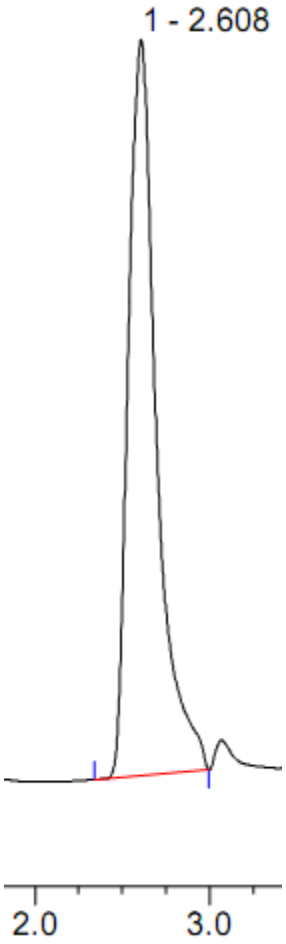


Figure 2.6 HPLC chromatogram of [AC-(10-NO_2)Cbs]$^+$ with retention time of 2.60 min using the isocratic elution programme, 3% methanol in acetic acid.

2.4.5 Synthesis of Coα,Coβ-dicyano(10-amino)cobyrinic Acid Heptamethyl Ester (dicyano-10-aminocobester, [DC-(10-NH_2)Cbs])

[DC-(10-NH_2)Cbs] was prepared by the reduction of [DC-(10-NO_2)Cbs] with sodium borohydride essentially as described by Gryko *et al.* [28] with a few modifications. [DC-(10-NO_2)Cbs] (250 mg, 0.22 mmol) was dissolved in methanol (13 mL) and stirred at -5 ^oC under Ar. Sodium borohydride (50 mg. 1.3 mmol) was added in three portions over a 1.5 h period. The reaction mixture was then quenched by pouring into sodium chloride aq. (50 mL), and the product was extracted by using dichloromethane (3 x 50 mL). The combined organic layers were

References on page 75

washed with 0.1 M sodium cyanide aq. (25 mL). The organic layer was then dried with sodium sulfate, filtered and rotary evaporated to dryness (40 ^{o}C). The crude compound was purified on a normal silica gel column with cyanide (5 mg). The eluting system was 3% methanol in ethyl acetate. Unfortunately [DC-(10-NH_2)Cbs] was unstable in solution, so to overcome this, it was immediately converted to [AC-(10-NH_2)Cbs]$^{+}$, using the same method as described in **Section 2.4.4.**

2.4.5.1 uv-vis Spectroscopy of [DC-(10-NH_2)Cbs]

The uv-vis spectrum of [DC-(10-NH_2)Cbs] has not been reported in the literature to the best of our knowledge. Its uv-vis spectrum was recorded in 50% isopropanol/water and, as expected, the principal bands were red-shifted to 600, 558 and 372 nm, respectively (**Figure 2.7**), because the NH_2 substituent at C10 acts as an electron donating group toward corrin ring and increases the charge density on the corrin ring.

2.4.5.2 ESI-MS of [DC-(10-NH_2)Cbs]

For reasons that are unclear, we were unable to obtain reliable MS data for this compound either in the positive or negative mode.

References on page 75

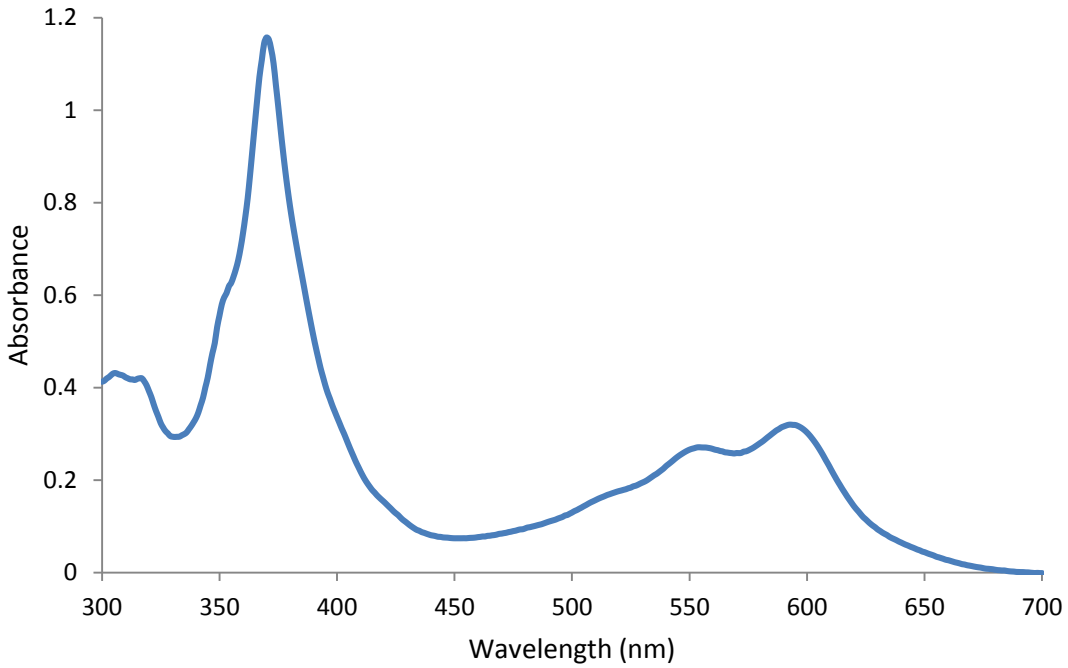


Figure 2.7 The uv-vis spectrum of [DC-(10-NH_2)Cbs].

2.4.5.3 NMR Spectroscopy of [DC-(10-NH_2)Cbs]

The NMR spectra for [DC-(10-NH_2)Cbs] were not recorded as it was unstable in $CDCl_3$.

2.4.6 Conversion of [DC-(10-NH_2)Cbs] to [AC-(10-NH_2)Cbs]$^+$

The same approach as described in **Section 2.4.4** was used for the conversion reaction. **Figure 2.8** shows the conversion of [DC-(10-NH_2)Cbs] to [AC-(10-NH_2)Cbs]$^+$ in 50% isopropanol/water. The γ band shifted from 372 to 362 nm, as the colour changed from blue to purple. Despite strenuous efforts, complete conversion to the aquacyano species could not be achieved (see small shoulder near 600 nm in the spectrum of the aquacyano species, **Figure 2.8**, indicative of the presence of ca. 10% dicyano species).

References on page 75

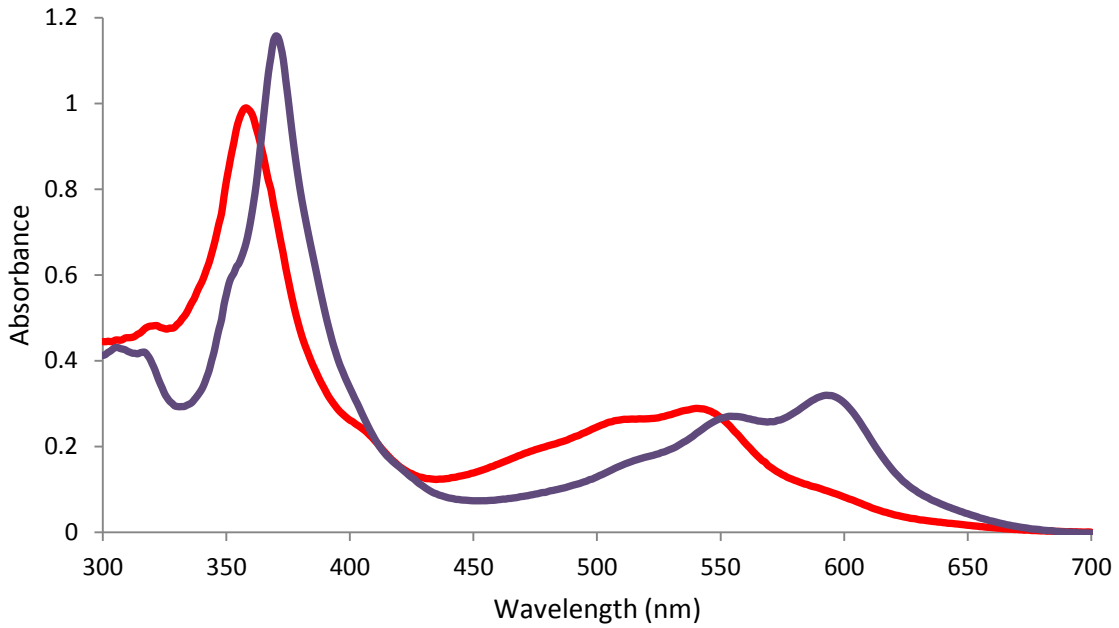


Figure 2.8 uv-vis spectra illustrate the full conversion of [DC-(10-NH_2)Cbs] (purple) to [AC-(10-NH_2)Cbs]$^+$ (red) in 50% isopropanol/water.

2.5 A Probe into the Solution Chemistry of C10-Modified Cobalt Corrinoids

2.5.1 Data analysis

All results were analysed with the computer programme SigmaPlot,[2] which employs the Marquardt's algorithm and a Newton-Raphson procedure.

2.5.2 Spectroscopic pK_a Investigations as a Function of pH

2.5.2.1 The effect of pH on the acid dissociation constant (pK_a) of [H_2O-(10-Br)Cbl]$^+$, [H_2OCbl]$^+$ and [H_2O-(10-Cl)Cbl]$^+$

pK_a values were determined for [H_2O-(10-Br)Cbl]$^+$, [H_2O-(10-Cl)Cbl]$^+$ and [H_2OCbl]$^+$, the last two compounds for comparison purposes. A sample of [H_2O-(10-Z)Cbl]$^+$ (Z= H, Br, Cl) was dissolved in a multi-component buffer (1 mM in each of 2-(*N*-morpholino)ethanesulfonic acid

References on page 75

(MES), (*N*-morpholino)propanesulfonic acid (MOPS), 4-(2-hydroxyethyl)-1-piperazineethanesulfonic acid (HEPES), *N*-cyclohexyl-2-aminoethanesulfonic acid (CHES), tris(hydoroxyethyl)aminomethane (TRIS) and *N*-cyclohexyl-3-aminopropanesulfonic acid (CAPS), μ = 0.5 M, Na_2SO_4) in a 50 mL thermostatted cell (25.0 ± 0.1 °C). A small magnetic stirrer bar was placed into the cell which was then placed on a stirring mantle to maintain a constant stirring and provide a homogeneous solution. The pH of the solution was changed from 5 to 12 in 0.5 unit increases by adding negligible volumes of concentrated NaOH solution with a drawn-out capillary tube. A peristaltic pump (Watson Marlow 101 U) was used to transfer the solution from the glass cell into a flow cell (Hellma) housed within a cell block of a Cary 300 Bio uv-vis spectrophotometer, where a full spectrum was recorded before returning of the sample to the glass cell.

The absorbance changes as a function of pH were analysed at multiple wavelengths. The experimental data were fitted using a non-linear least squares methods employing Newton-Raphson procedure to an ionisation isotherm (**Equation 2.1**), which is relevant when one acid-base equilibrium is present.[27]

$$A_\lambda = \left(\frac{A_0 10^{-pH} + A_1 10^{-pK_a}}{10^{-pH} + 10^{-pK_a}} \right) \qquad \textbf{(2.1)}$$

A is the absorbance at the monitoring wavelength, K_a is the acid dissociation constant, A_0 the initial absorbance and A_1 is the final absorbance. This equation was applied for each temperature at which the data were collected. Then pK_a was determined from a weighted average of the results, weighted by the reciprocal of the relative percentage error, where the error is the standard error of the fits.

2.5.2.2 Effect of pH on the Acid Dissociation Constant (pK_a) of [AC-(10-NO_2)Cbs]$^+$, [AC-(10-NH_2)Cbs]$^+$ and [ACCbs]$^+$

The acid dissociation constant (pK_a) of coordinated H_2O in [ACCbs]$^+$, [AC-(10-NO_2)Cbs]$^+$ and [AC-(10-NH_2)Cbs]$^+$ was determined using uv-vis spectroscopy. The compound in question was dissolved in a multi-component buffer,[38] (total 1 mM buffer made up of equal quantities of 2-(*N*-

morpholino)ethanesulfonic acid (MES), (*N*-morpholino)propanesulfonic acid (MOPS), tris(hydoroxyethyl)aminomethane (TRIS), *N*-cyclohexyl-2-aminoethanesulfonic acid (CHES) and *N*-cyclohexyl-3-aminopropanesulfonic acid (CAPS), 50% isopropanol) in a 50 mL thermostatted cell (25.0 ± 0.1 °C). The pH of the sample was adjusted by diffusing negligible volumes of 8 M NaOH with a drawn-out capillary tube. The sample was circulated through a 1 cm flow cell (Hellma) housed in the compartment of a Cary 300 Bio uv-vis spectrophotometer using a Watson-Marlow 101U peristaltic pump. The spectrum was recorded at intervals of approximately 0.5 pH units between pH 6 and 12. The changes in the absorbance spectrum as a function of pH, monitored at 3 or 4 wavelengths. The dependence of the absorbance spectrum on pH between pH 8 and pH 1 was also investigated for $[AC\text{-}(10\text{-}NO_2)Cbs]^+$ and $[AC\text{-}(10\text{-}NH_2)Cbs]^+$, in 1 mM potassium hydrogen phthalate (KHP), MES and MOPS in 50% isopropanol, by adjusting the pH with negligible volumes of solutions of appropriate concentration of H_2SO_4. The experimental data were fitted to an equation appropriate for one or two pK_as (**Equation 2.1** or **Equation 2.2**) as objective function, where A_λ is the absorbance measurement at the monitored wavelength and A_0, A_1 and A_2 and K_{a1} and K_{a2} are variables.

$$A_\lambda = \left(\frac{A_0 \left(10^{-pH}\right)^2 + A_1 10^{-pK_{a1}} 10^{-pH} + A_2 10^{-pK_{a1}} 10^{-pK_{a2}}}{\left(10^{-pH}\right)^2 + 10^{-pH} 10^{-pK_{a1}} + 10^{-pK_{a1}} 10^{-pK_{a2}}} \right) \quad \textbf{(2.2)}$$

2.5.3 Stability Constants (log K)

2.5.3.1 Stability Constants (log K) for Substitution of H_2O by Exogenous Ligands in $[H_2O\text{-}(10\text{-}Br)Cbl]^+$, $[H_2O\text{-}(10\text{-}Cl)Cbl]^+$ and $[H_2OCbl]^+$

The stability constants (log *K*) were determined spectrophotometrically as a function of pH for the substitution of the axially coordinated H_2O in $[H_2O\text{-}(10\text{-}Br)Cbl]^+$, $[H_2O\text{-}(10\text{-}Cl)Cbl]^+$ and

References on page 75

$[H_2OCbl]^+$ by a wide range of anionic ligands (N_3^-, NO_2^-, SCN^-, SO_3^{2-}) and neutral ligands (imidazole, DMAP), **Equation 1.1**.

$$DMB–Co–H_2O + L \overset{K}{\rightleftharpoons} DMB–Co–L + H_2O \qquad (\mathbf{1.1})$$

Ligand binding titrations were performed by the addition of aliquots of stock solution of the target ligand to a 20-50 μM solution of the Co(III) corrin solution in a 1 cm quartz cuvette housed in the thermostatted cell block of a Cary 100 uv-vis spectrophotometer. The temperature of the cell block was maintained at 25 ºC by a water circulating bath. Typically between 10 and 15 aliquot additions were made in each titration and absorbance readings were corrected for dilution.

The solutions were buffered at the appropriate pH which depends on the pK_a of the ligand (the ligand needs to be deprotonated) for the maximum complex formation. Hence, the samples were buffered with MES (for titrations performed at pH 6 with N_3^- and NO_2^-), MOPS (for titrations performed at pH 7.0 with SCN^-, SO_3^{2-}, imidazole), or CHES (for titration performed at pH 8.5 with DMAP). The ionic strength of 0.5 M was maintained for all titrations using Na_2SO_4. The stock ligand solution was prepared by dissolving the required amount of ligand in the appropriate buffer, and the pH was adjusted to the required pH by addition of NaOH or H_2SO_4. All log *K* values were determined at 25 ºC.

The log *K* was determined at a number of wavelengths where a considerable change in absorbance can be observed and away from the isosbestic points.

In cases where log *K* is relatively small (log $K < 4$), the absorbance data at wavelength λ were fitted using non-linear least squares methods to a simple binding isotherm (**Equation 2.3**) as objective function, with A_0, A_1 and *K* as the parameters to be optimized. A_0 and A_1 are the absorbance values at λ corresponding to 0 and 100% complex formation, respectively. The derivation of **Equation 2.3** can be found in **Appendix 2.7**.

$$A_\lambda = (A_0 + K A_1[L])/(1 + K[L]) \qquad (\mathbf{2.3})$$

References on page 75

When log *K* is relatively large (> 4), the implicit assumption in **Equation 2.3** that $[L]_{free} \approx [L]_{total}$ is not true because a significant fraction of the added ligand will be complexed to the metal ion. In this case [L] in **Equation 2.3** has to be replaced by an explicit expression for $[L]_{free}$. It can be shown[39] that $[L]_{free}$ is given by **Equation 2.4**, where only one root has physical meaning. In **Equation 2.4** $[M]_{total}$ is the total metal ion concentration.

$$[L]_{free} = \frac{-a_2 \pm \sqrt{a_2^2 - 4a_1a_3}}{2a_1}$$

$$a_1 = K;\ a_2 = 1 + K[M]_{total} - K[L]_{neutral};\ a_3 = -[L]_{neutral} \qquad \textbf{(2.4)}$$

It is well-established in cobalt corrin chemistry that hydroxide in [OHCbl] will not be displaced by an exogenous ligand X.[40-42] Moreover, it is usually the case that the protonated form of a ligand (e.g. imidazole) will not coordinate to a metal ion. Conditional stability constants, K_{obs}, determined at some pH values were therefore converted to pH-independent stability constants, *K*, using **Equation 2.5**, where pK_{aL} refers to the acid dissociation constant of the conjugate acid of the ligand L and pK_{aM}, to the acid dissociation constant of coordinated H_2O in $[H_2O\text{-}(10\text{-}Br)Cbl]^+$, $[H_2O\text{-}(10\text{-}Cl)Cbl]^+$ and $[H_2OCbl]^+$. The derivation of **Equation 2.5** can be found in **Appendix 2.8**.

$$K = K_{obs}\left(1+10^{pK_{aL}-pH}\right)\left(1+10^{pH-pK_{Co}}\right) \qquad \textbf{(2.5)}$$

2.5.3.2 Stability Constants (log K) for Substitution of H_2O by Exogenous Ligands in $[AC\text{-}(10\text{-}NO_2)Cbs]^+$, $[AC\text{-}(10\text{-}NH_2)Cbs]^+$, and $[ACCbs]^+$

References on page 75

The stability constants (log *K*) were determined spectrophotometrically as a function of pH for the substitution of the axially coordinated H_2O in $[AC\text{-}(10\text{-}NO_2)Cbl]^+$, $[AC\text{-}(10\text{-}NH_2)Cbl]^+$, and $[ACCbl]^+$ in a mixture of 50% isopropanol/water, by a range of anionic ligands (N_3^-, NO_2^-, SCN^-, SO_3^{2-}, CN^-) and neutral ligands (imidazole, methylamine, DMAP), **Equation 2.6**.

$$[CN\text{–}Co^{III}\text{–}H_2O]^+ + L^{n-} \overset{K}{\rightleftharpoons} [CN\text{–}Co^{III}\text{–}L]^{(1-n)} + H_2O \qquad (\mathbf{2.6})$$

The ligand binding titration was performed by the addition of aliquots of stock solution of the target ligand to a cobalt corrin solution in a 1 cm quartz cuvette housed in the thermostatted cell block of a Cary 100 uv-vis spectrophotometer. The temperature of the cell block was maintained at 25 ^oC by a water circulating bath. Typically between 10 and 15 aliquot additions were made in each titration and absorbance readings were corrected for dilution.

The solutions were buffered at the appropriate pH which depends on the pK_a of the ligand for the maximum complex formation. Hence, the samples were buffered with 0.1 M MOPS (for titrations performed at pH 7.0 with SCN^-, NO_2^-, N_3^- and imidazole), CHES (for titrations performed at pH 9.5 with DMAP and pH 9.0 with SO_3^{2-}), and CAPS (for titration performed at pH 10.0 with CN^-). Due to the solvent system the ionic strength was not adjusted. Stability constants for binding of CN^-[33] and SO_3^{2-} were large; therefore the values were determined in a competition experiment in the presence of 0.05 M N_3^-. Under this condition, there is > 99% formation of the azidocyano complex. Form this equation $K_{cyanide/sulfite} = K_{obs}K_{azide}$, *K* for binding of CN^-/SO_3^{2-} was determined, where the K_{obs} is the observed stability constant for binding of CN^-/SO_3^{2-} in the presence of excess N_3^-. Then the value was corrected for pK_a of HCN/H_2SO_3.[43]

The stock ligand solution was prepared by dissolving the required amount of ligand in the appropriate buffer in 50:50 isopropanol/water mixture, and the pH was adjusted to the required pH by addition of NaOH or H_2SO_4. All log *K* values were determined at 25 ^oC.

By analogy with $[ACCbl]^+$ and aquacyano-stable yellow cobester ($[ACSYCbs]^+$) both $[AC\text{-}(10\text{-}NO_2)Cbl]^+$ and $[AC\text{-}(10\text{-}NH_2)Cbl]^+$ exist as an equilibrium of two diastereomers in solution[33,44-48] *viz*. α-cyano, β-aqua and α-aqua, β-cyano. These two diastereomers are expected to have similar, but not identical, equilibrium constants. In such circumstances, a spectrophotometric

References on page 75

determination of log *K* shows a wavelength dependence, which is related to the relative extinction coefficients of the two diastereomers at the monitoring wavelength.[49]

Values of log *K* were determined for $[ACCbl]^+$, $[AC\text{-}(10\text{-}NO_2)Cbl]^+$ and $[AC\text{-}(10\text{-}NH_2)Cbl]^+$ following the same method of calculations as described in **Section 2.5.3.1**.

2.5.4 Kinetic Investigations of Ligand Substitution Reactions

2.5.4.1 Kinetic Investigations of Ligand Substitution Reactions of $[H_2O\text{-}(10\text{-}Br)Cbl]^+$

The kinetics of ligand substitution reactions for $[H_2O\text{-}(10\text{-}Br)Cbl]^+$ with N_3^- and imidazole were studied. **Equation 2.7** describes the reaction.

$$[DMB\text{–}Co\text{–}H_2O] + L \xrightarrow{k_{II}} [DMB\text{–}Co\text{–}L] + H_2O \qquad (\mathbf{2.7})$$

In this equation, L is an incoming ligand, which substitutes an axially coordinated water ligand. k_{II} is the second-order rate constant which was determined spectrophotometrically under pseudo first-order conditions.

The pseudo first-order rate constants, k_I^{obs}, were found by fitting the absorbance-time trace to **Equation 2.8** as objective function with A_1, A_2 and k_I^{obs} as variables using standard non-linear least squares methods. Since hydroxo-10-bromocobalamin ([OH-(10-Br)Cbl]) and [OHCbl] are inert to substitution,[42,50] values of k_1^{obs} were converted into a pH-independent value, *k*, using **Equation 2.9**,

$$A_\lambda = A_1 \exp(-k_1^{obs}\, t) + A_2 \qquad (\mathbf{2.8})$$

$$k = k_{obs}\,(1 + 10^{pH - pKCo}) \qquad (\mathbf{2.9})$$

References on page 75

where K_{Co} is the temperature-dependent acid dissociation constant for coordination of H_2O in $[H_2O\text{-}(10\text{-}Br)Cbl]^+$. Values of $\Delta H^{\ddagger}$ and $\Delta S^{\ddagger}$ were determined from the slope and intercept, respectively, of an Eyring plot of $\ln(k_{II}h/k_BT)$ against T^{-1}, where h *and* k_B are the Plank and Boltzman constants, respectively.

Solutions of $[H_2O\text{-}(10\text{-}Br)Cbl]^+$ were freshly prepared and buffered with 0.1 M of MES (for reaction performed with N_3^- at pH 6.0) and MOPS (for reaction performed with imidazole at pH 7.0) and 0.5 M of ionic strength was maintained with Na_2SO_4. 2.5 mL of the sample was added to a 1.0 cm pathlength cuvette (Hellma) and housed in a thermostatted cell block of the Agilent diode array spectrometer. Care was taken for thermal equilibration to be established. The ligand solution was also freshly prepared and buffered with MES or MOPS as described above; then the pH was adjusted to the same pH as that of the corrin solution and the total ionic strength of 0.5 M was maintained. A small aliquot of the ligand solution with known concentration was added to the cuvette and the rate of reaction was monitored by plotting the absorbance change for a number of wavelengths, for example 356, 373, 510 and 585 nm for the reaction of $[H_2O\text{-}(10\text{-}Br)Cbl]^+$ with N_3^- over the time. The second-order rate constants were studied as a function of temperature. At each temperature, between 6 and 8 ligand concentrations were used (by varying the volume of injected ligand), such that the ligand concentration spanned a factor of ten.

2.5.4.2 *Kinetic Investigations of Ligand Substitution Reactions of $[AC\text{-}(10\text{-}NO_2)Cbs]^+$, $[AC\text{-}(10\text{-}NH_2)Cbs]^+$ and $[ACCbs]^+$ Using Stopped-flow Spectrophotometry*

Prior to these experiments, preliminary spectroscopic investigations were carried out on a Cary 300 Bio uv-vis spectrometer to determine an appropriate wavelength at which the maximum absorbance change can be observed for the reactions with CN^-. Appropriate monitoring wavelengths were found to be 361, 372 and 370 nm for the reaction with $[AC\text{-}(10\text{-}NO_2)Cbs]^+$, $[AC\text{-}(10\text{-}NH_2)Cbs]^+$ and $[ACCbs]^+$, respectively.

All solutions were prepared freshly in 50% isopropanol/buffer mixtures (0.1 M CHES at pH 9.5); then a cobalt corrin solution with approximate concentration of 25 μM was added to the CHES

References on page 75

buffered solution. Cyanide solutions were freshly prepared in the same solvent system and were 0.5 and 5 mM in cyanide (on mixing) for reaction with $[ACCbs]^+$ an $[AC\text{-}(10\text{-}NH_2)Cbs]^+$, and between 2.5 and 25 mM for reaction with $[AC\text{-}(10\text{-}NO_2)Cbs]^+$. An example of a trace recorded for the reaction of CN^- (0.004 M) with $[ACCbs]^+$ is shown in **Figure 2.9**.

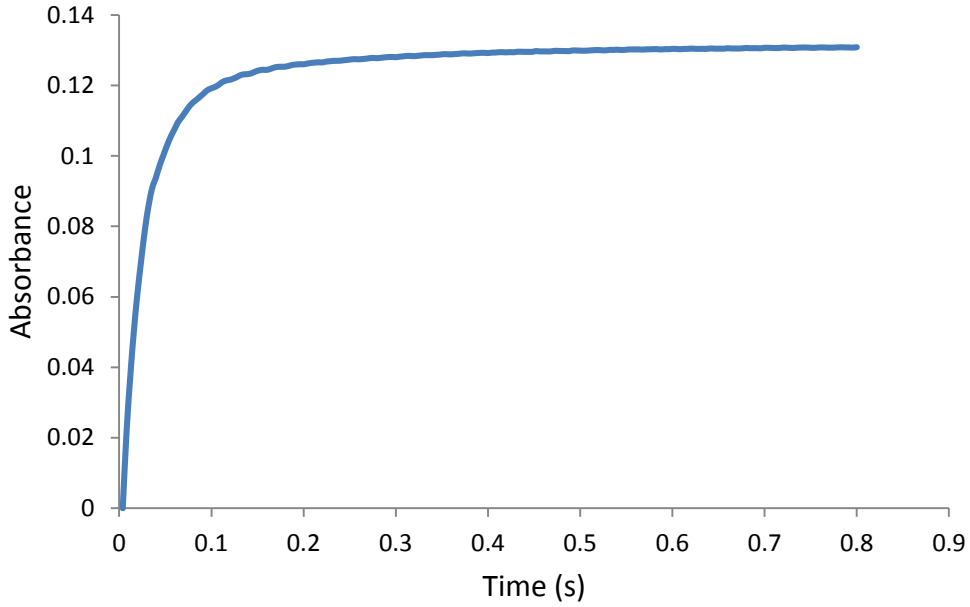


Figure 2.9 An example of a trace recorded for the reaction of CN^- with $[ACCbs]^+$ at 21 ^oC.

In all reactions, biphasic kinetics were observed due to the presence of the diaqua (or aquahydroxo) complex (see **Chapter 6**). The absorbance-time traces were therefore fitted to **Equation 2.10**, appropriate for parallel reactions. It is well-established for $[ACCbs]^+$[29] the faster phase corresponds to substitution of H_2O *trans* to CN^-, whereas the slower phase corresponds to substitution of H_2O *trans* to H_2O (or OH^-). In **Equation 2.10**, k_f and k_s are the pseudo first-order rate constants for the faster and slower phases, respectively, A_∞ is the absorbance at the end of the reaction, $|A_0 - A_1|$ the absorbance change associated with the faster phase and $|A_1 - A_\infty|$ that associated with the slower phase.

$$A_\lambda = A_\infty + (A_0 - A_1)e^{-k_f^{obs}t} + (A_1 - A_\infty)e^{-k_s^{obs}t} \quad \textbf{(2.10)}$$

References on page 75

The observed pseudo first-order rate constants were corrected (**Equation 2.11**) for the effect of pH since hydroxide is inert to substitution in the cobalt corrins, where pK_{Co} is the acid dissociation constant of coordinated H_2O on Co(III) in the cobester being studied;[41,42,51,52] the effective [CN^-] was corrected for the acid dissociation constant of HCN since HCN reacts negligibly slowly compared to CN^- itself.

$$k_i = k_i^{obs}\left(1+10^{\mathrm{pH}-\mathrm{p}K_{Co}}\right),\ (i = f,s) \qquad (\mathbf{2.11})$$

The second-order rate constants, k_{II}, were determined from weighed non-linear least squares plots of k_i, $i = f,s$, against the effective [CN^-]. Values of $\Delta H^{\ddagger}$ and $\Delta S^{\ddagger}$ were determined from the slope and intercept, respectively, of an Eyring plot of $\ln(k_{II}h/k_BT)$ against T^{-1}, where h and k_B are the Plank and Boltzmann constants, respectively.

2.6 Determination of Crystal Structure

2.6.1 Crystal Structural Determination of $[H_2O$-(10-Br)Cbl$]^+$ and $[N_3$-(10-Br)Cbl]

The growth of crystals of $[H_2O$-(10-Br)Cbl$]^+$ was attempted by dissolving ca. 10 mg in 1 mL deionised water, and placing the solution in an open glass vial which was placed in a larger vial containing acetone. The larger vial was sealed and kept at 4 ^oC; after a week very small, thin pellet-shaped crystals had formed which proved to diffract poorly. They are shown in **Figure 2.10** as capped sticks and ORTEP diagrams with the ellipsoids drawn at the 50% contour level in both diagrams waters of crystallisation omitted for clarity. This shows nicely how poor the aqua structure is. Crystallisation from a variety of solutions (neutral solution containing NaCl, LiCl, $NaClO_4$) was attempted several times, but with little success; either very poor quality crystals were obtained, or only an amorphous or micro-crystalline material formed. Therefore crystallising the azido complex was attempted, [N_3-(10-Br)Cbl]. Sodium azide (ca. 50 mg) was added to a 1 mL aqueous solution of aqua-10-bromo-cobalamin (15 mg) and dissolved. uv-vis and HPLC analysis confirmed the complete conversion to the azido complex. Crystallisation was by acetone vapour diffusion as described above. After 10 days at 4 ^oC needle-shaped crystals

References on page 75

had formed. The crystal structure of [N_3-(10-Br)Cbl] is illustrated in **Figure 2.10 and Figure 2.11**. Crystallographic data and tables of bond lengths, angles, torsions for [N_3-(10-Br)Cbl]$^+$ and [H_2O-(10-Br)Cbl]$^+$ can be found in **Appendix 2.7.**

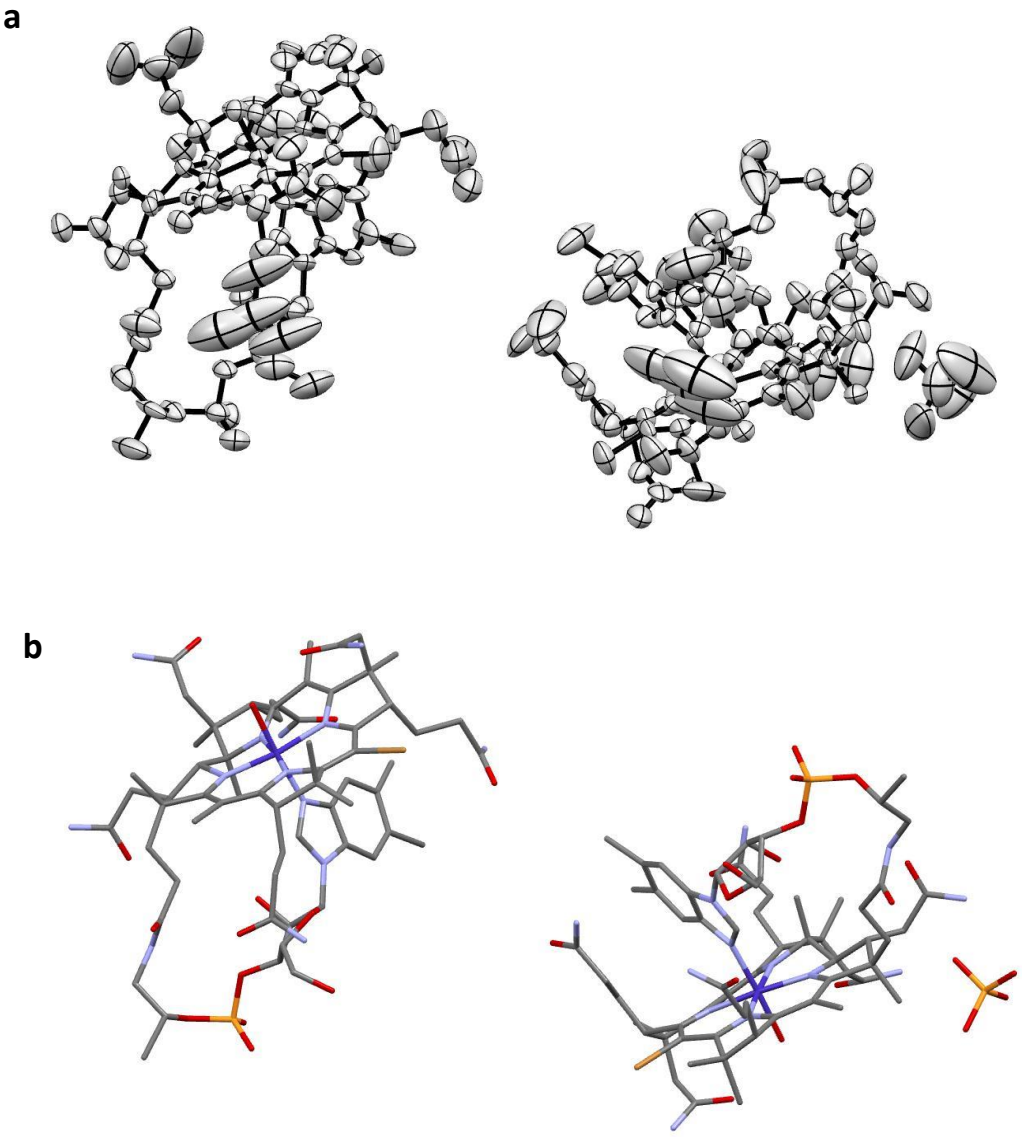


Figure 2.10 Crystal structure of [H_2O-(10-Br)Cbl]$^+$, (a) ORTEP diagrams with the ellipsoids drawn at the 50% contour level, (b) capped sticks diagram.

References on page 75

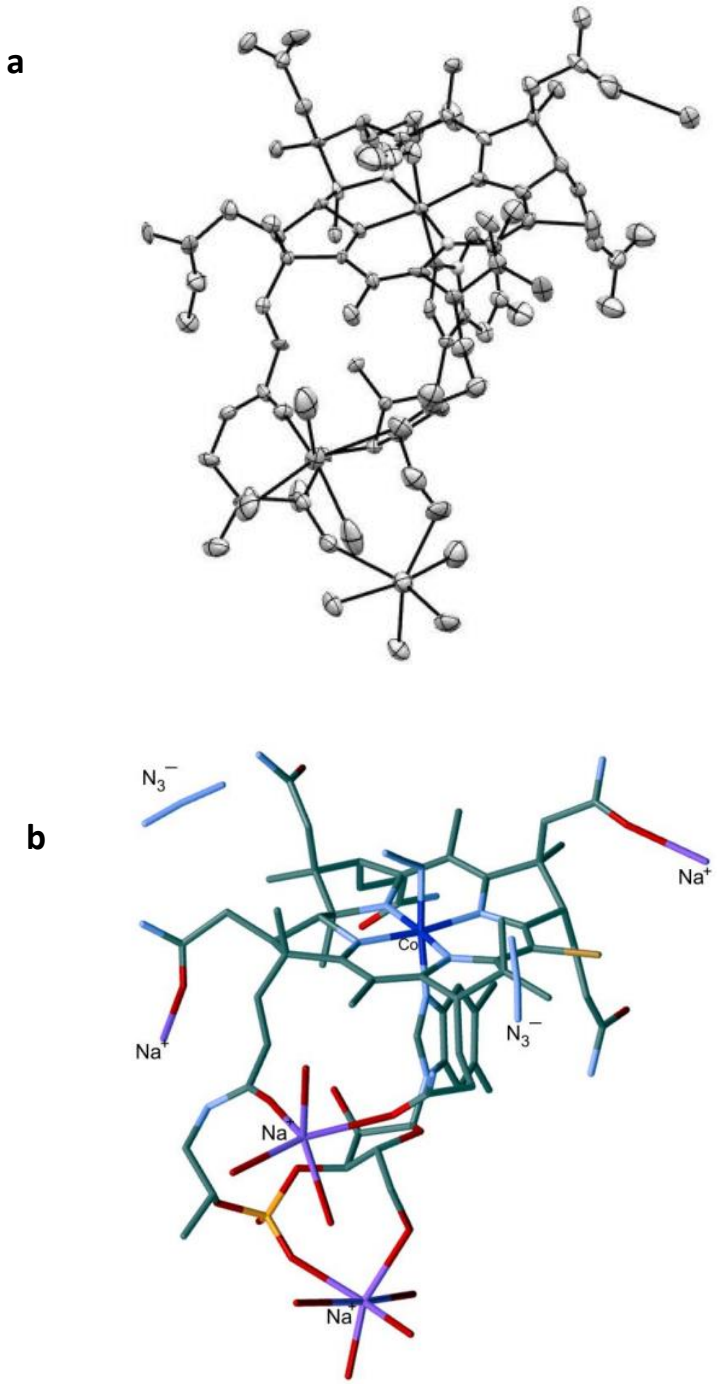


Figure 2.11 Crystal structure of of $[N_3\text{-}(10\text{-Br})Cbl]^+$, (a) ORTEP diagram with the ellipsoids drawn at the 50% contour level, (b) capped sticks diagram. Solvate molecules are omitted for clarity.

References on page 75

2.6.2 Crystal Structure Determination of [DC-(10-NO_2)Cbs]

Crystallisation of [DC-(10-NO_2)Cbs] was attempted using different methods. Initially it was attempted to recrystallise [DC-(10-NO_2)Cbs] in hexane/ethylacetate,[28] but only a red precipitate formed. It was also attempted to grow crystals in an H tube at room temperature by vapour diffusion of hexane into a solution of [DC-(10-NO_2)Cbs] in hexane. And lastly a slow evaporation of methanol/hexane was tried at room temperature. Unfortunately, only amorphous precipitates formed in all cases.

References on page 75

2.7 References

(1) Varian, 3.00(182) ed., Sax Software Crop., Australia, 2002.

(2) SigmaPlot, 12.3 ed., Synstat Software, San Jose, CA, 2008.

(3) MestReNova, 6.0.2-5475 ed., Mestrelab Research S. L., Santiago de Composiela, 2009.

(4) Bruker, Apex2, 2.0-1 ed., Bruker AXS Inc., Madison, Wisconsin, USA, 2005.

(5) Bruker, SAINT+, 7.60A ed., Bruker AXS Inc., Madison, Wisconsin, USA, 2005.

(6) Sheldrick, G. M. *Acta Crystallogr.* **2008**, *A64*, 112.

(7) Farrugia, L. *J. Appl. Cryst.* **1997**, *30*, 565.

(8) Frisch, M. J.; Trucks, G. W.; Schlegel, H. B.; Sucuseria, G. E.; Robb, M. A.; Cheeseman, J. R.; Scalmani, G.; Barone, V.; Mennucci, B.; Petersson, G. A.; Nakatsuji, H.; Caricato, M.; Li, X.; Hratchian, H. P.; Izmaylov, A. F.; Bloino, J.; Zheng, G.; Sonnenberg, J. L.; Hada, M.; Ehara, M.; Toyota, K.; Fukuda, R.; Hasegawa, J.; Ishida, M.; Nakajima, T.; Honda, Y.; Kitao, O.; Nakai, H.; Vreven, T.; Montgomery, J. J. A.; Peralta, J. E.; Ogliaro, F.; Bearpark, M.; Heyd, J. J.; Brothers, E.; Kudin, K. N.; Staroverov, V. N.; Kobayashi, R.; Normand, J.; Raghavachari, K.; Rendell, A.; Burant, J. C.; Iyengar, S. S.; Tomasi, J.; Cossi, M.; Rega, N.; Millam, N. J.; Kelene, M.; Knox, J. E.; Cross, J. B.; Bakken, V.; Adamo, C.; Jaramillo, J.; Gomperts, R.; Stratmann, R. E.; Yazyev, O.; Austin, A. J.; Cammi, R.; Pomelli, C.; Ochterski, J. W.; Martin, R. L.; Morokuma, K.; Zakrzewski, V. G.; Voth, G. A.; Salvador, P.; Dannenberg, J. J.; Dapprich, S.; Daniels, A. D.; Farkas, Ö.; Foresman, J. B.; Ortiz, J. V.; Cioslowski, J.; Fox, D. J.; Gaussian-09, Gaussian Inc.: Wallinford, CT, 2009.

(9) Perdew, J. P. *Phys. Rev. B* **1986**, *33*, 8822.

(10) Becke, A. D. *Phys. Rev. A* **1988**, *38*, 3098.

(11) Schäfer, A.; Horn, H.; Ahlrichs, R. *J. Chem. Phys.* **1992**, *97*, 2571.

(12) Schäfer, A.; Huber, C.; Ahlrichs, R. *J. Chem. Phys* **1994**, *100*, 5829.

(13) Dunlap, B. *J. Mol. Struct. (Theochem)* **2000**, *529*, 37.

(14) Dunlap, B. *J. Chem. Phys.* **1983**, *78*, 3140.

(15) Eichkorn, K.; Weigend, F.; Treutler, O.; Ahlrichs, R. *Theor. Chem. Acc.* **1997**, *97*, 119.

(16) Eichkorn, K.; Treutler, O.; Öhm, H.; Häser, M.; Ahlrichs, R. *Chem. Phys. Lett.* **1995**, *240*, 283.

(17) Bader, R. F. *Atoms in Molecules; A Quantum Theory*; Oxford University Press: Oxford, 1990.

(18) Keith, T. A. http://aim.tkgristmill.com, Overland Park, KS, 2011.

(19) Markwell, A. J.; Pratt, J. M.; Shaikjee, S. S.; Toerien, J. G. *J. Chem. Soc. Dalton Trans.* **1987**, 1349.

(20) Wagner, F. *Proc. Roy. Soc. Lond. A* **1965**, *288*, 344-347.

(21) Knapton, L.; Marques, H. M. *Dalton Trans.* **2005**, 889.

(22) Brown, K. L.; Brooks, H. B.; Gupta, B. D.; Victor, M.; Marques, H. M.; Scooby, D. C.; Goux, W. J.; Timkovich, R. *Inorg. Chem.* **1991**, *30*, 3430.

(23) Brown, K. L.; Zou, X. *J. Ame. Chem. Soc.* **1992**, *114*, 9643.

(24) Brown, K. L.; Zou, X.; Savon, S. R.; Jacobsen, W. *Biochemistry* **1993**, *32*, 8421.

(25) Brown, K. L.; Chang, C. K.; Marques, H. M. *Inorg. Chem.* **1995**, *34*, 3038.

(26) Brown, K. L. *in Chemistry and Biochemistry of B_{12}*; John Wiley & Sons: New York, 1999.

(27) Knapton, L. PhD, University of the Witwatersrand, 2005.

(28) Proinsias, K. Ó.; Kurcoń, S.; Gryko, D. *Eur. J. Org. Chem.* **2012**, 154.

(29) Chemaly, S. M.; Brown, K. L.; Fernandes, M. A.; Munro, O. Q.; Grimmer, C.; Marques, H. M. *Inorg. Chem.* **2011**, *50*, 8700.

(30) Schiebel, H. M.; Schulten, H. R. *Mass Spectrom. Rev.* **1986**, *5*, 249.

(31) Ernst, L. **1981**, *Liebigs. Ann. Chem.*, 376.
(32) Ernst, L. *J. Chem. Soc, Perkin Transactions 1* **1984**, 2267.
(33) Chemaly, S. M.; Florczak, M.; Dirr, H.; Marques, H. M. *Inorg. Chem.* **2011**, *50*, 8719.
(34) Ernst, L.; Magg, H. *Liebigs. Ann.* **1996**, 323.
(35) Gossauer, A.; Hwise, K. P.; Gotze, H.; Inhoffen, H. H. *Liebigs. Ann. Chem.* **1977**, 1480.
(36) Hamza, M. S. A. *Inorg. Biochem.* **1998**, *69*, 269.
(37) Palet, C.; Munoz, M.; Daunert, S.; Bachas, L. G.; Valiente, M. *Anal. Chem.* **1993**, *65*, 1533.
(38) Munro, O. Q.; Marques, H. M. *Inorg. Chem.* **1996**, *35*, 3752.
(39) Marques, H. M.; Bradley, J. C.; Campbell, L. A. *J. Chem. Soc. Dalton Trans.* **1992**, 2019.
(40) Boos, R. N.; Carr, J. E.; Conn, J. B. *Science.* **1953**, *117*, 603.
(41) Reenstra, W. W.; Jencks, W. P. *J. Am. Chem. Soc.* **1979**, *101*, 5780.
(42) Marques, H. M.; Brown, K. L.; Jacobsen, W. *J. Biol. Chem.* **1988**, *263*, 12378.
(43) Martell, A. E.; Smith, R. M.; Motekaites, R. J. NIST, Gaithersburg, MD, 2004.
(44) Friedrich, W. Z. *Naturforsch. B* **1966**, *21*, 595.
(45) Pratt, J. M. *The Inorganic Chemistry of Vitamin B_{12}*; Academic Press: London, 1972.
(46) Friedrich, W. Z.; Bieganowski, R. Z. *Naturforsch. B* **1967**, *22*, 741.
(47) Friedrich, W. Z.; Ohlms, H.; Sandeck, W.; Bieganowski, R. Z. *Naturforsch. B* **1967**, *22*, 839.
(48) Chemaly, S. M.; Kendall, L.; Nowakowska, M.; Pon, D.; Perry, C. B.; Marques, H. M. *Inorg. Chem.* **2013**, *52*, 1077.
(49) Johnson, G. D.; Bowen, R. E. *J. Am. Chem. Soc.* **1965**, *87*, 1655.
(50) Marques, H. M.; Breet, E. L. J.; Prinsloo, F. F. *J. Chem. Soc. Dalton Trans.* **1991**, 2941.
(51) Marques, H. M.; Baldwin, D. A.; Pratt, J. M. *J. Inorg. Biochem.* **1987**, *29*, 77.
(52) Marques, H. M.; Marsh, J. H.; Mellor, J. R.; Munro, O. Q. *Inorg. Chim. Acta.* **1990**, *170*, 259.

CHAPTER 3

The Thermodynamics of the Reactions of Aquacobalamin (vitamin B_{12a}), Aqua-10-chlorocobalamin and Aqua-10-bromocobalamin with Anionic and Neutral Ligands

3.1 Introduction

As mentioned in **Chapter 1**, the intriguing chemistry of vitamin B_{12}, and in particular that of aquacobalamin ($[H_2OCbl]^+$) has been the focus of attention of inorganic chemists for many years. The nature of Co(III) in the cobalt corrins (the derivatives of vitamin B_{12}) has been explored in an effort to elucidate the effect of the corrin ligand on chemistry of the axial coordination site of the metal ion.[1-11] Co(III) usually behaves as a hard and inert metal ion.[12] But surprisingly in vitamin B_{12} it behaves as a much softer and more labile ion, suggesting that it may have some Co(II)-like character. Reactions of B_{12a} with various anionic ligands revealed that in the case of $S_2O_3^{2-}$, NO_2^- and $SeCN^-$ the softer donor atom is preferred to coordinate to the metal atom, which can be evidence of a softer metal character due to the transfer of electron density from the corrin ring.[3]

Marques and co-workers suggested that an important factor in modifying the properties of normally inert Co(III) and conferring on it its unusual lability in the cobalt corrins is the delocalisation of electron density from the corrin equatorial ligand to Co(III), making the metal softer and imparting on it some measure of labile Co(II) character.[1,5,6,8,13]

To test this hypothesis, a number of strategies have been employed. Relating to this research a study was performed by Knapton and Marques where they perturbed the electronic structure of the corrin by substituting the H atom at C10 by either Cl (which is π electron-donating towards the corrin)[1,4] or NO (which is π electron-withdrawing).[2]

To extend this study the electronic structure of the corrin has been perturbed by substituting the H atom at C10 by Br, which is π electron-donating towards the corrin ring. In this chapter, acid dissociation constants, pK_a, for the deprotonation of coordinated H_2O, and stability constants, log K, for the substitution of coordinated H_2O by a variety of neutral and anionic ligands, are reported for aqua-10-bromocobalamin ($[H_2O\text{-}(10\text{-}Br)Cbl]^+$) as well as for $[H_2OCbl]^+$ and aqua-10-chlorocobalamin ($[H_2O\text{-}(10\text{-}Cl)Cbl]^+$). DFT calculations were used to rationalise the effect the

References on page 126

perturbation of the electronic structure of the corrin in these compounds has on the coordination chemistry of the axial coordination site of Co(III). In addition the crystal structures of $[H_2O\text{-}(10\text{-}Br)Cbl]^+$ and azido-10-bromocobalamin ($[N_3(10\text{-}Br)Cbl]$) are reported and compared to the available crystal structures of the relevant cobalamins.

3.2 pK_a Determination of $[H_2OCbl]^+$, $[H_2O\text{-}(10\text{-}Br)Cbl]^+$ and $[H_2O\text{-}(10\text{-}Cl)Cbl]^+$

3.2.1 Introduction

Axially coordinated water in vitamin B_{12} dissociates as illustrated in **Equation 3.1.**

$$DMB\text{–}Co\text{–}H_2O \rightleftharpoons DMB\text{–}Co\text{–}OH + H^+ \qquad (\mathbf{3.1})$$

The value for the dissociation constant (pK_a) is required to enable adjustments to be made to quantitative data from all kinetic and ligand binding studies in order to obtain pH-dependent values. This is important because the hydroxo species of the cobalt corrins species is inert to substitution.[4,6,14]

The acid dissociation constant (pK_a) for $[H_2OCbl]^+$ has been reported under different experimental conditions as: 7.8,[15] in the presence of Cl^- as KCl was used to adjust the ionic strength; 8.09,[4] where $NaNO_3$ was used as ionic strength adjustor; and 8.26[4] in 70% ethanol. This observed variation in pK_a values is the effect of ionic strength adjustor and solvent system. In a previous study the pK_a's for $[H_2O\text{-}(10\text{-}Cl)Cbl]^+$ and aqua-10-nitrosocobalamin ($[H_2O\text{-}(10\text{-}NO)Cbl]^+$) were reported[4] as 7.65 and 10.71, respectively, at 25 ^oC, I = 0.5 M ($NaNO_3$).

In this study, the pK_a of $[H_2O\text{-}(10\text{-}Br)Cbl]^+$ was determined as well as that of $[H_2O\text{-}(10\text{-}Cl)Cbl]^+$ and that of $[H_2OCbl]^+$ under the same experimental conditions, to ensure that all results are comparable ((1 mM in each of 2-(*N*-morpholino)ethanesulfonic acid (MES), (*N*-morpholino)propanesulfonic acid (MOPS), 4-(2-hydroxyethyl)-1-piperazineethanesulfonic acid (HEPES), *N*-cyclohexyl-2-aminoethanesulfonic acid (CHES), tris(hydroxoyethyl)aminomethane (TRIS) and *N*-cyclohexyl-3-aminopropanesulfonic acid (CAPS), μ = 0.5 M, Na_2SO_4). In addition, the pK_a value for $[H_2O\text{-}(10\text{-}Br)Cbl]^+$ was measured as a function of temperature.

References on page 126

3.2.2 Results and Discussion

3.2.2.1 Determination of the pK_a of $[H_2OCbl]^+$

The acid dissociation constant for the axially coordinated water ligand of $[H_2OCbl]^+$ was determined spectroscopically. The experimental data were fitted using non-linear least squares fit methods employing a Newton-Raphson procedure to an ionisation isotherm (**Equation 2.1**), which is relevant when one acid-base equilibrium is present.[4]

$$A_\lambda = \left(\frac{A_0 10^{-pH} + A_1 10^{-pK_a}}{10^{-pH} + 10^{-pK_a}} \right) \qquad (\mathbf{2.1})$$

A_λ is the absorbance at the monitoring wavelength, K_a is the acid dissociation constant, A_0 is the initial absorbance and A_1 is the final absorbance. This equation was applied for each temperature at which the data were collected. Then the pK_a was calculated from a weighted average of the results, weighted by the reciprocal of the relative percentage error, where the error is the standard error of the fits.

The pK_a value for $[H_2OCbl]^+$ was determined by titrating $[H_2OCbl]^+$ in an aqueous multi-component buffer system with negligible volumes of H_2SO_4 and NaOH between pH 6 to 10, as described in **Chapter 2, Section 2.5.2.1**.

The effect of pH change on the absorbance spectra of $[H_2OCbl]^+$ was monitored by uv-vis spectroscopy. It was noticed that as the pH increased the positions of α, β and γ bands underwent a red shift from 520, 498 and 352 nm to 540, 510 and 360 nm, respectively. The intensity of the peak of the γ band decreased approximately by 23 % and that of the α and β bands increased by 2 and 4%, respectively. **Figure 3.1** shows the spectroscopic changes in the spectrum of $[H_2OCbl]^+$ in an aqueous multi-component buffer system with varying the pH.

References on page 126

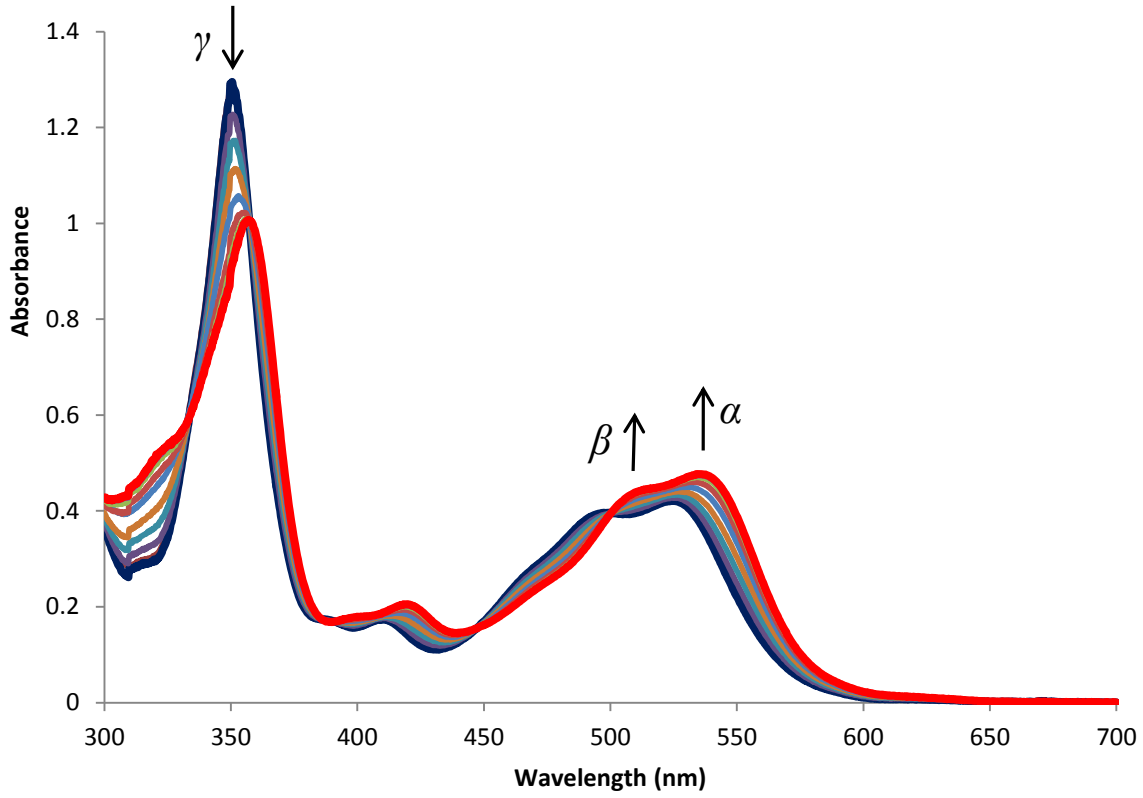


Figure 3.1 The effect of pH on the absorbance spectrum of $[H_2OCbl]^+$ at 25 °C in an aqueous solution, pH ranging from 5.5 (blue) to 10.6 (red).

The determination was repeated three times, and the values averaged, weighted by the reciprocal of the relative percentage error of the fit. The average value of the pK_a was 7.62 ± 0.01. An example of this fit is shown in **Figure 3.2** for data monitored at 352 nm.

References on page 126

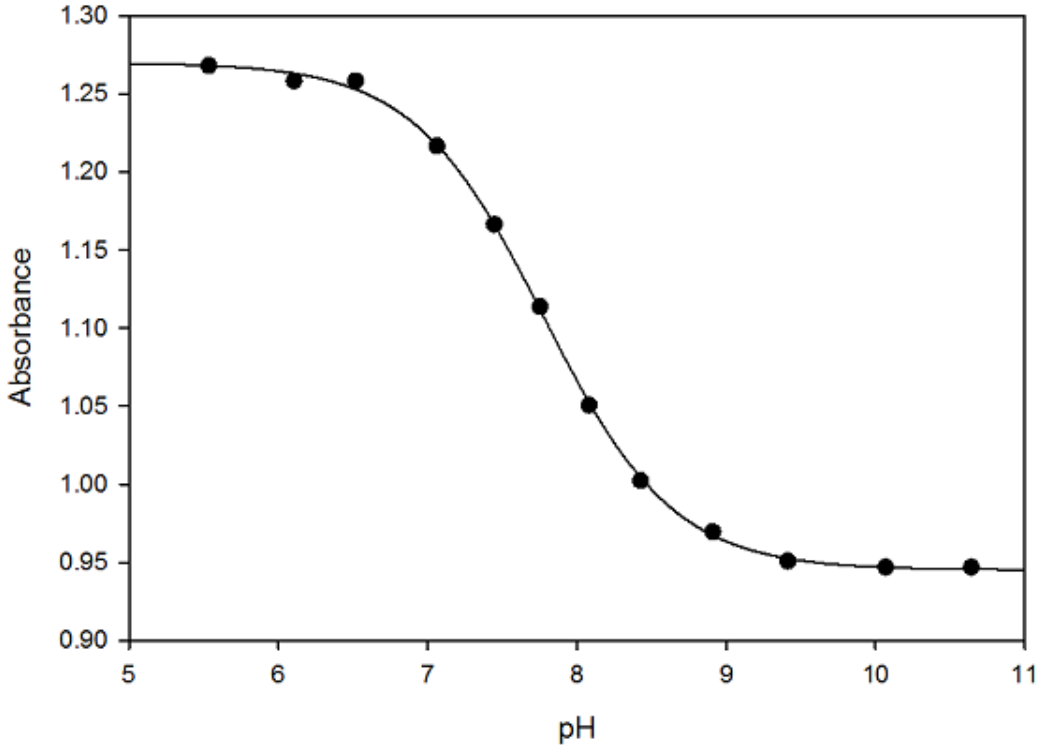


Figure 3.2 A plot of the change in absorbance of $[H_2OCbl]^+$ at 352 nm to which **Equation 2.1** has been fitted.

In a previous study,[4] the pK_a value of 8.09 ± 0.02 at 25 °C (I = 0.5 M, $NaNO_3$) was obtained for $[H_2OCbl]^+$. The reason for the difference between this and the value obtained in this study is unclear.

3.2.2.2 Determination of the pK_a of $[H_2O$-(10-Cl)Cbl$]^+$

The data collected for $[H_2O$-(10-Cl)Cbl$]^+$ was analysed in the same manner as that for $[H_2OCbl]^+$.

The absorbance spectrum of $[H_2O$-(10-Cl)Cbl$]^+$ is shown in **Figure 3.3** with distinctive isosbestic points at 525, 476, 361 and 339 nm. As the pH was increased, the position of α, β and γ bands shifted from 560, 522 and 356 nm to 568, 537 and 362 nm, respectively, with an increase in the intensity of the β and α bands of approximately 16 and 27%, respectively. The γ band intensity decreased by ~20% approximately.

References on page 126

The determination was repeated three times, and the values averaged, weighted by the reciprocal of the relative percentage error of the fit. An example of this fit is illustrated in **Figure 3.4** for data obtained at 356 nm. The average value of the pK_a was 7.22 ± 0.02.

Our findings are in reasonable agreement with previous results[4] where the pK_a for $[H_2O\text{-}(10\text{-}Cl)Cbl]^+$ was determined as 7.65 ± 0.05 at 25 °C (I = 0.5 M, $NaNO_3$).

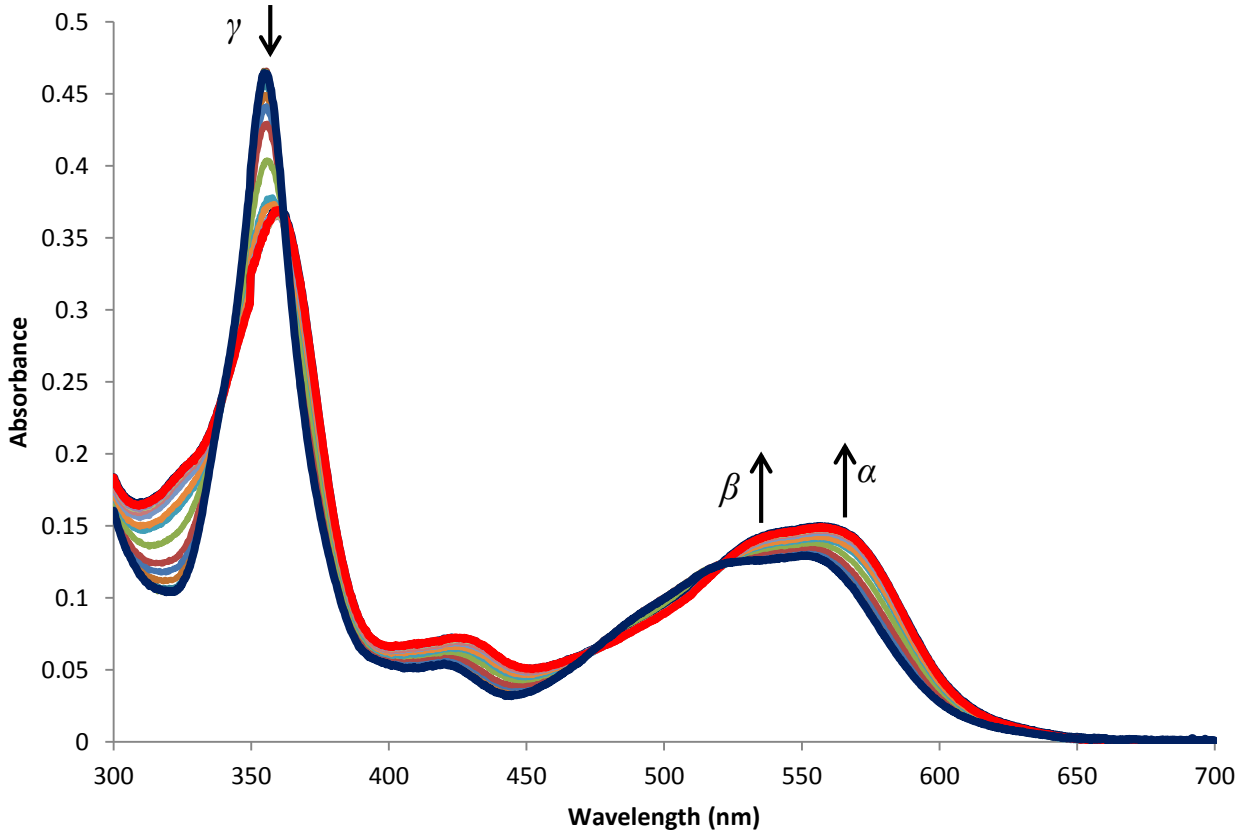


Figure 3.3 The effect of pH on the uv-vis spectrum of $[H_2O\text{-}(10\text{-}Cl)Cbl]^+$, varying pH from 4.7 (blue) to 10.4 (red).

References on page 126

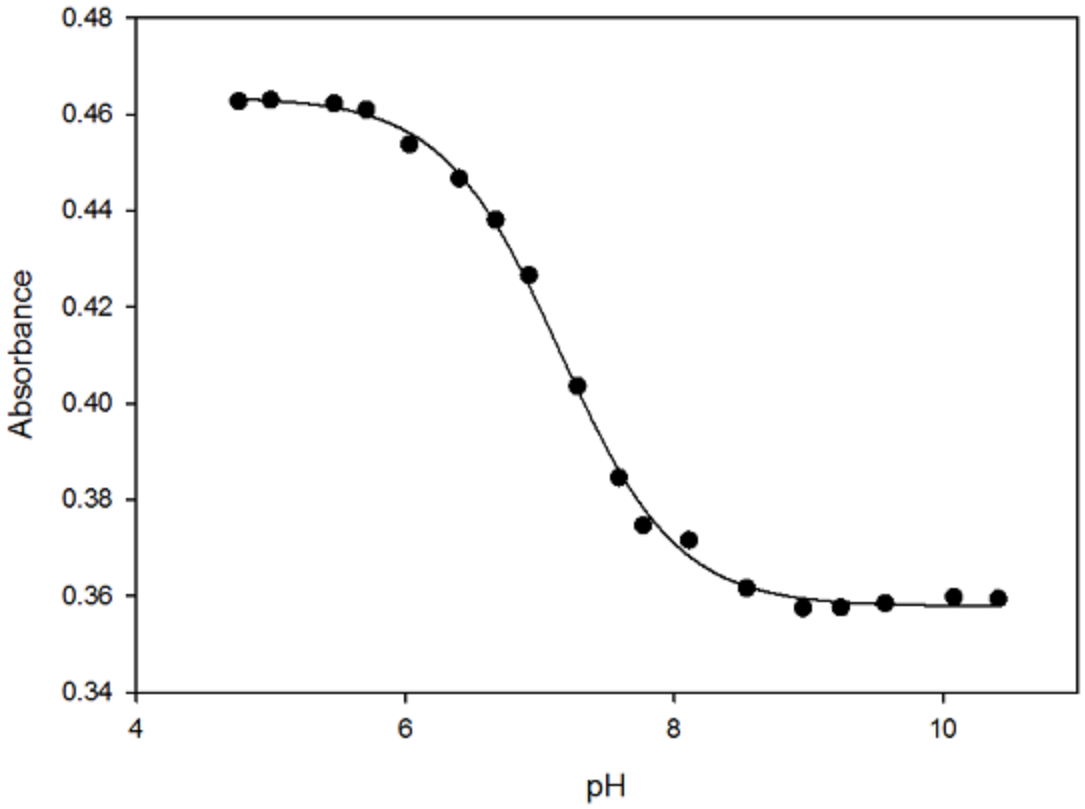


Figure 3.4 A plot of the change in absorbance of $[H_2O\text{-}(10\text{-}Cl)Cbl]^+$ at 356 nm to which **Equation 2.1** has been fitted.

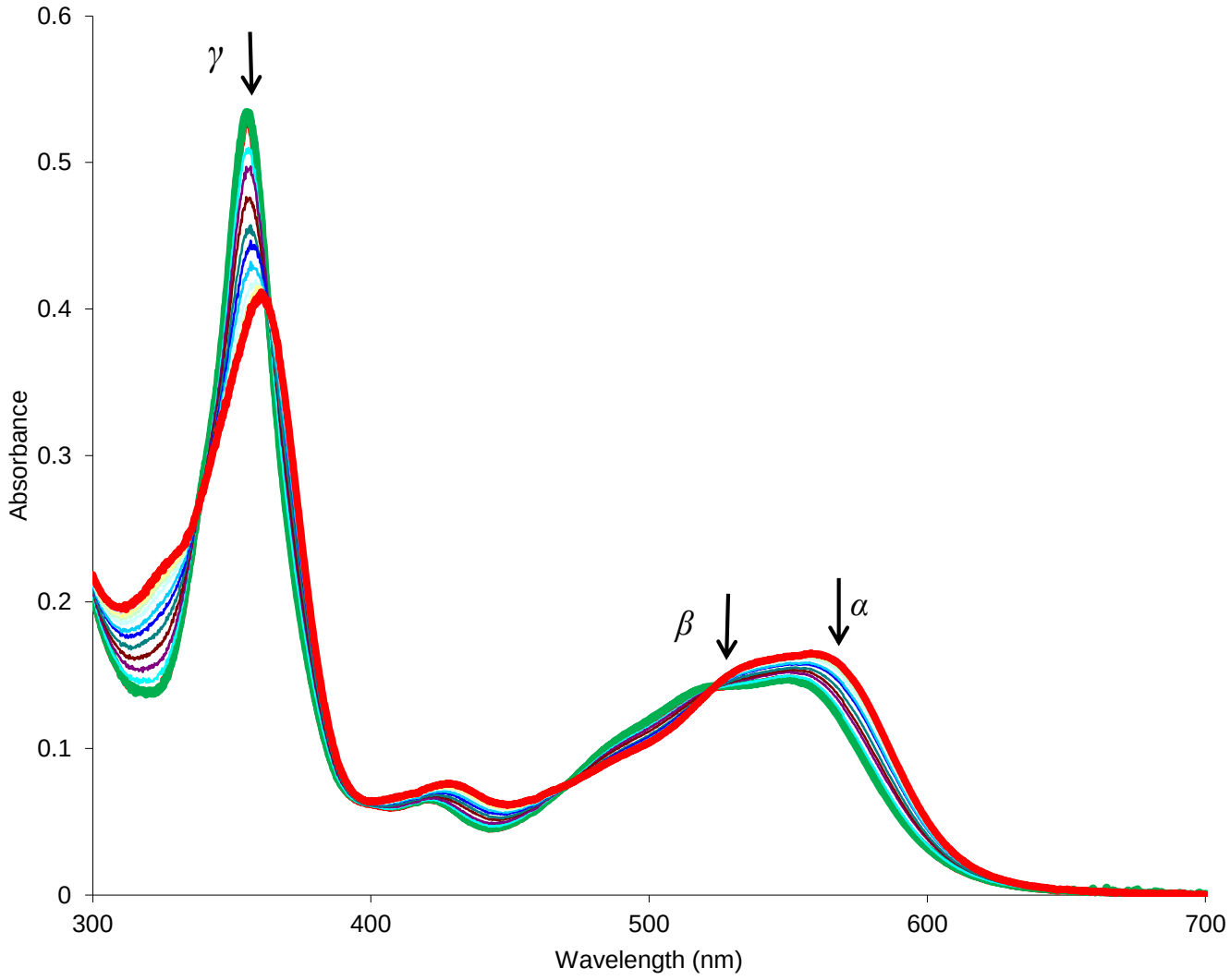
3.2.2.3 Determination of the pK_a of $[H_2O\text{-}(10\text{-}Br)Cbl]^+$

To determine the pK_a value of $[H_2O\text{-}(10\text{-}Br)Cbl]^+$, the sample was treated in the same manner as $[H_2OCbl]^+$ under the same experimental conditions. The pK_a of $[H_2O\text{-}(10\text{-}Br)Cbl]^+$ was studied as a function of temperature at 10, 15, 20, 25, 30 and 35 ^oC. **Figure 3.5** shows the absorbance spectrum of $[H_2O\text{-}(10\text{-}Br)Cbl]^+$ as a function of pH at 25 ^oC. It is obvious that as the pH varied from 5 to 10, the spectrum underwent a red shift as the α, β and γ bands shifted from 555, 522 and 357 nm to 567, 535 and 363 nm, respectively, with isosbestic points at 337, 363, 476 and 528 nm. The intensity of γ band decreased by approximately 23% and the intensity of β and α bands increased by 7 and 14%, respectively.

The changes in absorbance as a function of pH were analysed at 354, 430, 500, 565 and 590 nm (where the largest change in absorbance can be seen) using an acid dissociation isotherm (**Equation 3.2**) as explained before. The determination was repeated three times, and the values

References on page 126

averaged, weighted by the reciprocal of the relative percentage error of the fit. An example of this fit is illustrated in **Figure 3.6** at 355 nm. The average value of the pK_a was determined as 7.23 ± 0.03. The pK_a was determined as a function of temperature between 15 °C and 35 °C. From the van't Hoff plot (**Figure 3.7)** the thermodynamic parameters of the ionisation reaction were determined as ΔH = 34 ± 2 kJ mol^{-1} and ΔS = –26 ± 6 J K^{-1} mol^{-1}, from which pK_a = 7.28 at 25 °C.



References on page 126

Figure 3.5 The effect of pH on the uv-vis spectrum of $[H_2O\text{-}(10\text{-}Br)Cbl]^+$, on varying pH from 5.21 (green) to 9.9 (red).

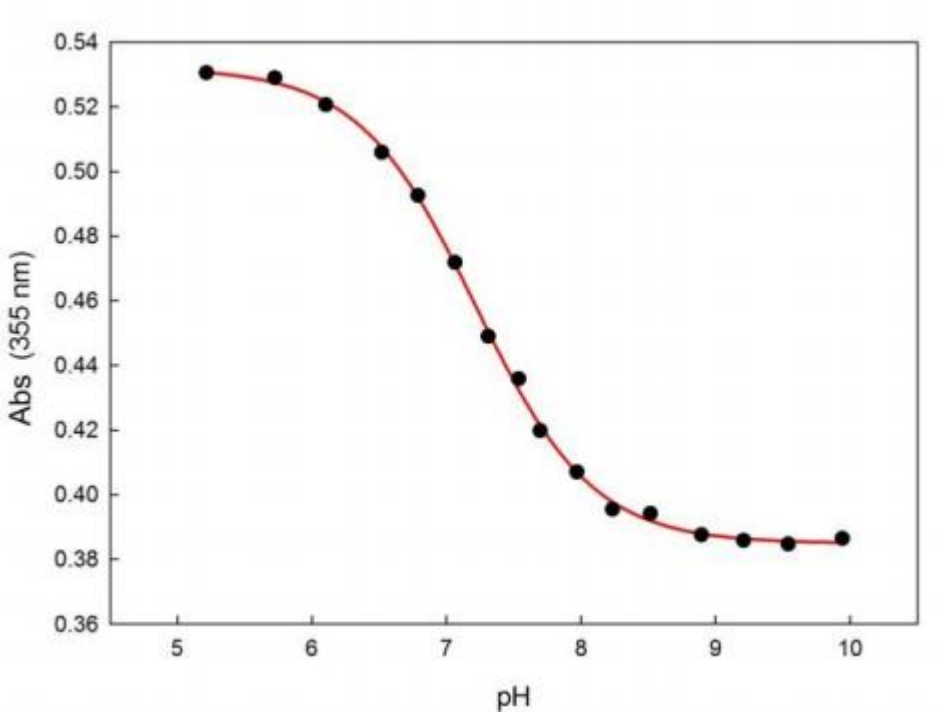


Figure 3.6 A plot of the change in absorbance of $[H_2O\text{-}(10\text{-}Br)Cbl]^+$ at 355 nm to which **Equation 2.1** has been fitted.

References on page 126

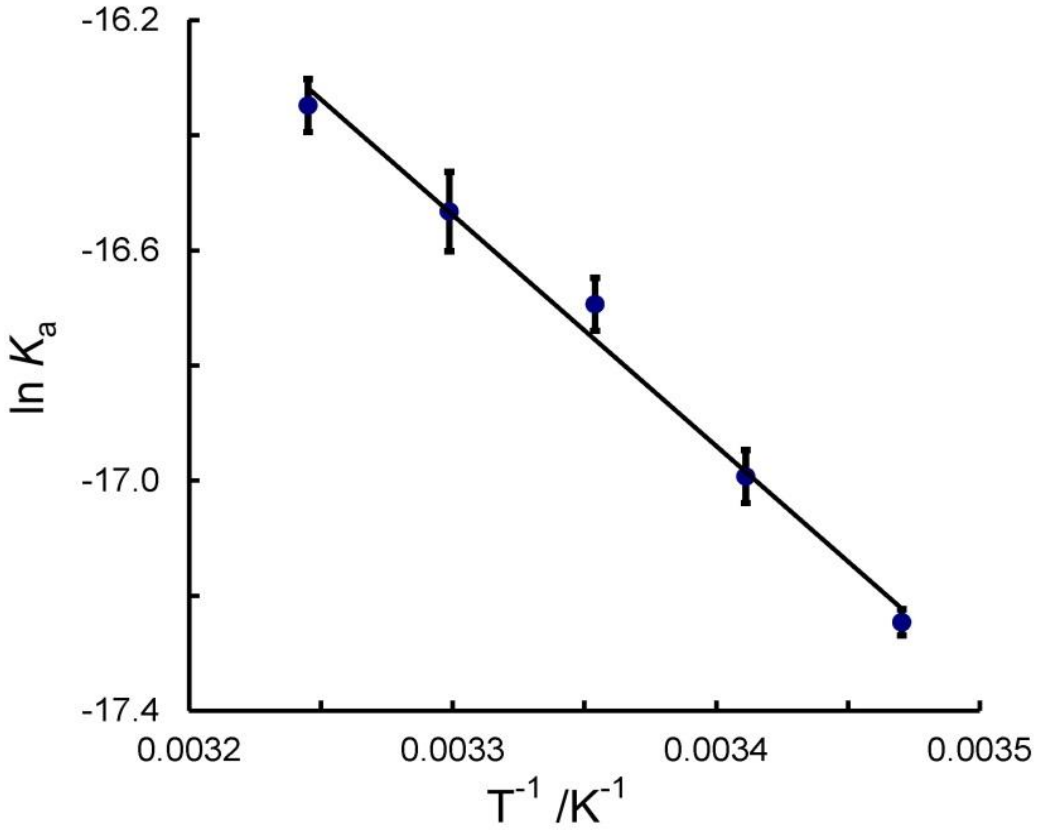


Figure 3.7 van't Hoff plot for the ionisation of coordinated H_2O in $[H_2O\text{-}(10\text{-}Br)Cbl]^+$. From the slope and intercept ΔH = 34 ± 2 kJ mol^{-1} and ΔS = –26 ± 6 J K^{-1} mol^{-1} were determined, respectively.

3.2.2.4 DFT Calculations

The DFT calculations on models of $[H_2O\text{-}(10\text{-}Z)Cbl]^{n+}$ show that as Z is changed from H to Cl to Br, the charge on the metal ion becomes less positive; the Bader charge on Co for $[H_2OCbl]^+$, $[H_2O\text{-}(10\text{-}Cl)Cbl]^+$ and $[H_2O\text{-}(10\text{-}Br)Cbl]^+$ are 1.2084, 1.2078 and 1.2074 e, respectively. Simultaneously, the charge on the axial ligands becomes more negative (the order is H < Br ≈ Cl for the negative charge on O of axial H_2O but H < Cl = Br for the negative charge on the N of axial imidazole), refer to **Table 3.11**. Hence the acidity of the axial H_2O ligand increases marginally resulting in lower pK_a for $[H_2O\text{-}(10\text{-}Br)Cbl]^+$ than for $[H_2OCbl]^+$ itself.

References on page 126

In a previous study, molecular orbital calculations were performed on $[H_2OCbl]^+$,[1] $[H_2O\text{-}(10\text{-}Cl)Cbl]^{+1}$ and $[H_2O\text{-}(10\text{-}NO)Cbl]^{+2}$ using the ZINDO/1 model. The partial charges found on the oxygen atom of the coordinated OH^- for $[H_2OCbl]^+$, $[H_2O\text{-}(10\text{-}Cl)Cbl]^+$ and $[H_2O\text{-}(10\text{-}NO)Cbl]^+$ were -0.503, -0.456 and -0.566, respectively; this led to the conclusion that as the electron withdrawing power of the C10 substitute increases the charge density on O atom increases, resulting in a more ionic metal hydroxide bond and a higher pK_a value for coordinated H_2O.

3.2.2.5 Conclusion

The pK_a values were determined for $[H_2OCbl]^+$, $[H_2O\text{-}(10\text{-}Cl)Cbl]^+$ and $[H_2O\text{-}(10\text{-}Br)Cbl]^+$ as 7.62 ± 0.01, 7.22 ± 0.02 and 7.23 ± 0.03, respectively at 25 ^oC. The data indicate that as the electron-donor ability of the C10 substituent increases the value of pK_a decreases. This is consistent with Br and Cl both donating electron density to the corrin ring and consequently increasing the negative charge on the O atom of coordinated H_2O; thus the acidity of the axial H_2O ligand increases marginally, resulting in a lower pK_a. The opposite effect was observed for $[H_2O\text{-}(10\text{-}NO)Cbl]^+$, in which it was shown that when C10 position is substituted by an electron withdrawing group the charge density on Co atom decreases, resulting in an increase in the pK_a value of coordinated H_2O to 10.71.[2]

References on page 126

3.3 Determination of the Stability Constants of $[H_2O\text{-}(10\text{-}Br)Cbl]^+$, $[H_2OCbl]^+$ and $[H_2O\text{-}(10\text{-}Cl)Cbl]^+$ with Various Anionic and Neutral Ligands

3.3.1 Introduction

The stability constants for the binding of various ligands to $[H_2OCbl]^+$ have been studied in both aqueous and multicomponent solvent systems.[16-18] In all cases it was observed that there is an obvious difference in both the thermodynamic and kinetic parameters as the identity of the solvent system varies. This is beyond the scope of the present study and all experiments were carried out in aqueous media. The values of stability constants for the reaction of $[H_2OCbl]^+$ with a selection of ligands reported in the literature are summarised in **Table 3.1**.

To investigate the *cis*-influence of the corrin ring, a study was recently carried out by Knapton to probe the *cis*-influence of the corrin ring by substitution of the H atom at C10 by Cl and NO. Stability constants of $[H_2O\text{-}(10\text{-}Cl)Cbl]^+$ with a variety of neutral and anionic ligands were determined and then compared with the results for $[H_2OCbl]^+$ under the identical experimental conditions. The data are tabulated in **Table 3.1.**

References on page 126

Table 3.1 Stability constants for the displacement of coordinated H_2O, in $[H_2OCbl]^+$ and $[H_2O$-(10-Cl)$Cbl]^+$.

Ligand	$[H_2OCbl]^+$		$[H_2O$-(10-Cl)$Cbl]^+$	
	log *K*	Reference	log *K*	Reference
NO_2^-	5.34 ± 0.03	13	5.52 ± 0.12	13
	5.3	19		
N_3^-	4.85 ± 0.13	13	4.97 ± 0.08	13
	4.74	19		
	4.61	20		
	4.75	20		
	4.9	21		
$S_2O_3^{2-}$	3.72 ± 0.02	13	4.35 ± 0.05	13
	3.76	20		
	3.86	22		
$NCSe^-$	3.77 ± 0.02	13	3.93 ± 0.03	13
	3.92	22		
SCN^-	3.03 ± 0.05	13	3.39 ± 0.18	13
	3.36	19		
	3.11	20		
	3.08	22		
OCN^-	2.57 ± 0.04	13	2.67 ± 0.07	13
	3.00	19		
	2.63	20		
	2.72	22		
Pyridine	1.23 ± 0.07	13	0.95 ± 0.09	13
Imidazole	4.63 ± 0.07	13	4.46 ± 0.19	13
	4.59	19		
CH_3NH_2	5.12 ± 0.08	13	4.82 ± 0.06	13
DMAP	3.99 ± 0.02	23	-	-

References on page 126

Comparison of the stability constants of $[H_2OCbl]^+$ with $[H_2O\text{-}(10\text{-}Cl)Cbl]^+$ showed that anionic ligands bind more strongly to $[H_2O\text{-}(10\text{-}Cl)Cbl]^+$ than to $[H_2OCbl]^+$ while the converse is true for neutral ligands. The data proved that modification of C10 position (i.e., a perturbation of the equatorial ligand) had an impact on the chemistry of the axial ligand of Co(III), showing that the *cis*-influence is not negligible in the chemistry of the Co(III) macrocycles.

The aim of this work was to further assess – and hence provide further evidence for - the *cis*-influence of the C10 position on the metal ion by substitution of the H atom on C10 by bromine which is more polarisable and less electronegative than chlorine. Then the results of the ligand binding properties of Co(III) in $[H_2O\text{-}(10\text{-}Br)Cbl]^+$, $[H_2OCbl]^+$ and in $[H_2O\text{-}(10\text{-}Cl)Cbl]^+$ are compared. Quantitatively, this was achieved by reacting $[H_2O\text{-}(10\text{-}Br)Cbl]^+$ with selected anionic and neutral ligands to obtain values of log *K*. On a qualitative level, this aim was achieved by observing the spectral changes for each reaction. Finally, these data are compared to analogous B_{12a} data in order to elucidate the effects of the substituent on C10 on the ligand binding properties of the Co(III) metal ion and hence further evaluate the importance of the *cis*-influence in these systems.

3.3.2 Results and Discussion

A stability constant is an equilibrium constant which provides a measure of the interaction between an incoming ligand and a metal in the formation of a complex; an example of this in this study is the formation of vitamin B_{12a} complexes with a variety of ligands, as shown in **Equation 1.1**.

$$DMB\text{–}Co\text{–}H_2O + L \overset{K}{\rightleftharpoons} DMB\text{–}Co\text{–}L + H_2O \qquad (\mathbf{1.1})$$

Stability constants (*K*) were determined spectroscopically as described in **Chapter 2, Section 2.5.3.1.** for substitution of axially coordinated H_2O of $[H_2O\text{-}(10\text{-}Br)Cbl]^+$, $[H_2O\text{-}(10\text{-}Cl)Cbl]^+$ and $[H_2OCbl]^+$ by a number of incoming ligands (L) which included anionic (N_3^-, NO_2^-, SCN^- and SO_3^{2-}) and neutral (imidazole and DMAP) ligands. Absorbance spectra for these ligand binding reactions were recorded and used in two separate approaches. Initially, spectra were qualitatively compared to observe any ligand-dependent spectral shifts. Secondly, changes in absorbance on titrating the cobalt corrin solution with a ligand were fitted to **Equation 2.3 or 2.4 (Chapter 2)**

References on page 126

using non-linear least squares fit methods to obtain log *K*. As already mentioned, the equilibrium constants with N_3^-, NO_2^-, SCN^- and imidazole have been reported before for $[H_2O\text{-}(10\text{-}Cl)Cbl]^+$and $[H_2OCbl]^+$ but in this study they were determined again under the identical experimental conditions, to ensure that all results are comparable. In addition, equilibrium constants with DMAP and SO_3^{2-} for $[H_2O\text{-}(10\text{-}Cl)Cbl]^+$ have been determined for the first time in this study.

3.3.2.1 The uv-vis Spectroscopic Changes of $[H_2O\text{-}(10\text{-}Br)Cbl]^+$ Toward Ligand Binding (Qualitative Investigation)

The reaction of $[H_2O\text{-}(10\text{-}Br)Cbl]^+$ with each of the ligands investigated here was recorded by uv-vis spectroscopy, and four significant bands were monitored for each ligand binding reaction (γ, *D*, β and α), as defined in **Figure 3.8**.

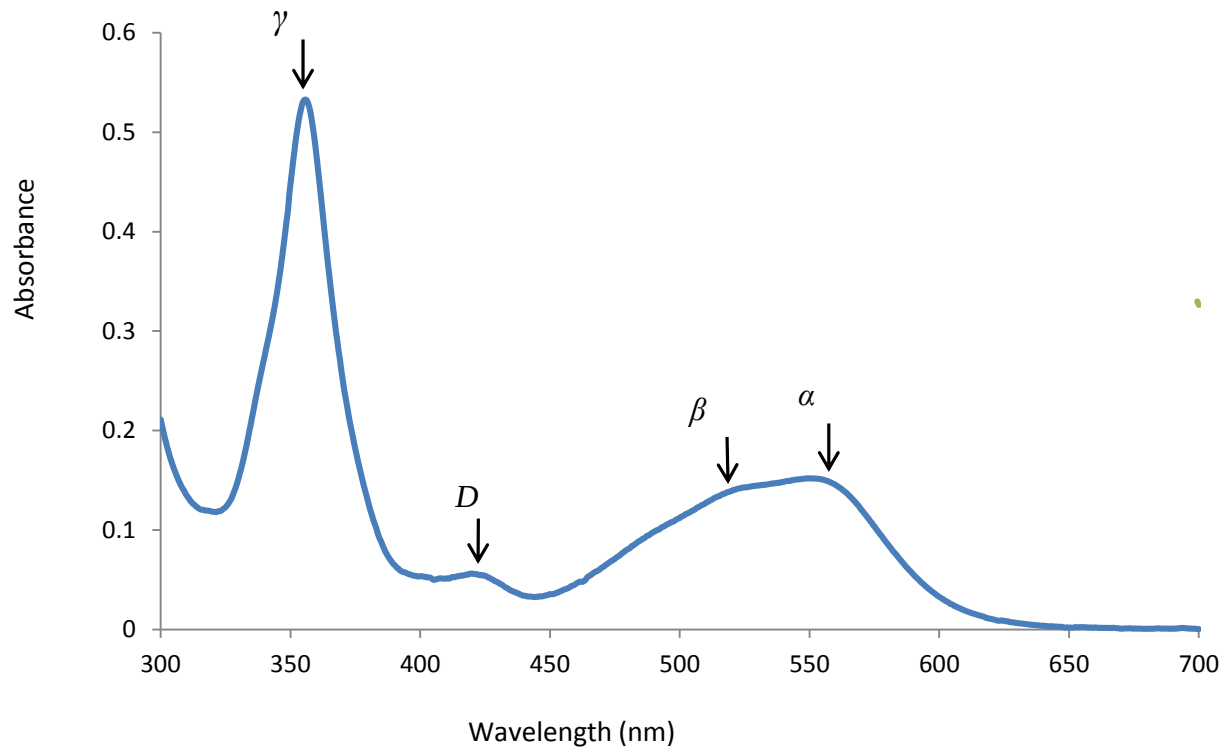


Figure 3.8 A uv-vis spectrum of $[H_2O\text{-}(10\text{-}Br)Cbl]^+$ in neutral pH at 25 ^oC.

References on page 126

The binding of anionic N- and S-donor ligands (N_3^-, NO_2^-, SCN^- and SO_3^{2-}) to $[H_2O\text{-}(10\text{-}Br)Cbl]^+$ yielded the spectra shown in **Figure 3.9**. The changes in the spectra as well as the isosbestic points are listed in **Table 3.2**. The details of the experimental procedures can be found in **Chapter 2, Section 2.5.3.1**.

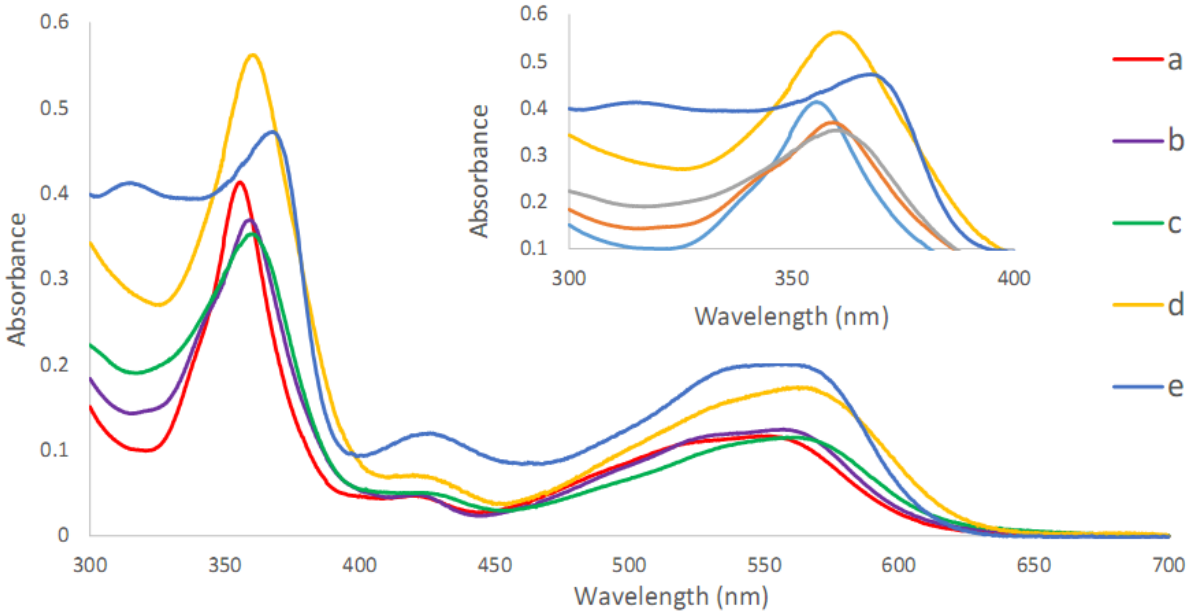


Figure 3.9 Absorption spectra of $[H_2O\text{-}(10\text{-}Br)Cbl]^+$, (a) in an aqueous solution of unbuffered neutral solution at 25 °C, in 1 cm pathlength cell, and in the presence of: (b) NO_2^-, (c) N_3^-, (d) SCN^- and (e) SO_3^{2-}.

References on page 126

Table 3.2 Shift in wavelength of the *γ*, *D*, *β* and *α* bands and isosbestic points on binding of anionic ligands to $[H_2O\text{-}(10\text{-}Br)Cbl]^+$.

Ligand	Wavelength (nm)				Isosbestic points (nm)
	γ	*D*	*β*	*α*	
H_2O (pH 6)	356	426	524	558	
H_2O (pH 7)	360	430	538	564	
NO_2^-	362	426	536	568	346, 360, 432, 519
N_3^-	362	433	532	571	350, 363, 546, 540
SCN^-	363	430	531	574	338, 363, 411, 575
SO_3^{2-}	371	430	538	576	346, 371, 479, 572

The binding of N_3^- to $[H_2O\text{-}(10\text{-}Br)Cbl]^+$ led to a decrease in intensity of the *γ* band at 357 nm, whereas the intensity of the *D* band increased at 426 nm. The *β* band at 524 nm decreased in intensity while the *α* band at 558 nm increased in intensity. For this binding reaction isosbestic points were observed at 350, 363, 546 and 540 nm, as illustrated in **Figure 3.10.**

References on page 126

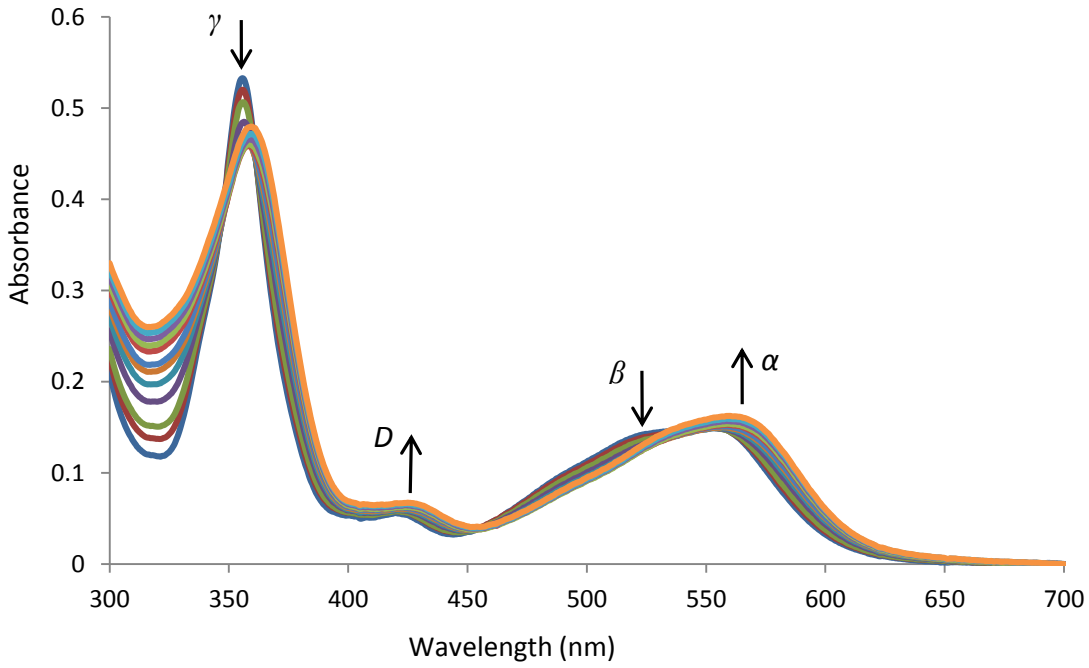


Figure 3.10 The absorbance changes observed for the binding of N_3^- to $[H_2O\text{-}(10\text{-}Br)Cbl]^+$.

In the case of the NO_2^- complex, the γ band at 357 nm decreased in intensity and *D* band remained unchanged. The β and α bands both increased in intensity at 525 and 560 nm, respectively. Isosbestic points were observed at 346, 360, 432 and 519 nm. The absorbance change spectrum can be found in **Appendix 3.1**.

For the binding of SCN^- (thiocyanate) there are two possibilities. The coordination of the ligand to the cobalt atom can occur either through the N or the S atom. It has been found that SCN^- is N-bound in the solid state,[3,24] however, NMR evidence showed that in solution it existed as a nearly equal mixture of two species which is assumed to be the N- and S- bound isothiocyanato and thiocyanato complexes.[13] There is also a report of a crystal structure of SCNCbl in which the SCN^- ligand is bound through S.[25] The uv-vis results obtained in this work showed that the intensity of the γ band decreased at 358 as well as the intensity of the *D* band at 428 nm. The β and α bands at 523 nm and 560 nm both decreased in intensity. Isosbestic points were observed at 338, 411, 575 and 363 nm **(Appendix 3.1).**

References on page 126

The binding of SO_3^{2-} led to an "atypical"[22] spectrum of $[H_2O\text{-}(10\text{-}Br)Cbl]^+$ as illustrated in **Figure 3.11**. The γ band at 360 nm decreased significantly in intensity and a shoulder appeared at 321 nm. The *D* band increased in intensity at 430 nm. The intensity of β and α bands at 538 and 564 nm both decreased. Isosbestic points were observed at 346, 371, 479 and 572 nm.

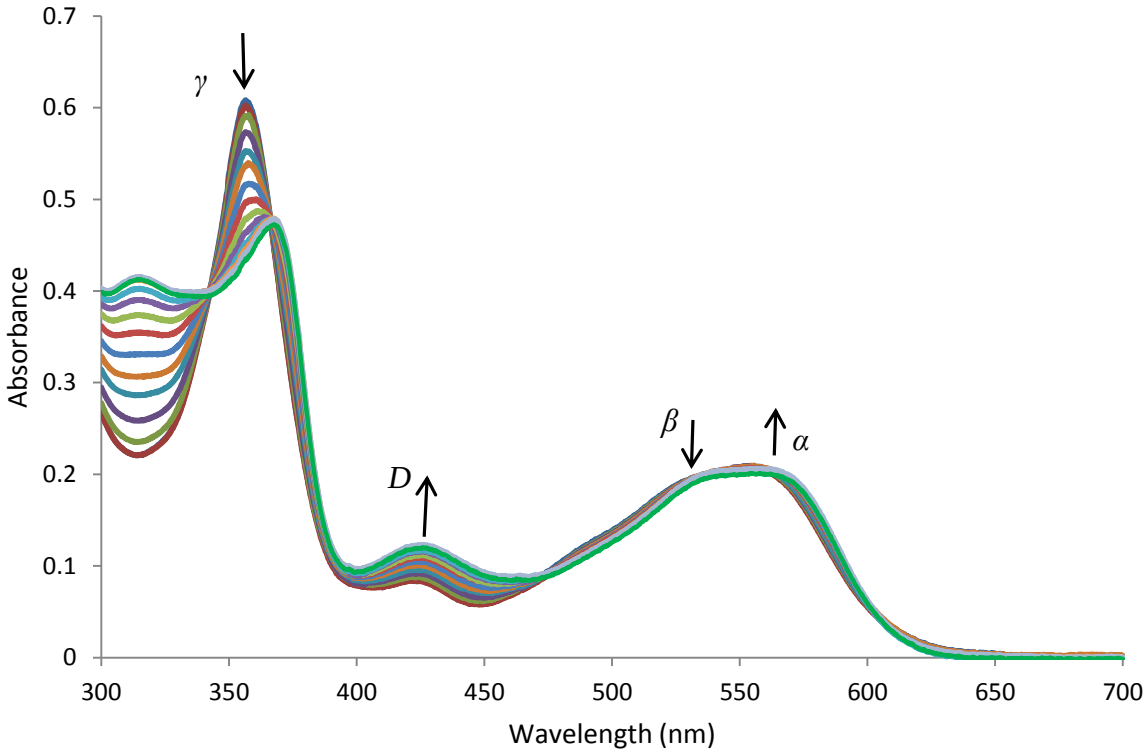


Figure 3.11 Spectroscopic changes associated with the binding of SO_3^{2-} to $[H_2O\text{-}(10\text{-}Br)Cbl]^+$.

Substitution of H_2O by anionic ligands in $[H_2O\text{-}(10\text{-}Br)Cbl]^+$ causes a bathochromic shift in the principal bands of the spectrum. In particular, γ, β and α bands underwent a red shift and the greatest shift was observed for the binding of SO_3^{2-} to $[H_2O\text{-}(10\text{-}Br)Cbl]^+$.

The binding of neutral ligands (DMAP and imidazole) to $[H_2O\text{-}(10\text{-}Br)Cbl]^+$ revealed virtually identical spectroscopic changes as observed when these ligands substituted H_2O in $[H_2OCbl]^+$ (**Appendix 3.1**). Binding of imidazole to $[H_2O\text{-}(10\text{-}Br)Cbl]^+$ caused the γ band to increase in

References on page 126

intensity and it shifted from 356 to 364 nm. The *D* band decreased slightly in intensity. The intensity of the *β* band at 528 nm also decreased, while the intensity of the *α* band at 565 nm increased, as illustrated in **Figure 3.12**. The isosbestic points were observed at 360, 402 and 563 nm.

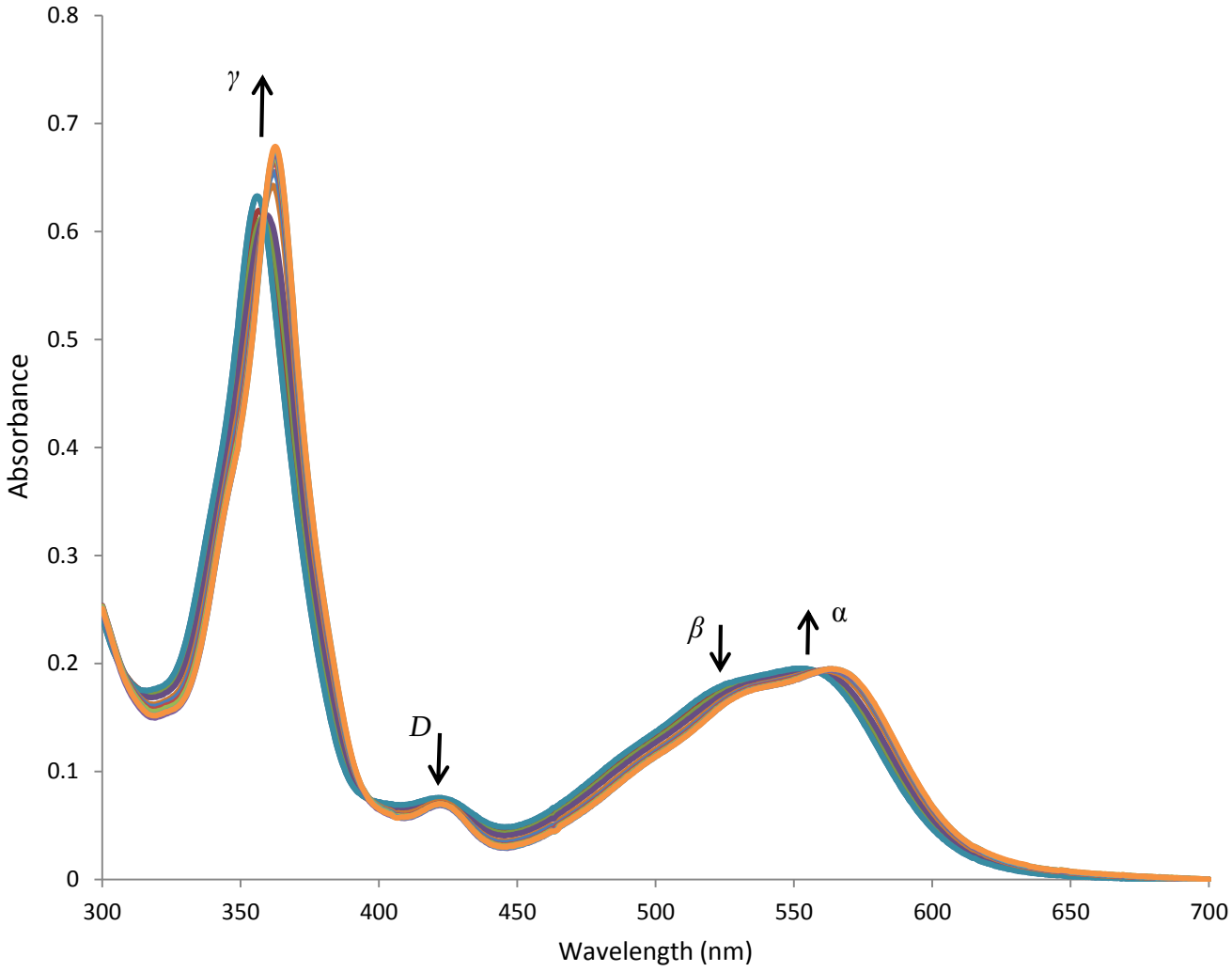


Figure 3.12 The spectral changes of binding of imidazole to the $[H_2O\text{-}(10\text{-}Br)Cbl]^+$.

References on page 126

Binding of DMAP to $[H_2O\text{-}(10\text{-}Br)Cbl]^+$ at pH 8.5 showed a large absorbance due to DMAP itself in the uv region around 310 nm. To overcome this, the same quantity of ligand was also added to the reference cuvette during the titration. In **Figure 3.13** the wavelength axis is only shown from 320 nm and the absorbance axis limited to 0.8 for convenience. The binding of DMAP to $[H_2O\text{-}(10\text{-}Br)Cbl]^+$ caused the γ band at 358 nm to increase in intensity and to shift to 367 nm. The *D* band also increased in intensity at 430 nm. The intensity of the β band at 534 nm decreased while the intensity of the α band increased at 566 nm; however only small changes were observed in the intensity of both β and α bands. Isosbestic points were observed at 432 and 564 nm.

In addition to these neutral ligands, methylamine, ethanolamine and ammonium nitrate were also tried but very slight spectroscopic changes were observed overnight which indicated that these reactions with $[H_2O\text{-}(10\text{-}Br)Cbl]^+$ were kinetically very slow. The stability constants for these reactions might be feasibly determined in an out-of-cell titration, but this was not investigated in this study. A summary of the shifts in the positions of the γ, *D*, β and α bands, and the isosbestic points on binding of neutral N- donor ligands to $[H_2O\text{-}(10\text{-}Br)Cbl]^+$ are given in **Table 3.3**.

Table 3.3 Shifts in γ, *D*, β and α bands and isosbestic points on ligand binding of neutral ligands to $[H_2O\text{-}(10\text{-}Br)Cbl]^+$.

Ligand	Wavelength (nm)				Isosbestic points (nm)
	γ	*D*	β	α	
H_2O (pH 7)	356	428	528	565	
H_2O (pH 8.5)	358	430	534	566	
Imidazole	364	429	535	572	360, 402, 563
DMAP	367	426	540	570	432, 564

References on page 126

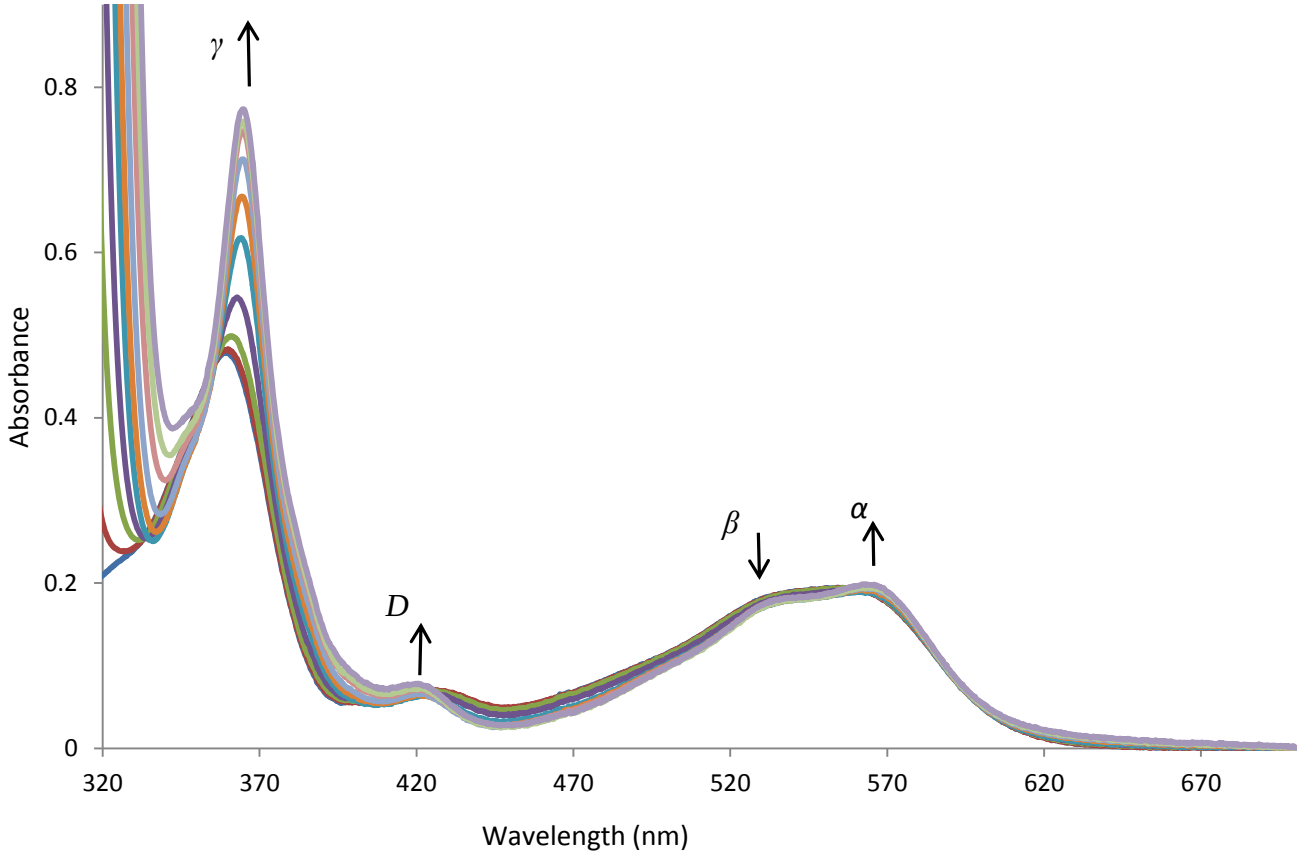


Figure 3.13 Spectroscopic changes associated with the binding of DMAP to $[H_2O\text{-}(10\text{-}Br)Cbl]^+$.

3.3.2.2 The uv-vis Spectroscopic Changes of $[H_2O\text{-}(10\text{-}Cl)Cbl]^+$ and $[H_2OCbl]^+$ Toward Ligand Binding (Qualitative Investigation)

Spectroscopic changes of the binding of variety of neutral and anionic ligands to $[H_2O\text{-}(10\text{-}Cl)Cbl]^+$ and $[H_2OCbl]^+$ were recorded by uv-vis spectroscopy. Although all the spectroscopic data for these compounds are available in the literature, they were determined under the identical conditions as the data obtained for $[H_2O\text{-}(10\text{-}Br)Cbl]^+$. Anionic N- and S-donor ligands (N_3^-, NO_2^-, NCS^- and SO_3^{2-}) and neutral N-donor ligands (imidazole and DMAP) bound to $[H_2O\text{-}(10\text{-}Cl)Cbl]^+$ and $[H_2OCbl]^+$ to yield similar-looking spectra to the spectrum of $[H_2O\text{-}(10\text{-}Br)Cbl]^+$ itself. For all cases a bathochromic shift was observed and the intensity of the *γ*, *D*, *β* and *α* bands either increased or decreased depending on the nature of the ligand. A summary of the shift in wavelength of *γ*, *D*, *β* and *α* bands and isosbestic points on binding of the ligands to $[H_2O\text{-}(10\text{-}Cl)Cbl]^+$ and $[H_2OCbl]^+$ are given in **Table 3.4** and **Table 3.5**, respectively. All the spectroscopic

References on page 126

changes associated with the binding of neutral and anionic ligands to $[H_2O\text{-}(10\text{-}Cl)Cbl]^+$and $[H_2OCbl]^+$ can be found in **Appendix 3.1**.

Table 3.4 Shift in wavelength of *γ*, *D*, *β* and *α* bands and isosbestic points on binding of anionic and neutral ligands to $[H_2O\text{-}(10\text{-}Cl)Cbl]^+$.

Ligand	Wavelength (nm)				Isosbestic points (nm)
	γ	*D*	*β*	*α*	
H_2O (pH 6)	356	424	520	559	
H_2O (pH 7)	357	425	528	561	
H_2O (pH 8.5)	357	430	534	566	
NO_2^-	360	424	530	561	347, 360, 408, 526
N_3^-	360	430	536	568	350, 363, 546, 540
NCS^-	361	427	558	574	338, 363, 411, 575
SO_3^{2-}	370	427	539	575	346, 371, 479, 572
Imidazole	362	429	535	572	360, 402, 563
DMAP	367	426	534	570	432, 564

References on page 126

Table 3.5 Shift in wavelength of *γ*, *D*, *β* and *α* bands and isobestic points on binding of anionic ligands to $[H_2OCbl]^+$.

Ligand	Wavelength (nm)				Isosbestic points (nm)
	γ	*D*	*β*	*α*	
H_2O (pH 6)	352	414	498	531	
H_2O (pH 7)	353	417	504	534	
H_2O (pH 8.5)	353	422	510	536	
N_3^-	360	424	516	544	343, 442, 534
NCS^-	359	420	515	547	337, 398, 545
SO_3^{2-}	366	418	516	542	341, 463, 504, 528
Imidazole	359	418	512	544	328, 354, 511, 535
DMAP	361	418	514	545	346, 421, 560

3.3.2.3 Conclusion

The results presented in **Table 3.6** show that when the H atom at the C10 position is replaced by Br, all the bands in $[L\text{-}(10\text{-}Br)Cbl]^{n+}$ shift to lower energies (L is any of the investigated ligand as shown in **Figure 3.9**); the same result was observed for $[L\text{-}(10\text{-}Cl)Cbl]^{n+}$. This implies that the substitution of the C10 position by an electron donating group such as Br causes an increase in the electronic density of the delocalised π electron system of the corrin ring and a decrease in the HOMO-LUMO gap.

References on page 126

Table 3.6 Summary of the position of the principal bands in the uv-vis spectrum of complexes of $[LCbl]^{n+}$ and the 10-Cl and 10-Br analogues.

L	$[LCbl]^{n+}$			$[L\text{-}(10\text{-}Cl)Cbl]^{n+}$			$[L\text{-}(10\text{-}Br)Cbl]^{n+}$		
	γ/ nm	β/ nm	α/ nm	γ/ nm	β/ nm	α/ nm	γ/ nm	β/ nm	α/ nm
H_2O	351	527	554	355	536	558	356	539	555
N_3^-	357	523	546	360	543	565	359	547	563
NO_2^-	356	504	535	360	530	559	360	527	560
SO_3^{2-}	364	525	548	367	550	570	370	540	568
NCS^-	360	517	550	362	540	575	363	545	575
Imidazole	358	520	545	361	544	574	363	544	574
DMAP[a]	362	514	547	366	542	572	367	541	572

[a] *N*,*N*-dimethylaminopyridine.

Comparison of $[LCbl]^{n+}$ and $[L\text{-}(10\text{-}Br)Cbl]^{n+}$ (where L is the axial ligand) spectra revealed that the electronic spectra of these compounds closely parallel each other ($R^2 = 0.92$, for the γ band). **Figure 3.14** shows this correlation where the plot of γ band is shown. from the observations in this study are in the agreement with the results of $[L\text{-}(10\text{-}Cl)Cbl]^{n+}$.[4] It has been concluded from both studies that there is a direct electronic communication between the axial coordination site of the metal and the equatorial macrocycle (corrin ring). Therefore it is reasonable to suppose that perturbation of the electronic structure of the corrin ring will materially affect the chemistry of the axial coordination site of Co(III) in the cobalt corrins.

References on page 126

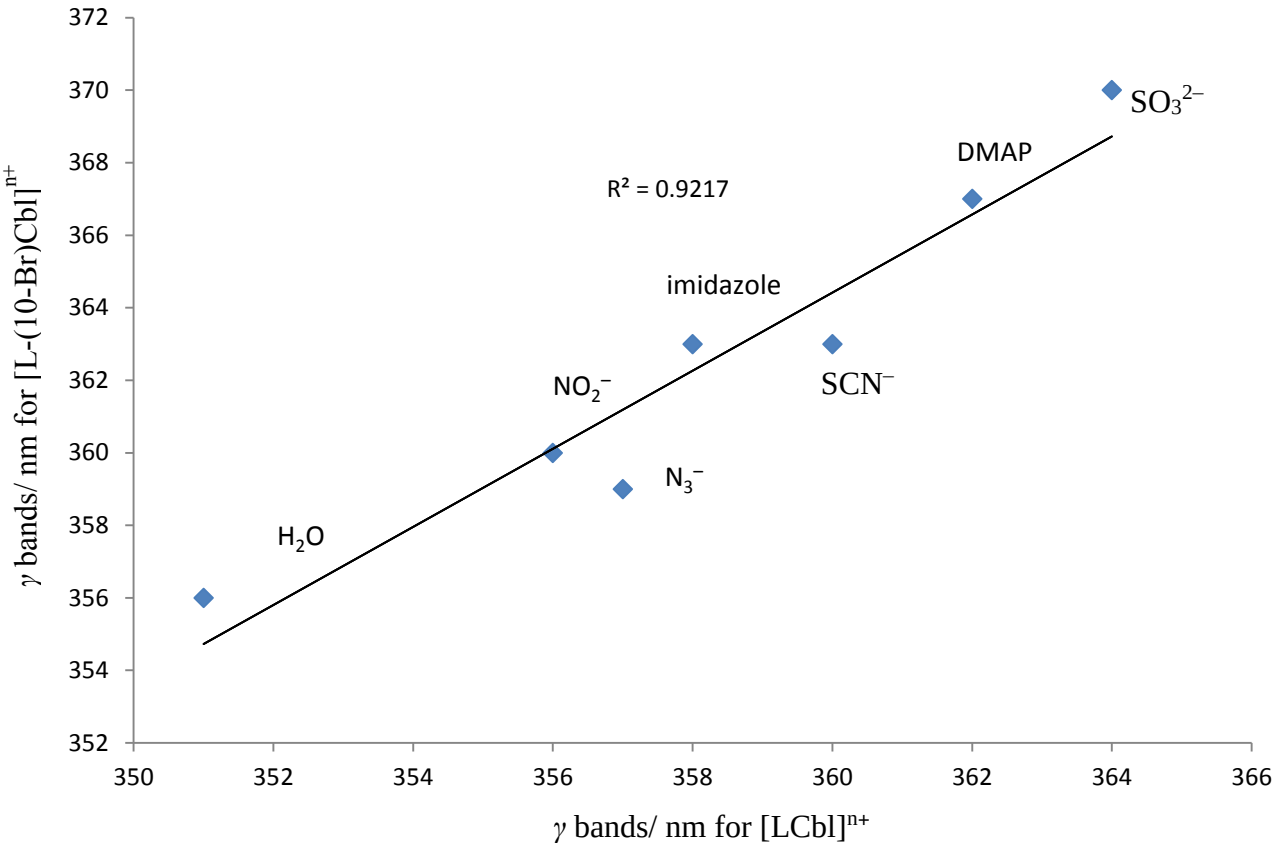


Figure 3.14 Relationship between the γ bands of both $[LCbl]^{n+}$ and $[L\text{-}(10\text{-}Br)Cbl]^{n+}$ ($R^2 = 0.92$).

3.3.2.4 Determination of Stability Constants (Quantitative Investigation)

The stability constants were determined for the binding of various neutral and anionic ligands to $[H_2O\text{-}(10\text{-}Br)Cbl]^+$, $[H_2O\text{-}(10\text{-}Cl)Cbl]^+$ and $[H_2OCbl]^+$ (**Equation 1.1**), in an aqueous multicomponent buffer system and the ionic strength was adjusted to 0.5 M. Others have suggested that the ideal solvent system for the study of vitamin B_{12} which most closely mimics the biological environment of B_{12} is a multi-component system containing more non-polar solvent, such as methanol.[17] However, using such a solvent system precludes the study from being done at higher temperatures because of the volatility of the solvent. Hence all the work reported here was done in an aqueous medium.

The stability constants were determined by fitting the absorbance data obtained during the titrations to **Equation 2.3** (where log K is < 4) or **Equation 2.4** (where log K is > 4), and are

References on page 126

reported in **Table 3.7**. An example of a fit for titration of $[H_2O\text{-}(10\text{-}Br)Cbl]^+$ with N_3^- is shown in **Figure 3.15.**

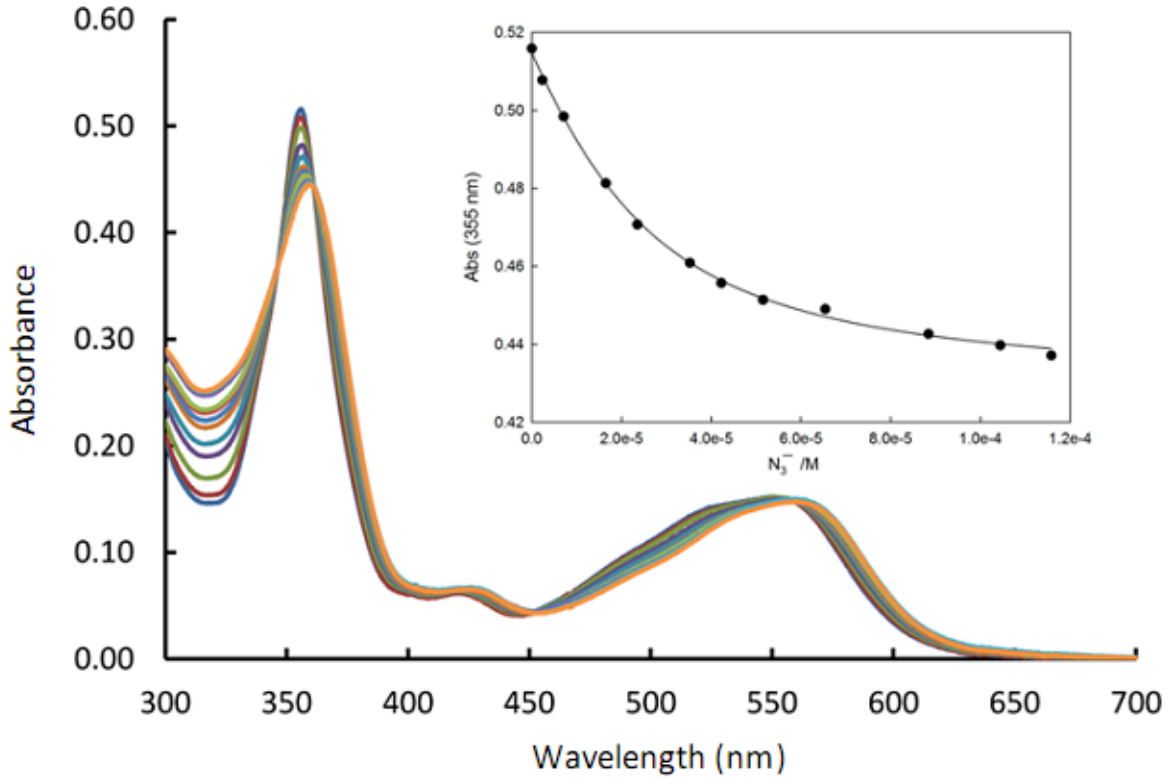


Figure 3.15 Changes in the uv-vis spectrum on substituting coordinated H_2O in $[H_2O\text{-}(10\text{-}Br)Cbl]^+$ by N_3^- at 25 ºC, pH 6.5. The insert shows a fit of the absorbance change at 355 nm to the binding isotherm given by **Equation 2.4** of the text.

References on page 126

Table 3.7 Stability constants (as log *K* values) for the substitution of coordinated H_2O in $[H_2O\text{-}(10\text{-}Z)Cbl]^+$ (Z = H, Cl, Br) by an exogenous ligand L.[a,b]

L	$[H_2OCbl]^+$	$[H_2O\text{-}(10\text{-}Cl)Cbl]^+$	$[H_2O\text{-}(10\text{-}Br)Cbl]^+$	$\Delta K = \log K_{10H} - \log K_{10Z}$ [c]		
				Z=Cl	Z=Br	Average Δ
$S_2O_3^{2-}$	*3.72(2)*	*4.35(5)*		*-0.63*		-0.63
SO_3^{2-}	4.10(8)	4.45(7)	4.72(7)	-0.35	-0.62	-0.49
NO_2^-	5.32(6)	5.47(24)	5.83(13)	-0.08	-0.58	-0.28
	5.34(3)	*5.52(12)*		*-0.18*		
SCN^-	3.21(3)	3.29(6)	3.26(4)	-0.08	-0.05	-0.16
	3.03	*3.39*		*-0.36*		
$SeCN^-$	*3.77(2)*	*3.93(3)*		*-0.16*		-0.16
N_3^-	4.68(7)	4.85(3)	4.84(6)	-0.17	-0.16	-0.15
	4.85(13)	*4.97(8)*		*-0.12*		
CNO^-	*2.57(4)*	*2.67(7)*		*-0.10*		-0.10
Imidazole	4.63(2)	4.32(7)	4.27(5)	0.31	0.36	0.28
	4.63(7)	*4.46(19)*		*0.17*		
pyridine	*1.23(7)*	*0.95(9)*		*0.28*		0.28
DMAP [d]	3.76(18)	3.47(19)	3.47(21)	0.29	0.29	0.29
CH_3NH_2	*5.12(8)*	*4.82(6)*		*0.30*		0.30

[a] See **Equation 1.1** . [b] Values in italics from Knapton & Marques;[4] all others from this work. [c] Difference in log *K* values when the C10 position is occupied by H and when it is occupied by Z = Cl or Br. [d] *N*,*N*-dimethylaminopyridine.

References on page 126

The results show that anionic ligands bind more strongly to $[H_2O\text{-}(10\text{-}Br)Cbl]^+$ than to $[H_2OCbl]^+$ with log *K* values between 0.05 and 0.62 (average 0.33) larger. It was also reported by Knapton[13] that the substitution of the C10 position by Cl favoured the coordination of anionic ligands with log *K* values between 0.1 and 0.63 (average 0.26) larger than $[H_2OCbl]^+$. So our findings are in good agreement with the previous study. There is a linear correlation between the log *K* values of $[H_2O\text{-}(10\text{-}Br)Cbl]^+$ and $[H_2OCbl]^+$, as illustrated in **Figure 3.16.** Hence, the behaviour of these ligands towards Co(III) is, unsurprisingly, similar. The same trend was observed when comparing the log *K* values for $[H_2O\text{-}(10\text{-}Br)Cbl]^+$ and those for $[H_2O\text{-}(10\text{-}Cl)Cbl]^+$ (**Figure 3.17**).

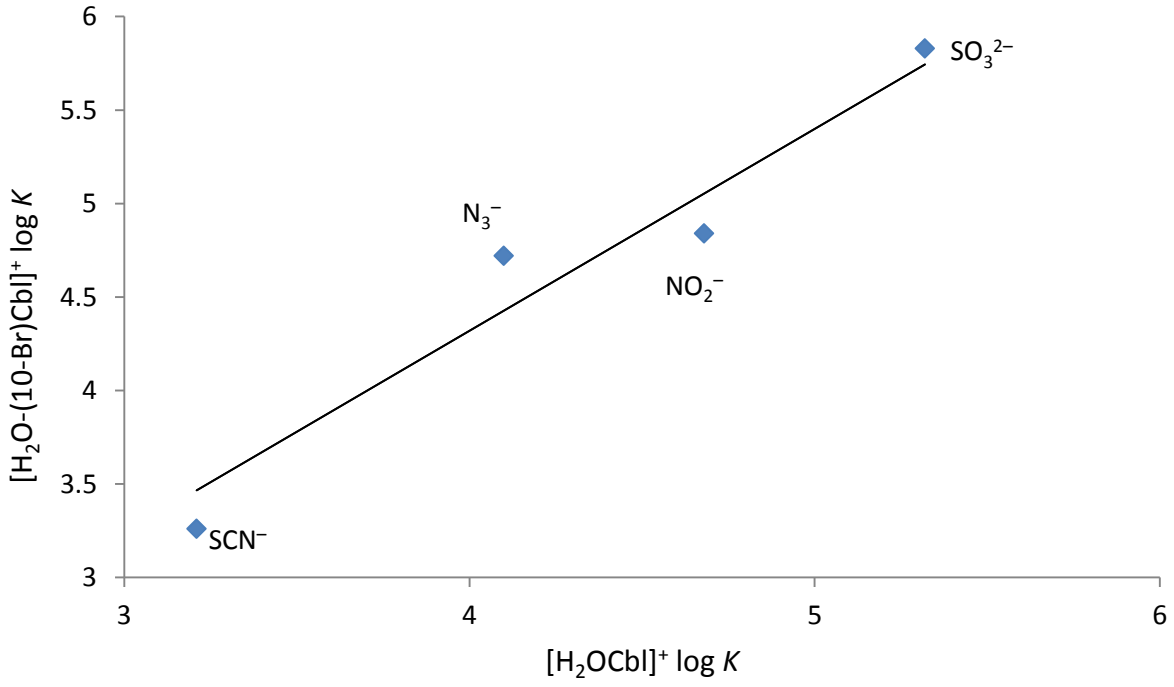


Figure 3.16 The correlation between the stability constants for $[H_2O\text{-}(10\text{-}Br)Cbl]^+$ and $[H_2OCbl]^+$ complexes with anionic ligands.

References on page 126

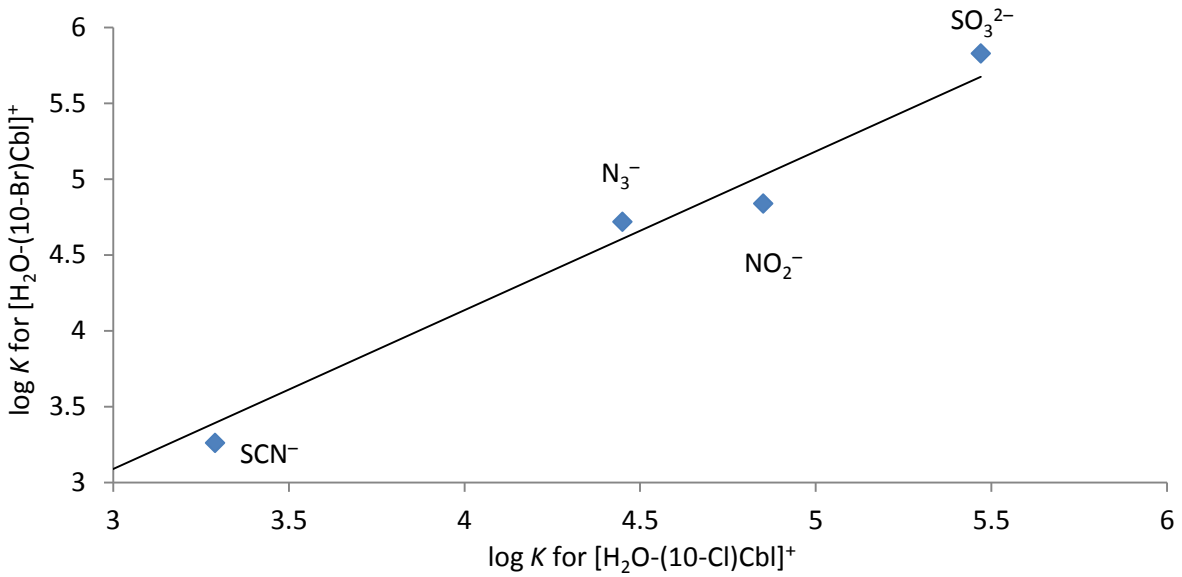


Figure 3.17 The correlation between the stability constants for $[H_2O\text{-}(10\text{-}Br)Cbl]^+$ and $[H_2O\text{-}(10\text{-}Cl)Cbl]^+$ complexes with anionic ligands.

The neutral ligands (imidazole and DMAP) bind less strongly to $[H_2O\text{-}(10\text{-}Br)Cbl]^+$ than to $[H_2OCbl]^+$ with log *K* values between 0.29 and 0.36 (average 0.33) smaller. It was reported in the previous study[13] that neutral ligands (methylamine, pyridine, imidazole) binds less strongly to $[H_2O\text{-}(10\text{-}Cl)Cbl]^+$than to $[H_2OCbl]^+$ with log *K* between 0.17 and 0.3 (average 0.25) smaller. These observations were similar to the previous observations.[13] To help rationalise these observations, the charge distribution in the DFT models of a representative complex with a neutral (H_2O) and an anionic (N_3^-) ligand was employed, see **Section 3.4**.

References on page 126

3.3.2.5 Conclusion

The spectroscopic changes observed on the binding of ligands to $[H_2O\text{-}(10\text{-}Br)Cbl]^+$ were similar for the same class of ligands for both $[H_2OCbl]^+$ and $[H_2O\text{-}(10\text{-}Cl)Cbl]^+$. For both $[H_2O\text{-}(10\text{-}Br)Cbl]^+$ and $[H_2O\text{-}(10\text{-}Cl)Cbl]^+$, all the bands shifted to lower energies (red-shifted) compared to $[H_2OCbl]^+$. The halogen substituents Br and Cl at the C10 position, although categorised as σ withdrawing, also have π donor character toward the π system of corrin; this explains the red shift in the spectra of $[H_2O\text{-}(10\text{-}Br)Cbl]^+$ and $[H_2O\text{-}(10\text{-}Cl)Cbl]^+$ presumably because of a narrowing of the HOMO–LUMO gap (see **Chapter 1**, **Section 1.6**), as transitions with predominantly $\pi\rightarrow\pi^*$ character dominate the electronic spectrum of the cobalt corrins.

Substitution of the C10 H by Br had a similar effect as the substitution of H by Cl on the stability constants of $[H_2O\text{-}(10\text{-}Br)Cbl]^+$ with a representative set of anionic and neutral ligands. In the case of $[H_2O\text{-}(10\text{-}Br)Cbl]^+$ anionic ligands were found to bind more strongly while the opposite is true for neutral ligands. Similar observations were reported in the case of $[H_2O\text{-}(10\text{-}Cl)Cbl]^+$, which indicates that cobalt atom behaves in a similar fashion towards ligand binding in both $[H_2O\text{-}(10\text{-}Br)Cbl]^+$ and $[H_2O\text{-}(10\text{-}Cl)Cbl]^+$, and serves to confirm the previous results.

3.4 QTAIM Calculations

QTAIM calculations were used to gain insight into the nature of the bonding between the metal and its ligands in $[H_2O\text{-}(10\text{-}Z)Cbl]^+$, based on the value of ρ, the electron density at the bond critical point. Simplified DFT models of $[H_2O\text{-}(10\text{-}Z)Cbl]^+$ with Z = H, Cl, Br and $[N_3\text{-}(10\text{-}Z)Cbl]$ with Z = H, Cl, Br are shown in **Figure 3.18**.

The electron density at the bond critical point of a bond, ρ, indicates the strength of a bond between two atoms.[10] An increase in ρ is indicative of increase in the bond strength, and is usually accompanied by a decrease in the bond length. The ratio of the potential and the kinetic energy densities at a bond critical point, $|V(r)|/G(r)$, can be used to characterise the nature of a chemical bond.[10] A bond is characterised as ionic if $|V(r)|/G(r) < 1$, covalent if $|V(r)|/G(r) > 2$ or of intermediate character if $1 < |V(r)|/G(r) < 2$.[26] From the data in **Table 3.8**, it is clear that all of the metal-ligand bonds are of intermediate character; however the $Co–N_{ax}$ bond presents with a more

References on page 126

covalent character than the Co–OH_2 bond as might be expected, given that aromatic N-donor ligands are better ligands for Co(III) in the cobalt corrins than H_2O.

The DFT calculations on models of [X-(10-Z)Cbl]$^{n+}$, X = H_2O or N_3^-, *n* = 1 or 0, confirmed that as Z is changed from H to Cl to Br, the charge on the metal ion becomes less positive (**Table 3.8**), although the effect is very small. It is suggested that the trends rather than the actual numerical values are indicative and informative. Simultaneously, the charge on the axial ligands becomes more negative (the order is H < Br ≈ Cl for the negative charge on O of axial H_2O but H < Cl = Br for the negative charge on the N of axial imidazole). A similar trend is evident in the DFT models of the azido complexes (**Table 3.8**); Co becomes less positive as Z is varied from H to Cl to Br; the negative charge on the N donor of N_3^- increases monotonically; and the negative charge on the N donor of axial imidazole also increases (now H < Br ≈ Cl).

Knapton[4] investigated the partial charge on Co and oxygen atoms in [H_2OCbl]$^+$ and [H_2O-(10-Cl)Cbl]$^+$ using the ZINDO/1 model. It was found that in [H_2OCbl]$^+$ the partial charges on the oxygen and cobalt atoms were –0.342 and 0.004e, while the partial charges for oxygen and cobalt in [H_2O-(10-Cl)Cbl]$^+$ were –0.340 and –0.009e, respectively. This confirmed that the cobalt atom was more negative in [H_2O-(10-Cl)Cbl]$^+$ than in [H_2OCbl]$^+$ due to the Cl atom at the C10 position. The partial charge on the chlorine atom in [H_2O-(10-Cl)Cbl]$^+$ and [OH-(10-Cl)Cbl] was also investigated and found to be –0.266 and –0.298e, respectively. Thus, the Cl at the C10 position acts as an electron donor to the corrin ring when the charge on the metal atom is quite low but also accommodates any charge increase in the system.

References on page 126

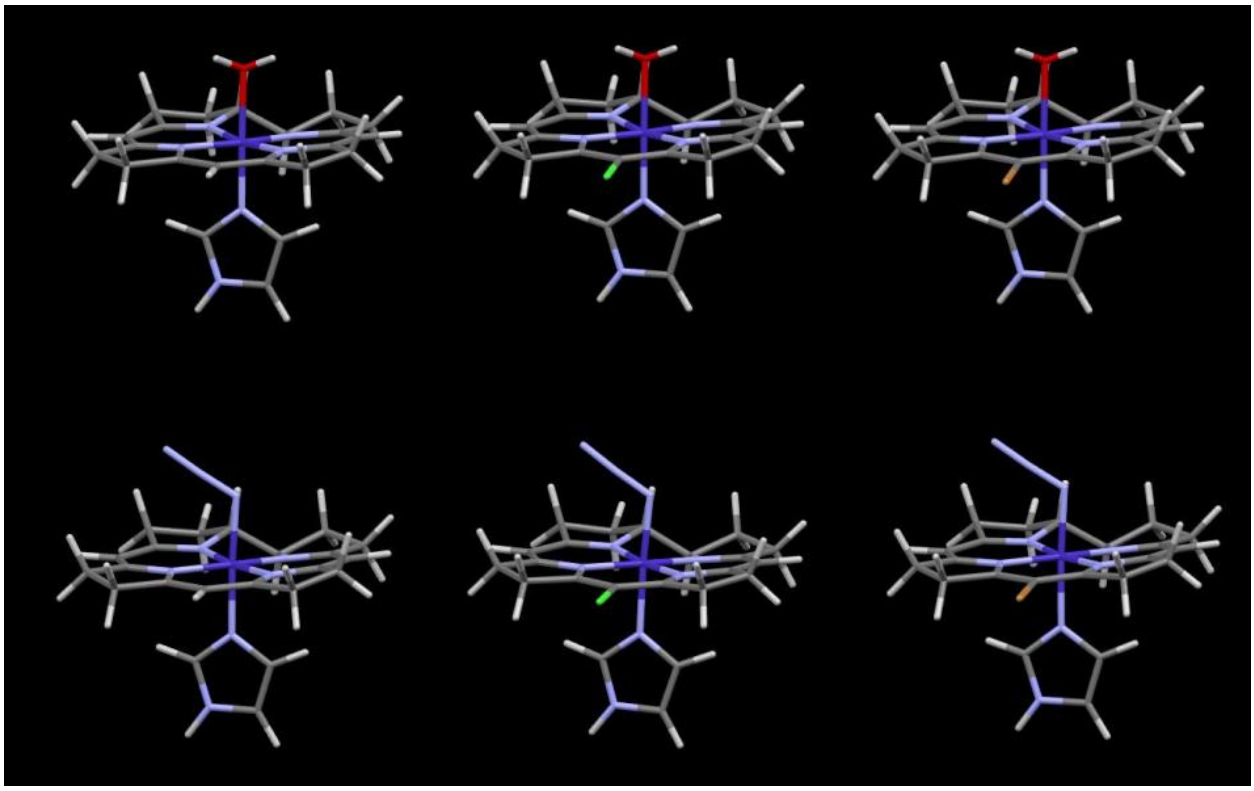


Figure 3.18 Energy-minimised DFT models of (top) $[H_2O\text{-}(10\text{-}Z)Cbl]^+$ with (left to right) Z = H, Cl, Br; and (bottom) $[N_3\text{-}(10\text{-}Z)Cbl]$ with (left to right) Z = H, Cl, Br.

References on page 126

Table 3.8 Axial bond lengths and QTAIM properties at the bond critical point in DFT models of [L-(10-Z)Cbl]$^{n+}$, X = H_2O or N_3^-, *n* = 1 or 0, Z = H, Cl or Br [a].

[H_2O-(10-Z)Cbl]$^+$					**[N_3-(10-Z)Cbl]**				
Co–OH_2					**Co–N_3**				
Z	**/Å**	***ρ***	**$\nabla^2\rho$**	***|V|/G***	**Z**	**/Å**	***ρ***	**$\nabla^2\rho$**	***|V|/G***
H	2.087	0.05791	0.31489	1.08994	H	1.969	0.09525	0.30233	1.25543
Cl	2.095	0.05684	0.3064	1.09049	Cl	1.969	0.09545	0.30154	1.25693
Br	2.094	0.05693	0.30698	1.09058	Br	1.969	0.09545	0.30146	1.25699
Co–N_{ax}					**Co–N_{ax}**				
Z	**/Å**	***ρ***	**$\nabla^2\rho$**	***|V|/G***	**Z**	**/Å**	***ρ***	**$\nabla^2\rho$**	***|V|/G***
H	1.898	0.11132	0.44908	1.20569	H	1.999	0.08556	0.3716	1.16999
Cl	1.897	0.11157	0.44792	1.20736	Cl	2	0.08552	0.36933	1.17138
Br	1.897	0.11155	0.44819	1.20712	Br	2	0.08551	0.36933	1.1713
Bader charges, q /e					**Bader charges, q /e**				
Z	**Co**	**O**	**N_{ax}**		**Z**	**Co**	**N (N_3^-)**	**N_{ax}**	
H	1.2084	-1.0535	-1.0027		H	1.1794	-0.2857	-1.0106	
Cl	1.2078	-1.0555	-1.0035		Cl	1.1791	-0.2860	-1.0122	
Br	1.2074	-1.0551	-1.0035		Br	1.1789	-0.2863	-1.0120	
Corrin fold angle					**Corrin fold angle**				
Z	**/deg**				**Z**	**/deg**			
H	5.15				H	7.12			
Cl	5.58				Cl	7.18			
Br	6.03				Br	7.8			

References on page 126

DFT calculations were used to interpret the data from the stability constant studies. Three effects were noted on changing Z from H to Cl or Br. Firstly, the positive charge on Co decreases; the metal becomes more electron rich and δ_{Co}(Z–H) becomes more negative. This effect is somewhat more pronounced if the β axial ligand is neutral H_2O rather than anionic N_3^-. Secondly, the substitution at C10 also causes an increase in the negative charge on the donor atom, D (δ_D(Z-H) becomes more negative); again this is more significant with a neutral than an anionic axial ligand. Finally, replacing neutral H_2O by anionic N_3^- causes the charge on Z to become more negative (δ_Z(*a*-*n*) is negative, and significantly more so if Z is Cl or Br than if Z is H).

This therefore suggests that $[H_2O\text{-}(10\text{-}Z)Cbl]^+$, Z = Cl or Br, will discriminate against a neutral ligand because the metal is more electron rich and will be less capable of accepting charge donation from the axial donor. If the ligand is an anion, however, the charge donation can be accepted by delocalisation onto the C10 Cl or Br; the C10 substituent acts as a charge reservoir for the additional charge. Anions are therefore bound more favourably by $[H_2O–(10\text{-}Z)Cbl]^+$, Z = Cl or Br, than by $[H_2OCbl]^+$ itself. Knapton[4] also reported that the cobalt atom in $[H_2O\text{-}(10\text{-}Cl)Cbl]^+$ was more electron rich than it was in $[H_2OCbl]^+$ and thus less likely to accept more electron density from the neutral ligands. This was the rationalisation advanced why the stability constants for the binding of neutral ligands to $[H_2O\text{-}(10\text{-}Cl)Cbl]^+$ were lower.

The differential stability of anionic ligands with the 10-Cl and 10-Br derivatives of $[H_2OCbl]^+$ offers an explanation for the lower pK_a values of these compounds (7.22 and 7.28) compared to $[H_2OCbl]^+$ (7.62, see **Section 3.2.1**). If the anionic ligand OH^- coordinates preferentially to the 10-Cl and 10-Br derivatives, then it will be a poorer Lewis base towards H^+. Similar observations were reported by Knapton[4] regarding the lower pK_a for the coordinated H_2O in $[H_2O\text{-}(10\text{-}Cl)Cbl]^+$ than in $[H_2OCbl]^+$: the charge on the O atom is lower in $[H_2O\text{-}(10\text{-}Cl)Cbl]^+$ hence OH^- is a poor Lewis base towards H^+.

3.4.1 Conclusion

DFT calculations were carried out on simplified DFT models of $[H_2O\text{-}(10\text{-}Z)Cbl]^+$ with Z = H, Cl, Br; and $[N_3\text{-}(10\text{-}Z)Cbl]$ with Z = H, Cl, Br. The QTAIM analyses verified that the substitution of the C10 position by Br or Cl led to a decrease on the positive charge of Co, and it became more electron rich. This rationalises why both complexes ($[H_2O\text{-}(10\text{-}Br)Cbl]^+$ and $[H_2O\text{-}(10\text{-}Cl)Cbl]^+$)

References on page 126

favoured the binding of anionic ligands and conversely discriminated against the binding of neutral ligands compared to $[H_2OCbl]^+$ itself.

The QTAIM analyses also verified that the substitution of the C10 position by Br caused the negative charge on O atom increases; thus the acidity of the axial H_2O ligand increases marginally, resulting in lower pK_a compare to the pK_a of $[H_2OCbl]^+$.

3.5 X-ray Crystallography of $[H_2O$-(10-Br)Cbl$]^+$ and $[N_3$-(10-Br)Cbl$]$

As mentioned in **Chapter 2, Section 2.6.1,** crystals of $[H_2O$-(10-Br)Cbl$]^+$ and azido-10-bromocobalamin ($[N_3$-(10-Cl)Cbl]) were obtained by vapour diffusion of acetone into aqueous solutions of the compounds. However it is unfortunate that the crystals of $[H_2O$-(10-Br)Cbl$]^+$ diffracted poorly, and that, despite several attempts, we were unable to produce better quality crystals. The structure contains one phosphate anion (presumably as HPO_4^{2-} for charge neutrality, although we were unable to locate the proton) per pair of $[H_2O$-(10-Br)Cbl$]^+$ ions in the asymmetric unit; this resulted in the compound crystallising in a triclinic rather than the usual orthorhombic space group (**Figure 3.19**). This low symmetry cell and small crystals exacerbated the data collection problem. The metrics obtained from the structure have to be treated with caution. The data of crystallography can be found in **Appendix 2.7**.

The Co–OH_2 bond length (1.933(7) Å and 1.943(8) Å in the two molecules in the asymmetric unit) is marginally shorter, although not statistically significantly different, to that found in the crystal structure of $[H_2OCbl]^+$ itself (1.952 Å)[27] and to that found in $[H_2O$-(10-Cl)Cbl$]^+$ (1.948 Å).[1] The Co–N_{ax} bond to the N-donor of axial 5,6-dimethylbenzimidazole (DMB) is significantly longer in the 10-Br and 10-Cl derivatives (1.975 and 1.961 Å; 1.967 Å,[1] respectively) than in $[H_2OCbl]^+$ itself (1.925 Å[27]). Given the well-established *trans*-influence in the cobalt corrins,[28,29] this suggests that the Co–OH_2 bond is stronger in the 10-Br and 10-Cl derivatives than in $[H_2OCbl]^+$ itself. The Co–N bond lengths to the corrin N-donors in the 10-Br and 10-Cl derivatives are somewhat longer than in $[H_2OCbl]^+$ (**Table 3.9**); the corrin cavity has expanded and the corrin fold angle (the angle between the mean planes defined by N21, C4, C5, C6, N22, C9, C10 and C10, C11, N23, C14, C15, C16, N24)[30] is somewhat larger. There are therefore some structural changes to the corrin on replacing the C10 H with Cl or Br.

References on page 126

The crystal structure of the azido complex is, by contrast, a much higher quality structure with a relatively low *R* factor (6.36%; only 31 of the 104 cobalamin structures listed in the CSD[6] have a lower *R* factor). Like the majority of cobalamin structures (88.6% of those in the CSD), it crystallised in the orthorhombic space group $P2_12_12_1$. [N_3-(10-Br)Cbl] co-crystallised with two equivalents of NaN_3, three acetone and five solvent H_2O molecules in the asymmetric unit (**Figure 3.19**). The Co–N_3^- bond length is 1.942(6) Å, while Co–N_{ax}, the bond between Co(III) and the axial base, is 1.974(6) Å. In the structure of N_3Cbl itself (co-crystallised with LiCl, *R* = 5.13%, 100 K) the values are 1.984(3) and 1.999(3) Å, respectively.[31] (There is an older structure[32] but it is of poor quality, *R* = 20.0%, collected at 293 K, and can be ignored). In contrast to the aqua complex, the azido complex of 10-Br has shorter bond lengths to the two axial ligands compared to the analogous complex of the normal cobalamin. By contrast, the Co–C bond length in cyano-10-chlorocobalamin ([CN-(10Cl)Cbl]) is longer than in ([CNCbl]) itself (1.97(2) Å, compared to 1.867(7),[33] 1.877(2)[34] and 1.886(4) Å[33]), while the Co–N_{ax} bond lengths are very similar (2.04(7) Å; 2.029(5), 2.028(2) and 2.041(3) Å, respectively). In methyl-10-chlorocobalamin ([Me-(10Cl)Cbl]), the Co–C bond length, 1.979(7) Å, is similar to that in methylcobalamin ([MeCbl]) itself (1.979(4) Å in the structure reported by Randaccio and co-workers,[33] marginally longer at 1.990(1) Å in the report of Luger and co-workers),[35] while the Co–N_{ax} bond length is somewhat longer (2.200(7) Å, compared to 2.163(4) and 2.156(1) Å, respectively). There is therefore no clear trend that emerges from the crystallographic values on how the bond length between Co(III) and an anionic axial ligand changes when C10 H is replaced by Cl or Br.

The Co–N21 and Co–N23 bond lengths are longer in [N_3-(10-Br)Cbl] than in [N_3Cbl] whereas the Co–N22 and Co–N24 bonds are shorter; hence the corrin cavity has undergone a distortion with the N21•••N23 distance increasing but the N22•••N24 distance decreasing when C10 H is substituted by Br. The 10-Br derivative is also marginally more folded (the corrin fold angle in [N_3-(10-Br)Cbl] is 18.5º but 16.3º in [N_3Cbl]). Whether these effects are really a consequence of the substitution of H by Br at C10, or a result of crystal packing forces is unclear.

References on page 126

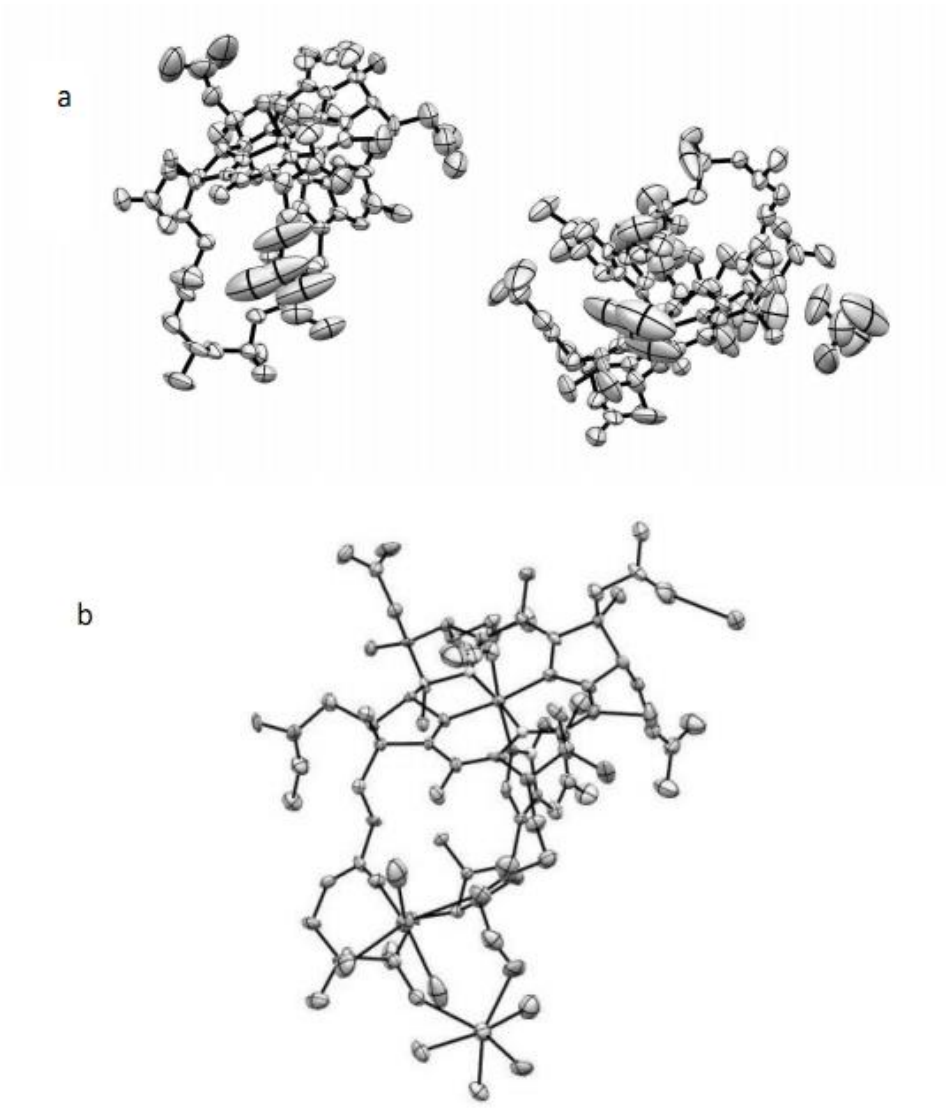


Figure 3.19 ORTEP diagrams with the ellipsoids drawn at the 50% contour level (a) [H_2O-(10-Br)Cbl]$^+$ and (b) [N_3-(10-Br)Cbl]$^+$. Solvate molecules are omitted for clarity.

References on page 126

Table 3.9 A comparison of structural metrics in the crystal structures of $[H_2OCbl]^+$,[27] $[H_2O\text{-}(10\text{-}Cl)Cbl]^{+1}$ and $[H_2O\text{-}(10\text{-}Br)Cbl]^+$ and of $[N_3Cbl]$[31] and $[N_3\text{-}(10\text{-}Br)Cbl]$.

[a]The axial ligand X is either H_2O or N_3^-. [b]There are two molecules in the asymmetric unit.

	Co–X /Å [a]	**Co–N_{ax} /Å**	**Co–N21 /Å**	**Co–N22 /Å**	**Co–N23 /Å**	**Co–N24 /Å**	**N21•••N23 /Å**	**N22•••N24 /Å**	**Fold Angle /deg**
$[H_2OCbl]^+$	1.952	1.925	1.881	1.897	1.904	1.879	3.779	3.764	18.7
$[H_2O\text{-}(10\text{-}Cl)Cbl]^+$	1.948	1.967	1.887	1.913	1.929	1.892	3.812	3.795	19.9
$[H_2O\text{-}(10\text{-}Br)Cbl]^{+b}$	1.933	1.975	1.894	1.922	1.912	1.902	3.813	3.801	26.8
	1.943	1.961	1.916	1.944	1.905	1.909	3.817	3.841	20.1
$[N_3Cbl]$	1.984	1.999	1.882	1.911	1.923	1.989	3.798	3.800	16.3
$[N_3\text{-}(10\text{-}Br)Cbl]$	1.942	1.974	1.914	1.899	1.936	1.887	3.845	3.777	18.5

References on page 126

3.5.1 Conclusion

It was noted from the crystallographic data of 10-Br derivatives, that the Co–X (X= O, N) bond is stronger in X-10-bromocobalamin than in X-cobalamin itself (see **Table 3.12**). Substituting of the Br atom at the C10 position also resulted in a more folded corrin ring as the corrin cavity underwent a distortion with the N21•••N23 distance increasing but the N22•••N24 distance decreasing in [N_3-(10-Br)Cbl] while the latter decreased in [H_2O-(10-Br)Cbl]$^+$. All these effects may be a consequence of the substitution of H by Br at C10 although one cannot discount the possibility that they are the result of crystal packing effects.

3.6 Summary of the Chapter

The work in this Chapter assessed the *cis*-influence exerted by the corrin ring on the metal ion in C10 substituted cobalamins. The electronic structure of the corrin ring is a leading factor in labilising of the Co(III) metal ion, therefore, perturbing the electronic structure of the corrin ring by replacement of C10 H by Br influenced the chemistry of the axial coordination sites; consequently this had an effect on the thermodynamics of the ligand substitution reactions. The results from the coordination of various anionic and neutral ligands by the Co(III) centre in [H_2O-(10-Br)Cbl]$^+$ showed that the Co(III) metal ion binds preferentially to anionic ligands than in [H_2OCbl]$^+$ and discriminates against the neutral ligands. These observations were in good agreement with the previous study for [H_2O-(10-Cl)Cbl]$^+$.[4] These findings were rationalised by DFT calculations which highlights the impact of the electron density on the lability of the Co(III) metal. As the electron density increases on the Co(III) metal ion, the metal becomes softer and more Co(II)-like character. The electron density on the cobalt atom varied as the nature of the C10 substituent was changed. When C10 is substituted by Br or Cl both cause the electron density increases on the cobalt metal and becomes more electron rich and more labile.

References on page 126

Inorganica Chimica Acta 436 (2015) 29–38

Contents lists available at ScienceDirect

Inorganica Chimica Acta

journal homepage: www.elsevier.com/locate/ica

Probing the nature of the Co(III) ion in cobalamins: The reactions of aquacobalamin (vitamin B_{12a}), aqua-10-chlorocobalamin and aqua-10-bromocobalamin with anionic and neutral ligands ☆

Nafise Ghadimi [a], Christopher B. Perry [a], Manuel A. Fernandes [a], Penny P. Govender [b], Helder M. Marques [a,*]

[a] Molecular Sciences Institute, School of Chemistry, University of the Witwatersrand, P.O. Wits, Johannesburg 2050, South Africa
[b] Department of Applied Chemistry, University of Johannesburg, P.O. Box 17011, Doornfontein, Johannesburg 2028, South Africa

ARTICLE INFO

Article history:
Received 19 April 2015
Received in revised form 3 June 2015
Accepted 10 July 2015
Available online 23 July 2015

Keywords:
Aquacobalamin
Vitamin B_{12}
Co(III)
Ligand substitution reactions
Reaction kinetics

ABSTRACT

The preparation of aqua-(10-bromo)cobalamin, $[H_2O\text{-}(10\text{-}Br)Cbl]^+$, in which the C-10 H of aquacobalamin is substituted by Br, and its characterisation by spectroscopic and by single crystal XRD is described. Equilibrium constants for substitution of H_2O by anionic (SO_3^{2-}, NO_2^-, SCN^-, N_3^-) and neutral N-donor (imidazole, 4-*N*,*N*-dimethylaminopyridine) ligands in $[H_2OCbl]^+$, $[H_2O\text{-}(10\text{-}Cl)Cbl]^+$ and $[H_2O\text{-}(10\text{-}Br)Cbl]^+$ are reported. Rate constants and $\Delta H^{\ddagger}$ and $\Delta S^{\ddagger}$ values for the substitution of H_2O in $[H_2O\text{-}(10\text{-}Br)Cbl]^+$ by N_3^- and imidazole are reported, and are compared with values available for $[H_2OCbl]^+$ and $[H_2O\text{-}(10\text{-}Cl)Cbl]^+$. Br at C-10 is resonance donating to the corrin. Substitution of the C-10 H by Cl or Br favours the coordination of anionic ligands, but discriminates against the binding of neutral N-donor ligands. DFT (BP86/TZVP) calculations are used to rationalise these observations. When H is changed to Cl or Br, the metal ion becomes less positive and the corrin nucleus becomes more positive, so favouring the coordination of anionic ligands. The kinetics of the substitution of H_2O by N_3^- and imidazole show that both react more slowly with $[H_2O\text{-}(10\text{-}Br)Cbl]^+$ than with $[H_2OCbl]^+$. Although $\Delta H^{\ddagger}$ values are smaller, they do not compensate for significantly more negative values of $\Delta S^{\ddagger}$, indicative of a transition state that occurs earlier along the reaction coordinate. Thus perturbation of the electronic structure of a corrin can markedly affect the chemistry of the axial coordination site of Co(III), providing evidence of the importance of cis effects in the chemistry of Co(III) macrocycles.

© 2015 Elsevier B.V. All rights reserved.

1. Introduction

We have been exploring the nature of Co(III) in the cobalt corrins (derivatives of vitamin B_{12}) in an effort to elucidate the effect of the corrin ligand on the chemistry of the metal ion [1–12]. We have suggested that an important factor in modifying the properties of normally inert Co(III) and conferring on it the unusual lability found in the cobalt corrins is the delocalisation of electron density from the corrin equatorial ligand onto Co(III), making the metal softer and imparting on it some measure of labile Co(II) character.

We have used a number of strategies to test this hypothesis. Firstly, we have perturbed the electronic structure of the corrin by substituting the H atom at C-10 (see Fig. 1 for numbering) by either Cl (which is π electron-donating towards the corrin) [1,4] or NO (which is π electron-withdrawing) [2]; secondly, we have disrupted the π conjugated system by oxidising the C5–C6 double bond [6,7,9]; thirdly, we have prepared an aquacobalamin (vitamin B_{12a}, H_2OCbl^+) analogue containing a porphyrin [10]; and more recently we have prepared a B_{12a} analogue containing a corrole [12]. In each case we have compared the physical properties and the thermodynamics (and in some cases the kinetics) of the substitution of the axial H_2O by a series of neutral and anionic ligands to determine the effect that perturbing the electronic structure of the corrin, or exchanging a corrin for a porphyrin or a corrole, has on the chemistry of Co(III). We have also used density functional theory (DFT) modelling to probe these cis effects in the cobalt corrins [8,11].

Briefly, we have demonstrated that there is indeed electronic communication between the axial and the equatorial ligands in the cobalt corrins [5] and that the C-10–Cl bond length in [X-(10-Cl)Cbl] depends on the nature of the axial ligand X [1]; that

☆ Supplementary materials is available at http://dx.doi.org/.

* Corresponding author.
E-mail address: Helder.Marques@wits.ac.za (H.M. Marques).

http://dx.doi.org/10.1016/j.ica.2015.07.019
0020-1693/© 2015 Elsevier B.V. All rights reserved.

References on page 126

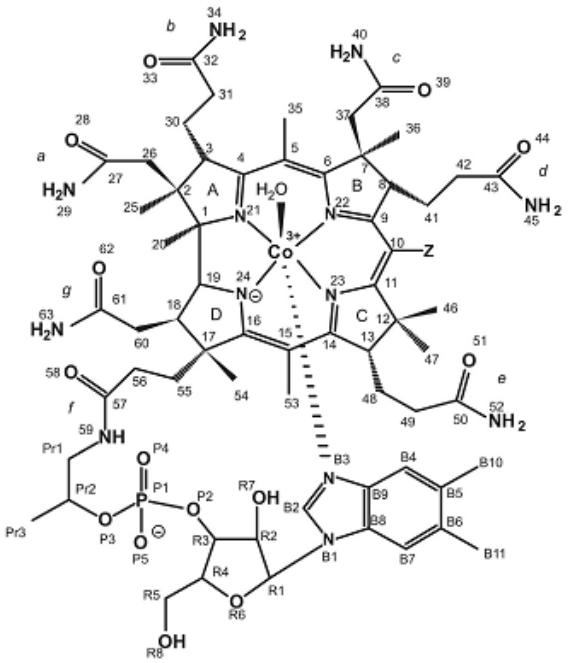


Fig. 1. Standard view of the cobalamins and atom numbering. The axial ligand 5,6-dimethylbenzimidazole occupies the lower or α coordination site; the β coordination site is occupied by H_2O. The portion of the molecule from C6 through C14 is referred to as the "eastern" part of the molecule.

substituting the C-10 H by NO deactivates the metal ion [2]; that the ligand substitution reactions of $[H_2O\text{-}(10\text{-}Cl)Cbl]^+$ are slower than those of vitamin B_{12a}, $[H_2OCbl]^+$, itself [4]; that interrupting the conjugation of the corrin makes the metal ion harder [7,9]; and that the difference in charge on the macrocyle (−3 in corroles, −2 in porphyrins and −1 in corrins), which modifies the net charge at the metal centre, plays an important role in controlling and modifying the chemistry of the metal ion [10,12].

During the course of attempting a synthesis of 10-alkyl cobalamins, we prepared the intermediate aqua-10-bromocobalamin, $[H_2O\text{-}(10\text{-}Br)Cbl]^+$. We have characterised this by single crystal X-ray diffraction (as the azido complex, the aqua complex having given poor quality crystals) and NMR spectroscopy. We have undertaken a comparison of the equilibrium constants for the substitution of axial H_2O by a range or exogenous ligands, X, and compared values of log *K* (Eq. (2), Z = H, Cl or Br) with those for $[H_2OCbl]^+$ and $[H_2O\text{-}(10\text{-}Cl)Cbl]^+$, and report our findings in this paper.

$$X^{n-} + [H_2O\text{-}(10\text{-}Z)Cbl]^+ \overset{K}{\rightleftharpoons} [X\text{-}(10\text{-}Z)Cbl]^{(1-n)+} + H_2O \qquad (1)$$

2. Experimental

2.1. Materials and methods

Hydroxocobalamin was from Roussel. All solvents (Merck) and reagents (Sigma Aldrich) were of the highest purity available and used as received. Deionised water was produced by a Millipore RO unit, and further purified by reverse osmosis using a Millipore MilliQ Ultra-Pure system (18 MΩ cm). The measurement of pH was performed using a Metrohm 780 pH meter with Metrohm LL UnitrodePt 1000 glass electrode calibrated against standard potassium hydrogen phthalate, KH_2PO_4/K_2HPO_4 and borax buffers. HPLC analyses were performed on a Supelco Sigma–Aldrich Discovery C18 reverse phase column (25 cm × 4.6 mm, 5 μm) coupled to a C18 guard column (4.0 cm × 3.0 mm), a Dionex Ultimate 3000 pump and photodiode array detector at a constant flow rate of 1.00 ml min^{-1}. The mobile phase used consisted of 25 mM phosphate buffer, pH 3, and CH_3CN with gradient elution from 98:2 to 75:25 buffer:CH_3CN over 15 minutes. All UV–Vis spectra were recorded on either a Cary 300 UV–Vis spectrophotometer or on an Agilent 100 diode array spectrometer, using 1.00 cm pathlength quartz cuvettes. The cell compartment temperature was kept constant with a water-circulating bath set at 25.0 °C. Mass spectra were obtained using a Waters Synapt G2 time-of-flight mass spectrometer with sample injection into a stream of CH_3CN and 0.1% formic acid; the lock mass was provided by leucine enkaphalin. One-dimensional (^1H, $^{13}C\{^1H\}$ and dept135), two-dimensional proton homonuclear (COSY, TOCSY, NOESY and ROESY) and two-dimensional heteronuclear (^1H–^{13}C) experiments (HSQC and HMBC) NMR spectra were recorded on 15 mg samples dissolved in 700 μL of MeOD at 300 K on a Bruker Avance III 500 spectrometer operating at 500.133 MHz (^1H) and 125.770 MHz (^{13}C) using a 5-mm PABBO broad band probe. All NMR spectra were internally referenced to TMS. NMR spectra were processed using Bruker Topspin 3.0 (Avance III 500) and Topspin 2.1 (Avance III 300) software packages.

2.2. Preparation of aqua-10-bromo-cobalamin

$[H_2O\text{-}(10\text{-}Br)Cbl]^+$ was prepared by the reaction of ethylcobalamin (EtCbl) with *N*-bromosuccinamide (NBS) essentially as described by Wagner for the reaction of methylcobalamin (MeCbl) with NBS [13]. Freshly acid-washed Zn granules (1 g) were placed in a two-necked round bottom flask through which was passed a steady stream of Ar. Hydoxocobalamin (OHCbl, 200 mg, 0.15 mmol) was dissolved in 50 mL of a 10% acetic acid/methanol solution in a separate flask; after deaeration (Ar), this was cannula-transferred to the flask containing the Zn metal (room temperature). The solution rapidly turned from red to brown to grey, consistent with the reduction to Co(I). After complete reduction (20 min), ethyl bromide (15 mmol) was added and left to react for one hour in the dark under Ar. The progress of the alkylation was monitored by HPLC. After essentially quantitative conversion of OHCbl to EtCbl the reaction mixture was cannula-transferred to a separate flask and rotary evaporated to dryness (50 °C). The EtCbl was dissolved in 40 mL of acetic acid after deaeration (Ar), NBS (0.18 mmol) was added, and the mixture was left to react for one hour. The progress of the bromination reaction was monitored by HPLC. When the reaction was complete, the reaction mixture was cannula-transferred to a round bottom flask and rotatory evaporated to dryness (50 °C) under ambient light. The product was dissolved in 30 mL of 0.1 M HCl and exposed to the light for a few hours; the conversion of $[Et\text{-}(10\text{-}Br)Cbl]$ to $[H_2O\text{-}(10\text{-}Br)Cbl]^+$ was monitored by HPLC. The product was neutralised with $NaHCO_3$ and rotary evaporated to dryness (50 °C) and then was dissolved in a minimum amount of deionised water and chromatographed on a 230 × 15 mm C18 column using a Büchi Sepacore chromatographic system consisting of two C-605 pump modules, a C-615 pump manager, a C-660 fraction collector, and a C-635 UV photometer. A gradient of phosphate buffer (25 mM, pH 3) and CH_3CN from 0% to 40% CH_3CN at a flow rate of 3 ml min^{-1} was used to elute the product from the column as well as a small amount of $[H_2OCbl]^+$. UV–Vis, λ/nm ($\varepsilon/10^3$ M^{-1} cm^{-1}), pH 6.9, 0.5 M MOPS: 356 (25.9); 526 (7.5); 555 (8.0). ESI-MS (positive mode): 704.74, $(M-H_2O+H)^{2+}$, calc. 704.68, 100%; 715.73, $(M-H_2O+Na)^{2+}$, calc. 715.68, 19.5%; 1408.48, $(M-H_2O)^+$, calc. 1408.36, 3.3%; 1431.47, $(M-H_2O-H+Na)^+$, calc. 1431.36, 1.0%.

References on page 126

2.3. Preparation of aqua-10-chloro-cobalamin

$[H_2O\text{-}(10\text{-}Cl)Cbl]^+$ was prepared as previously described [4].

2.4. Crystallography

We attempted to grow crystals of $[H_2O\text{-}(10\text{-}Br)Cbl]^+$ by dissolving ca. 10 mg in 1 mL deionised water, and placing the solution in an open glass vial which was placed in a larger vial containing acetone. The larger vial was sealed and kept at 4 °C; after a week very small, pellet-shaped crystals had formed which proved to diffract poorly. Intensity data from these crystals were collected at −100(2) °C on a Bruker X8 Proteum diffractometer equipped with a PLATINUM 135 CCD detector and Montel 200 optics, using Cu Kα radiation (45 kV, 60 mA) from a Microstar rotating-anode generator. The collection method involved ω-scans of width 0.5° and 1024 × 1024 bit data frames. Details of the crystallographic data are given in Table 1.

We attempted the crystallisation several times from a variety of solutions (neutral solution containing NaCl, LiCl, $NaClO_4$), but with little success; either very poor quality crystals were obtained, or only an amorphous or micro-crystalline material formed. We therefore resorted to crystallising the azido complex, $[N_3\text{-}(10\text{-}Br)Cbl]$. Sodium azide (ca. 50 mg) was added to a 1 mL aqueous solution of $[H_2O\text{-}(10\text{-}Br)Cbl]^+$ (15 mg) and dissolved. UV–Vis and HPLC analysis confirmed the complete conversion to the azido complex. Crystallisation was by acetone vapour diffusion as described above. After 10 days at 4 °C needle-shaped crystals had formed. The compound co-crystallised with two equivalents of Na^+ and N_3^- ions per unit cell, as well as an acetone molecule and five H_2O solvent molecules. Intensity data were collected at −100(2) °C on a Bruker APEX II CCD area detector diffractometer with graphite monochromated Mo Kα radiation (50 kV, 30 mA). The collection method involved ω-scans of width 0.5° and 512 × 512 bit data frames.

Data collection for both samples were carried out using the APEX 2 [14] data collection software followed by data reduction using the program SAINT+[14] and multiscan absorption corrections using SADABS [14]. The crystal structures were solved by direct methods using SHELXS-97 [15]. Non-hydrogen atoms were first refined isotropically followed by anisotropic refinement by full matrix least-squares calculations based on F^2 using SHELXL-97 [15]. Hydrogen atoms were first located in the difference map then positioned geometrically and allowed to ride on their respective parent atoms, with isotropic thermal parameters fixed at 1.2 (CH, CH_2 and NH_2) or 1.5 (CH_3 and OH) times those of their corresponding parent atoms. It was not possible to locate the hydrogen atoms on several of the water molecules. The contribution of these hydrogen atoms has, however, been accounted for in the chemical formula and related data such as crystal density and F(000). Figures were prepared using ORTEP-3 [16]. Details of the crystallographic data for both samples are given in Table 1. The structure files for $[H_2O\text{-}(10\text{-}Br)Cbl]^+$ and $[N_3\text{-}(10\text{-}Br)Cbl]$ have been deposited at the Cambridge Structural Database (deposition numbers CCDC-1057492 and CCDC-1057493, respectively). A list of bond length and angles is given in Table S1 for $[H_2O\text{-}(10\text{-}Br)Cbl]^+$ and Table S2 for $[N_3\text{-}(10\text{-}Br)Cbl]$ in the Supplementary material.

Table 1
Crystallographic data for bis(aqua-(10-bromo)cobalamin) hydrogen phosphate pentatriacontahydrate and azido-(10-bromo)cobalamin di(sodium azide) triacetone solvate pentahydrate.

CCDC deposition code	CCDC 1057492	CCDC 1057493
Empirical formula	$(C_{62}H_{88}BrCoN_{13}O_{15}P)_2$, HPO_4, $35(H_2O)$	$C_{62}H_{88}BrCoN_{13}O_{15}P$, $2(NaN_3)$, $3(C_3H_6O)$, $5(H_2O)$
Formula weight	3578.07	1932.70
T (K)	173(2)	173(2)
λ (Å)	1.54178	0.71073
Crystal system	triclinic	orthorhombic
Space group	$P1$	$P2_12_12_1$
Unit cell dimensions		
a (Å)	12.0184(4)	15.3745(4)
b (Å)	14.8684(5)	23.4023(6)
c (Å)	25.7024(8)	25.3443(7)
α (°)	89.348(2)	
β (°)	80.785(2)	
γ (°)	85.911(2)	
V (Å³)	4522.1(3)	9118.8(4)
Z	1	4
$D_{calc.}$ (Mg m^{-3})	1.314	1.408
Absorption coefficient (mm^{-1})	2.981	0.739
F(000)	1895	4072
Crystal size (mm)	0.10 × 0.10 × 0.05	0.60 × 0.07 × 0.05
θ range for data collection (°)	2.98–49.39	1.55–25.00
Index ranges	$-11 \leqslant h \leqslant 11$, $-14 \leqslant k \leqslant 13$, $-24 \leqslant l \leqslant 24$	$-15 \leqslant h \leqslant 18$, $-27 \leqslant k \leqslant 27$, $-30 \leqslant l \leqslant 30$
Reflections collected	36423	62372
Independent reflections (R_{int})	15262 (0.0611)	16040 (0.2016)
Completeness to θ	49.39°, 91.8%	26.00°, 100.0%
Absorption correction	Semi-empirical from equivalents	Semi-empirical from equivalents
Refinement method	Full-matrix least-squares on F^2	Full-matrix least-squares on F^2
Data/ restraints/parameters	15262/199/2001	16040/0/1115
Goodness-of-fit (GOF) on F^2	1.113	0.938
Final R indices [$I > 2\sigma(I)$]	$R_1 = 0.0928$, $wR_2 = 0.2395$	$R_1 = 0.0636$, $wR_2 = 0.0929$
R indices (all data)	$R_1 = 0.1055$, $wR_2 = 0.2529$	$R_1 = 0.1976$, $wR_2 = 0.1232$
Absolute structure parameter	−0.016(5)	−0.010(10)
Largest diff. peak and hole (e Å^{-3})	0.699 and −0.568	0.752 and −0.654

2.5. Acid dissociation constant

The acid dissociation constant of coordinated H_2O in $[H_2O\text{-}(10\text{-}Br)Cbl]^+$ was determined using UV–Vis spectroscopy. $[H_2O\text{-}(10\text{-}Br)Cbl]^+$ was dissolved in a multi-component buffer [17] (1 mM in each of 2-(*N*-morpholino)ethanesulfonic acid (MES), (*N*-morpholino)propanesulfonic acid (MOPS), 4-(2-hydroxyethyl)-1-piperazineethanesulfonic acid (HEPES), *N*-cyclohexyl-2-aminoethanesulfonic acid (CHES) and *N*-cyclohexyl-3-aminopropanesulfonic acid (CAPS), $\mu = 0.5$ M, Na_2SO_4) in a 50 mL thermostatted cell (25.0 ± 0.1 °C). The pH of the sample was adjusted by diffusing negligible volumes of 8 M NaOH or conc. H_2SO_4 with a drawn-out capillary tube. The sample was circulated through a 1 cm flow cell (Hellma) housed in the compartment of a Cary 3E UV–Vis spectrophotometer using a Watson-Marlow 101U peristaltic pump. The spectrum was recorded at intervals of approximately 0.5 pH units. The changes in the absorbance spectrum as a function of pH were fitted to Eq. (2) as objective function and A_0, A_1 and K_a as variables, where A_λ is the absorbance measurement at the monitored wavelength; A_0 and A_f are the initial and final absorbance measurements respectively at the monitored wavelength; and K_a is the equilibrium constant for ionization of coordinated H_2O. The acid dissociation constant is reported as a pK_a.

$$A_\lambda = \left(\frac{A_0 10^{-pH} + A_1 10^{-pK_a}}{10^{-pH} + 10^{-pK_a}}\right) \quad (2)$$

References on page 126

2.6. Equilibrium constants

The equilibrium constants, K, for the coordination of the ligands by $[H_2O\text{-}(10\text{-Br})Cbl]^+$, $[H_2O\text{-}(10\text{-Cl})Cbl]^+$ and $[H_2OCbl]^+$, Eq. (2), were determined by addition of aliquots of a stock solution of the appropriate ligand to a 20–50 μM solution of the Co(III) corrin contained in a 1.00 cm path length cuvette housed in the thermostatted cell block of a Cary 100 UV–Vis spectrophotometer. All work was done in aqueous solution with $\mu = 0.50$ M (Na_2SO_4). Typically between 10 and 15 aliquot additions were made in each titration and absorbance readings were corrected for dilution. For cases where log K is relatively small (log $K < 4$), the absorbance data at the monitoring wavelength λ were fitted using non-linear least squares methods to a simple binding isotherm (Eq. (3)) as objective function, with A_0, A_1 and K as the parameters to be optimized. A_0 and A_1 are the absorbance values at λ corresponding to 0 and 100% complex formation, respectively.

$$A_\lambda = (A_0 + KA_1[X])/(1 + K[X]) \quad (3)$$

When log K is relatively large (>4), the implicit assumption in Eq. (3) that $[X]_{free} \approx [X]_{total}$ is not true because a significant fraction of the added ligand will be complexed to the metal ion. In this case [X] in Eq. (3) has to be replaced by an explicit expression for $[X]_{free}$. It can be shown [18] that $[X]_{free}$ is given by Eq. (4), where only one root has physical meaning. In Eq. (4), $[M]_{total}$ is the total metal ion concentration.

$$[X]_{free} = \frac{-a_2 \pm \sqrt{a_2^2 - 4a_1a_3}}{2a_1} \quad (4)$$

$$a_1 = K; \quad a_2 = 1 + K[M]_{total} - K[L]_{total}; \quad a_3 = -[L]_{total}$$

It is well-established in cobalt corrin chemistry that hydroxide in hydroxocobalamin will not be displaced by an exogenous ligand X [19–21]. Moreover, it is usually the case that the protonated form of a ligand (for example, imidazole) will not coordinate to a metal ion. Conditional stability constants, K_{obs}, determined at some pH value, were therefore converted to pH-independent equilibrium constants, K, using Eq. (5), where pK_{aX} refers to the acid dissociation constant of the conjugate acid of the ligand X and pK_{aM}, to the acid dissociation constant of coordinated H_2O in $[H_2O\text{-}(10\text{-}Z)Cbl]^+$, Z = H, Cl or Br.

$$K = K_{obs}(1 + 10^{pK_{aX} - pH})(1 + 10^{pH - pK_{aM}}) \quad (5)$$

2.7. Kinetics

The kinetics of the displacement of H_2O from $[H_2O\text{-}(10\text{-Br})Cbl]^+$ by imidazole (Im) and N_3^- were studied as a function of temperature (between 10 °C and 35 °C, pH 6, 2-(*N*-morpholino)ethanesulfonic acid (MES) buffer, $\mu = 0.50$ M, Na_2SO_4 for azide; between 15 °C and 35 °C, pH 7, 3-morpholinopropane-1-sulfonic acid (MOPS) buffer, $\mu = 0.50$ M, Na_2SO_4 for imidazole) by monitoring the change in absorbance at four wavelengths (356, 373, 501 and 585 nm for azide; 362, 373, 510 and 585 nm for imidazole) using an Agilent 100 diode array spectrometer. Between five and eight different ligand concentrations were used at each temperature by injecting the appropriate volume of a stock solution of the ligand into a solution of 20 μM $[H_2O\text{-}(10\text{-Br})Cbl]^+$. The pseudo first order rate constants, k_l^{obs}, were found by fitting the absorbance-time trace to Eq. (6) as objective function with A_1, A_2 and k_l^{obs} as variables using standard non-linear least squares methods.

$$A_\lambda = A_1 \exp(-k_l^{obs} t) + A_2 \quad (6)$$

Since the hydroxo complex [HO-(10-Br)Cbl], by analogy with [HOCbl], is expected to be substitution inert [20,21], and the conjugate acids HN_3 and HIm^+ are unlikely to coordinate Co(III), k_l^{obs} was converted to a pH-independent first order rate constant, k_l by applying the equivalent of Eq. (5). The second order rate constant for the reaction symbolised by Eq. (7) ($X^{n-} = N_3^-$ or Im) was then obtained from the slope of a weighted linear least squares fit of k_l against $[X^{n-}]$. The weighting factor was the reciprocal of the relative percentage standard error of the non-linear least squares fit of the absorbance-time trace. The intercept of such a plot, if statistically significantly different from zero, corresponds to the reverse rate constant, k_r.

$$[H_2O\text{-}(10\text{-Br})Cbl]^+ + X^{n-} \underset{k_r}{\overset{k_{II}}{\rightleftharpoons}} [X\text{-}(10\text{-Br})Cbl]^{(1-n)+} + H_2O \quad (7)$$

The enthalpy and entropy of activation, $\Delta H^\ddagger$ and $\Delta S^\ddagger$, were obtained from the slope and intercept of a weighted linear least squares Eyring plot of $\ln(k_{II}h/k_BT)$ against T^{-1}, where h and k_B are the Planck and Boltzman constants, respectively.

2.8. Molecular modelling

Starting from the crystallographic coordinates of $[H_2OCbl]^+$ [22], models of $[H_2O\text{-}(10\text{-}Z)Cbl]^+$, Z = H, Cl or Br, in which all substituents of the corrin ring were truncated to H and with imidazole as the α axial ligand, were explored using density functional theory (DFT) calculations. These calculations were performed with the Gaussian-09 program [23], the GGA BP86 functional [24,25] and the TZVP basis set [26,27]. Both the density-fitting approximation [28,29] and the density-fitting TZVP basis set [30,31] was used so as to minimize calculation time. To explore the topological properties of the electron density, wavefunction files were generated with Gaussian-09 and analysed using Bader's QTAIM [32] as implemented in AIMALL [33].

Calculated gas-phase values of ΔE and ΔG for the deprotonation reactions (Eq. (8)) were determined using models of $[H_2O\text{-}(10\text{-}Z)Cbl]^+$, Z = H, Cl or Br, in which all substituents of the corrin ring were truncated to H (except for the *c* side chain, which was retained since axial ligands may hydrogen bond to it) using ORCA 3.0.3 [34] with the BP86 functional, and TZVP basis set. Both the 'Resolution of the Identity' (RI) [30,31,35–39] approximation, and the corresponding TZVP auxiliary basis set were used to reduce computational costs. Frequency calculations were performed to obtain thermodynamic corrections to the energy, as well as to verify that the system was in a ground state conformation.

$$H_2O + [H_2O\text{-}(10\text{-}Z)Cbl]^+ \overset{k_a}{\rightleftharpoons} [HO\text{-}(10\text{-}Z)Cbl)] + H_3O^+ \quad (8)$$

3. Results

3.1. The spectroscopic properties and structure of [HO-(10-Z)Cbl]$^+$

The ^1H and ^{13}C NMR spectra of $[H_2O\text{-}(10\text{-Br})Cbl]^+$ were assigned using the methodology developed by Brown [40–44]. The full assignments are given in Tables S3 and S4 of the Supplementary material, and a brief account of the methodology used is given there as well.

As expected, because of the substitution of the C-10 H by Br, the ^{13}C resonance of C-10 shifts downfield ($\Delta\delta_{[H_2O\text{-}(10\text{-Br})Cbl]^+ - [H_2OCbl]^+} = 10.49$ ppm, Table S4), as do those of C8, C12 and C47, while there are upfield shifts in the resonances of C9, C11 and C46. These changes are similar to those observed when substituting C-10 H with Cl (Table S5).

The substitution of the C-10 H by Br causes a red shift in the γ, β and α bands as reported by Wagner [13] and as observed for $[H_2O\text{-}(10\text{-Cl})Cbl]^+$,[4] with very little change to the intensity of the absorbance. The position of the bands of the aqua complexes (pH 7) and some complexes with a variety of other ligands are compared in Table 2.

References on page 126

It is unfortunate that the crystals of [H_2O-(10-Br)Cbl]$^+$ diffracted poorly, and that, despite several attempts, we were unable to produce better quality crystals. The structure contains one phosphate anion (presumably as HPO_4^{2-} for charge neutrality, although we were unable to locate the proton) per pair of [H_2O-(10-Br)Cbl]$^+$ ions in the asymmetric unit; this resulted in the compound crystallizing in a triclinic rather than the usual orthorhombic space group. This low symmetry cell and small crystals exacerbated the data collection problem. The metrics obtained from the structure must be treated with caution.

The Co–OH_2 bond length (1.933(7) Å and 1.943(8) Å in the two molecules in the asymmetric unit) is marginally shorter, although not statistically significantly different, to that found in the crystal structure of [H_2OCbl]$^+$ itself (1.952 Å) [22] and to that found in [H_2O-(10-Cl)Cbl]$^+$ (1.948 Å) [1]. The Co–N_{ax} bond to the N-donor of axial 5,6-dimethylbenzimidazole (dmbzm) is significantly longer in the 10-Br and 10-Cl derivatives (1.975 Å and 1.961 Å; 1.967 Å [1], respectively) than in [H_2OCbl]$^+$ itself (1.925 Å [22]). Given the well-established trans influence in the cobalt corrins [45,46], this suggests that the Co–OH_2 bond is stronger in the 10-Br and 10-Cl derivatives than in [H_2OCbl]$^+$ itself. The Co–N bond lengths to the corrin N-donors in the 10-Br and 10-Cl derivatives are somewhat longer than in H_2OCbl$^+$ (Table S5 of the Supplementary material); the corrin cavity has expanded and the corrin fold angle (the angle between the mean planes defined by N21, C4, C5, C6, N22, C9, C-10 and C-10, C11, N23, C14, C15, C16, N24 [47]) is somewhat larger. There therefore appear to be some structural changes to the corrin on replacing the C-10 H with Cl or Br.

The crystal structure of the azido complex is, by contrast, a much higher quality structure with a relatively low *R* factor (6.36%; only 31 of the 104 cobalamin structures listed in the CSD [48] have a lower *R* factor). Like the majority of cobalamin structures (88.6% of those in the CSD), it crystallised in the orthorhombic space group $P2_12_12_1$. [N_3-(10-Br)Cbl] co-crystallised with two equivalents of NaN_3, three acetone and five solvent H_2O molecules in the asymmetric unit (Fig. 2; ORTEP diagrams of this and the aqua structure are given in Fig. S1 of the Supplementary material). The Co–N_3^- bond length is 1.942(6) Å, while Co–N_{ax}, the bond between Co(III) and the axial base, is 1.974(6) Å. In the structure of [N_3Cbl] itself (co-crystallised with LiCl, *R* = 5.13%, 100 K) the values are 1.984(3) and 1.999(3) Å, respectively [49]. (There is an older structure [50] but it is of poor quality, *R* = 20.0%, collected at 293 K, and can be ignored.) The azido complex of [(10-Br)Cbl] has shorter bond lengths to the two axial ligands compared to the analogous complex of the normal cobalamin. By contrast, the Co–C bond length in [NC-(10-Cl)Cbl] is *longer* than in cyanocobalamin itself (1.97(2) Å; compared to 1.867(7) [51], 1.877(2) [52] and 1.886(4) Å [51]), while the Co–N_{ax} bond lengths are very similar (2.04(7) Å; 2.029(5), 2.028(2) and 2.041(3) Å, respectively). In [Me-(10-Cl)Cbl], the Co–C bond length, 1.979(7) Å, is similar to that in [MeCbl] itself (1.979(4) Å in the structure reported by Randaccio and co-workers [51], marginally longer at 1.990(1) Å in the report of Luger and co-workers [53]), while the Co–N_{ax} bond length is somewhat longer (2.200(7) Å, compared to 2.163(4) and 2.156(1) Å, respectively). There is therefore no clear trend that emerges from the crystallographic evidence on how the bond length between Co(III) and an anionic axial ligand changes when C-10 H is replaced by Cl or Br.

The Co–N21 and Co–N23 bond lengths are longer in [N_3-(10-Br)Cbl] than in [N_3Cbl] whereas the Co–N22 and Co–N24 bonds are shorter; hence the corrin cavity has undergone a distortion with the N21···N23 distance increasing but the N22···N24 distance decreasing when C-10 H is substituted by Br. The 10-Br derivative is also marginally more folded (the corrin fold angle in [N_3-(10-Br)Cbl] is 18.5° but 16.3° in N_3Cbl). Whether these effects are really a consequence of the substitution of H by Br at C-10, or a result of crystal packing forces is unclear.

3.2. Acid dissociation constants

The titration of 20.5 μM [H_2O-(10-Br)Cbl]$^+$ from pH 5.22 to 9.94 causes the γ band to move from 355 to 360 nm with a decrease in intensity by 24%. The γ band becomes broader, and the N-band emerges as a shoulder at 325 nm. The β band shifts from 525 to 535 nm and the α band from 552 to 562 nm, both gaining in intensity (Fig. S2 of the Supplementary material). The absorbance changes at 355, 430, 500, 565 and 590 nm were fitted to Eq. (2). An example is shown as the insert to Fig. S2 of the Supplementary material. The determination was repeated three times, and the values averaged, weighted by the reciprocal of the relative percentage error of the fit. The average value of the pK_a was 7.23 ± 0.03. The pK_a was determined as a function of temperature between 15 °C and 35 °C. From the van't Hoff plot (Fig. S3) we find $\Delta H = 34 \pm 2$ kJ mol^{-1} and $\Delta S = -26 \pm 6$ J K^{-1} mol^{-1}, from which pK_a (25 °C) = 7.28, the value we used in calculations of log *K* values (*vide infra*).

Under the same conditions (μ = 0.50 M, Na_2SO_4), we found the pK_a for [H_2OCbl]$^+$ = 7.62 ± 0.01 and pK_a = 7.22 ± 0.02 for [H_2O-(10-Cl)Cbl]$^+$. The substitution of C-10 H by Cl and Br therefore marginally increases the acidity of coordinated H_2O.

3.3. DFT modelling

The DFT models of [X-(10-Z)Cbl]$^{n+}$, X = H_2O or N_3^-, *n* = 1 or 0, Z = H, Cl or Br, are shown in Fig. S4 of the Supplementary material. Structural metrics are given in Table 3, as are key parameters derived from a QTAIM analysis of the wavefunction files. A comparison of selected structural metrics crystallographically observed in [N_3-(10-Br)Cbl] and its DFT model is given in Table S6 of the Supplementary Information. Bond lengths are reproduced to within approximately 0.02 Å, and bond angles to better than 1°, which is typical for DFT modelling [54,55]. The values of ΔE and ΔG for the reaction represented by Eq. (8) determined by DFT methods are given in Table 4.

3.4. Equilibrium constants

As an example, the spectroscopic changes accompanying the replacement of coordinated H_2O in [H_2O-(10-Br)Cbl]$^+$ by N_3^- at 25 °C, pH 6.5, are shown in Fig. 3. The insert to the Fig. shows the best fit of the absorbance changes at 355 nm to Eq. (4). Applying Eq. (5) with pK_a(HN_3) = 4.37 [56] and pK_a([H_2O-(10-Br)Cbl]$^+$) = 7.28 (*vide supra*) gives a pH-independent value of log *K* = 4.85. Typically, the spectroscopic changes at between 3 and 5 wavelengths were fitted to Eq. (4) (or Eq. (3) if appropriate), and the log *K* values obtained were averaged. These are reported in Table 5 and are the average of 3 titrations.

3.5. Kinetics

Examples of absorbance-time traces for the reactions of N_3^- and Im with [H_2O-(10-Br)Cbl]$^+$ are shown in Fig. S5 of the Supplementary material. The primary kinetic data are listed in Tables S7 and S8 of the Supplementary material. Examples of plots of k_I and [X^{n-}] for the two ligands studied are given in Fig. S6 of the Supplementary material. The reaction with N_3^- produces intercepts that are statistically different from zero (i.e., k_r in Eq. (7) is not negligible); however, k_r is negligibly small for the reaction with imidazole. The Eyring plots is shown in Fig. S7 of the Supplementary material, while that for k_r for N_3^- is shown in Fig. S8. The values of k_{Ii}, k_r, and of $\Delta H^{\ddagger}$ and $\Delta S^{\ddagger}$ deduced from these plots, as well as

References on page 126

Table 2
Comparison of the position of the principal bands in the UV–Vis spectrum of complexes of $[H_2OCbl]^+$ and the 10-Cl and 10-Br analogues.

X	$[XCbl]^{n+}$			$[X\text{-}(10\text{-}Cl)\text{-}Cbl]^{n+}$			$[X\text{-}(10\text{-}Br)\text{-}Cbl]^{n+}$		
	γ (nm)	β (nm)	α (nm)	γ (nm)	β (nm)	α (nm)	γ (nm)	β (nm)	α (nm)
H_2O	351	527	554	355	536	558	356	539	555
N_3^-	357	523	546	360	543	565	359	547	563
SO_3^{2-}	364	525	548	367	550	570	370	540	568
NCS^-	360	517	550	362	540	575	363	545	575
Imidazole	358	520	545	361	544	574	363	544	574

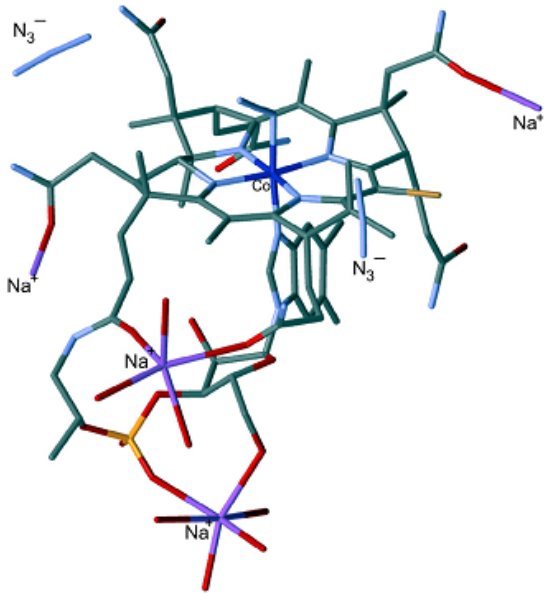


Fig. 2. The crystal structure of $[N_3\text{-}(10\text{-}Br)Cbl]$. The azido ligand is coordinated in a bent fashion, and oriented over C15. Two equivalent of NaN_3 co-crystallise with the cobalamin. Solvate molecules are omitted for clarity.

those available for the analogous reactions with $[H_2O\text{-}Cbl]^+$ and $[H_2O\text{-}(10\text{-}Cl)Cbl]^+$ are summarised in Table 6.

4. Discussion

The electronic effect of the substituent at C-10 can be deduced from the positions of the main transitions in the UV–Vis spectrum. When Z = H the α, β and γ bands of $[CN_2Cbl]$ occur at 580, 550 and 367 nm, respectively [60]. When Z = NO [2], which is strongly electron-withdrawing, the respective bands in the spectrum of $[CN_2\text{-}(10\text{-}NO)Cbl]$ are blue-shifted to 568, 530 and 356 nm. By contrast, when Z = NH_2, which is electron-donating towards the corrin, the bands are red-shifted to 655, 610 and 379 nm, respectively [13]. A similar effect is seen by comparing the spectra of $[H_2OCbl]^+$ (554, 527, 351 nm) [61] and $[H_2O\text{-}(10\text{-}NO)Cbl]^+$ (535, 507, 345 nm) [2]. The principal UV–Vis bands in $[H_2O\text{-}(10\text{-}Cl)Cbl]^+$ occur at 558, 536 and 355 nm, respectively (Table 2, this work; 555, 522 and 355 nm reported previously [4]), while those in $[H_2O\text{-}(10\text{-}Br)Cbl]^+$ are found at 555, 539 and 356 nm. This confirms that Cl and Br at C-10 are resonance-donating towards the corrin, with Br slightly more donating, consistent with its greater softness and lower electronegativity.

This is supported by the DFT calculations on models of $[X\text{-}(10\text{-}Z)Cbl]^{n+}$, X = H_2O or N_3^-, n = 1 or 0, Z = H, Cl or Br, although the effect is very small. As Z is changed from H to Cl to Br, the charge on the metal ion becomes less positive (Table 3). Simultaneously, the charge on the axial ligands becomes more negative (the order is H < Br ≈ Cl for the negative charge on O of axial H_2O and H < Br = Cl for the negative charge on the N of axial imidazole). A

Table 3
Axial bond lengths and QTAIM properties at the bond critical point in DFT models of $[X\text{-}(10\text{-}Z)Cbl]^{n+}$, X = H_2O or N_3^-, n = 1 or 0, Z = H, Cl or Br.[a]

$H_2O\text{-}(10\text{-}Z)Cbl^+$					$N_3\text{-}(10\text{-}Z)Cbl$				
Co–OH_2					Co–N_3				
Z	/Å	ρ	$\nabla^2\rho$	|V|/G	Z	/Å	ρ	$\nabla^2\rho$	|V|/G
H	2.087	0.05791	0.31489	1.08994	H	1.969	0.09525	0.30233	1.25543
Cl	2.095	0.05684	0.3054	1.09049	Cl	1.969	0.09545	0.30154	1.25693
Br	2.094	0.05693	0.30698	1.09058	Br	1.969	0.09545	0.30146	1.25699
Co–N_{ax}					Co–N_{ax}				
Z	/Å	ρ	$\nabla^2\rho$	|V|/G	Z	/Å	ρ	$\nabla^2\rho$	|V|/G
H	1.898	0.11132	0.44908	1.20569	H	1.999	0.08556	0.3716	1.16999
Cl	1.897	0.11157	0.44792	1.20736	Cl	2	0.08552	0.36933	1.17138
Br	1.897	0.11155	0.44819	1.20712	Br	2	0.08551	0.36933	1.1713
Bader charges (q/e)					Bader charges (q/e)				
Z	Co	O	N_{ax}		Z	Co	N (N_3^-)	N_{ax}	
H	1.2084	−1.0535	−1.0027		H	1.1794	−0.2857	−1.0106	
Cl	1.2078	−1.0555	−1.0035		Cl	1.1791	−0.2860	−1.0122	
Br	1.2074	−1.0551	−1.0035		Br	1.1789	−0.2863	−1.0120	
Corrin fold angle					Corrin fold angle				
Z	/°				Z	/°			
H	5.15				H	7.12			
Cl	5.58				Cl	7.18			
Br	6.03				Br	7.8			

[a] See also Table 5 for further analysis of the Bader charges on atoms in these models.

References on page 126

Table 4
Gas-phase values of ΔE and ΔG for the deprotonation of $[H_2O\text{-}(10\text{-}Z)Cbl]^+$ determined by DFT modelling (BP86/TZVP).

	BP86/TZVP			Experimental
	ΔE (kJ mol^{-1})	ΔG (kJ mol^{-1})	pK_a	pK_a (25 °C)
$[H_2OCbl]^+$	36.51	35.47	6.22	7.62(1)
$[H_2O\text{-}(10\text{-}Cl)Cbl]^+$	34.71	34.80	6.10	7.22(2)
$[H_2O\text{-}(10\text{-}Br)Cbl]^+$	35.01	34.10	5.98	7.23(3); 7.28[a]

[a] The value of 7.23(3) is the average of three experimental determinations at 25 °C; the value of 7.28 is from the values of ΔH and ΔS from a van't Hoff plot between 15 °C and 35 °C at T = 25 °C.

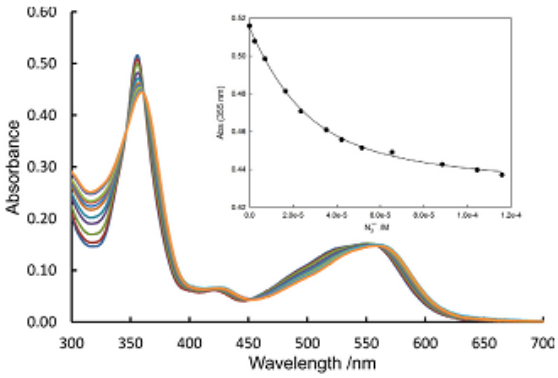


Fig. 3. Changes in the UV–Vis spectrum on substituting coordinated H_2O in 20.1 μM $[H_2O\text{-}(10\text{-}Br)Cbl]^+$ by N_3^- at 25 °C, pH 6.5. The insert shows a fit of the absorbance change at 355 nm to the binding isotherm given by Eq. (4) of the text.

similar trend is evident in the DFT models of the azido complexes (Table 3); Co becomes less positive as Z is varied from H to Cl to Br; the negative charge on the N donor of N_3^- increases monotonically; and the negative charge on the N donor of axial imidazole also increases (now H < Br ≈ Cl).

We inferred from the crystallographic data that the Co–OH_2 bond is stronger in $[H_2O\text{-}(10\text{-}Br)Cbl]^+$ and $[H_2O\text{-}(10\text{-}Cl)Cbl]^+$ than in $[H_2OCbl]^+$ itself (see Results). This would certainly be consistent with the acidity of coordinated H_2O increasing when C-10 H is substituted by Cl or Br. However, the DFT modelling contradict this; it shows the Co–OH_2 bond length increases when Br and Cl replace H at C-10, and the Co–N_{ax} bond length decreases marginally (Table 3). As a consequence, the Co–OH_2 becomes weaker (ρ at bond critical point decreases). Counter-intuitively, however, the covalency of the Co–OH_2 bond increases on substituting C-10 H by Cl and Br (the Laplacian $\nabla^2\rho$ decreases and the ratio of the potential energy density V and the kinetic density G, $|V|/G$, increases [62–66]). It is therefore difficult to rationalise the difference in the pK_as of the complexes based on the crystallographic data (which, as we pointed out above, have to be treated with some caution) and the DFT modelling. We shall return to this point below.

The principal focus of this work was to determine what effect substituting the C-10 H with Cl and Br, which are resonance donating to the corrin system, has on the equilibrium constants, log K, for substitution of coordinated H_2O by a number of anionic and neutral ligands (Eq. (2)). We previously showed [4] that anionic ligands (NO_2^-, SCN^-, N_3^-, OCN^-, $S_2O_3^{2-}$, $NCSe^-$) bind more strongly to $[H_2O\text{-}(10\text{-}Cl)Cbl]^+$ than to $[H_2OCbl]^+$ with log K values between 0.10 and 0.63 (average 0.26) larger, while neutral ligands (CH_3NH_2, pyridine, imidazole) conversely binds less strongly to $[H_2O\text{-}(10\text{-}Cl)Cbl]^+$ than to $[H_2OCbl]^+$ with log K between 0.17 and 0.3 (average 0.25) smaller. The data for NO_2^-, SCN^-, N_3^- and imidazole reported here for $[H_2O\text{-}(10\text{-}Br)Cbl]^+$, and augmented with log K values for SO_3^{2-} and DMAP, confirm our previous findings that substitution of the C-10 H by Cl or Br favours the coordination of anionic ligands, but discriminates against the binding of neutral N-donor ligands (Table 5).

The charge distribution in the DFT models of a representative complex with a neutral (H_2O) and an anionic (N_3^-) ligand provide some insight into possible reasons for these observations (Table 7). While the differences are small, we believe that the trends are illuminating. (We are grateful to a reviewer for suggesting that we investigate the charge distribution on the corrin nucleus in its entirety; we had focussed our attention primarily on the charge on Co, on the donor atom D of the β axial ligand, and on the C10 substituent, Z).

We note four effects that occur on changing Z from H to Cl or Br. Firstly, the charge on the corrin nucleus becomes more positive (δ_{corr}(Z-H) > 0, Table 7) while there is very little difference to the charge on the trans imidazole ligand (i.e., this is predominantly a cis effect). The effect is more pronounced if the β ligand is an anion. Secondly, the positive charge on Co decreases (although the effect

Table 5
Equilibrium constants (as log K values) for the substitution of coordinated H_2O in $[H_2O\text{-}(10\text{-}Z)Cbl]^+$ (Z = H, Cl, Br) by an exogenous ligand X[a,b] at 25 °C.

X	$[H_2OCbl]^+$	$[H_2O\text{-}(10\text{-}Cl)Cbl]^+$	$[H_2O\text{-}(10\text{-}Br)Cbl]^+$	ΔK = log K_{10H} − log K_{10Z} [c]		
				Z = Cl	Z = Br	Average Δ
$S_2O_3^{2-}$	3.72(2)	4.35(5)		−0.63		−0.63
SO_3^{2-}	4.10(8)	4.45(7)	4.72(7)	−0.35	−0.62	−0.49
NO_2^-	5.32(6)	5.47(24)	5.83(13)	−0.08	−0.58	−0.28
	5.34(3)	*5.52(12)*		*−0.18*		
SCN^-	3.21(3)	3.29(6)	3.26(4)	−0.08	−0.05	−0.16
	3.03(5)	*3.39(18)*		*−0.36*		
$SeCN^-$	3.77(2)	3.93(3)		*−0.16*		−0.16
N_3^-	4.68(7)	4.85(3)	4.84(6)	−0.17	−0.16	−0.15
	4.85(13)	*4.97(8)*		*−0.12*		
CNO^-	*2.57(4)*	*2.67(7)*		*−0.10*		−0.10
Imidazole	4.63(2)	4.32(7)	4.27(5)	0.31	0.36	0.28
	4.63(7)	*4.46(19)*		*0.17*		
Pyridine	*1.23(7)*	0.95(9)		0.28		0.28
DMAP[d]	3.76(18)	3.47(19)	3.47(21)	0.29	0.29	0.29
CH_3NH_2	*5.12(8)*	*4.82(6)*		*0.30*		0.30

[a] See Eq. (2).
[b] Values in italics from Knapton and Marques; [4] all others from this work.
[c] Difference in log K values when the C-10 position is occupied by H and when it is occupied by Z = Cl or Br.
[d] 4-*N*,*N*-dimethylaminopyridine.

References on page 126

Table 6
Rate constants and activation parameters for the reaction of N_3^- and imidazole with $[H_2O\text{-}(10\text{-Br})Cbl]^+$.

X	Cobalt corrin	Temp (°C)	k_{II} ($M^{-1}\,s^{-1}$)	$\Delta H^{\ddagger}$ (kJ mol^{-1})	$\Delta S^{\ddagger}$ (J $K^{-1}\,mol^{-1}$)	k_{II} (25 °C)[a] ($M^{-1}\,s^{-1}$)	k_r ($10^{-2}\,s^{-1}$)	$\Delta H^{\ddagger}$ (kJ mol^{-1})	$\Delta S^{\ddagger}$ (J $K^{-1}\,mol^{-1}$)	k_r (25 °C)[a] (s^{-1})	Refs
N_3^-	$[H_2O\text{-}(10\text{-Br})Cbl]^+$	10.0	108(3)	54(5)	−13(17)	362	0.21(2)	89(5)	20(17)	1.73	This work
		15.0	138(10)				0.31(1)				
		17.5	176(24)				0.69(19)				
		20.0	277(5)				0.85(2)				
		25.0	339(19)				1.74(9)				
		30.0	530(63)				2.78(20)				
		35.0	685(122)				4.53(47)				
N_3^-	$[H_2OCbl]^+$			68(2)	34(8)	447					[57]
N_3^-	$[H_2O\text{-}(10\text{-Cl})Cbl]^+$			50(1)	−32(5)	228					[4]
Im	$[H_2O\text{-}(10\text{-Br})Cbl]^+$	15.0	2.5(2)	66(4)	−8(15)	6.4					This work
		20.0	4.6(1)								
		25.0	6.6(1)								
		30.0	11.7(3)								
		35.0	16.6(7)								
Im	$[H_2OCbl]^+$			82(2)	57(8)	24.9					[58]
NMeIm[b]	$[H_2OCbl]^+$			73(3)	21(11)	12.5					[59]

[a] Interpolated from the activation parameters.
[b] *N*-methylimidazole.

Table 7
Bader charges in DFT models of $[X\text{-}(10\text{-Z})Cbl]^{n+}$, X = H_2O or N_3^-, n = 1 or 0, Z = H, Cl or Br.

	Z	q_{corr}[a]	q_{Im}[a]	q_Z[a]	q_D[a]	q_{Co}[a]	δ_{corr}(Z-H)[b]	δ_{Co}(Z-H)[c]	δ_D(Z-H)[d]	$\delta_Z(a\text{-}n)$[e]
$[H_2O(10\text{-Z})Cbl]^+$	H	1.4665	0.3249	0.0824	−1.0535	1.2084				
	Cl	1.6709	0.3278	−0.1227	−1.0555	1.2078	0.2044	−0.0006	−0.0020	
	Br	1.5123	0.3276	0.0361	−1.0551	1.2074	0.0458	−0.0010	−0.0016	
$[N_3(10\text{-Z})Cbl]$	H	1.2296	0.1981	0.0559	−0.2857	1.1794				−0.0265
	Cl	1.4513	0.1978	−0.1743	−0.2860	1.1791	0.2217	−0.0003	−0.0003	−0.0516
	Br	1.3059	0.1957	−0.0285	−0.2863	1.1789	0.0763	−0.0005	−0.0006	−0.0646

[a] Bader charges (in *e*) on the corrin nucleus (including Co, but excluding Z), the imidazole axial ligand, the substituent Z on C-10, the donor atom, D, of the β axial ligand (O in $[H_2O(10\text{-Z})Cbl]^+$ and N in $[N_3(10\text{-Z})Cbl]$, and on Co, respectively.
[b] The difference in charge on the corrin nucleus between Z = H, Cl or Br and Z = H in $[H_2O(10\text{-Z})Cbl]^+$ (first two entries) and (last two entries in column) in $[N_3(10\text{-Z})Cbl]$.
[c] As for footnote b, but for Co.
[d] As for footnote b, but for the donor atom, D.
[e] The difference in charge on the C-10 substituent Z when β ligand is changed from anionic N_3^- to neutral H_2O.

is very small); the metal becomes more electron rich and δ_{Co}(Z-H) becomes more negative. This effect is somewhat more pronounced if the β axial ligand is neutral H_2O rather than anionic N_3^-. Thirdly, the substitution at C-10 also causes an increase in the negative charge on the donor atom, D(δ_D(Z-H) becomes more negative); again this is more significant with a neutral ligand than with an anionic axial ligand. Finally, replacing neutral H_2O by anionic N_3^- causes the charge on Z to become more negative ($\delta_Z(a\text{-}n)$ is negative, and significantly more so if Z is Cl or Br than if Z is H).

This suggests that $[H_2O\text{-}(10\text{-Z})Cbl]^+$, Z = Cl or Br, will discriminate against a neutral ligand because the corrin nucleus is more positive (as pointed out by a reviewer) and the metal is more electron rich and hence less capable of accepting charge donation from the axial donor. If the ligand is an anion, however, binding of an anionic ligand will be favoured because of electrostatic interaction with the corrin, and, moreover, the charge donation can be accepted by the corrin and by delocalisation onto the C-10 Cl or Br. Anions are therefore bound more favourably by $[H_2O\text{-}(10\text{-Z})Cbl]^+$, Z = Cl or Br, than by $[H_2OCbl]^+$ itself.

This is unlikely to be the only factor at play, since, on this basis, $[H_2O\text{-}(10\text{-Cl})Cbl]^+$ should bind anionic ligands better than $[H_2O\text{-}(10\text{-Br})Cbl]^+$; there is little difference, within experimental error, in the log *K* values (Table 3). We have previously shown that a cobalamin will usually coordinate an ambident nucleophile through the softer of the two potential donor atoms, as in $\underline{Se}CN^-$, $\underline{NO}_2^-$ and $\underline{S}_2O_3^{2-}$ [3]. SO_3^{2-} is S-bound as in sulfito-cobalamin [67,68]. An exception we found was SCN^- which is N-bound in the solid state; however, we obtained NMR evidence to show that in solution it existed as a nearly equal mixture of two species which we took to be the N- and S-bound thiocyanato complexes. There is also a report of a crystal structure of SCNCbl in which the thiocyanato ligand is bound through S.[†] Recent DFT calculations (BP86, B3LYP) suggest that the isothiocyanato isomer predominates in complexes with cob(III)alamin and cob(II)alamin [69]. For the anionic ligands we note that values of $\Delta K = \log K_{10H} - \log K_{10Z}$ roughly correlate with the spectrochemical series [70], *viz*, $\underline{S}CN^- < N_3^- < \underline{N}CS^- < NO_2^- < SO_3^{2-}$ (although NO_2^- is usually [71] higher in the spectrochemical series than SO_3^{2-}). If this is indeed the case – and we plan to investigate this in detail using computational methods – then as the π acceptor ability of the anion increases, the better it coordinates to the more electron-rich metal in the 10-Cl and 10-Br derivatives of $[H_2OCbl]^+$. The relatively higher stability of complexes between anionic ligands and $[H_2O\text{-}(10\text{-Z})Cbl]^+$, Z = Cl or Br, is therefore likely to be due to the ability of the system to redistribute charge onto the C-10 substituent and by back-donation onto the ligand itself.

We have shown elsewhere that imidazoles and pyridines are π acceptors from Fe(II) and π donors towards Fe(III) porphyrins [72]. We note (Table 5) that $\Delta K = \log K_{10H} - \log K_{10Z}$ for imidazole and

[†] J. M. Pratt, *Inorganic Chemistry of B_{12}*, Academic Press, London, 1972, p. 152, quotes a personal communication with D. C. Hodgkin.

References on page 126

two pyridines is identical to that for a primary amine, CH_3NH_2. If π bonding played a significant role, one would expect (as we found for the anionic ligands) that ΔK would have been larger for the aromatic N-donor ligands. This too will be investigated computationally and reported elsewhere.

The differential stability of anionic ligands with the 10-Cl and 10-Br derivatives of $[H_2OCbl]^+$ offers an explanation for the lower pK_a values of these compounds (7.22 and 7.28) compared to $[H_2OCbl]^+$ (7.62, *vide supra*). If the anionic ligand OH^- coordinates preferentially to the 10-Cl and 10-Br derivatives, then it will be a poorer Lewis base towards H^+. Modelling of the deprotonation of $[H_2O$-(10-X)Cbl$]^+$ (Table 4) gave ΔE and ΔG values that are broadly in line with the experimental results (calculated pK_a $[H_2OCbl]^+$ > pK_a $[H_2O$-(10-Cl)Cbl$]^+$ > pK_a $[H_2O$-(10-Br)Cbl$]^+$; experimentally observed pK_a $[H_2OCbl]^+$ > pK_a $[H_2O$-(10-Cl)Cbl$]^+$ ≈ pK_a $[H_2O$-(10-Br)Cbl$]^+$). The BP86/TZVP energy-minimized models of [HO-(10-Cl)Cbl] and [HO-(10-Br)Cbl] have identical Co–O bond lengths that are marginal shorter than that in [HOCbl] (1.893 and 1.894 Å, respectively) while the Co–N bond to the trans imidazole ligand (also identical) is marginally longer (2.050 and 2.048 Å, respectively); the effect is very small, but in line with the experimental results.

The rate constants given in Table 6 show that both N_3^- and imidazole react more slowly with $[H_2O$-(10-Br)Cbl$]^+$ than with $[H_2OCbl]^+$, consonant with our previous observations [4] of the reaction of N_3^- and pyridine with $[H_2O$-(10-Cl)Cbl$]^+$ and $[H_2OCbl]^+$. The differences are not large, but are significant. They arise from values of $\Delta H^{\ddagger}$ than are smaller for the reactions with the 10-Cl and 10-Br derivatives than for that with $[H_2OCbl]^+$, but which fail to compensate for $\Delta S^{\ddagger}$ values that are much more negative. We have previously interpreted this in terms of the well-established dissociative interchange mechanism of the ligand substitution reactions of the cobalt corrins [4]. The smaller $\Delta H^{\ddagger}$ and more negative $\Delta S^{\ddagger}$ values are indicative of a transition state that occurs earlier along the reaction coordinate in the reactions of these ligands with the 10-Cl and 10-Br derivatives than in their reactions with $[H_2OCbl]^+$. In an early transition state, the extent of bond breaking between the metal and the departing ligand is smaller than in a late transition state, lowering the value of $\Delta H^{\ddagger}$; conversely, the freedom of the departing ligand is lower, and fails to compensate for the loss of freedom associated with bond formation between the metal and the entering ligand. That the transition state occurs later along the reaction coordinate with $[H_2OCbl]^+$ than with the 10-Cl and 10-Br derivatives, we suggest, is a consequence of the lower charge density on the metal, making it a better electrophile both towards the incoming and the departing ligand.

This work has provided further evidence that perturbing the electronic structure of the corrin can have a small, but significant, effect on the stability of Co(III) corrin complexes with axial ligands. These cis effects may play a role in the labilisation of coenzyme B_{12}, and should not be overlooked when assessing the origin of the remarkable lability of this cofactor.

Acknowledgements

Funding for this work was provided by the Department of Science and Technology/National Research Foundation South African Research Chairs Initiative (GUN 64799), and the University of the Witwatersrand.

Appendix A. Supplementary material

CCDC 1057492 and 1057493 contains the supplementary crystallographic data for this paper. These data can be obtained free of charge from The Cambridge Crystallographic Data Centre via http://www.ccdc.cam.ac.uk/data_request/cif. Supplementary data associated with this article can be found, in the online version, at http://dx.doi.org/10.1016/j.ica.2015.07.019.

References

[1] K.L. Brown, S. Cheng, X. Zou, J.D. Zubkowski, E.J. Valente, L. Knapton, H.M. Marques, Inorg. Chem. 36 (1997) 3666.
[2] H.M. Marques, L. Knapton, X. Zou, K.L. Brown, J. Chem. Soc., Dalton Trans. (2002) 3195.
[3] C.B. Perry, M.A. Fernandes, K.L. Brown, X. Zou, E.J. Valente, H.M. Marques, Eur. J. Inorg. Chem. (2003) 2095.
[4] L. Knapton, H.M. Marques, Dalton Trans. (2005) 889.
[5] C.B. Perry, H.M. Marques, S. Afr. J. Chem. 58 (2005) 9.
[6] S.M. Chemaly, K.L. Brown, M.A. Fernandes, O.Q. Munro, C. Grimmer, H.M. Marques, Inorg. Chem. 50 (2011) 8700.
[7] S.M. Chemaly, M. Florczak, H. Dirr, H.M. Marques, Inorg. Chem. 50 (2011) 8719.
[8] P.P. Govender, I. Navizet, C.B. Perry, H.M. Marques, Chem. Phys. Lett. 550 (2012) 150.
[9] C.F. Zipp, J.P. Michael, M.A. Fernandes, S. Mathura, C.B. Perry, I. Navizet, P.P. Govender, H.M. Marques, Inorg. Chem. 53 (2014) 4418.
[10] S. Mathura, D. Sannasy, A.S. de Sousa, C.B. Perry, I. Navizet, H.M. Marques, J. Inorg. Biochem. 123 (2013) 66.
[11] P.P. Govender, I. Navizet, C.B. Perry, H.M. Marques, J. Phys. Chem. A 117 (2013) 3057.
[12] C.F. Zipp, J.P. Michael, M.A. Fernandes, S. Mathura, C.B. Perry, I. Navizet, P.P. Govender, H.M. Marques, Inorg. Chem. (2014) (in press).
[13] F. Wagner, Proc. R. Soc. London A A228 (1965) 344.
[14] Bruker AXS Inc., Madison, Wisconsin, USA, 2005.
[15] P.P. Govender, I. Navizet, C.B. Perrry, H.M. Marques, J. Phys. Chem. A 117 (2013) 3057.
[16] L.J. Farrugia, J. Appl. Crystallogr. 30 (1997) 565.
[17] O.Q. Munro, H.M. Marques, Inorg. Chem. 35 (1996) 3752.
[18] H.M. Marques, O.Q. Munro, M.L. Crawcour, Inorg. Chim. Acta 196 (1992) 221.
[19] J.B. Conn, T.G. Wartman, Science 115 (1952) 72.
[20] W.W. Reenstra, W.P. Jencks, J. Am. Chem. Soc. 101 (1979) 5780.
[21] H.M. Marques, K.L. Brown, D.W. Jacobsen, J. Biol. Chem. 263 (1988) 12378.
[22] C. Kratky, G. Farber, K. Gruber, K. Wilson, Z. Dauter, H.F. Nolting, R. Konrat, B. Krautler, J. Am. Chem. Soc. 117 (1995) 4654.
[23] M.J. Frisch, G.W. Trucks, H.B. Schlegel, G.E. Scuseria, M.A. Robb, J.R. Cheeseman, G. Scalmani, V. Barone, B. Mennucci, G.A. Petersson, H. Nakatsuji, M. Caricato, X. Li, H.P. Hratchian, A.F. Izmaylov, J. Bloino, G. Zheng, J.L. Sonnenberg, M. Hada, M. Ehara, K. Toyota, R. Fukuda, J. Hasegawa, M. Ishida, T. Nakajima, Y. Honda, O. Kitao, H. Nakai, T. Vreven, J.J.A. Montgomery, J.E. Peralta, F. Ogliaro, M. Bearpark, J.J. Heyd, E. Brothers, K.N. Kudin, V.N. Staroverov, R. Kobayashi, J. Normand, K. Raghavachari, A. Rendell, J.C. Burant, S.S. Iyengar, J. Tomasi, M. Cossi, N. Rega, J.M. Millam, M. Klene, J.E. Knox, J.B. Cross, V. Bakken, C. Adamo, J. Jaramillo, R. Gomperts, R.E. Stratmann, O. Yazyev, A.J. Austin, R. Cammi, C. Pomelli, J.W. Ochterski, R.L. Martin, K. Morokuma, V.G. Zakrzewski, G.A. Voth, P. Salvador, J.J. Dannenberg, S. Dapprich, A.D. Daniels, Ö. Farkas, J.B. Foresman, J.V. Ortiz, J. Cioslowski, D.J. Fox, Gaussian-09, Gaussian Inc., Wallinford, CT, 2009.
[24] A.D. Becke, Phys. Rev. A 38 (1988) 3098.
[25] J.P. Perdew, Phys. Rev. B 33 (1986) 8822.
[26] A. Schäfer, H. Horn, R. Ahlrichs, J. Chem. Phys. 97 (1992) 2571.
[27] A. Schäfer, C. Huber, R. Ahlrichs, J. Chem. Phys. 100 (1994) 5829.
[28] B.I. Dunlap, J. Chem. Phys. 78 (1983) 3140.
[29] B.I. Dunlap, J. Mol. Struct. (Theochem) 529 (2000) 37.
[30] K. Eichkorn, O. Treutler, H. Ohm, M. Ahser, R. Ahlrichs, Chem. Phys. Lett. 240 (1995) 283.
[31] K. Eichkorn, F. Weigend, O. Treutler, R. Ahlrichs, Theor. Chem. Acc. 97 (1997) 119.
[32] R.F. Bader, Atoms in Molecules: A Quantum Theory, Oxford University Press, Oxford, 1990.
[33] T.A. Keith, http://aim.tkgristmill.com, Overland Park, KS, 2011.
[34] F. Neese, WIREs Comput. Mol. Sci. 2 (2012) 73.
[35] E.J. Baerends, D.E. Ellis, P. Ros, Chem. Phys. 2 (1973) 41.
[36] B.I. Dunlap, J.W.D. Connolly, J.R. Sabin, J. Chem. Phys. 71 (1979) 3396.
[37] C. Van Alsenoy, J. Comput. Chem. 9 (1988) 620.
[38] R.A.R.A. Kendall, H.A. Früchtl, Theor. Chem. Acc. 97 (1997) 158.
[39] J.L. Whitten, J. Chem. Phys. 58 (1973) 4496.
[40] K.L. Brown, H.B. Brooks, B.D. Gupta, M. Victor, H.M. Marques, D.C. Scooby, W.J. Goux, R. Timkovich, Inorg. Chem. 30 (1991) 3430.
[41] K.L. Brown, X. Zou, J. Am. Chem. Soc. 114 (1992) 9643.
[42] K.L. Brown, X. Zou, S.R. Savon, D.W. Jacobsen, Biochemistry 32 (1993) 8421.
[43] K.L. Brown, X. Zou, G.Z. Wu, J.D. Zubkowski, E.J. Valente, Polyhedron 14 (1995) 1621.
[44] K.L. Brown, in: R. Banerjee (Ed.), Chemistry and Biochemistry of B_{12}, John Wiley & Sons Inc, New York, 1999, p. 197.
[45] C.B. Perry, H.M. Marques, S. Afr. J. Sci. 100 (2004) 368.
[46] J. Kuta, J. Wuerges, L. Randaccio, P.M. Kozlowski, J. Phys. Chem. A 113 (2009) 11604.
[47] J.P. Glusker, in: D. Dolphin (Ed.), B_{12}, vol. 1, Wiley-Interscience, New York, 1982, p. 23.
[48] CCDC, Cambridge, UK, 2011.
[49] L. Randaccio, M. Furlan, S. Geremia, M. Šlouf, Inorg. Chem. 37 (1998) 5390.

References on page 126

3.7 References

(1) Brown, K. L.; Cheng, S.; Zou, X.; Zubkowski, J. D.; Valente, E. J.; Knapton, L.; Marques, H. M. *Inorg. Chem.* **1997**, *36*, 3666.

(2) Marques, H. M.; Knapton, L.; Zou, X.; Brown, K. L. *J. Chem. Soc. Dalton Trans.* **2002**, 3195.

(3) Perry, C. B.; Fernandes, M. A.; Brown, K. L.; Zou, X.; Valente, E. J.; Marques, H. M. *Eur. J. Inorg. Chem.* **2003**, 2095.

(4) Knapton, L. PhD, University of the Witwatersrand, 2005.

(5) Perry, C. B.; Marques, H. M. *S. Afr. J. Chem.* **2005**, *58*, 9.

(6) Chemaly, S. M.; Brown, K. L.; Fernandes, M. A.; Munro, O. Q.; Grimmer, C.; Marques, H. M. *Inorg. Chem.* **2011**, *50*, 8700.

(7) Navizet, I.; Perry, C. B.; Govender, P. P.; Marques, H. M. *J. Phys. Chem. B.* **2012**, *116*, 8836.

(8) Chemaly, S. M.; Kendall, L.; Nowakowska, M.; Pon, D.; Perry, C. B.; Marques, H. M. *Inorg. Chem.* **2013**, *52*, 1077.

(9) Mathura, S. PhD, University of the Witwatersrand, 2013.

(10) Govender, P. P.; Navizet, I.; Perry, C. B.; Marques, H. M. *J. Phys. Chem. A.* **2013**, *117*, 3057.

(11) Zipp, C. F.; Michael, J. P.; Fernandes, M. A.; Mathura, S.; Perry, C. B.; Navizet, I.; Govender, P. P.; Marques, H. M. *Inorg. Chem.* **2014**, *53*, 4418.

(12) Pearson, R. G. *J. Am. Chem.* **1963**, *85*, 3533.

(13) Knapton, L.; Marques, H. M. *Dalton Trans.* **2005**, 889.

(14) Chemaly, S. M.; Florczak, M.; Dirr, H.; Marques, H. M. *Inorg. Chem.* **2011**, *50*, 8719.

(15) Rubinson, K. A.; Parekh, H. V.; Itabashi, E.; Mark, H. B. *Inorg. Chem.* **1983**, *22*, 458.

(16) Balt, S.; van Herk, A. M. *Transition Met. Chem.* **1983**, *8*, 152.

(17) Moreno-Esparza, R.; Lopez, M.; Peannell, K. H. *J. Chem. Soc. Dalton Trans.* **1992**, 1791.

(18) Balt, S.; de Bolster, M. W. G.; van Herk, A. M. *Inorg. Chim. Acta.* **1985**, *107*, 13.

(19) Randall, W. C.; Alberty, R. A. *Biochem.* **1967**, *6*, 1520.

(20) Thusius, D. *J. Am. Chem. Soc.* **1971**, *93*, 2629.

(21) Firth, R. A.; Hill, H. A. O.; Pratt, J. M.; Thorp, R. G.; Williams, R. J. P. *J. Chem. Soc. A.* **1969**, 381.

(22) Pratt, J. M.; Thorp, R. G. *J. Chem. Soc. A.* **1966**, 187.

(23) Zipp, C. F. PhD, University of the Witwatersrand, 2013.

(24) Garau, G.; Geremia, S.; Marzilli, L. G.; Nardin, G.; Randaccio, L.; Tauzher, G. *Acta Cryst., Sec. B: Struct. Sci* **2003**, *59*, 51.

(25) Pratt, J. M. *The Inorganic Chemistry of Vitamin B_{12}*; Academic Press: London, 1972.

(26) Epinosa, E.; Molins, E.; Lecomte, C. *Chem. Phys. Lett.* **1998**, *285*, 170.

(27) Krautler, B.; Caderas, C.; Konrat, R.; Puchberger, M.; Kratky, C. *Helv. Chim. Acta.* **1995**, *78*, 581.

(28) Perry, C. B. PhD, University of the Witwatersrand, 2004.

(29) Kuta, J.; Wuerges, J.; Randaccio, L.; Kozlowski, P. M. *J. Phys. Chem. A.* **2009**, *113*, 11604.

(30) Glusker, J. P. *in B_{12}*; Wiley-Interscience: New York, 1982.

(31) Randaccio, L.; Furlan, M.; Geremia, S.; Slouf, M. *Inorg. Chem.* **1998**, *37*, 5390.

(32) Hinrichs, L.; Klar, G.; Kopf, J.; Wiese, J. *Acta Crystallogr. A.* **1984**, *40*, C304.

(33) Randaccio, L.; Furlan, M.; Geremia, S.; Slouf, M.; Srnova, I.; Toffoli, D. *Inorg. Chem.* **2000**, *39*, 3403.

(34) Marino, N.; Rabideau, A. E.; Doyle, R. P. *Inorg. Chem.* **2011**, *50*, 220.
(35) Mebs, S.; Henn, J.; Dittrich, B.; Paulmann, C.; Luger, P. *J. Phys. Chem. A* **2009**, *113*, 8366.

CHAPTER 4

The Kinetics of the Reaction of Aqua-10-bromocobalamin with Azide and Imidazole

4.1 Introduction

Co(III) is the classic example of an inert transition metal ion, but the Co(III) at the centre of the corrin ring is remarkably labile toward axial ligand substitution.[1,2] This could be due to the delocalised π electron system of the corrin ring. Thus, a comparison of second-order rate constants (k_{II}) for substitution of H_2O by an incoming ligand (L) in Co(III) complexes with four N-donor equatorial ligands (N_4) (**Equation 4.1**) shows that the lability ratio of Co(III) ion toward substitution in corrin, porphyrin, cobaloxime and amine systems is approximately 10^9:10^6:10^4 :1, respectively.[3,4] Moreover, the substitution of water by thiocyanate has been shown to be nine orders of magnitude faster when the *cis* ligand is corrin than when it is $(NH_3)_4$; the data are given in **Table 4.1** .

$$X–Co^{III}(N_4)–OH_2 + L \xrightarrow{k_{II}} X–Co^{III}(N_4)–L + H_2O \qquad \textbf{(4.1)}$$

This remarkable increase in the lability of the inert cobalt ion is almost certainly a function of its coordination environment.[3-7]

References on page 137

Table 4.1 Second-order rate constants for ligand substitution of X by L in various $Co^{III}(N_4)$ complexes.

X	Complex	L	k_{II}/ M^{-1} s^{-1}	Reference
OH^-	Corrin	N_3^-	1.6×10^5	8
OH^-	Porphyrin[a]	N_3^-	7.2×10^2	9
H_2O	Corrin	I^-	2.2×10^3	1
H_2O	Porphyrin[a]	I^-	1.62	10
I^-	Corrin	SCN^-	1.5×10^2	1
I^-	Corrin	$S_2O_3^{2-}$	6.8	6
I^-	Cobaloxime[b]	SCN^-	1.2×10^{-3}	11
H_2O	Corrin	SCN^-	8.2×10^2	1
H_2O	$(NH_3)_4$	SCN^-	8.6×10^{-7}	12

[a] Tetrakis-(4-N-methylpyridyl)porphinato. [b] Bis(dimethylglyoximato).

The rate of substitution of coordinated H_2O in aquacobalamin ($[H_2OCbl]^+$) with various ligands have been determined.[13-17] The determination of the activation parameters for these reactions can give insights into the reaction mechanism[16,18,19] as well as insights into the effect of different substituents and different incoming ligands, depending on their electron-donating or -withdrawing abilities.

In a previous study in our research group, Knapton[5] examined the influence of perturbing the electronic structure of the corrin ring when the H of C10 was substituted by an electron π donor atom, Cl, on the second-order rate constants and their activation parameters. The data obtained implied that aqua-10-chlorocobalamin ($[H_2O$-(10-Cl)Cbl$]^+$) reacted more slowly with N_3^- (used in that study as an example of an anionic ligand) and pyridine (an example of a neutral ligand) compared to $[H_2OCbl]^+$ because the metal had a lower partial charge in $[H_2OCbl]^+$ than in $[H_2O$-

References on page 137

(10-Cl)Cbl]$^+$; therefore, it was argued that Co in the former complex is a better Lewis acid? From the activation parameters, a compensating effect was noted. As $\Delta H^{\ddagger}$ became more negative and the reaction became enthalpically less favoured, there was a compensating increase in $\Delta S^{\ddagger}$ that favoured the reaction. This was interpreted to mean that in the reaction of [H_2O-(10-Cl)Cbl]$^+$ with the incoming ligands, the transition state occurred earlier along the reaction coordinate, there was less bond breaking in transition state and $\Delta H^{\ddagger}$ was lower; as a consequence $\Delta S^{\ddagger}$ was less positive as the departing ligand H_2O had less freedom.

In this study, the rate of substitution of coordinated H_2O in aqua-10-bromocobalamin ([H_2O-(10-Br)Cbl]$^+$) by N_3^- and imidazole has been determined as have the activation parameters to gain insight into the effect of the C10 substituent on the chemistry of the Co(III) metal ion toward these two incoming ligands. A comparison is made with available data for [H_2OCbl]$^+$.

4.2 Results and Discussion

The rates of substitution reactions, and the associated activation parameters $\Delta H^{\ddagger}$ and $\Delta S^{\ddagger}$, for the substitution of coordinated H_2O in [H_2O-(10-Br)Cbl]$^+$ by N_3^- and imidazole were determined. These reactions were monitored as a function of temperature by uv-vis spectroscopy (**Chapter 2**, **Section 2.5.4.1**). The first-order rate constants (k_I) were determined using **Equation 2.8**, and can be found in **Appendix 4.1**. Examples of the results and regression analysis of the standard non-linear least squares curve fitting data can be found in **Digital Appendix D**. The second-order rate constants (k_{II}) were determined from the slope of a plot of the first-order rate constant against ligand concentration, at each monitoring temperature. The enthalpy and entropy of activation, $\Delta H^{\ddagger}$ and $\Delta S^{\ddagger}$, were obtained from the slope and intercept of a weighted linear least squares Eyring plot as in **Equation 4.2**. k_{II} is the pH-independent second-order rate constant, h and k_B are the Planck and Boltzman constants, respectively.

$$\ln\frac{k_{II}h}{k_BT} = \frac{-\Delta H^{\ddagger}}{RT} + \frac{\Delta S^{\ddagger}}{R} \qquad \textbf{(4.2)}$$

References on page 137

The reaction between $[H_2O\text{-}(10\text{-}Br)Cbl]^+$ and N_3^- was monitored at seven temperatures (10, 15, 17.5, 20, 25, 30 and 35 ^oC) as an absorbance decrease at 356 nm, the wavelength at which the greatest absorbance change occurs. The reaction between $[H_2O\text{-}(10\text{-}Br)Cbl]^+$ and imidazole was monitored at six temperatures (10, 15, 20, 25, 30 and 35 ^oC) and the reaction progression was monitored at 362 nm. In this case, there was an absorbance increase. Examples of absorbance-time traces for the reactions of N_3^- and imidazole with $[H_2O\text{-}(10\text{-}Br)Cbl]^+$ are shown in **Figure 4.1**.

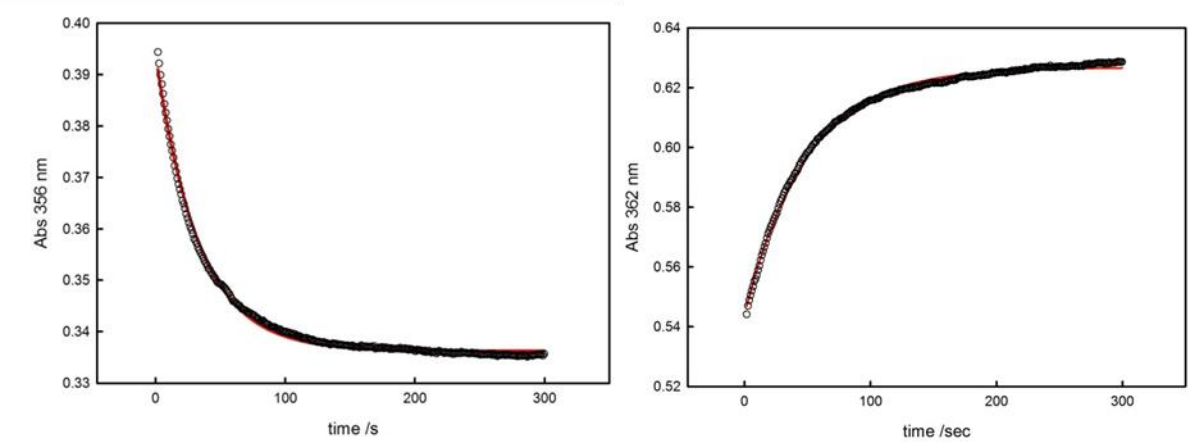


Figure 4.1 Absorbance-time traces for the reaction of (left) N_3^- with $[H_2O\text{-}(10\text{-}Br)Cbl]^+$ (66 μM N_3^-, 25.0 ^oC, pH 5.85 MES buffer, μ = 0.50 M, Na_2SO_4) and (right) imidazole with $[H_2O\text{-}(10\text{-}Br)Cbl]^+$ (6.5 mM Im, 25.0 ^oC, pH 6.9, MOPS buffer, μ = 0.50 M, Na_2SO_4). The red line is the best fit of **Equation 2.10** of the text (**Chapter 2**) to the experimental data which gave k_I^{obs} = 3.02(2) × 10^{-2} s^{-1} and 3.88(4) × 10^{-2} s^{-1}, respectively.

The values k_{II}, k_r, and of $\Delta H^{\ddagger}$ and $\Delta S^{\ddagger}$ deduced from the Eyring plots, as well as those available for the analogous reactions with $[H_2OCbl]^+$ and $[H_2O\text{-}(10\text{-}Cl)Cbl]^+$ are summarised in **Table 4.2**. Examples of plots of k_I against $[L^{n-}]$ for the two ligands studied are given in **Figure 4.2**. The reaction with N_3^- produces intercepts that are statistically different from zero (i.e., k_r in **Equation 2.10** is not negligible); however, k_r is negligibly small for the reaction with imidazole. The Eyring plots are shown in **Figure 4.3**, while that for k_r for N_3^- is shown in **Figure 4.4**.

References on page 137

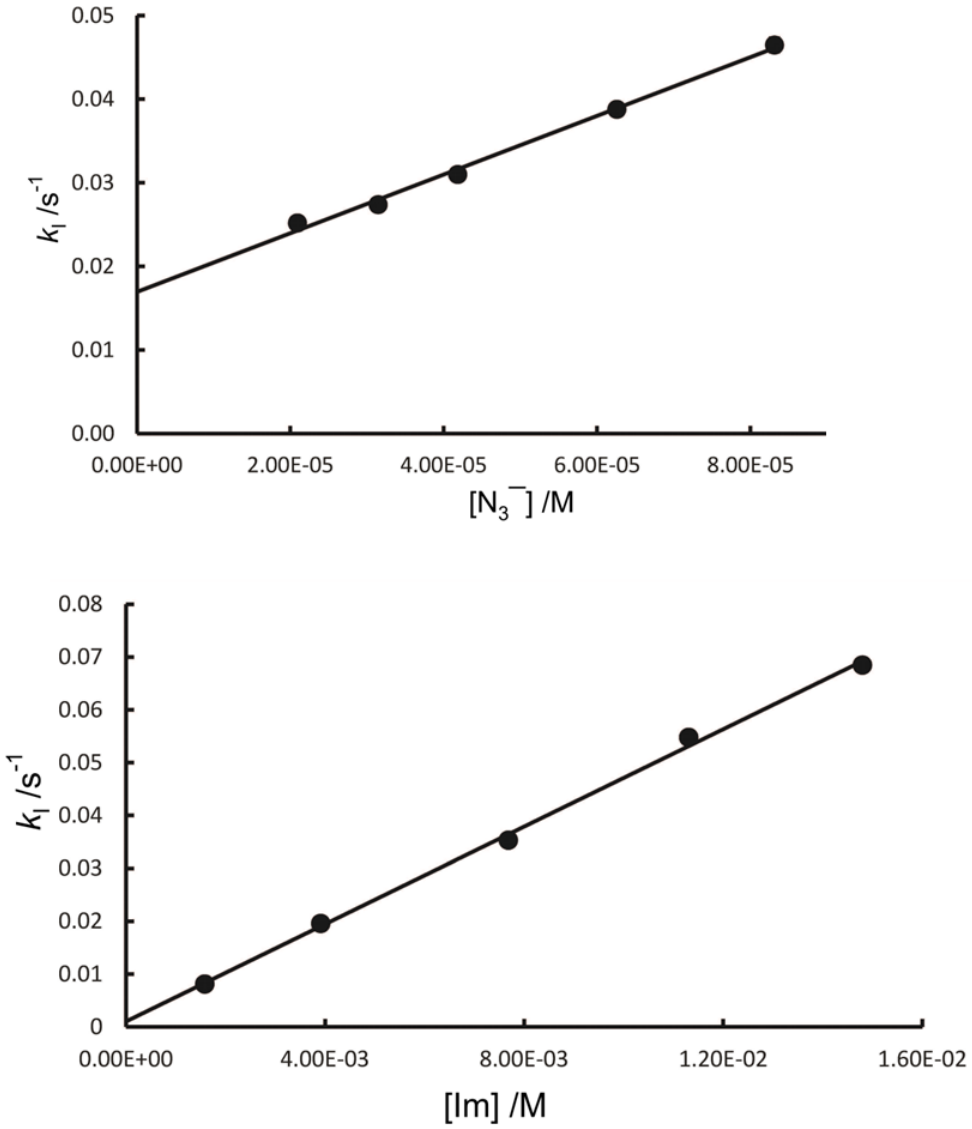


Figure 4.2 Plots of k_I against (top) $[N_3^-]$ (25.0 ^oC) and (bottom) imidazole (20.0 ^oC). The intercept in the first case is significant statistically different from zero, but not in the second case. The gradients give the second order-rate constant, k_{II}.

References on page 137

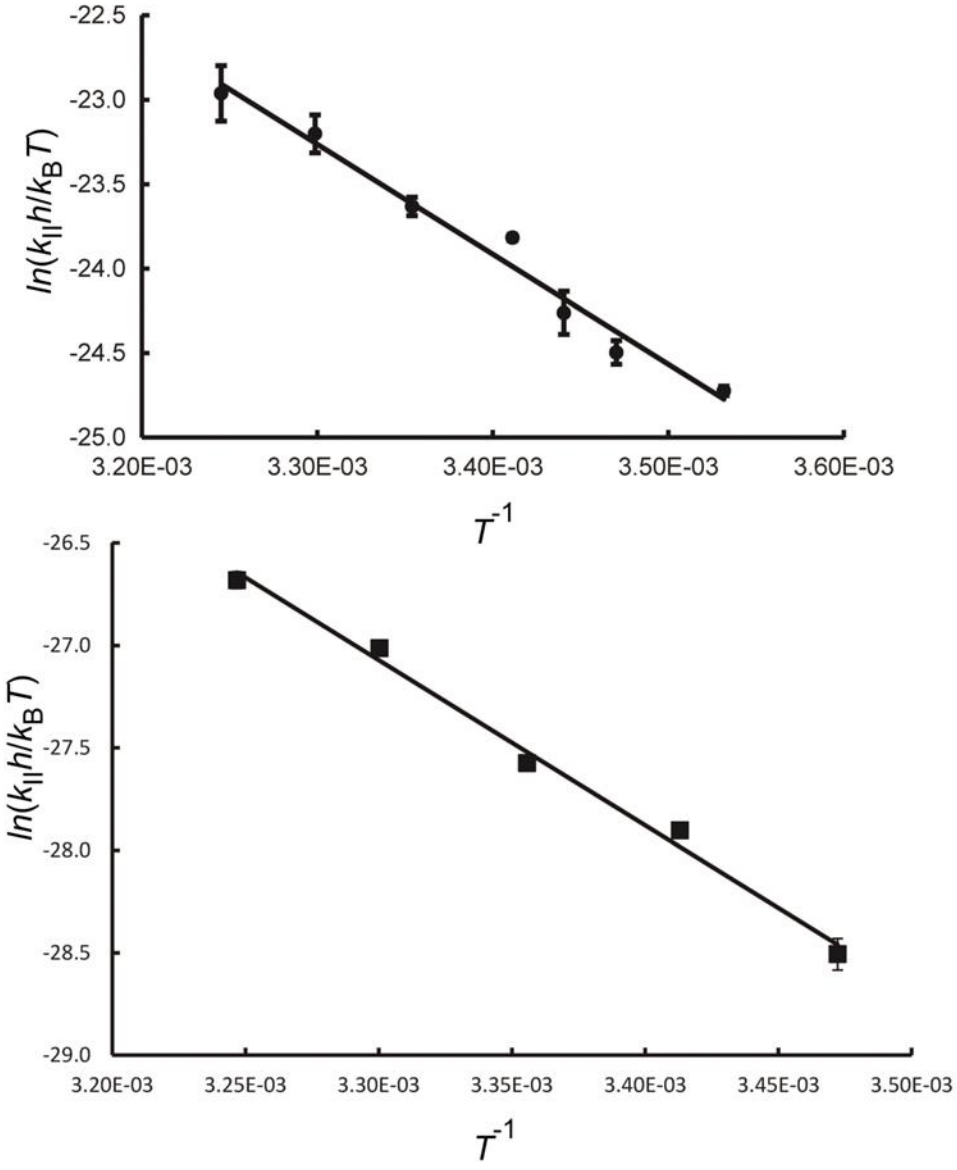


Figure 4.3 Eyring plots for the reaction of N_3^- (top) and imidazole (bottom) with $[H_2O\text{-}(10\text{-}Br)Cbl]^+$.

References on page 137

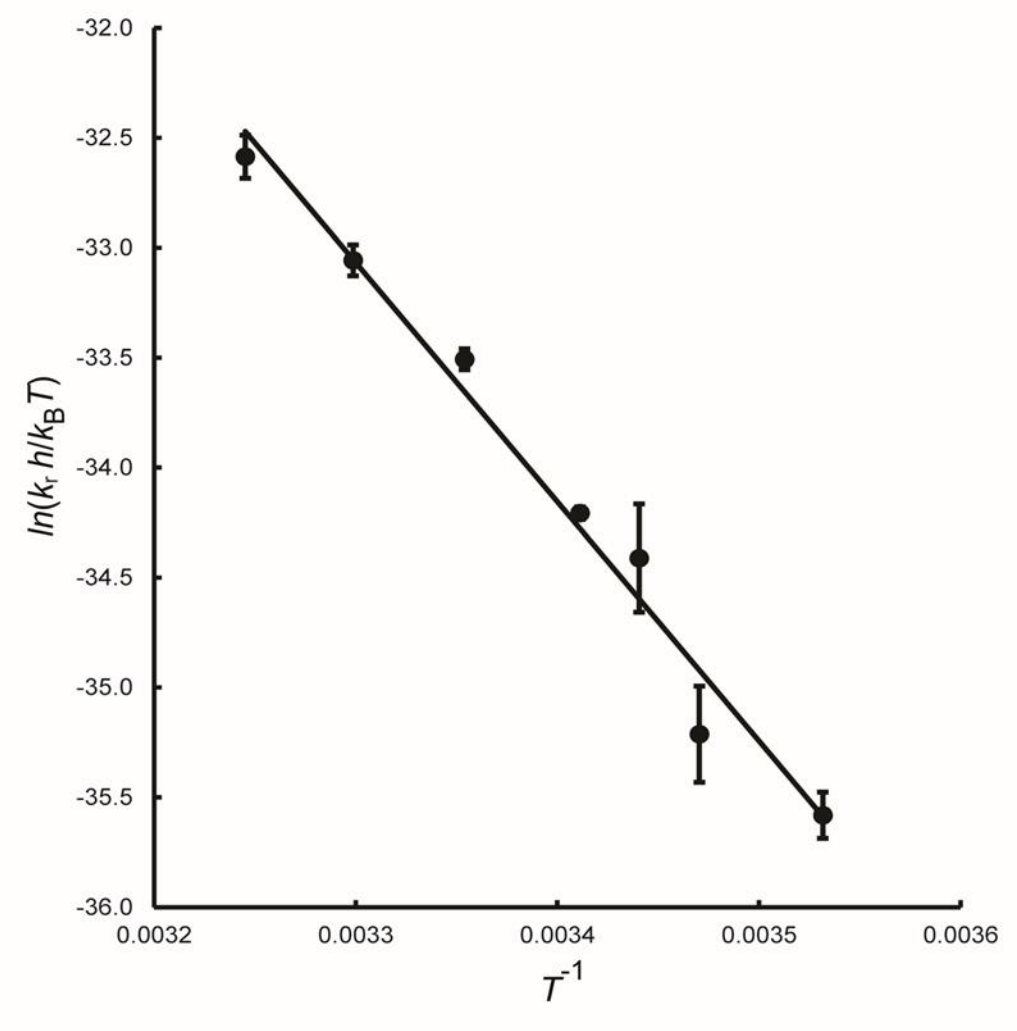


Figure 4.4 Eyring plots for the reverse rate constant of the reaction of N_3^- with $[H_2O\text{-}(10\text{-}Br)Cbl]^+$.

References on page 137

Table 4.2 Rate constants and activation parameters for the reaction of N_3^- and imidazole with $[H_2O\text{-}(10\text{-}Br)Cbl]^+$, $[H_2O\text{-}(10\text{-}Cl)Cbl]^+$ and $[H_2OCbl]^+$.

L	Cobalt corrin	Temp /°C	k_{II} /M^{-1} s^{-1}	$\Delta H^{\ddagger}$ /kJ mol^{-1}	$\Delta S^{\ddagger}$ /J K^{-1} mol^{-1}	k_{II}(25 °C) [a] /M^{-1} s^{-1}	k_r /10^{-2} s^{-1}	$\Delta H^{\ddagger}$ /kJ mol^{-1}	$\Delta S^{\ddagger}$ /J K^{-1} mol^{-1}	k_r(25 °C) [a] /s^{-1}	Ref
N_3^-	$[H_2O\text{-}(10\text{-}Br)Cbl]^+$	10.0	108(3)	54(5)	-13(17)	362	0.21(2)	89(5)	20(17)	1.73	This work
		15.0	138(10)				0.31(1)				
		17.5	176(24)				0.69(19)				
		20.0	277(5)				0.85(2)				
		25.0	339(19)				1.74(9)				
		30.0	530(63)				2.78(20)				
		35.0	685(122)				4.53(47)				
N_3^-	$[H_2OCbl]^+$			68(2)	34(8)	447					4
N_3^-	$[H_2O\text{-}(10\text{-}Cl)Cbl]^+$			50(1)	-32(5)	228					5
Imidazole	$[H_2O\text{-}(10\text{-}Br)Cbl]^+$	15.0	2.5(2)	66(4)	-8(15)	7.0					This work
		20.0	4.6(1)								
		25.0	6.6(1)								
		30.0	11.7(3)								
		35.0	16.6(7)								
Imidazole	$[H_2OCbl]^+$			82(2)	57(8)	24.9					20
NMeIm [b]	$[H_2OCbl]^+$			73(3)	21(11)	12.5					21

[a]Interpolated from the activation parameters. [b]*N*-methylimidazole.

References on page 137

The rate constants given in **Table 4.2** show that both N_3^- and imidazole react more slowly with $[H_2O\text{-}(10\text{-Br})Cbl]^+$ than with $[H_2OCbl]^+$, consonant with the previous observations[5] of the reaction of N_3^- and pyridine with $[H_2O\text{-}(10\text{-Cl})Cbl]^+$ and $[H_2OCbl]^+$. The differences are not large, but are significant. They arise from values of $\Delta H^{\ddagger}$ than are smaller for the reactions with the 10-Cl and 10-Br derivatives than for that with $[H_2OCbl]^+$, but which are compensated for by $\Delta S^{\ddagger}$ values that are much more negative. This matter was previously interpreted in terms of the well-established dissociative interchange mechanism of the ligand substitution reactions of the cobalt corrins.[5] The smaller $\Delta H^{\ddagger}$ and more negative $\Delta S^{\ddagger}$ values are indicative of a transition state that occurs early along the reaction coordinate in the reactions of these ligands with the 10-Cl and 10-Br derivatives than in their reactions with $[H_2OCbl]^+$. In an early transition state, the extent of bond breaking between the metal and the departing ligand is smaller than in a late transition state, lowering the value of $\Delta H^{\ddagger}$; conversely, the degree of freedom of the departing ligand is lower, and fails to compensate for the loss of freedom associated with bond formation between the metal and the entering ligand. That the transition state occurs earlier along the reaction coordinate with the 10-Cl and 10-Br derivatives than with $[H_2OCbl]^+$ might be a consequence of the lower charge density on the metal in the latter, making it a better electrophile both towards the incoming and the departing ligand.

4.3 Conclusion

An investigation was undertaken into the kinetics of the reactions of $[H_2O\text{-}(10\text{-Br})Cbl]^+$ with N_3^- and imidazole to make a comparison with the available kinetic results for $[H_2OCbl]^+$ and $[H_2O\text{-}(10\text{-Cl})Cbl]^+$. The results showed that both N_3^- and imidazole react more slowly with $[H_2O\text{-}(10\text{-Br})Cbl]^+$ than with $[H_2OCbl]^+$, consonant with the previous observations[3] of the reaction of N_3^- and pyridine with $[H_2O\text{-}(10\text{-Cl})Cbl]^+$ and $[H_2OCbl]^+$. The transition state occurs earlier along the reaction coordinate in $[H_2O\text{-}(10\text{-Br})Cbl]^+$ and $[H_2O\text{-}(10\text{-Cl})Cbl]^+$ whereas the transition state occurs later along the reaction coordinate with $[H_2OCbl]^+$. It is assumed that this is a consequence of the lower charge density on the metal in $[H_2OCbl]^+$, making it a better Lewis acid both towards the incoming and the departing ligand. This provides evidence to show how perturbing the electronic structure of the corrin can modify the kinetics of the ligand substitution reactions of the axial coordination site, emphasising the importance of the *cis*-effect in the chemistry of Co(III) macrocyclic complexe

References on page 137

4.4 References

(1) Betterton, E. A. PhD, University of the Witwatersrand, 1982.

(2) Mathura, S.; Perry, C. B.; Navizet, I.; de Sousa, A. S.; Sannasy, D.; Marques, H. M. *J. Inorg. Biochem.* **2013**, *123*, 66.

(3) Knapton, L.; Marques, H. M. *Dalton Trans.* **2005**, 889.

(4) Brown, K. L.; Cheng, S.; Zou, X.; Zubkowski, J. D.; Valente, E. J.; Knapton, L.; Marques, H. M. *Inorg. Chem.* **1997**, *36*, 3666.

(5) Knapton, L. PhD, University of the Witwatersrand, 2005.

(6) Marques, H. M.; Knapton, L.; Zou, X.; Brown, K. L. *J. Chem. Soc. Dalton Trans.* **2002**, 3195.

(7) Perry, C. B.; Marques, H. M. *S. Afr. J. Chem.* **2005**, *58*, 9.

(8) Marques, H. M.; Bradley, J. C.; Brown, K. L.; Brooks, H. *J. Chem. Soc. Dalton Trans.* **1993**, 3475.

(9) Pasternack, R. F.; Gillies, B. S.; Stromsted, J. P. *Bioinorg. Chem.* **1978**, *8*, 33.

(10) Ashley, K. R.; Berggren, M.; Cheng, M. *J. Am. Chem. Soc.* **1975**, *97*, 1422.

(11) Hague, D. N.; Halpern, H. *J. Inorg. Chem.* **1967**, *6*, 2059.

(12) Jackson, W. G.; Jurisson, S. S.; McGregor, B. C. *Inorg. Chem.* **1985**, *24*, 1788.

(13) Pratt, J. M. *The Inorganic Chemistry of Vitamin B_{12}*; Academic Press: London, 1972.

(14) Reenstra, W. W.; Jencks, W. P. *J. Am. Chem. Soc.* **1979**, *101*, 5780.

(15) Marques, H. M.; Brown, K. L.; Jacobsen, W. *J. Biol. Chem.* **1988**, *263*, 12378.

(16) Thusius, D. *J. Am. Chem. Soc.* **1971**, *93*, 2629.

(17) Hill, H. A. O.; Pratt, J. M.; Williams, R. J. P. *Chem. Br.* **1969**, *5*, 156.

(18) Langford, C. H.; Gray, H. B. *Ligand substitution processes*; Benjamin, W. A. Inc.: New York, 1965.

(19) Hasinoff, B. B. *Can. J. Chem.* **1974**, *52*, 910.

(20) Marques, H. M.; Bradley, J. C.; Campbell, L. A. *J. Chem. Soc. Dalton Trans.* **1992**, 2019.

(21) Mathura, S. PhD, University of the Witwatersrand, 2013.

CHAPTER 5

The Thermodynamics of the Reactions of Aquacyanocobester, Aquacyano-10-nitrocobester and Aquacyano-10-aminocobester with Anionic and Neutral Ligands

5.1 Introduction

Co(III) is an example of a kinetically inert metal ion from the first row of the *d* block. However, it is usually labile in cobalt corrins. It is hypothesised that this exceptional lability may be a consequence of the delocalisation of electron density from the equatorial ligand imparting on the metal some measure of labile Co(II)-like character.[1-3] If this is the case, then clearly the electronic structure of the equatorial ligand influences the chemistry of the axial coordination site and, conversely, perturbing that electronic structure should lead to an observable effect on that chemistry. To check this hypothesis, the electronic structure of the corrin ring has been perturbed by a number of approaches. As mentioned in **Chapter 3**, the electronic structure of the corrin ring was perturbed by substitution of the H atom at C10 by Cl (which is π electron-donating towards the corrin)[1] and by NO (which is π electron-withdrawing).[4] The results showed that the C10-Cl bond length in [L-(10-Cl)Cbl] depends on the nature of the axial ligand L.[2] The ligand substitution reactions of $[H_2O\text{-}(10\text{-}Cl)Cbl]^{+1}$ are slower than those of $[H_2OCbl]^+$ itself; and also substitution of the C10 H by Cl favours the coordination of anionic ligands, but discriminates against the binding of neutral N-donor ligands.[1] Substituting the C10 H by NO deactivates the metal ion.[4]

Recent studies in our research group have focused on aquacyanocobester ($[ACCbs]^+$);[5-7] aquacyano-stable yellow cobester ($[ACSYCbs]^+$),[5-7] in which the C5 carbon is oxidized and the 13 atom, 14 π-e^- delocalized system of normal corrins is interrupted leading to a 10 π-e^- system between N21 and N24, and an isolated double bond between N21 and C4; and 5-seco-aquacyanocobester ([5-seco-ACCbs]),[8] in which a part of the corrin ring is cleaved at the C5 position by photosensitized oxygenation, and resulting in diminishing conjugation of the corrin (structures are shown in **Figure 5.1**). The thermodynamic results showed that the softer metal in $[ACCbs]^+$ has a preference for softer ligands and the harder metal in $[ACSYCbs]^+$ and [5-seco-ACCbs] for the harder ligands. For neutral ligands $[ACSYCbs]^+$ showed a lower affinity toward

References on page 190

the incoming ligands (except for NH_3) than $[ACCbs]^+$ itself, which showed that the distinction between the harder Co(III) in $[ACSYCbs]^+$ and softer Co(III) in $[ACCbs]^+$ is maintained for neutral N-donor ligands.[7]

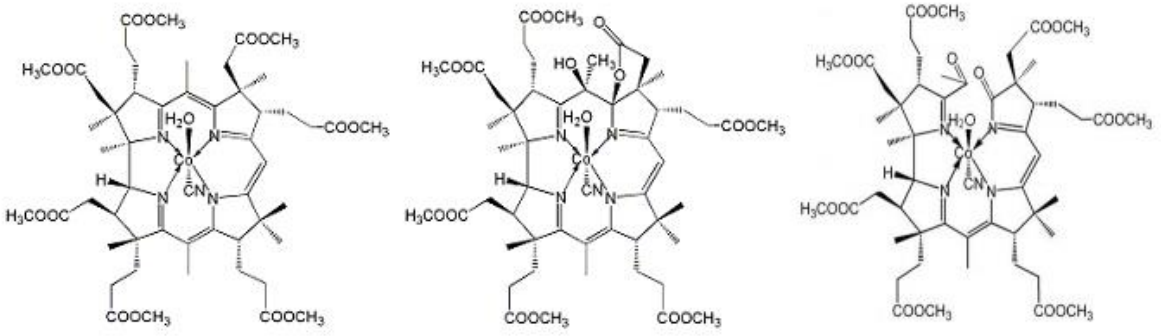


Figure 5.1 The structures of $[ACCbs]^+$ **(1)**, $[ACSYCbs]^+$ **(2)** and [5-seco-ACCbs] **(3)**.[8]

In this chapter, acid dissociation constants, pK_a, for the deprotonation of coordinated H_2O, and stability constants, log K, for the substitution of coordinated H_2O by a variety of neutral and anionic ligands, are reported for $[ACCbs]^+$, aquacyano(10-nitro)cobester, $[AC\text{-}(10\text{-}NO_2)Cbs]^+$ in which the C10 H is replaced by NO_2, which is strongly electron-withdrawing, and aquacyano(10-amino)cobester, $[AC\text{-}(10\text{-}NH_2)Cbs]^+$, in which C10 carries a strongly electron donating NH_2 group. In addition, DFT calculations were used to rationalise the effect that perturbation of the electronic structure of the corrin in these closely related compounds has on the coordination chemistry of the axial coordination site of Co(III).

References on page 190

5.2 pK_a Determination of $[ACCbs]^+$, $[AC\text{-}(10\text{-}NO_2)Cbs]^+$ and $[AC\text{-}(10\text{-}NH_2)Cbs]^+$

5.2.1 Introduction

Axially coordinated water in corrin complexes such as $[ACCbs]^+$ dissociates as illustrated in **Equation 5.1**. As mentioned in **Chapter 3**, for an elucidation of the solution chemistry it is essential to know the value of the dissociation constant to allow for adjustments to be made in both ligand binding and kinetics investigations in order to obtain pH-independent values of equilibrium and rate constants. This is very important at basic pH, when a proton is removed from the axial water group, resulting in the formation of hydroxo species which is inert to substitution reactions.[5,6,9]

$$[CN\text{–}Co\text{–}H_2O]^+ \rightleftharpoons [CN\text{–}Co\text{–}OH] + H^+ \qquad (\mathbf{5.1})$$

It has been reported that the determination of the acid dissociation constant of coordinated H_2O in the cobesters is difficult because of competing hydrolysis of the ester moieties[6] and also the product had a very similar uv-vis spectrum to that of aquacyano complex, but significantly higher pK_a. Chemaly reported a pK_a of 10.56 ± 0.08[7] for $[ACCbs]^+$ which seems reasonable as ester hydrolysis occurs at pH >11.

In this work, the pK_a values for $[AC\text{-}(10\text{-}NO_2)Cbs]^+$ and $[AC\text{-}(10\text{-}NH_2)Cbs]^+$ were determined as well as $[ACCbs]^+$ under the identical experimental conditions (described in **Chapter 2**, **Section 2.5.2.2**), to ensure that all results are comparable (1 mM in each of 2-(*N*-morpholino)ethanesulfonic acid (MES), (*N*-morpholino)propanesulfonic acid (MOPS), 4-(2-hydroxyethyl)-1-piperazineethanesulfonic acid (HEPES), *N*-cyclohexyl-2-aminoethanesulfonic acid (CHES), Tris(hydroxylmethyl)-aminoethane and *N*-cyclohexyl-3-aminopropanesulfonic acid (CAPS)), in 50% isopropanol, between pH 6 to pH 12. The changes in the absorbance spectrum as a function of pH were monitored at 3 or 4 wavelengths. The dependence of the absorbance spectrum on pH between pH 8 and pH 1 was also investigated, in 1 mM potassium hydrogen phthalate (KHP), MES and MOPS in 50% isopropanol for $[AC\text{-}(10\text{-}NO_2)Cbs]^+$ and $[AC\text{-}(10\text{-}NH_2)Cbs]^+$, by adjusting the pH with negligible volumes of solutions of an appropriate concentration of H_2SO_4. We had to balance a slow electrode response in the aqueous isopropanol

References on page 190

solvent with the knowledge[5] that the ester side chains of cobesters are subject to hydrolysis. The data therefore are more scattered than might have been hoped for. The experimental data were fitted to an equation appropriate for one or two pK_as (**Equation 2.1** or **Equation 2.2**), where A_λ is the absorbance measurement at the monitored wavelength and A_0, A_1 and A_2 and K_{a1} and K_{a2} are variables.

$$A_\lambda = \left(\frac{A_0 10^{-pH} + A_1 10^{-pK_a}}{10^{-pH} + 10^{-pK_a}} \right) \qquad \textbf{(2.1)}$$

$$A_\lambda = \left(\frac{A_0 \left(10^{-pH}\right)^2 + A_1 10^{-pK_{a1}} 10^{-pH} + A_2 10^{-pK_{a1}} 10^{-pK_{a2}}}{\left(10^{-pH}\right)^2 + 10^{-pH} 10^{-pK_{a1}} + 10^{-pK_{a1}} 10^{-pK_{a2}}} \right) \qquad \textbf{(2.2)}$$

pK_a was calculated from a weighted average of the results, weighted by the reciprocal of the relative percentage error, where the error is the standard error of the fits. In addition, the pK_a values for these compounds were also determined as a function of temperature to obtain the values of ΔH and ΔS from plots of ln K against T^{-1}.

5.2.2 Results and Discussion

5.2.2.1 Determination of the pK_a of [ACCbs]$^+$

The absorbance changes as a function of pH (see **Figure 5.2**) for a solution of [ACCbs]$^+$ were fitted to a single pK_a and we attributed the relatively poor fits (**Figure 5.3**) to the slow electrode response as mentioned in **Section 5.2.1**. On a subsequent re-examination of the data, the data were fitted to a two pK_a model (**Equation 2.2**) with one pK_a around 8 and the other around 10, as listed in **Table 5.1**. Since the pK_a at around 10 is associated with much larger spectroscopic changes than that around 8, which, in the case of [ACCbs]$^+$ is hardly detectable, the former is

References on page 190

attributed to the ionisation of coordinated H_2O and the second to the ionisation of coordinated H_2O in the diaqua (or aquahydoxo) complex that is always present in $[ACCbs]^+$ solutions, and is an intermediate in the interconversion of the two diastereomers.[5] The inadequacy of the fit to a single pK_a model is more obvious at 585 and 354 nm as illustrated in **Figure 5.3 (A, C)**. **Figure 5.3** shows examples of the dependence of the absorbance at two of several wavelengths monitored to determine the pK_a of coordinated H_2O in $[ACCbs]^+$ in 50% isopropanol/buffer solutions at 25 ^oC. The absorbance change at 354 nm was fitted to a single pK_a value of 10.63 ± 0.04 (**Figure 5.3 (A)**). **Figure 5.3 (B)** shows a significantly better fit with two pK_as at 8.4 ± 0.8 and 10.69 ± 0.05. This is seen more clearly at 585 nm where a single pK_a (10.71 ± 0.05) does not fit the data very well around pH 9 (**Figure 5.3 (C)**), whereas two pK_as at 8.4 ± 0.6 and 10.80 ± 0.05 give a very good fit (**Figure 5.3 (D)**).

The changes in the absorbance spectrum as a function of pH showed that as the pH increased the positions of α, β and γ bands underwent a red shift from 530, 500 and 355 nm to 544, 511 and 365 nm, respectively, with isosbestic points at 330, 364, 395, 414 and 538 nm, as shown in **Figure 5.2**. The average value of the pK_a was 10.71 ± 0.05.

References on page 190

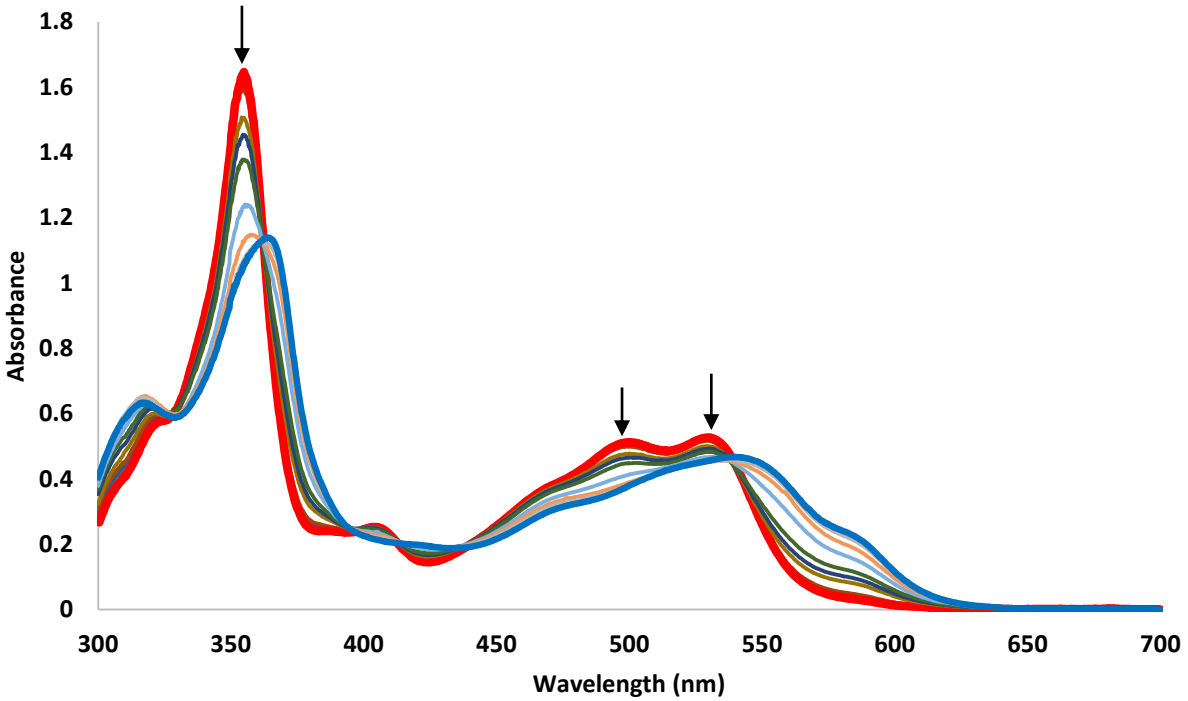


Figure 5.2 The effect of pH on the uv-vis spectrum of $[ACCbs]^+$, on varying pH from 5.8 (red) to 12.0 (blue).

References on page 190

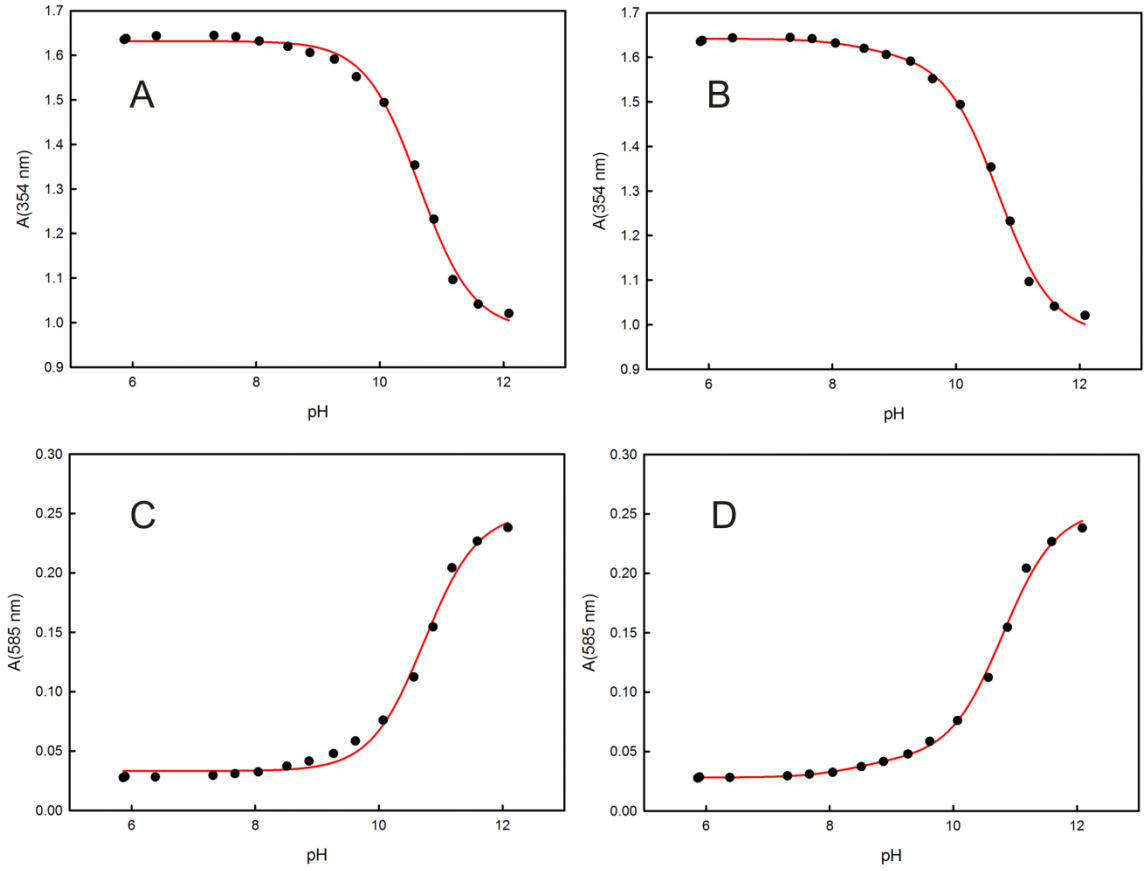


Figure 5.3 Plots of the change in absorbance of $[ACCbs]^+$ in 50% isopropanol/buffer solutions at 25 °C, (A) at 354 nm fitted to a single pK_a model, (B) at 354 nm fitted to a two pK_a model (C) at 585 nm fitted to a single pK_a mpdel, (D) at 585 nm fitted to a two pK_a model.

The pK_a was determined as a function of temperature between 10 °C and 30 °C (**Table 5.1**). From the van't Hoff plot (**Figure 5.4)** the thermodynamic parameters of the ionisation of coordinated H_2O in $[ACCbs]^+$ were determined as ΔH = 86 ± 10 kJ mol^{-1} and ΔS = 85 ± 34 J K^{-1} mol^{-1}, from which the interpolated pK_a at 25°C is 10.6.

References on page 190

Table 5.1 The acid dissociation constants of $[ACCbs]^+$, in 50% isopropanol/buffer Solutions.

Temperature /°C	pK_{a1} [a]	ΔH /kJ mol^{-1}	ΔS /J K^{-1} mol^{-1}	pK_{a1} (25 °C) [c]
13.0	9.3 ± 0.1	102 ± 13	182 ± 43	8.4
18.0	8.67 ± 0.13			
21.0	8.6 ± 0.1			
25.0	8.5 ± 0.1			
30.0	8.1 ± 0.0			
Temperature /°C	pK_{a2} [b]	ΔH /kJ mol^{-1}	ΔS /J K^{-1} mol^{-1}	pK_{a2} (25 °C) [c]
13.0	11.22 ± 0.07	86 ± 10	85 ± 34	10.6
18.0	10.96 ± 0.07			
21.0	10.82 ± 0.07			
25.0	10.71 ± 0.05			
	10.56 ± 0.08 [d]			
30.0	10.28 ± 0.06			

[a] Attributed to ionisation of coordinated H_2O in aquahydroxocobester

[b] Attributed to ionisation of coordinated H_2O in $[ACCbs]^+$

[c] From the thermodynamic parameters

[d] In aqueous solution[7]

References on page 190

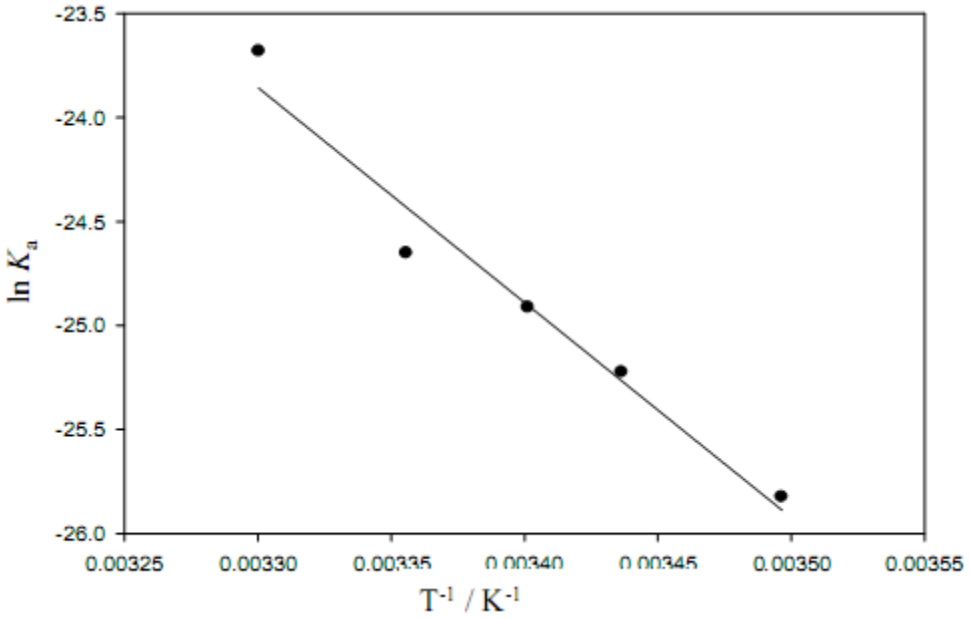


Figure 5.4 van't Hoff plot for the ionisation of coordinated H_2O in $[ACCbs]^+$.

5.2.2.2 Determination of the pK_a of [AC-(10-NO_2)Cbs]$^+$

The pK_a value for $[AC\text{-}(10\text{-}NO_2)Cbs]^+$ was determined in the same manner as that for $[ACCbs]^+$. The spectroscopic changes for the absorbance spectra of $[AC\text{-}(10\text{-}NO_2)Cbs]^+$ were monitored by uv-vis spectroscopy as a function of pH (**Figure 5.5**); as the pH increased the positions of α, β and γ bands underwent a red shift from 543, 512 and 359 nm to 561, 521 and 369 nm, respectively, with isosbestic points at 366, 433 and 555 nm.

An example of fits at several wavelengths are illustrated in **Figure 5.6.** Systematic and reproducible deviations of a fit of the experimental data to a single pK_a model were found, and the data fitted much more satisfactorily to a two pK_a model with one pK_a around 8 and the other around 10 (see **Figure 5.6**). As mentioned in **Section 5.2.2.3** the pK_a at around 10 is attributed to the ionisation of coordinated H_2O and the pK_a at around 8 is attributed to the ionisation of coordinated H_2O in the diaqua (or aquahydoxo) complex.

The pK_a was determined as a function of temperature between 10 ^oC and 30 ^oC as listed in **Table 5.2**. From the van't Hoff plot (**Figure 5.7)** the thermodynamic parameters of the ionisation of

References on page 190

coordinated H_2O in $[AC\text{-}(10\text{-}NO_2)Cbs]^+$ were determined as ΔH = 84 ± 11 kJ mol^{-1} and ΔS = 87 ± 39 J K^{-1} mol^{-1} from which the interpolate pK_a at 25 °C is 10.3.

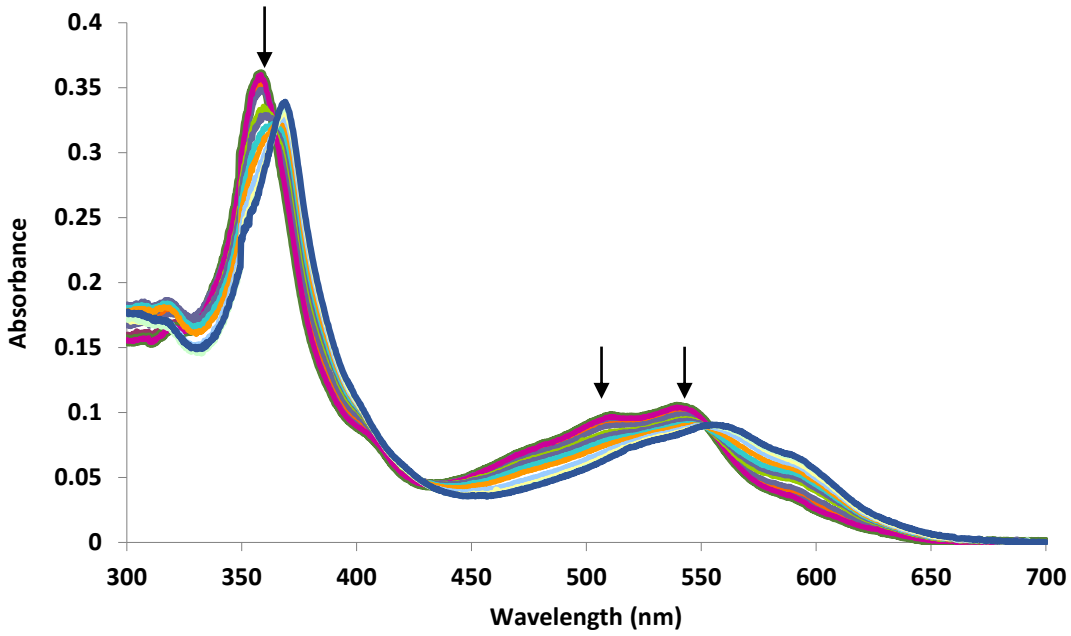


Figure 5.5 The effect of pH on the uv-vis spectrum of $[AC\text{-}(10\text{-}NO_2)Cbs]^+$, on varying pH from 6.7 (purple) to 12.3 (blue).

References on page 190

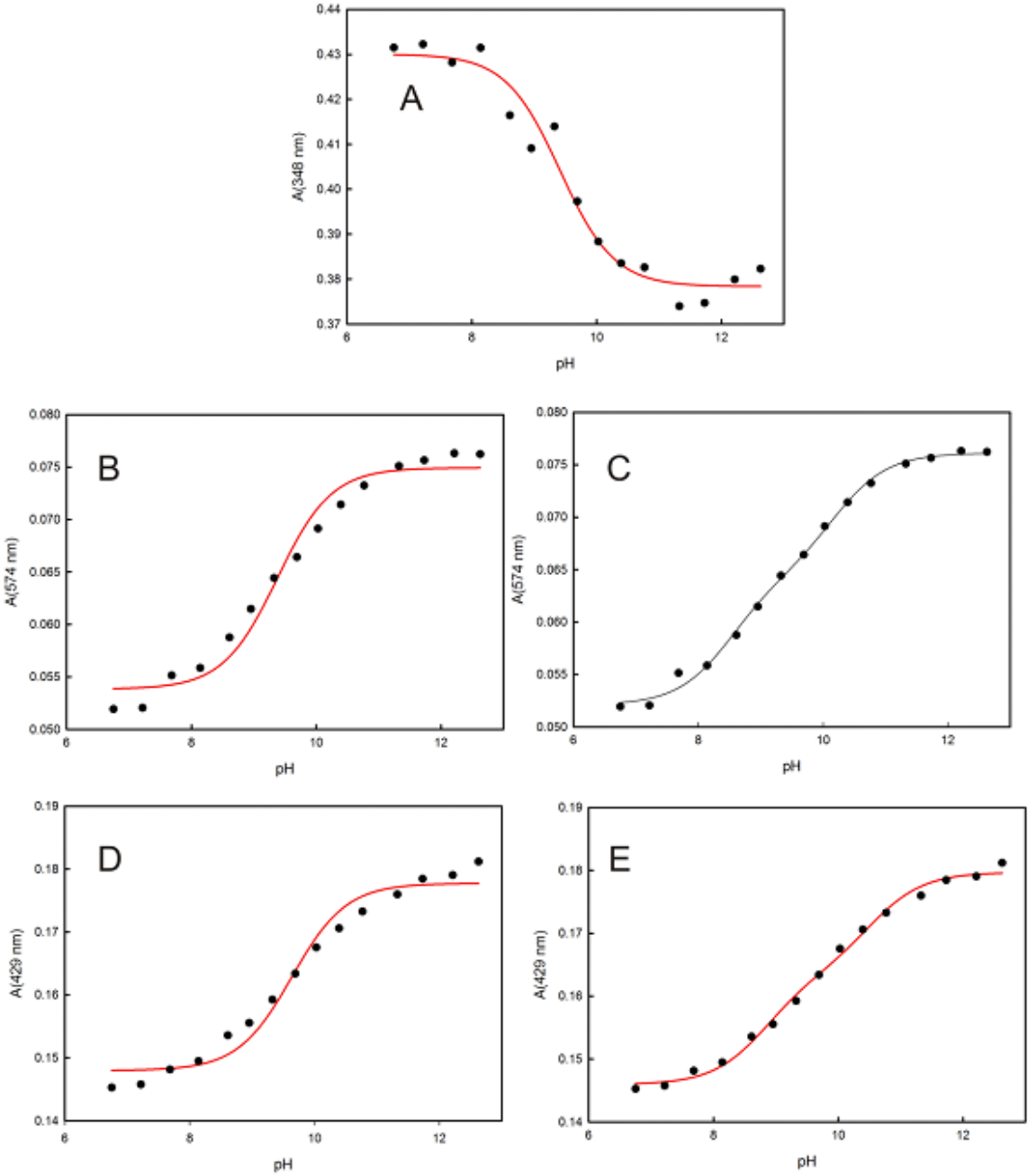


Figure 5.6 Monitoring the absorbance change with pH (A) an example of a fit to a single pK_a fit at the γ band of [AC-(10-NO_2)Cbs]$^+$, (B, D) examples of a fit to a single pK_a model and (C, E) examples of a fit to a two pK_a model.

References on page 190

Table 5.2 The acid dissociation constants of [AC-(10-NO_2)Cbs]$^+$, in 50% isopropanol/buffer Solutions.

Temperature /^{o}C	pK_{a1} [a]	ΔH /kJ mol^{-1}	ΔS /J K^{-1} mol^{-1}	pK_{a1} (25 ^{o}C) [c]
11.0	9.63 ± 0.01	106 ± 9	189 ± 32	8.7
18.0	8.87 ± 0.26			
21.5	9.23 ± 0.11			
25.0	8.63 ± 0.13			
30.0	8.40 ± 0.01			
Temperature /^{o}C	pK_{a2} [b]	ΔH /kJ mol^{-1}	ΔS /J K^{-1} mol^{-1}	pK_{a2} (25 ^{o}C) [c]
11.0	10.92 ± 0.04	84 ± 11	87 ± 39	10.3
18.0	10.72 ± 0.11			
21.0	10.55 ± 0.14			
25.0	10.32 ± 0.13			
30.0	9.90 ± 0.08			

[a] Attributed to ionisation of coordinated H_2O in aquahydroxocobester

[b] Attributed to ionisation of coordinated H_2O in [AC-(10-NO_2)Cbs]$^+$

[c] From the thermodynamic parameters

References on page 190

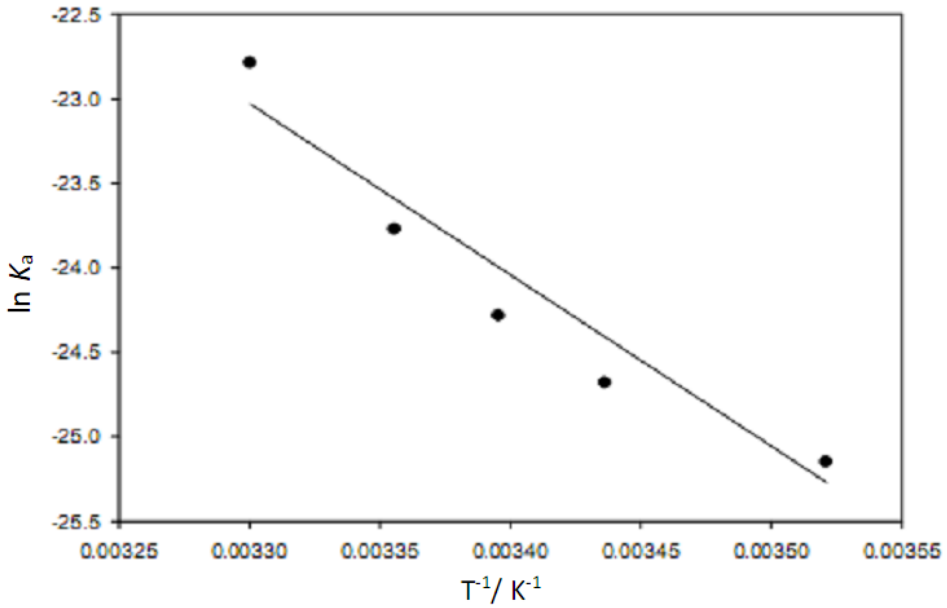


Figure 5.7 van't Hoff plot for the ionisation of coordinated H_2O in $[AC\text{-}(10\text{-}NO_2)Cbs]^+$.

5.2.2.3 Determination of the pK_a of $[AC\text{-}(10\text{-}NH_2)Cbs]^+$

The collected data for the titration of $[AC\text{-}(10\text{-}NH_2)Cbs]^+$ was analysed in the same way as that of $[AC\text{-}(10\text{-}NO_2)Cbs]^+$ and $[ACCbs]^+$.

The effect of pH change on the absorbance spectra of $[AC\text{-}(10\text{-}NH_2)Cbs]^+$ was recorded by uv-vis spectroscopy. It was noticed as the pH was increased the position of α, β and γ bands shifted from 522, 511 and 359 nm to 559, 544 and 369 nm, with distinctive isosbestic points at 321, 364, 429 and 555 nm, **Figure 5.8**. An example of the fits is illustrated in **Figure 5.9** at 360, 600, 374 and 510 nm. As illustrated in **Figure 5.9 (A),** monitoring the absorbance change with pH at the γ band (360 nm) of $[AC\text{-}(10\text{-}NH_2)Cbs]^+$ also appeared to be adequately described by a single pK_a (9.42 ± 0.09). At other wavelengths, and in particular at 374 nm (**Figure 5.9 (F)**), it is clear that a single pK_a (**Figure 5.9 (B, D, F)**) is an inadequate description of the absorbance changes with pH and at least two pK_as are required (**Figure 5.9 (C, E,G)**). As discussed above a two pK_a model indicates two pK_as, one around 8 which is corresponded to the ionisation of H_2O in diaqua or aquahydroxo complex and the other around 10 which is associated with much larger spectroscopic changes and corresponds to the ionisation of H_2O in $[AC\text{-}(10\text{-}NH_2)Cbs]^+$.

References on page 190

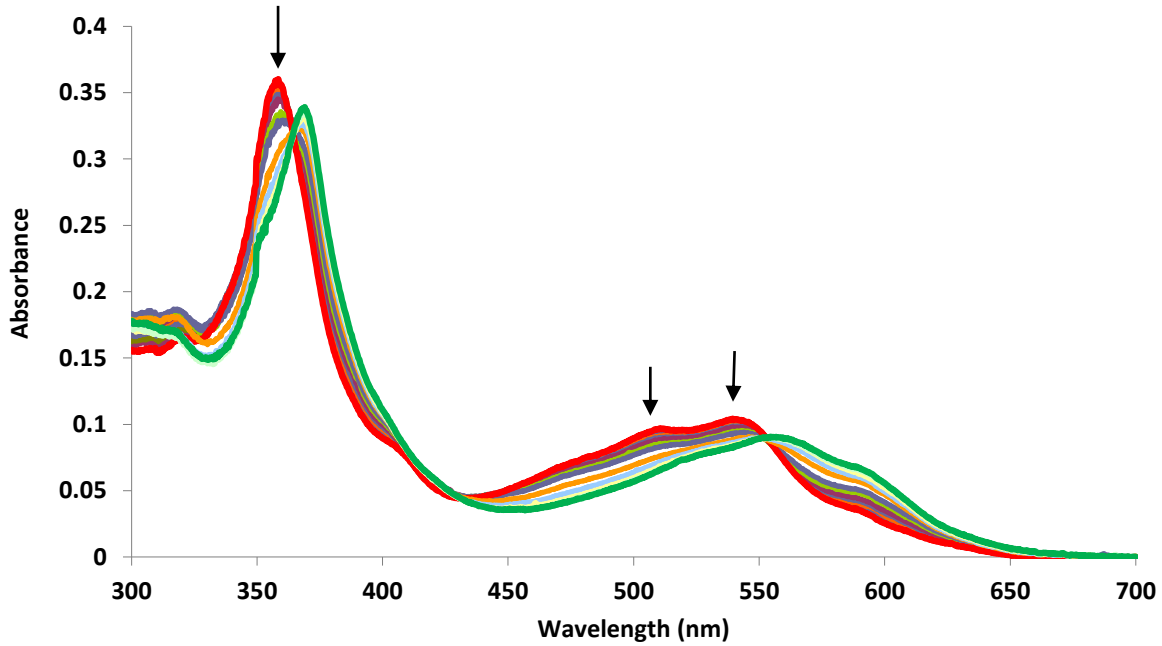


Figure 5.8 The effect of pH on the uv-vis spectrum of [AC-(10-NH_2)Cbs]$^+$, varying pH from 6.2 (red) to 12.6 (green).

References on page 190

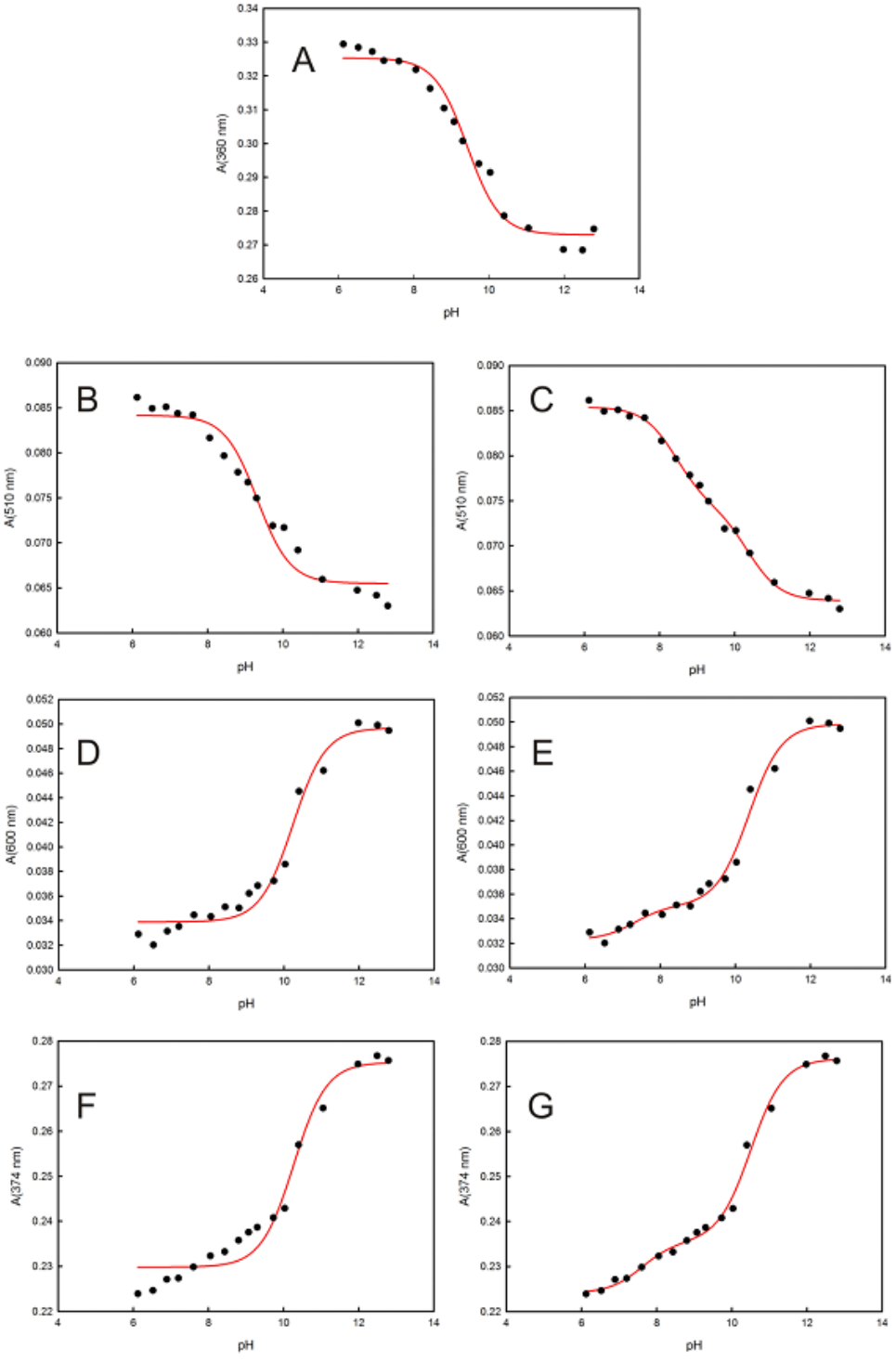


Figure 5.9 Monitoring the absorbance change with pH, (A) at the γ band of $[AC\text{-}(10\text{-}NH_2)Cbs]^+$ using a single pK_a model, (B, D, F) examples of a fit of the experimental data to a single pK_a model at 510, 600 and 374 nm, respectively and (C, E,G) examples of a fit to a two pK_a model with one pK_a around 8 and the other > 10.

References on page 190

The pK_a determination was studied as a function of temperature (**Table 5.3**), ranged from 10 to 30 ^oC. Thermodynamics parameters, ΔH = 89 ± 11 kJ mol^{-1} and ΔS = 100 ± 39 J K^{-1} mol^{-1} were determined for the ionisation of H_2O in $[AC\text{-}(10\text{-}NH_2)Cbs]^+$ from the slope and the intercept of the van't Hoff plot, as shown in **Figure 5.10**. The pK_a was determined as 10.4 at 25 ^oC from the thermodynamic parameters.

Table 5.3 The acid dissociation constants of $[AC\text{-}(10\text{-}NH_2)Cbs]^+$ in 50% isopropanol/buffer solutions.

Temperature /^oC	pK_{a1} [a]	ΔH /kJ mol^{-1}	ΔS /J K^{-1} mol^{-1}	pK_{a1} (25 ^oC) [c]
13.0	8.9 ± 0.2	39 ± 7	-34 ± 23	8.7
18.0	8.85 ± 0.16			
21.5	8.8 ± 0.2			
25.0	8.7 ± 0.3			
30.0	8.5 ± 0.2			
Temperature /^oC	pK_{a2} [b]	ΔH /kJ mol^{-1}	ΔS /J K^{-1} mol^{-1}	pK_{a2} (25 ^oC) [c]
13.0	11.01 ± 0.05	89 ± 11	100 ± 39	10.4
18.0	10.87 ± 0.07			
21.0	10.54 ± 0.13			
25.0	10.30 ± 0.14			
30.0	10.16 ± 0.15			

[a] Attributed to ionisation of coordinated H_2O in aquahydroxocobester

[b] Attributed to ionisation of coordinated H_2O in $[AC\text{-}(10\text{-}NH_2)Cbs]^+$

[c] From the thermodynamic parameters

References on page 190

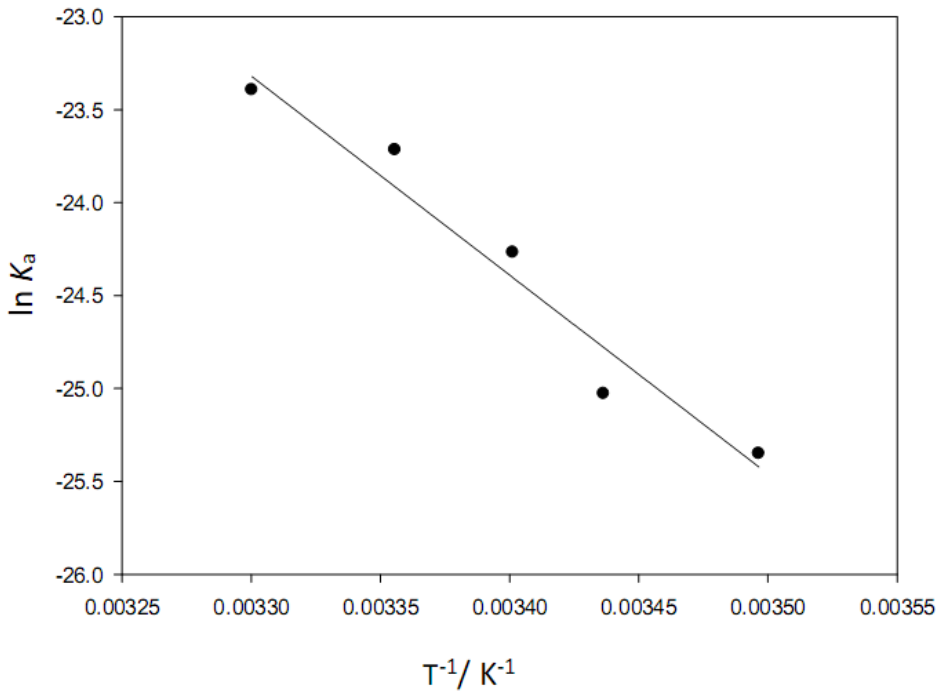


Figure 5.10 van't Hoff plot for the ionisation of coordinated H_2O in $[AC\text{-}(10\text{-}NH_2)Cbs]^+$.

In addition, an extensive investigation was undertaken to measure the pK_b of the 10-NH_2 substituent in $[AC\text{-}(10\text{-}NH_2)Cbs]^+$. When it is protonated, the 10-NH_2 group in $[AC\text{-}(10\text{-}NH_2)Cbs]^+$ amino group is no longer electron-donating towards the corrin, and should behave very much like 10-H in $[ACCbs]^+$ itself; the principal absorption bands in the uv-vis spectrum of $[AC\text{-}(10\text{-}NH_2)Cbs]^+$ should shift to shorter wavelength. However the experimental data showed that this is not the case; the bands remained red-shifted relative to those of $[ACCbs]^+$ throughout the pH range from 6 to 12.5 (for example, the γ band of $[ACCbs]^+$ shifted from 354 nm at pH 5.9 to 364 nm at pH 12.1; that of $[AC\text{-}(10\text{-}NH_2)Cbs]^+$ shifted from 359 nm at pH 6.1 to 369 nm at pH 12.5). Therefore protonation of 10-NH_2 must occur below pH 7.

The changes in the uv-vis spectrum of $[AC\text{-}(10\text{-}NH_2)Cbs]^+$ were monitored between pH 8 and pH 1 and very small changes in absorbance were found, and significantly, without a change in band positions (**Figure. 5.11**). The data were adequately fitted to a single pK_a = 5.1 ± 0.1 (average of three titrations, each monitored at three different wavelengths). Provide the pH remained above 2, the absorbance changes were completely reversible. At lower pH irreversible changes occurred which are attributed to the hydrolysis of the ester side chains. Similar changes

References on page 190

were observed in the uv-vis spectrum of $[AC\text{-}(10\text{-}NO_2)Cbs]^+$ in the acid region (**Figure 5.11**) pK_a = 3.4 ± 0.3 (average of three titrations, each monitored at two different wavelengths). Since firstly the absorbance changes are very small; secondly, there is no significant change in the band positions; and thirdly a similar process is observed in solutions of $[AC\text{-}(10\text{-}NO_2)Cbs]^+$, we conclude this cannot be due to protonation of the 10-NH_2 group. Either this occurs in the pH 8-10 region and there are actually three pK_as in that region (no reliable fits were obtained with a three pK_a model) but the lack of a blue-shift in the band positions makes this unlikely; or the protonation is spectroscopically silent in the uv-vis (also unlikely); or, surprisingly, the protonation of the 10-NH_2 group occurs below pH 2. In the absence of further evidence, we tentatively conclude that the latter is the case. The pK_a at around 4 was assigned to the ionisation of coordinated H_2O in the diaqua(10-Z)cobester ($[diaqua\text{-}(10\text{-}Z)Cbs]^{2+}$) , Z = NO_2, NH_2 ; that at around 8 to the aquahydroxo(10-Z)cobester ($[aquahydroxo\text{-}(10\text{-}Z)Cbs]^+$); and that around 10 to that of the $[AC(10\text{-}Z)Cbs]^+$.

References on page 190

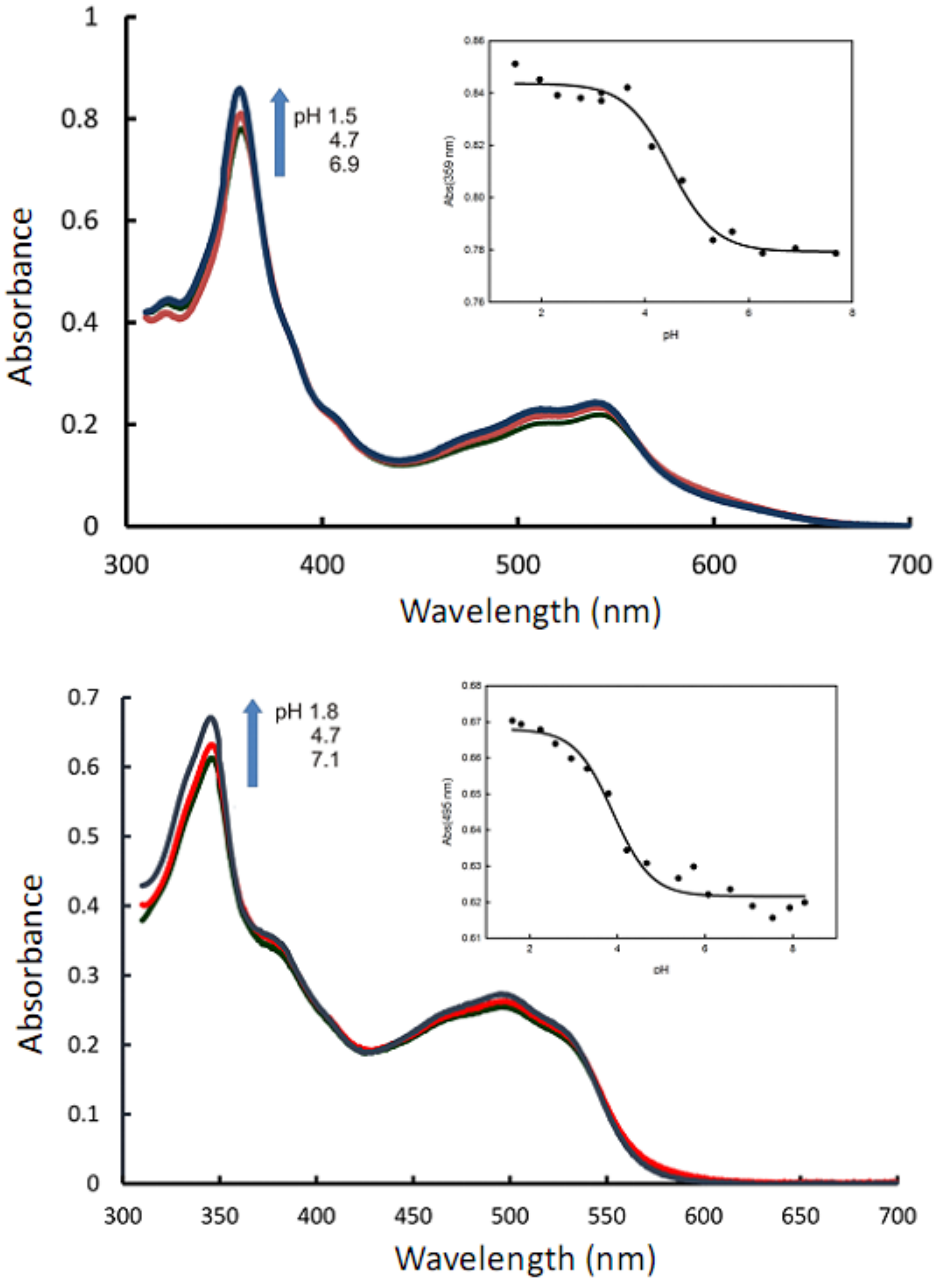


Figure 5.11 Absorbance changes on titrating (top) $[AC\text{-}(10\text{-}NH_2)Cbs]^+$ and (bottom) $[AC\text{-}(10\text{-}NO_2)Cbs]^+$ between pH 8 and pH 1.5. The inserts show fitting of the data at the γ-band maximum to an expression for a single pK_a at 5.1 ± 0.1 for $[AC\text{-}(10\text{-}NH_2)Cbs]^+$ and 3.4 ± 0.3 for $[AC(10\text{-}NO_2)Cbs]^+$. (The results are average results of three titrations monitored at three and two different wavelengths, respectively).

References on page 190

5.2.2.4 Summary of pK_a values

The p*K*a values and thermodynamic parameters for [AC-(10-NO_2)Cbs]$^+$, [AC-(10-NH_2)Cbs]$^+$ and [ACCbs]$^+$ are summarised in **Table 5.4**.

Table 5.4 The Acid Dissociation Constants of the Cobesters [AC-(10-Z)Cbs]$^+$, Z = H, NO_2, NH_2, in 50% Aqueous Isopropanol Solutions.

Z	Temp /°C	pK_{a1} [a]	ΔH /kJ mol^{-1}	ΔS /J K^{-1} mol^{-1}	pK_{a1} (25 °C) [c]	pK_{a2} [b]	ΔH /kJ mol^{-1}	ΔS /J K^{-1} mol^{-1}	pK_{a2} (25 °C) [c]
H	13.0	9.3 ± 0.1	102 ± 13	182 ± 43	8.4	11.22 ± 0.07	86 ± 10	85 ± 34	10.6
	18.0	8.7 ± 0.1				10.96 ± 0.07			
	21.0	8.6 ±0.1				10.82 ± 0.07			
	25.0	8.5 ± 0.1				10.71 ± 0.05			
	30.0	8.15 ± 0.05				10.28 ± 0.06			
	25.0					10.56 ± 0.08 [d]			
NO_2	11.0	9.63 ± 0.01	106 ± 9	189 ± 32	8.7	10.92 ± 0.04	84 ± 11	87 ± 39	10.2
	18.0	8.9 ± 0.3				10.72 ± 0.11			
	21.5	9.2 ± 0.1				10.55 ± 0.14			
	25.0	8.6 ± 0.1				10.32 ± 0.13			
	30.0	8.4 ± 0.01				9.90 ± 0.08			
NH_2	11.8	8.9 ± 0.2	39 ± 7	-34 ± 23	8.7	11.01 ± 0.05	89 ± 11	100 ± 39	10.4
	18.0	8.9 ± 0.2				10.87 ± 0.07			
	21.3	8.8 ± 0.2				10.54 ± 0.13			
	25.0	8.7 ± 0.3				10.30 ± 0.14			
	30.0	8.5 ± 0.2				10.2 ± 0.2			

[a] Attributed to ionization of coordinated H_2O in aquahydroxo(10-Z)Cbs

[b] Attributed to ionization of coordinated H_2O in aquacyano(10-Z)Cbs

[c] From the thermodynamic parameters

[d] In aqueous solution[7]

References on page 190

5.2.3 Conclusions

The pK_a studies indicated that a two pK_a model is more adequate for fitting the experimental data. The results showed that the pK_as of $[ACCbs]^+$, $[AC\text{-}(10\text{-}NH_2)Cbs]^+$ and $[AC\text{-}(10\text{-}NO_2)Cbs]^+$ are similar within experimental error. As indeed are the thermodynamic parameters (ΔH = 86 ± 10 kJ mol^{-1} and ΔS = 85 ± 34 J K^{-1} mol^{-1} for $[ACCbs]^+$; ΔH = 89 ± 11 kJ mol^{-1} and ΔS = 100 ± 39 J K^{-1} mol^{-1} for $[AC\text{-}(10\text{-}NH_2)Cbs]^+$; ΔH = 84 ± 11 kJ mol^{-1}; ΔS = 87 ± 39 J K^{-1} mol^{-1} for $[AC\text{-}(10\text{-}NO_2)Cbs]^+$).

5.3 Determination of the Stability Constants of $[ACCbs]^+$, $[AC\text{-}(10\text{-}NO_2)Cbs]^+$ and $[AC\text{-}(10\text{-}NH_2)Cbs]^+$, with Various Anionic and Neutral Ligands

5.3.1 Introduction

Stability constants are a measure of the affinity of a metal ion for an exogenous ligand and can provide insight into the nature of that metal ion. Relevant to this study, the stability constants for the formation of complexes of a variety of ligands with $[ACCbs]^+$,[6] $[ACSYCbs]^+$,[6] and [5-seco-ACCbs][8] have been determined. The stability constants for substitution of water by a series of anionic ligands in these complexes are reported in **Table 5.5**. The results showed that the interruption of the conjugation system in $[ACSYCbs]^+$ and [5-seco-ACCbs], results in a less electron rich and more Co(III)-like metal ion, in the order $[ACCbs]^+ > [ACSYCbs]^+ > [5\text{-seco-}ACCbs]^+$. Thus the π donor ligands (N_3^-, SCN^-, $S_2O_3^{2-}$) bound preferentially to the less electron rich metal ion in $[ACSYCbs]^+$ and [5-seco-ACCbs]. Whereas, the π acceptor ligands (CN^-, SO_3^{2-}, NO_2^-) bound preferentially to the more electron rich metal ion in $[ACCbs]^+$. For the coordination of anionic ligands by $[ACCbs]^+$ and $[ACSYCbs]^+$, the thermodynamics of the ligand substitution reaction of H_2O (by the anionic ligands N_3^-, NO_2^-, CN^-, SO_3^{2-}) were compared and showed that the ligands with a harder donor atom (N in N_3^- and NO_2^-) produce ΔH values that are more negative in their reactions with $[ACSYCbs]^+$ than with $[ACCbs]^+$, whereas ligands with a softer donor (C in CN^-, S in SO_3^{2-}) have ΔH values that are less positive, or more negative, for their reactions with $[ACCbs]^+$ than with $[ACSYCbs]^+$. The softer metal in $[ACCbs]^+$ has a preference for softer ligands and the harder metal in $[ACSYCbs]^+$ for the harder

References on page 190

ligands. The stability constants for the coordination of neutral N-donor ligands by $[ACCbs]^+$ and $[ACSYCbs]^+$ showed that the values of log *K* for the coordination of the neutral ligands by $[ACSYCbs]^+$ are generally lower than those coordinated by $[ACCbs]^+$, except for NH_3 (**Table 5.6**).[7] The reactions of aliphatic amines with $[ACSYCbs]^+$ produce more negative ΔH values than the reactions with $[ACCbs]^+$; thus the Co(III) in $[ACSYCbs]^+$ has a higher affinity for the harder N-donor ligands (N in NH_3), while the Co(III) in $[ACCbs]^+$ has a greater affinity the softer aromatic N-donor ligands (N in pyridine). It was subsequently shown that the distinction between the harder Co(III) in $[ACSYCbs]^+$ and softer Co(III) in $[ACCbs]^+$ is maintained for neutral N-donor ligands.[7]

References on page 190

Table 5.5 Stability constants for the substitution of water by anionic ligands in $[ACCbs]^+$, $[ACSYCbs]^+$ and [5-seco-ACCbs] at 25 °C.

	log *K*		
Ligand	$[ACCbs]^+$	$[ACSYCbs]^+$	$[5\text{-seco-ACCbs}]^+$
SO_3^{2-}	5.00 ± 0.02[a]	3.06 ± 0.02[a]	3.4 ± 0.01[b]
NO_2^-	2.89 ± 0.01[a]	2.38 ± 0.01[a]	2.17 ± 0.09[b]
CN^-	8.10 ± 0.1[a]	7.10 ± 0.05[a]	6.2 ± 0.01[b]
N_3^-	2.595 ± 0.1[a]	2.64 ± 0.03[a]	2.6 ± 0.01[b]
SCN^-	1.53 ± 0.04[b]	1.80 ± 0.08[b]	2.02 ± 0.02[b]
$S_2O_3^{2-}$	0.51 ± 0.04[a]	-0.2 ± 0.01[a]	1.80 ± 0.08[b]

[a] Reference 5. [b] Reference 8.

References on page 190

Table 5.6 Stability constants for the substitution of water by neutral ligands in $[ACCbs]^+$ and $[ACSYCbs]^+$ at 25 °C.[7]

	log K[a]	
Ligand	$[ACCbs]^+$	$[ACSYCbs]^+$
Py[b]	2.19	< -1[c]
4MePy	3.36	0.38
N-MeI	4.29	1.56
$CF_3CH_2NH_2$	0.4	< -2[a]
NH_3	2.75	2.94
NH_2EtOH	1.91	1.52
NH_2EtOCH_3	1.84	1.74

[a] Interpolated value of log K at 25 °C from the values of ΔH and ΔS. [b] Py = pyridine. [c] Estimated.

The aim of the present study was to provide further information on the *cis*-influence of the equatorial ligands on the metal ion by substitution of C10 H by NO_2 (strongly electron-withdrawing) and NH_2 (strongly electron-donating) in cobesters. The stability constants for $[AC\text{-}(10\text{-}NO_2)Cbs]^+$ and $[AC\text{-}(10\text{-}NH_2)Cbs]^+$ were compared to those for $[ACCbs]^+$ to elucidate the effects of modification of the electronic structure of the corrin ring on the ligand binding properties of the Co(III) metal ion and highlight the importance of the *cis* influence in these systems.

References on page 190

5.3.2 Results and Discussion

The equilibrium constants (log *K*) for the ligand substitution reaction represented in **Equation 2.6** were determined spectrophotometrically in a 50% isopropanol/buffer solution at 25.0 ± 0.1 ^{o}C, where the exogenous ligand L was N_3^-, NO_2^-, SCN^-, SO_3^{2-}, CN^-, imidazole, methylamine or 4-*N*,*N*-dimethylaminopyridine (DMAP), and corrin is either the intact corrin of $[ACCbs]^+$ or the C10 substituted corrins of $[AC\text{-}(10\text{-}NO_2)Cbs]^+$ and $[AC\text{-}(10\text{-}NH_2)Cbs]^+$.

$$[CN\text{–}Co^{III}\text{–}H_2O]^+ + L^{n-} \overset{K}{\rightleftharpoons} [CN\text{–}Co^{III}\text{–}L]^{(1-n)+} + H_2O \qquad \textbf{(2.6)}$$

Titrations were performed by the addition of aliquots of a stock solution of the ligand to a cobalt corrin solution, as described in **Chapter 2, Section 2.5.3.2**. Absorbance spectra for these ligand binding reactions were recorded, and changes in absorbance on titrating the cobalt corrin solution with a ligand were fitted to **Equation 2.3 or 2.4 (Chapter 2)** using non-linear least squares fit methods to obtain log *K*. To check reproducibility, each titration was repeated three to four times.

5.3.2.1 Ligand Binding Studies with Nitrite

Aliquots of a nitrite (NO_2^-) solution (0.008 M) were added to a solution of $[AC\text{-}(10\text{-}Z)Cbs]^+$ (Z = H, NO_2, NH_2) buffered in MOPS (pH 7.1). On formation of the complex, the absorbance spectra underwent a red shift with isosbestic points at 324, 351, 432, and 508 nm for $[AC\text{-}(10\text{-}NO_2)Cbs]^+$; at 332, 364, 409 and 547 nm for $[AC\text{-}(10\text{-}NH_2)Cbs]^+$; and at 332, 367, 395 and 508 nm for $[ACCbs]^+$ (**Figure 5.12**).

The experimental data were analysed at 347, 359, 470, 520 and 555 nm for $[AC\text{-}(10\text{-}NO_2)Cbs]^+$; at 360, 375, 480 and 570 nm $[AC\text{-}(10\text{-}NH_2)Cbs]^+$; and at 354, 378, 468 and 561 nm for $[ACCbs]^+$, by fitting the absorbance to **Equation 2.4.** The values of log *K* at the four wavelengths were then averaged. The log *K* values were determined as 5.22 ± 0.03, 4.8 ± 0.2 and 4.2 ± 0.1 for the substitution of H_2O in $[AC\text{-}(10\text{-}NO_2)Cbs]^+$, $[AC\text{-}(10\text{-}NH_2)Cbs]^+$ and $[ACCbs]^+$, respectively.

References on page 190

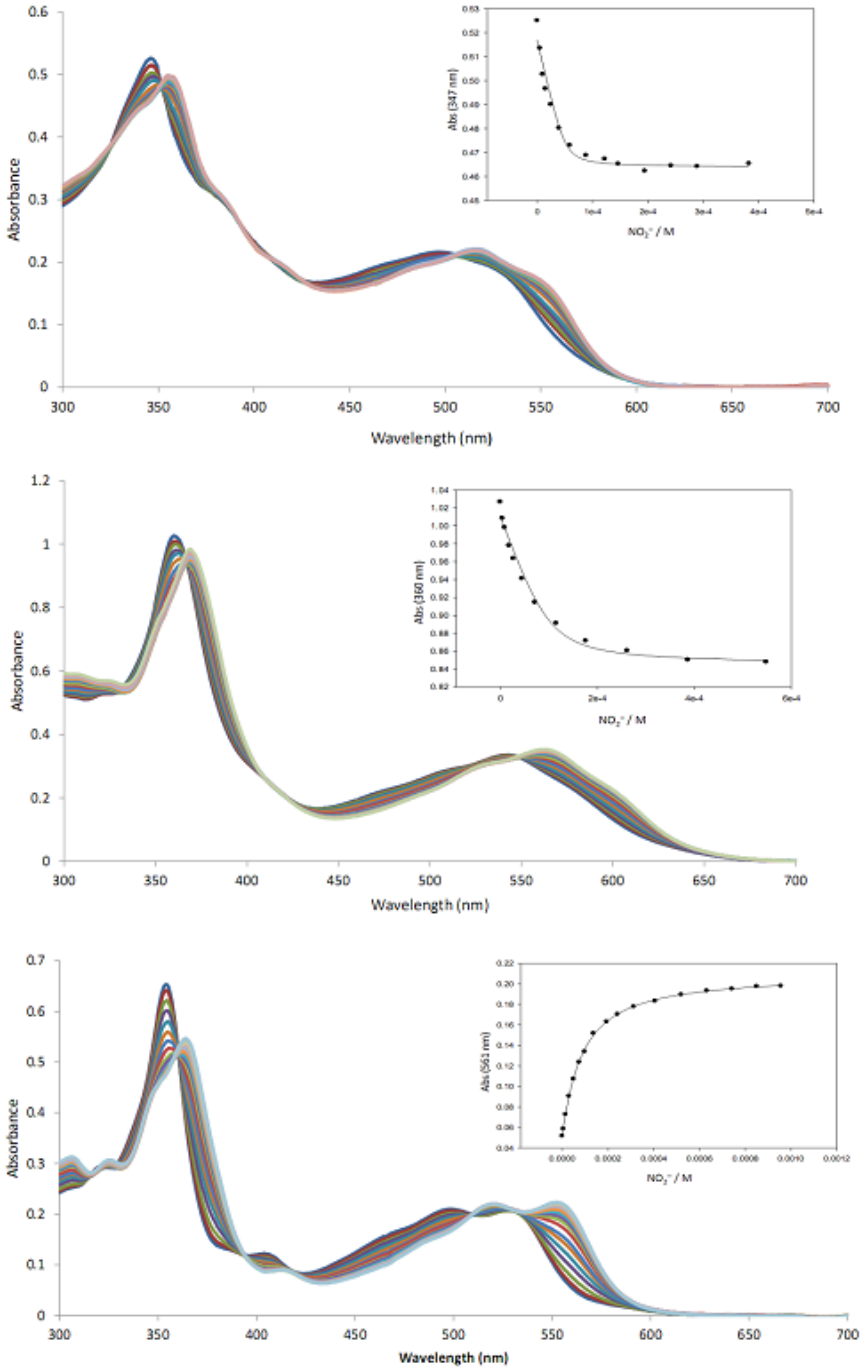


Figure 5.12 Changes in the uv-vis spectrum on substituting coordinated H_2O in (top) [AC-(10-NO_2)Cbs]$^+$, (middle) [AC-(10-NH_2)Cbs]$^+$ (bottom) [ACCbs]$^+$ by NO_2^- at 25 ^oC, pH 7.1. The insert shows a fit of the absorbance change at 347, 360 and 561 nm, (from top to bottom) to the binding isotherm given by **Equation 2.4**.

References on page 190

5.3.2.2 Ligand Binding Studies with Azide

Aliquots of an azide (N_3^-) solution (0.010 M) was added to a solution of $[AC\text{-}(10\text{-}Z)Cbs]^+$ buffered with MOPS (pH 6.9) in 50% isopropanol. Aliquots of N_3^- solution were also added to the reference cuvette to cancel out the effect of N_3^- absorbing in the same wavelength range region as $[AC\text{-}(10\text{-}Z)Cbs]^+$. On the coordination of N_3^- to $[AC\text{-}(10\text{-}Z)Cbs]^+$ the electronic absorption spectra underwent a red shift with isosbestic points at 323, 354, 450 and 513 nm for $[AC\text{-}(10\text{-}NO_2)Cbs]^+$; at 332, 370, 440 and 553 nm for $[AC\text{-}(10\text{-}NH_2)Cbs]^+$; and at 329, 360, 390, 436 and 515 nm for $[ACCbs]^+$, as shown in **Figure 5.13**.

The experimental data were analysed at 347 and 575 nm for $[AC\text{-}(10\text{-}NO_2)Cbs]^+$; at 360, 383, 510 and 607 nm for $[AC\text{-}(10\text{-}NH_2)Cbs]^+$; at 355 and 575 nm for $[ACCbs]^+$, by fitting the absorbance to **Equation 2.4 or 2.3.** The values of log *K* at multiple wavelengths were then averaged, resulting in log *K* values of 4.53 ± 0.09, 4.27 ± 0.07 and 3.55 ± 0.03 for the substitution of H_2O in $[AC\text{-}(10\text{-}NO_2)Cbs]^+$, $[AC\text{-}(10\text{-}NH_2)Cbs]^+$ and $[ACCbs]^+$, respectively.

References on page 190

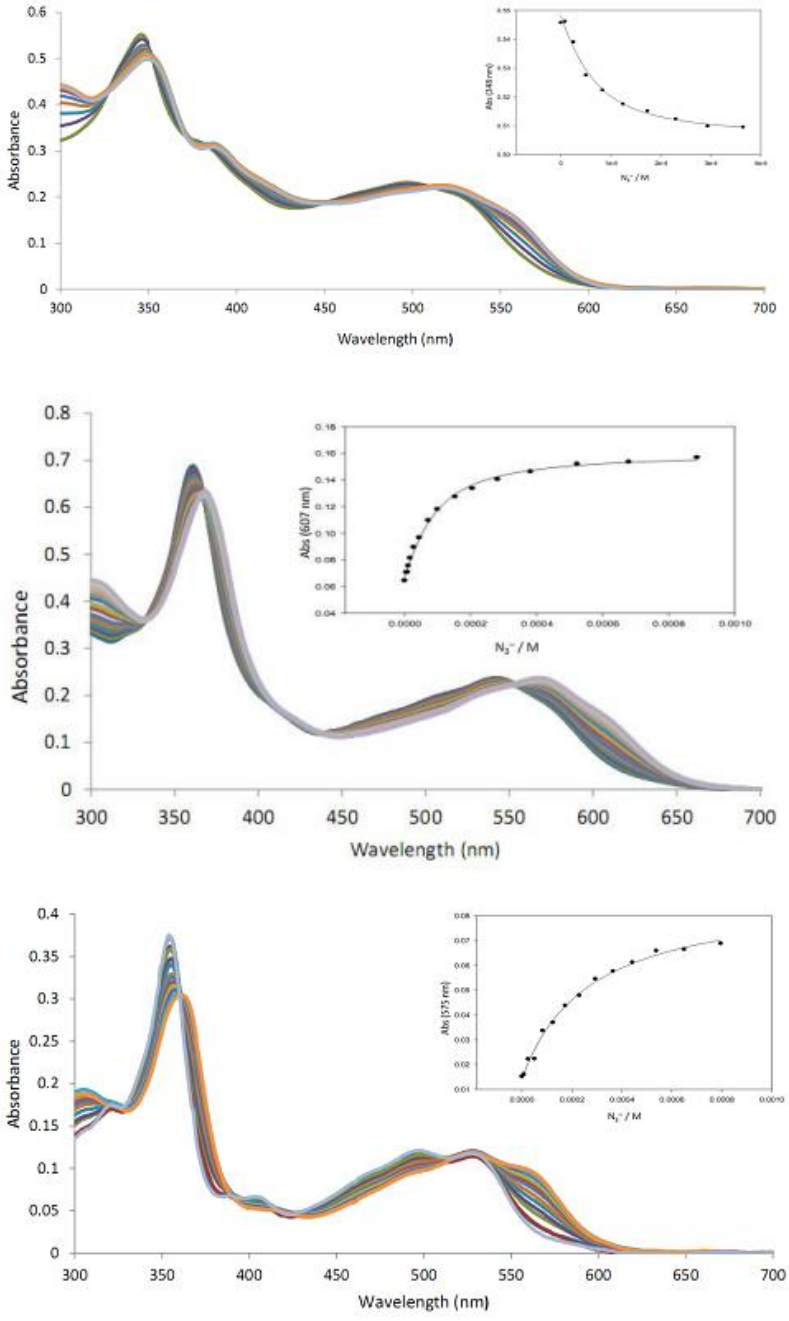


Figure 5.13 Changes in the uv-vis spectrum on substituting coordinated H_2O in (top) [AC-(10-NO_2)Cbs]$^+$, (middle) [AC-(10-NH_2)Cbs]$^+$ and (bottom) [ACCbs]$^+$ by N_3^- at 25 ^{o}C, pH 6.9. The insert shows a fit of the absorbance change at 348, 607 and 575 nm, (from top to bottom) to the binding isotherm given by **Equation 2.4** and **Equation 2.3** (for [ACCbs]$^+$).

References on page 190

5.3.2.3 Ligand Binding Studies with Thiocyanate

The binding constant for the coordination of thiocyanate (SCN^-) to $[AC\text{-}(10\text{-}Z)Cbs]^+$ was determined by addition of aliquots of a SCN^- solution (0.084 M) to a $[AC\text{-}(10\text{-}Z)Cbs]^+$ solution buffered with MOPS (pH 7.2). Binding of SCN^- to $[AC\text{-}(10\text{-}Z)Cbs]^+$ caused the absorbance spectra to undergo a red shift with isosbestic points at 349, 316, 442 and 508 nm for $[AC\text{-}(10\text{-}NO_2)Cbs]^+$; at 364, 406 and 555 nm for $[AC\text{-}(10\text{-}NH_2)Cbs]^+$; at 312, 360 and 510 nm for $[ACCbs]^+$, as shown in **Figure 5.14**.

The experimental data were analysed at 300, 348, 365, 475 and 570 nm for $[AC\text{-}(10\text{-}NO_2)Cbs]^+$; at 350, 360, 515 and 593 nm for $[AC\text{-}(10\text{-}NH_2)Cbs]^+$; at 355, 368, 502 and 558 nm for $[ACCbs]^+$, by fitting the absorbance to **Equation 2.3.** The average values of log *K* were determined as 3.9 ± 0.1, 3.1 ± 0.2 and 3.16 ± 0.03 for $[AC\text{-}(10\text{-}NO_2)Cbs]^+$, $[AC\text{-}(10\text{-}NH_2)Cbs]^+$ and $[ACCbs]^+$, respectively.

References on page 190

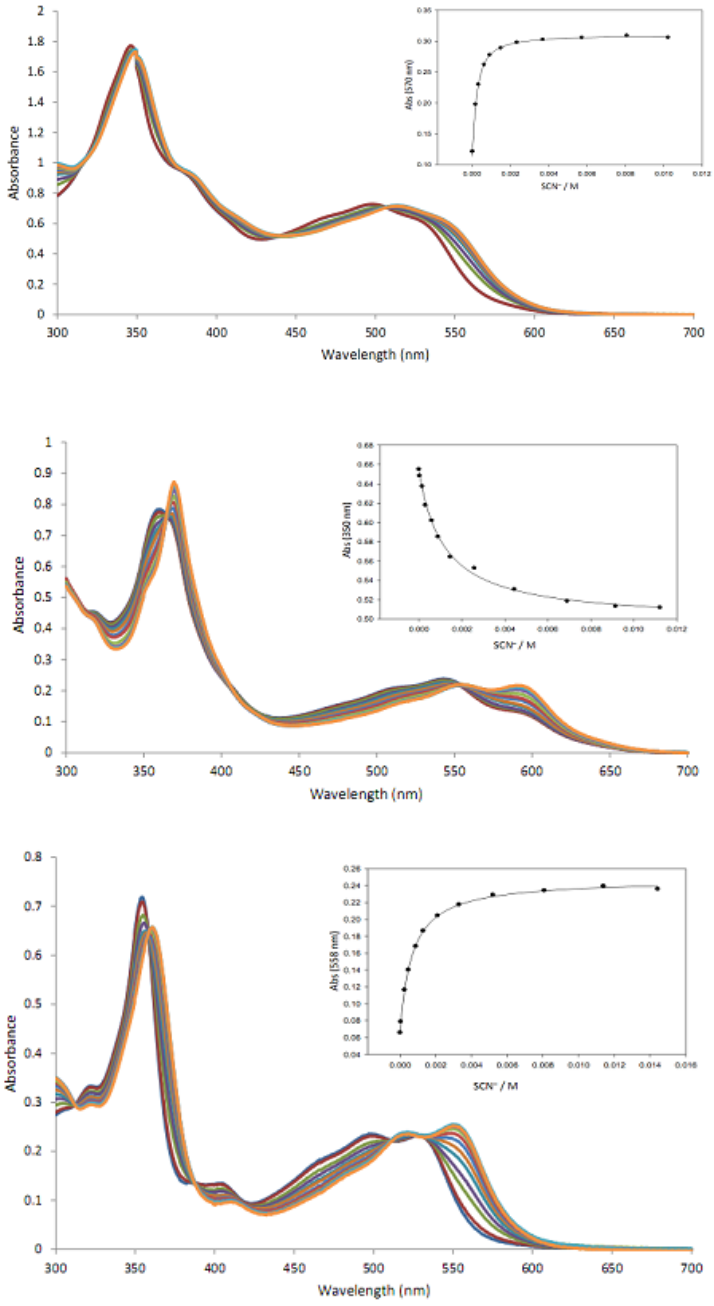


Figure 5.14 Changes in the uv-vis spectrum on substituting coordinated H_2O in (top) [AC-(10-NO_2)Cbs]$^+$, (middle) [AC-(10-NH_2)Cbs]$^+$ (bottom) [ACCbs]$^+$ by SCN^- at 25 ^oC, pH 7.2. The insert shows a fit of the absorbance change at 348, 607 and 575 nm, (from top to bottom) to the binding isotherm given by **Equation 2.3**.

References on page 190

5.3.2.4 Ligand Binding Studies with Sulfite

The stability constant for the reaction of sulfite (SO_3^{2-}) to $[AC\text{-}(10\text{-}Z)Cbs]^+$ was large; therefore the values were determined in a competition experiment in the presence of 0.05 M N_3^- (described in **Chapter 2, Section 2.5.3.2**). The competition reaction was performed by addition of aliquots of a SO_3^{2-} solution (0.07 M) to azidocyano(10-Z)cobester ($[N_3CN\text{-}(10\text{-}Z)Cbs]$) buffered with MES (pH 8.9) in 50% isopropanol. On formation of the sulfite complex, a shoulder appeared between 320-330 nm resulting in an "atypical" spectrum. As illustrated in **Figure 5.15** the absorbance spectra underwent a blue shift with well-defined isosbestic points at 338, 393, 488 nm for $[N_3CN\text{-}(10\text{-}NO_2)Cbs]$; at 350, 395 and 513 nm for $[N_3CN\text{-}(10\text{-}NH_2)Cbs]$. The absorbance spectra for $[N_3CNCbs]$ underwent a red shift with isosbestic points at 337, 381, 480, 482 and 582 nm.

To obtain the log *K* values for these reactions, the data were analysed at 326, 346, 418 and 530 nm for $[N_3CN\text{-}(10\text{-}NO_2)Cbs]$; at 325, 370, 450 and 570 nm for $[N_3CN\text{-}(10\text{-}NH_2)Cbs]$; and at 312, 365, 440, 525 and 550 nm for $[N_3CNCbs]$ by fitting the absorbance to **Equation 2.4**. The values of log K_{obs} were then averaged at the four wavelengths and determined as 1.51 ± 0.06, 4.28 ± 0.10 and 4.39 ± 0.06 for the substitution of SO_3^{2-} in $[N_3CN\text{-}(10\text{-}NO_2)Cbs]$, $[N_3CN\text{-}(10\text{-}NH_2)Cbs]$ and $[N_3CNCbs]$, respectively. Then the log *K* value for the substitution of SO_3^{2-} in $[AC\text{-}(10\text{-}NO_2)Cbs]^+$, $[AC\text{-}(10\text{-}NH_2)Cbs]^+$ and $[ACCbs]^+$ were determined as 6.04 ± 0.06, 8.6 ± 0.1 and 7.94 ± 0.06, respectively since $K_{sulfite} = K_{obs}K_{azide}$ as described in **Chapter 2**, **Section 2.5.3.2**.

References on page 190

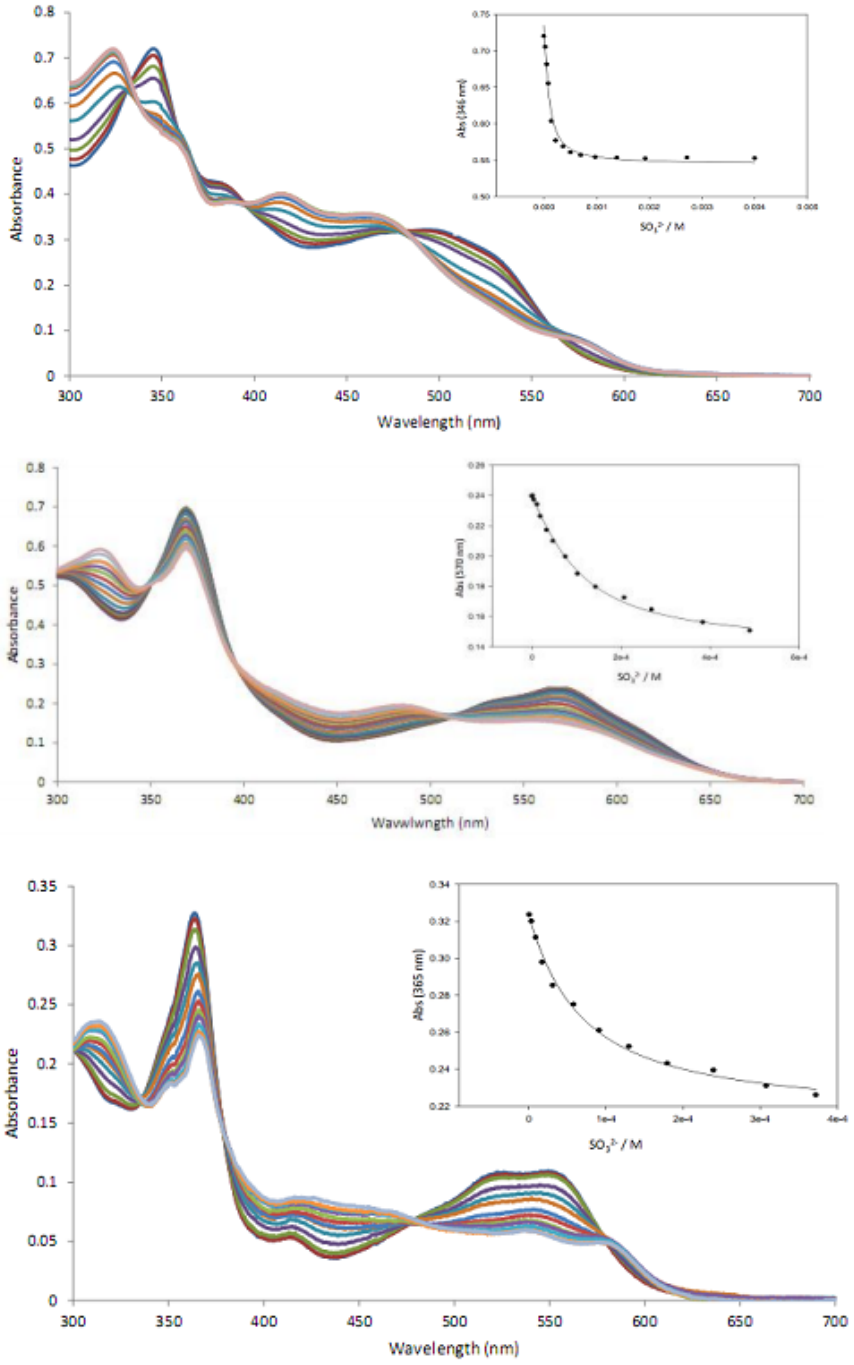


Figure 5.15 Changes in the uv-vis spectrum on substituting coordinated N_3^- in (top) [N_3CN-(10-NO_2)Cbs], (middle) [N_3CN-(10-NH_2)Cbs] and (bottom) [N_3CNCbs] by SO_3^{2-} at 25 °C, pH 8.9. The insert shows a fit of the absorbance change at 346, 570 and 365 nm, (from top to bottom) to the binding isotherm given by **Equation 2.4**.

References on page 190

5.3.2.5 Ligand Binding Studies with Cyanide

As mentioned in **Chapter 2, section 2.5.3.2,** the stability constant for the binding of cyanide (CN^-) to $[AC\text{-}(10\text{-}Z)Cbs]^+$ was expected to be large by analogy with observations obtained for the binding reaction of cyanide with $[ACCbs]^+$ $[ACSYCbs]^+$.[5] Therefore the values of log *K* were determined in a competition experiment in the presence of 0.05 M N_3^-. The stability constants for the coordination of the CN^- ligand by $[N_3CN\text{-}(10\text{-}Z)Cbs]$ were determined by addition of aliquots of a CN^- solution (0.005 M) to $[N_3CN\text{-}(10\text{-}Z)Cbs]$ buffered with CAPS (pH 10.1) in 50% isopropanol. **Figure 5.16** shows the spectra underwent a red shift with isosbestic points at 350, 376 and 528 for $[N_3CN\text{-}(10\text{-}NO_2)Cbs]$; at 363, 420 and 576 nm for $[N_3CN\text{-}(10\text{-}NH_2)Cbs]$; and at 363, 400, 534 and 560 nm for $[N_3CNCbs]$.

To determine the log *K* values, the data were analysed at 330, 362 and 584 nm $[N_3CN\text{-}(10\text{-}NO_2)Cbs]$; at 330, 370 and 595 nm for $[N_3CN\text{-}(10\text{-}NH_2)Cbs]$; and at 330, 370, 525 and 585 nm for $[N_3CNCbs]$ by fitting the absorbance to **Equation 2.4**. The average log *K* values for the coordination of CN^- by $[N_3CN\text{-}(10\text{-}NO_2)Cbs]$, $[N_3CN\text{-}(10\text{-}NH_2)Cbs]$ and $[N_3CNCbs]$ at several wavelengths were determined as 2.86 ± 0.10, 5.30 ± 0.14 and 5.70 ± 0.12, respectively. Then the average log *K* values for the substitution of CN^- in $[AC\text{-}(10\text{-}NO_2)Cbs]^+$, $[AC\text{-}(10\text{-}NH_2)Cbs]^+$ and $[ACCbs]^+$ were determined as 7.39 ± 0.08, 10.0 ± 0.3 and 9.6 ± 0.1 respectively (described in **Chapter 2**, **Section 2.5.3.2**).

References on page 190

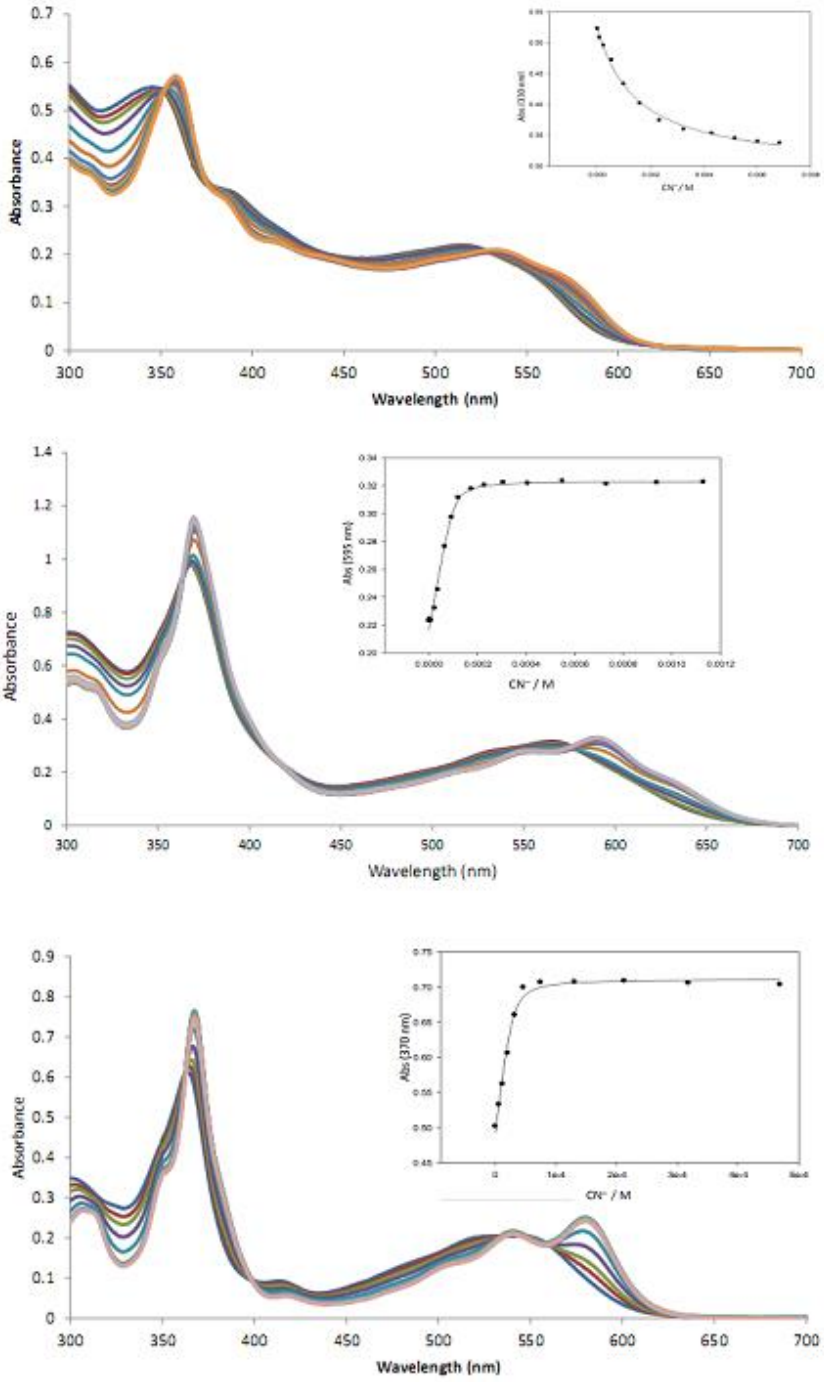


Figure 5.16 Changes in the uv-vis spectrum on substituting coordinated N_3^- in (top) [N_3CN-(10-NO_2)Cbs], (middle) [N_3CN-(10-NH_2)Cbs] and (bottom) [N_3CNCbs] by CN^- at 25 ^oC, pH 10.1. The insert shows a fit of the absorbance change at 362, 595 and 370 nm, (from top to bottom) to the binding isotherm given by **Equation 2.4**.

References on page 190

5.3.2.6 Ligand Binding Studies with Imidazole

Aliquots of imidazole (0.025 M) were added to a solution of $[AC\text{-}(10\text{-}Z)Cbs]^+$ buffered with MOPS (pH 6.9) in 50% isopropanol. The experimental data were analysed at 355 and 564 nm for $[AC\text{-}(10\text{-}NO_2)Cbs]^+$; at 330, 368, 500 and 570 nm for $[AC\text{-}(10\text{-}NH_2)Cbs]^+$; and at 363 and 556 nm for $[ACCbs]^+$, and fitted using **Equation 2.4**. The average values of log *K* for the coordination of imidazole to $[AC\text{-}(10\text{-}NO_2)Cbs]^+$, $[AC\text{-}(10\text{-}NH_2)Cbs]^+$ and $[ACCbs]^+$ were determined as 4.37 ± 0.04, 4.5 ± 0.2 and 4.66 ± 0.06, respectively. The absorption spectra underwent a red shift with isosbestic points at 347, 428 and 509 nm for $[AC\text{-}(10\text{-}NO_2)Cbs]^+$; at 360, 400 and 555 nm for $[AC\text{-}(10\text{-}NH_2)Cbs]^+$; at 363 and 556 nm for $[ACCbs]^+$, as shown in **Figure 5.17**.

References on page 190

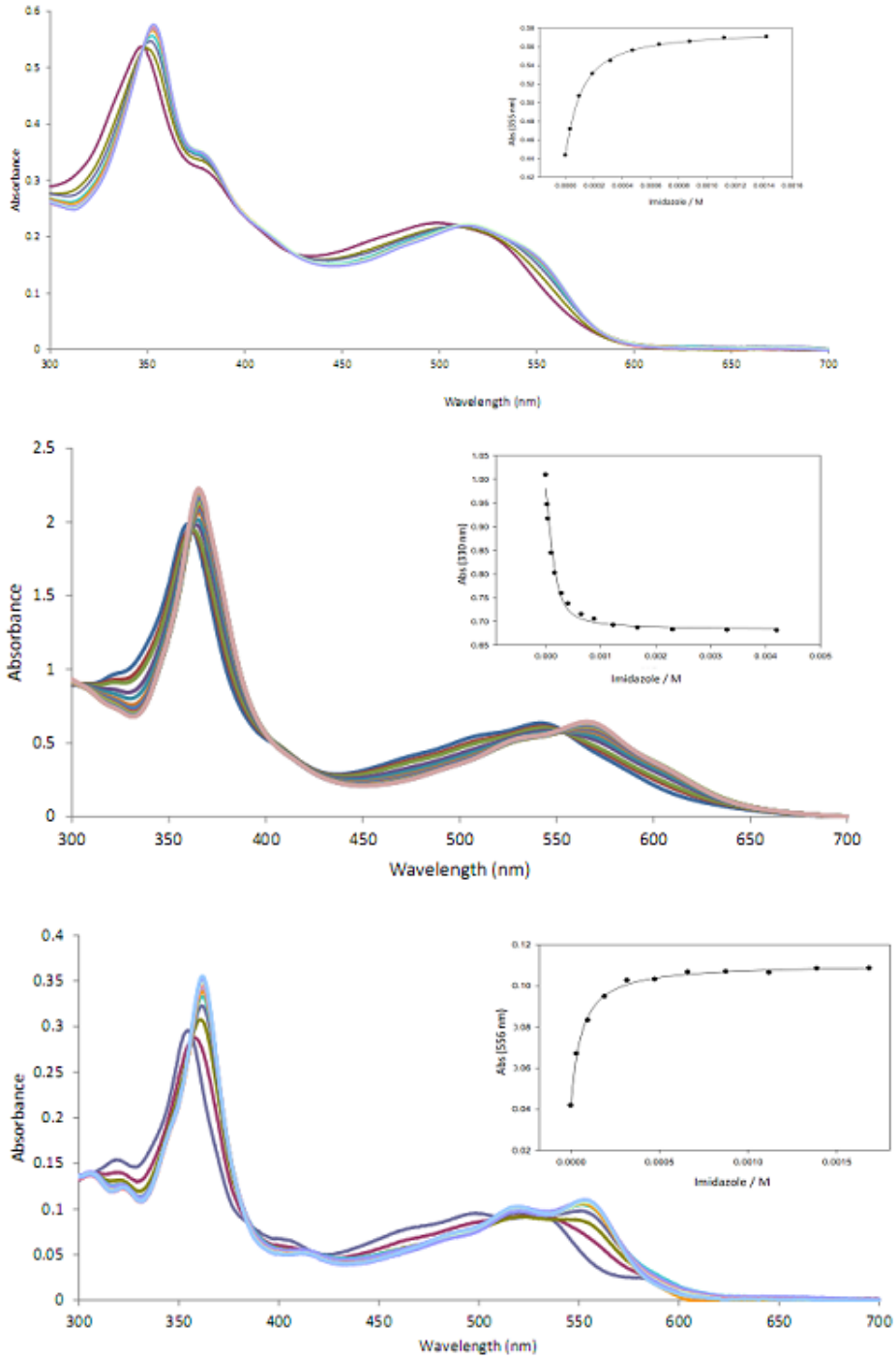


Figure 5.17 Changes in the uv-vis spectrum on substituting coordinated H_2O in (top) [AC-(10-NO_2)Cbs]$^+$, (middle) [AC-(10-NH_2)Cbs]$^+$ (bottom) [ACCbs]$^+$ by imidazole at 25 ^oC, pH 6.9. The insert shows a fit of the absorbance change at 355, 330 and 363 nm, (from top to bottom) to the binding isotherm given by **Equation 2.4.**

References on page 190

5.3.2.7 Ligand Binding Studies with Methylamine

The stability constant for the coordination of methylamine ($MeNH_2$) to $[AC\text{-}(10\text{-}Z)Cbs]^+$ was determined by the addition of aliquots of a $MeNH_2$ solution (0.12 M) to a solution of $[AC(10\text{-}Z)Cbs]^+$ buffered with CAPS (pH 10.3) in 50% isopropanol. **Figures 5.18** shows as the formation of methylamine complexes increased the spectra underwent a red shift with isosbestic points at 347, 394 and 513 nm for $[AC\text{-}(10\text{-}NO_2)Cbs]^+$; at 360, 403 and 550 nm for $[AC\text{-}(10\text{-}NH_2)Cbs]^+$; and at 358, 386 and 511 nm for $[ACCbs]^+$. The changes in absorbance were analysed at 335, 355, 470 and 560 nm for $[AC\text{-}(10\text{-}NO_2)Cbs]^+$; at 333, 367, 500 and 578 nm for $[AC\text{-}(10\text{-}NH_2)Cbs]^+$; and at 354, 363, 470 and 555 nm for $[ACCbs]^+$, to which a binding isotherm (**Equation 2.3**) was fitted. The averaged log *K* values were found to be 3.13 ± 0.06, 3.52 ± 0.07 and 3.2 ± 0.1 for $[AC\text{-}(10\text{-}NO_2)Cbs]^+$, $[AC\text{-}(10\text{-}NH_2)Cbs]^+$ and $[ACCbs]^+$, respectively.

References on page 190

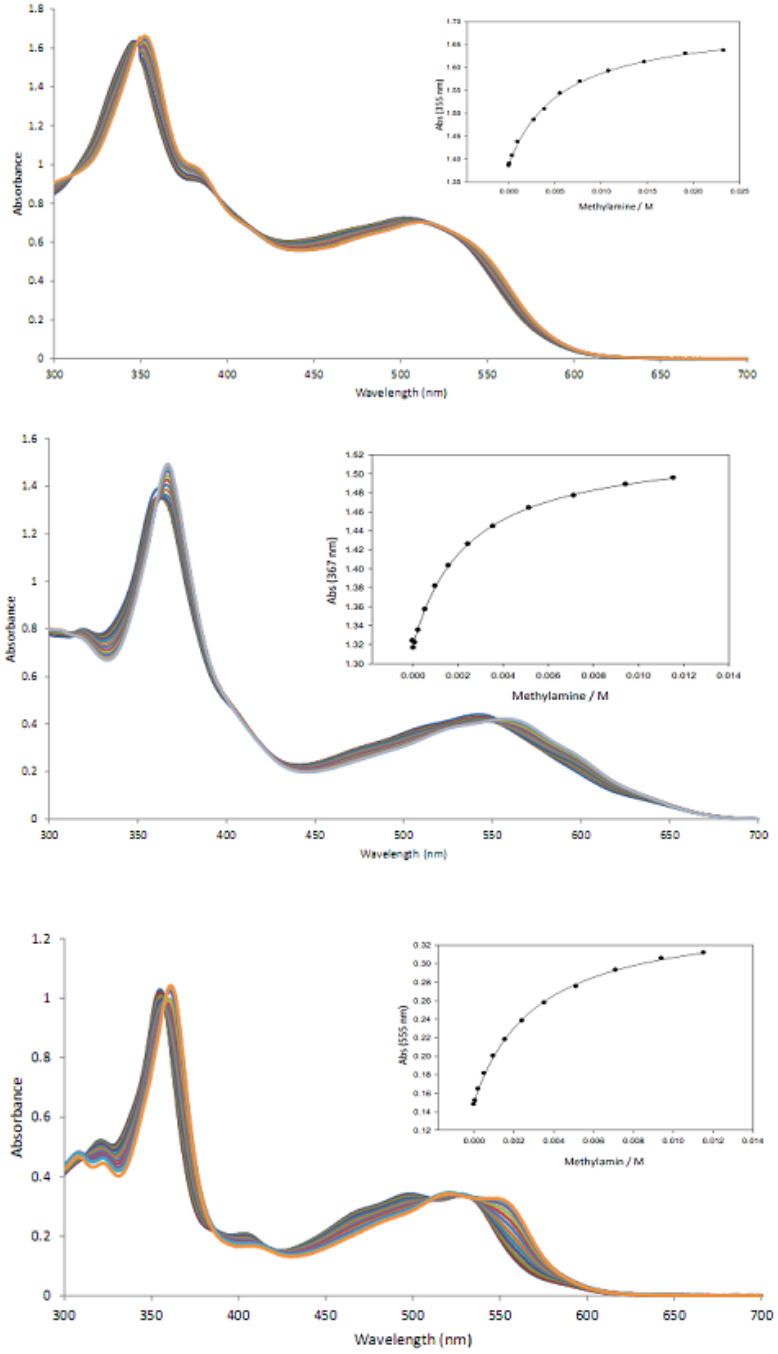


Figure 5.18 Changes in the uv-vis spectrum on substituting coordinated H_2O in (top) [AC-(10-NO_2)Cbs]$^+$, (middle) [AC-(10-NH_2)Cbs]$^+$ (bottom) [ACCbs]$^+$ by $MeNH_2$ at 25 ^oC, pH 10.3. The insert shows a fit of the absorbance change at 355, 367 and 555 nm, (from top to bottom) to the binding isotherm given by **Equation 2.3.**

References on page 190

5.3.2.8 Ligand Binding Studies with DMAP

The stability constant for the binding of DMAP to [AC-(10-Z)Cbs]$^+$ was obtained by addition of aliquots of a DMAP solution (0.047 M) to a [AC-(10-Z)Cbs]$^+$ solution buffered with CHES (pH 9.5) in 50% isopropanol. Binding of DMAP to [AC-(10-Z)Cbs]$^+$ showed a large absorbance due to DMAP itself in the uv region around 310 nm (**Figure 5.19**). To overcome this issue the same quantity of DMAP ligand was added to the reference cuvette simultaneously. Coordination of the DMAP to [AC-(10-Z)Cbs]$^+$ occurred slowly and required at least 15 min between each addition for equilibrium to be reached. Absorption spectra of the three cobesters underwent a red shift, although for [AC-(10-NO_2)Cbs]$^+$ the shift is very small in the region of 400-700 nm and the wavelength axis is only shown from 320 nm for convenience, as shown in (**Figure 5.19**). Isosbestic points were observed at 376 nm for [AC-(10-NO_2)Cbs]$^+$; at 323, 360 and 548 nm for [AC-(10-NH_2)Cbs]$^+$; and at 357, 386 and 510 nm for [ACCbs]$^+$.

The absorbance change was analysed at 425, 450, 475 and 500 nm for [AC-(10-NO_2)Cbs]$^+$; at 365, 465, 485, 510 and 565 nm for [AC-(10-NH_2)Cbs]$^+$; and at 362, 380, 465 and 555 nm for [ACCbs]$^+$, and fitted to **Equation 2.4** or **Equation 2.3** (for [AC-(10-NO_2)Cbs]$^+$). The average log *K* values were obtained as 2.91 ± 0.09, 4.9 ± 0.2 and 4.97 ± 0.03 for [AC-(10-NO_2)Cbs]$^+$, [AC-(10-NH_2)Cbs]$^+$and [ACCbs]$^+$, respectively.

References on page 190

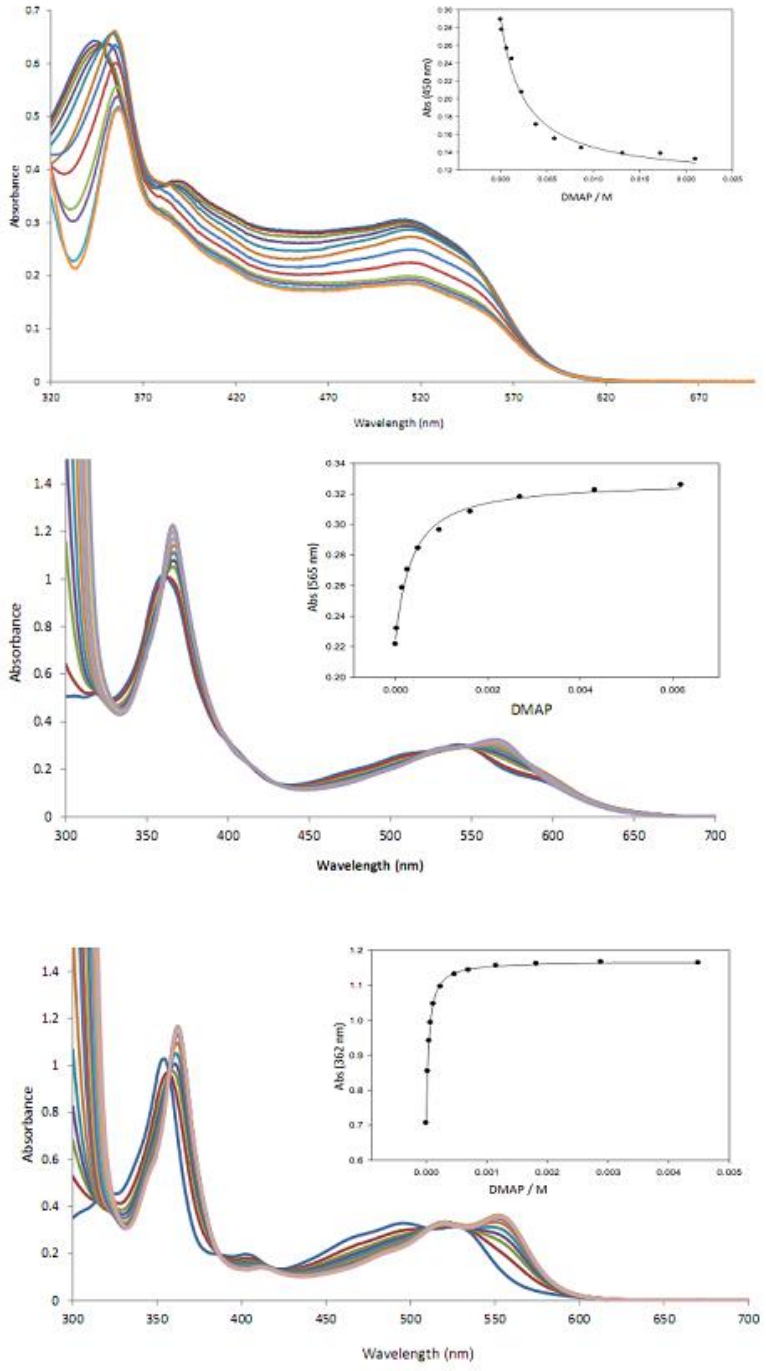


Figure 5.19 Changes in the uv-vis spectrum on substituting coordinated H_2O in (top) [AC-(10-NO_2)Cbs]$^+$, (middle) [AC-(10-NH_2)Cbs]$^+$ and (bottom) [ACCbs]$^+$ by DMAP at 25 ^oC, pH 8.5. The insert shows a fit of the absorbance change at 450, 565 and 362 nm, (from top to bottom) to the binding isotherm given by **Equation 2.4 and Equation 2.3** (for [AC-(10-NO_2)Cbs]$^+$).

References on page 190

5.3.3 Summary of Results and Conclusions

The log *K* values in **Table 5.7** show that the affinity of the softest ligands studied, CN^- and SO_3^{2-}, parallels the softness of the metal ion ($[AC\text{-}(10\text{-}NH_2)Cbs]^+$ > $[ACCbs]^+$ > $[AC\text{-}(10\text{-}NO_2)Cbs]^+$), with a discrimination spanning two orders of magnitude. The case is less clear for the N-donor ligands; DMAP clearly has a higher affinity for $[AC\text{-}(10\text{-}NH_2)Cbs]^+$ and $[ACCbs]^+$ than for $[AC\text{-}(10\text{-}NO_2)Cbs]^+$, but there is little discrimination in the case of imidazole and $MeNH_2$. The harder anions SCN^-, N_3^- and NO_2^- are bound better by the harder Co(III) centre in $[AC\text{-}(10\text{-}NO_2)Cbs]^+$ than in $[ACCbs]^+$ or $[AC\text{-}(10\text{-}NH_2)Cbs]^+$, ($SCN^-$ is found bound to cob(III)alamin in the isothiocyanato form in the solid state[3,10,11] although there is NMR evidence[6] of a mixture of the thiocyanato and isothiocyanato isomers in solution, and a report of a crystal structure of the thiocyanato form).[12] This indicates that the electron density at the metal centre is a primary discriminator for the affinity of the metal for an exogenous ligand. Anionic ligands with a hard donor are favoured by a cobalt corrin with a hard metal centre; but in particular, the softer metal centre found when Z = H, NH_2 heavily favours the softer anions.

Generally, there is a greater discrimination between $[ACCbs]^+$ and $[AC(10\text{-}NO_2)Cbs]^+$ than between $[ACCbs]^+$ and $[AC(10\text{-}NH_2)Cbs]^+$. We have noted[13] in a BP86/6-311+G(d,p) study of complexes of the type $[(CN)_2(10\text{-}Z)corrin]$ that the symmetric and anti-symmetric NC—Co—CN stretching frequencies respond linearly with values of the Hammett para constant, σ_p, for Z provided $\sigma_p > 0$, but is insensitive when $\sigma_p < 0$. Why the *cis*-effect on the ground state properties the cobalt corrin complexes is more prominent when the C10 substituent is more electron-withdrawing than H than when it is more electron-donating, is still unclear and merits further investigation. Nevertheless, the present results illustrate how perturbing the electronic structure of the cis corrin ligand can significantly affect the affinity of Co(III) in the cobalt corrins for its axial ligands.

References on page 190

Table 5.7 Values of log *K* for replacement of coordinated H_2O in the cobesters $[AC\text{-}(10\text{-}Z)Cbs]^+$, Z = H, NO_2, NH_2, in 50% aqueous isopropanol solutions by exogenous ligands L at 25.0 °C.[a]

L	$[AC\text{-}(10\text{-}NH_2)Cbs]^+$	$[ACCbs]^+$	$[AC\text{-}(10\text{-}NO_2)Cbs]^+$
CN^-	10.0 ± 0.3	9.6 ± 0.1	7.39 ± 0.08
SO_3^{2-}	8.6 ± 0.1	7.94 ± 0.06	6.04 ± 0.06
DMAP	4.9 ± 0.2	4.97 ± 0.03	2.91 ± 0.09
Imidazole	4.5 ± 0.2	4.66 ± 0.06	4.37 ± 0.04
$MeNH_2$	3.52 ± 0.07	3.2 ± 0.1	3.13 ± 0.06
SCN^-	3.1 ± 0.2	3.16 ± 0.03	3.9 ± 0.1
N_3^-	4.27 ± 0.07	3.55 ± 0.03	4.53 ± 0.09
NO_2^-	4.8 ± 0.2	4.2 ± 0.1	5.22 ± 0.03

[a] **Equation 5.3**.

References on page 190

5.4 QTAIM Analysis

QTAIM analyses are used here to gain insight into factors that may account for the differences in the thermodynamics and kinetics of the ligand substitution reactions of the cobalt corrins. As explained in **Chapter 3**, **Section 3.4** parameters which are used to interpret the calculations are: ρ, electron density at the bond critical point of a bond; $|V(r)|/G(r)$, the ratio of the potential and the kinetic energy densities at a bond critical point; and the Bader charge on cobalt and on the donor atoms of the axial ligands.

Models of $[L(CN)(10\text{-}Z)Cbs]^{n+}$, with the axial ligands L and CN^-, and C10 substituent Z, L = H_2O, imidazole (Im), CN^- or NO_2^-, Z = H, NO_2 or NH_2, were constructed and used to study the *cis*-influence of the corrin ring on the properties of the Co–β bond toward a ligand binding reaction. **Table 5.8** gives the structural metrics, the topological properties of the electron density at the bond critical point of the Co–β bond, and the Bader charges on Co and the two donor atoms of the axial ligands, as deduced from the DFT modelling. Three representative modelled structures are shown in **Figure 5.20.**

References on page 190

Table 5.8 Structural and electronic properties of $[L(CN)(10\text{-}Z)Cbs]^{n+}$; L = H_2O, imidazole, CN^- and NO_2^-; Z = H, NO_2, NH_2; from BP86/TZVP models.[a]

$[(H_2O)(CN)(10\text{-}Z)Cbs]^+$				
C-10 substituent, Z		H	NO_2	NH_2
Axial Ligands	α	CN^-	CN^-	CN^-
	β	H_2O	H_2O	H_2O
Bond lengths /Å	Co–OH_2	2.236	2.222	2.292
	δ(Co–O)		-0.014	0.056
	Co–CN	1.828	1.829	1.828
	δ(Co–CN)		0.001	0.000
Topological properties of Co–β	ρ	0.0411	0.0423	0.0370
	δρ		0.0012	-0.0042
	$\nabla^2\rho$	0.1836	0.1925	0.1504
	δ$\nabla^2\rho$		0.0089	-0.0332
	$\lvert V(r)\rvert/G(r)$	1.1183	1.1120	1.1451
	δ($\lvert V(r)\rvert/G(r)$)		-0.0064	0.0267
Bader charges /e	Co	1.1404	1.1428	1.1363
	δCo		0.0024	-0.0041
	O (H_2O)	-1.1236	-1.1256	-1.1273
	δO		-0.0020	-0.0037
	C (CN^-)	0.7849	0.7818	0.7843
	δC		-0.0032	-0.0006
$[(Im)(CN)(10\text{-}Z)Cbs]^+$				
C-10 substituent	Z	H	NO_2	NH_2
Axial Ligands	α	CN^-	CN^-	CN^-
	β	Im	Im	Im
Bond lengths /Å	Co-N(Im)	2.070	2.063	2.080
	δ(Co–N)		-0.007	0.010
	Co–CN	1.859	1.861	1.857
	δ(Co–CN)		0.002	-0.002
Topological properties of Co–β	ρ	0.0726	0.0741	0.0709

References on page 190

	$\delta\rho$		0.0015	-0.0017
	$\nabla^2\rho$	0.3241	0.3290	0.3127
	$\delta\nabla^2\rho$		0.0050	-0.0114
	$\lvert V(r)\rvert/G(r)$	1.1289	1.1308	1.1322
	$\delta(\lvert V(r)\rvert/G(r))$		0.0019	0.0033
Bader charges /e	Co	1.1556	1.1542	1.1548
	δCo		-0.0014	-0.0008
	N (Im)	-1.1121	-1.1173	-1.1116
	δN		-0.0052	0.0005
	C (CN^-)	0.7697	0.7649	0.7709
	δC		-0.0048	0.0012
[$(CN)_2$(10-Z)Cbs]				
C-10 substituent	Z	H	NO_2	NH_2
Axial Ligands	α	CN^-	CN^-	CN^-
	β	CN^-	CN^-	CN^-
Bond lengths /Å	Co–CN	1.935	1.933	1.937
	δ(Co–CN)		-0.002	0.002
	Co–CN	1.935	1.933	1.935
	δ(Co–CN)		-0.002	0
Topological properties of Co–β	ρ	0.1145	0.1151	0.1135
	$\delta\rho$		0.0005	-0.0010
	$\nabla^2\rho$	0.2903	0.2888	0.2860
	$\delta\nabla^2\rho$		-0.0015	-0.0043
	$\lvert V(r)\rvert/G(r)$	1.3747	1.3787	1.3762
	$\delta(\lvert V(r)\rvert/G(r))$		0.0040	0.0015
Bader charges /e	Co	1.1521	1.1514	1.1545
	δCo		-0.0007	0.0024
	C (CN^-)	0.7461	0.7414	0.7469
	δC		-0.0047	0.0008
	C (CN^-)	0.7460	0.7413	0.7461

References on page 190

	δC		-0.0046	0.0001
[(NO₂)(CN)(10-Z)Cbs]				
C-10 substituent	Z	H	NO_2	NH_2
Axial Ligands	α	CN^-	CN^-	CN^-
	β	NO_2^-	NO_2^-	NO_2^-
Bond lengths /Å	Co–N (NO_2^-)	2.020	2.017	2.022
	δ(Co–N)		-0.003	0.002
	Co–CN	1.921	1.922	1.922
	δ(Co–CN)		0.001	0.001
Topological properties of Co–β	ρ	0.0903	0.0912	0.0898
	δρ		0.0009	-0.0004
	$\nabla^2\rho$	0.3293	0.3298	0.3255
	δ$\nabla^2\rho$		0.0005	-0.0038
	$\lvert V(r)\rvert/G(r)$	1.2025	1.2069	1.2045
	δ($\lvert V(r)\rvert/G(r)$)		0.0044	0.0020
Bader charges /e	Co	1.1564	1.1523	1.1573
	δCo		-0.0041	0.0009
	N (NO_2^-)	0.4212	0.4211	0.4216
	δN		-0.0001	0.0004
	C (CN^-)	0.7542	0.7491	0.7546
	δC		-0.0050	0.0004

[a] Explanation of symbols used. δ is the difference of a parameter where Z = NO_2 or NH_2 and when Z = H. ρ and $\nabla^2\rho$ is the charge density and the Laplacian of the charge density (in au), respectively, at the bond critical point; 1 au of ρ = 6.7483 e Å^{-3} and 1 au of $\nabla^2\rho$ = 24.099 e Å^{-5}. $V(r)$ and $G(r)$ are the potential and kinetics energies densities, respectively, at the bond critical point.

References on page 190

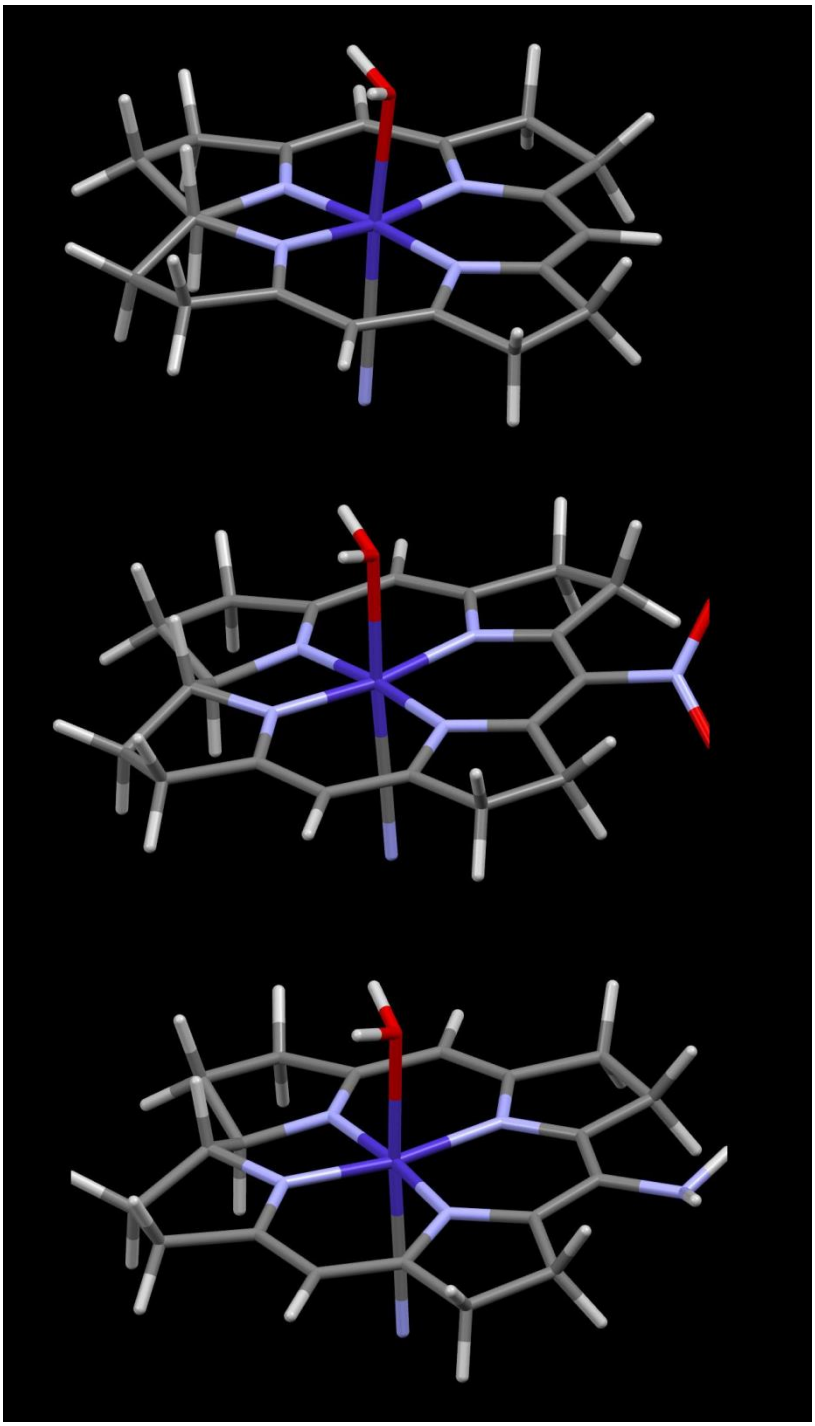


Figure 5.20 BP86/TVZP models of (from top) $[(H_2O)(CN)Cbs]^+$, $[(H_2O)(CN)(10\text{-}NO_2)Cbs]^+$ and $[(H_2O)(CN)(10\text{-}NH_2)Cbs]^+$.

References on page 190

The DFT modelling confirms the trends in log *K* values as reported in **Table 5.7** and also highlights the following changes. Firstly, it was noted a normal *trans* influence is reproduced in the models of the four complexes. As the Co–*β* bond length decreases, the Co–CN bond length to the *α* CN^- ligand increases monotonically (**Figure 5.21**).

Secondly, the partial charge on the metal in $[(H_2O)(CN)(10\text{-}Z)Cbs]^+$ (as assessed from the Bader charges obtained from a QTAIM analysis) becomes more positive as Z = H is changed to Z = NO_2 (i.e., the metal becomes harder) and less positive on changing Z from H to NH_2 (the metal becomes softer).

Thirdly, substitution of C10 H by electron-withdrawing NO_2 causes the bond length between Co and the *β* ligand to decrease, while the bond to the *α* CN^- hardly changes; conversely if the C10 substituent is electron-donating NH_2, the Co–*β* bond length increases. The responsiveness of the Co–*β* bond length to the *cis* influence of the corrin is inversely proportional to the its bond strength, i.e., δ(Co–*β*), the change in the length of the Co–*β* bond when C10 is changed from H to NO_2 or NH_2 is in the order H_2O > Im > NO_2^- > CN^- while *ρ*, the charge density at the bond critical point of the Co–*β* bond, and a measure of its bond strength,[14-21] varies in the order H_2O < Im < NO_2^- < CN^-, **Table 5.8**. This is presumably a consequence of a decrease in the charge density on the metal ion when NO_2 replaces H at C10, and an increase when the substituent is NH_2.

References on page 190

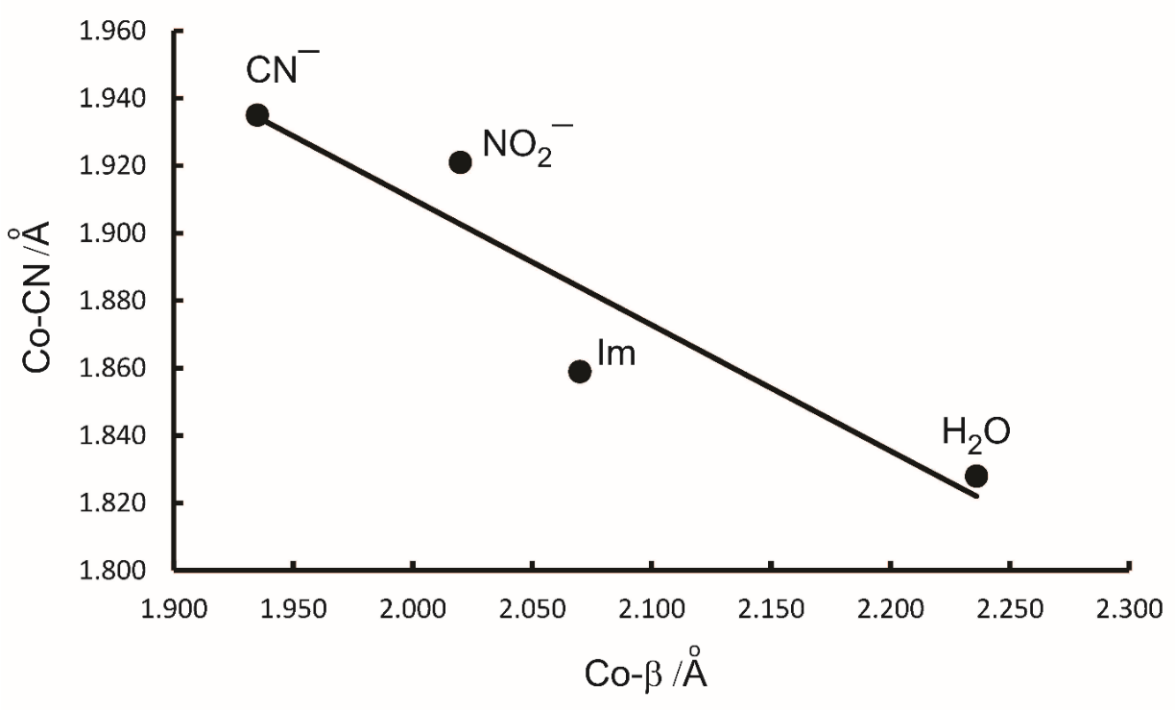


Figure 5.21 The normal *trans* influence is reproduced in BP86/TZVP models of $[(L)(CN)Cbs]^{n+}$. The bond length between Co and the β ligand, L = H_2O, Im, NO_2^-, CN^-, is plotted against the *trans* Co–CN bond length.

The change in length of the Co–OH_2 and the Co–N(Im) bonds on changing the C10 substituent has a small but significant effect on their nature. Metal-ligand bonds are usually characterised by having $\rho < 0.1$ but $\nabla^2\rho > 0$,[22,23] as found here for bonds between Co and the axial ligands. The ratio of the potential and kinetic energy densities can be used to characterise the nature of a chemical bond.[24] Interactions with $|V_b|/G_b < 1$ are characteristic of ionic interactions; those with $|V_b|/G_b > 2$ are typically covalent interactions; and $1 < |V_b|/G_b < 2$ is diagnostic of interactions of intermediate character. As has been shown for a wide variety of compounds,[13,25-29] metal-ligand bonds are usually intermediate in character. Focusing on the four compounds in **Table 5.8** with Z = H, we note that $|V_b|/G_b$ varies from 1.118 for the Co–OH_2 bond, to 1.129 for Co–N(Im), 1.203 for Co–NO_2^-, to 1.375 for Co–CN^-, i.e., the covalent character of the Co–β bond increases across this series. Now focusing on the aqua complexes, it is noted that the covalent character increases marginally when the C10 substituent is electron-donating NH_2, but decreases with

References on page 190

electron-withdrawing NO_2. The effect is very small in the complexes with the other three ligands, where in every case there is a marginal increase in the covalent character of the bond.

In summary, the complexes $[(H_2O)(CN)(10\text{-}Z)Cbs]^+$ have a relatively weak Co–OH_2 bond which is close to being ionic in nature ($|V_b|/G_b \approx 1.1$ is near the ionic threshold of 1). This bond decreases in length, strengthens, and becomes more ionic, as Z is varied from NH_2 to H to NO_2, as the partial charge on the metal ionic becomes more positive and the metal becomes harder. This is summarized graphically in **Figure 5.22**.

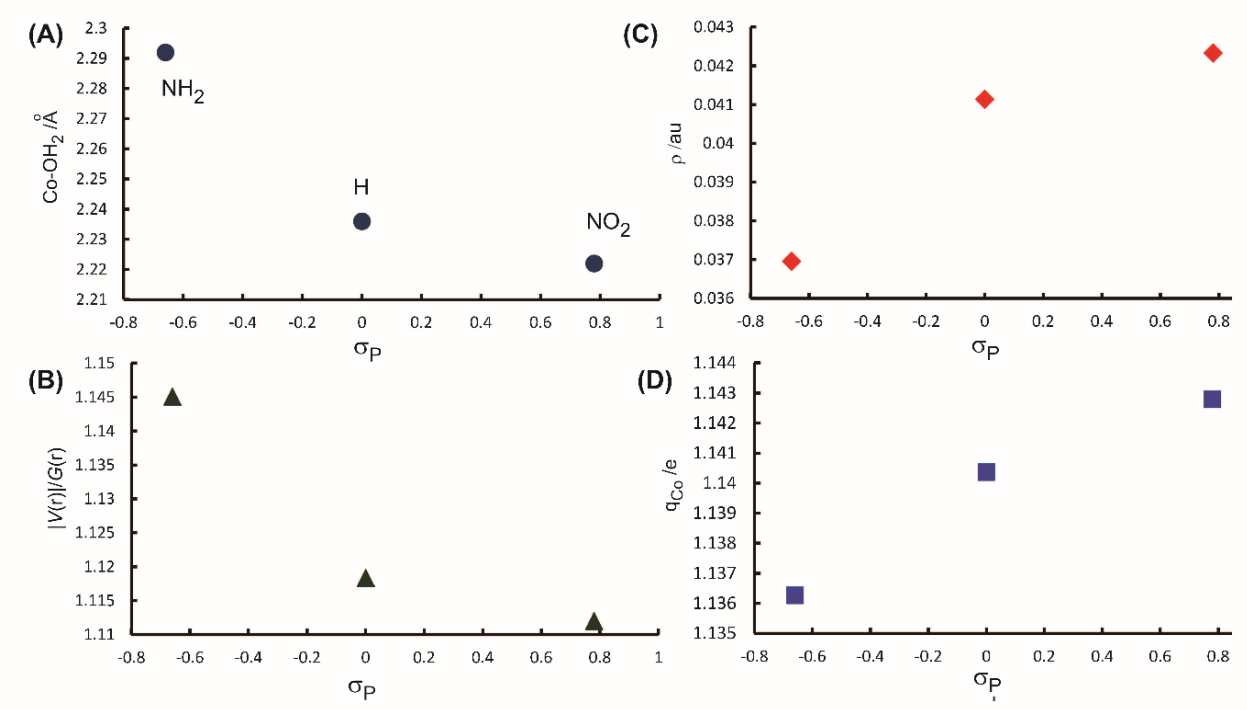


Figure 5.22 The dependence of (A) the Co–OH_2 bond length, (B) the ratio of the potential and kinetic energy densities at the bond critical point (bcp) of the Co–OH_2 bond, (C) the charge density at the bcp of the Co–OH_2 bond, and (D) the Bader charge on Co in BP86/TZVP models of $[(H_2O)(CN)Cbs]^+$ on the Hammett para constant, σ_p, of the C10 substituent.

References on page 190

5.4.1 Conclusions

DFT calculations were performed on models of $[L(CN)(10\text{-}Z)Cbs]^{n+}$, with the axial ligands L and CN^-, and C10 substituent Z, L = H_2O, imidazole, CN^- or NO_2^-, Z = H, NO_2 or NH_2. The QTAIM analyses verified that when the C10 substituent (Z) is varied from NO_2 to H to NH_2, the positive charge on the cobalt atom decreases (as assessed from the Bader charges obtained from a QTAIM analysis) and the metal becomes more electron rich and softer. This rationalised why the softer anions (CN^- and SO_3^{2-}) are bound better by the softer Co(III) centre in aquacyanocobester and aquacyano-10-aminocobester, while the harder Co(III) centre in aquacyano-10-nitrocobester favours the binding to the harder anions (N_3^-, NO_2^- and SCN^-).

In all four complexes metal-ligand bonds have intermediate character ($1 < |V_b|/G_b < 2$). However, the covalent character of the Co–β bond increases across this series when Z is H Co–CN^- > Co–NO_2 > Co–N(Im) > Co–OH_2. In aqua complexes the covalent character of the Co–*β* bond increases significantly when Z is NH_2 and decreases when Z is NO_2.

When Z is changed from electron-donating (NH_2) to electron-withdrawing (NO_2), the positive charge increases on cobalt atom and becomes harder and consequently the Co–*β* bond decreases in length, strengthens and becomes more ionic, that the modelling confirms that there is direct electronic communication between the axial coordination site of the metal and the corrin ring. Therefore it is reasonable to expect that altering the electronic structure of the equatorial ligand will modify the chemistry of the metal's axial coordination site.

References on page 190

5.5 Summary of This Chapter

We hypothesised that the electronic structure of the corrin ring plays a critical role in conferring lability on the cobalt atom and consequently on the chemistry of the Co–*β* ligand. To test this, the electronic structure of the corrin in cobesters was perturbed by replacement of C10 H by NO_2 and NH_2. Then ligand binding investigations were carried out on $[AC\text{-}(10\text{-}NO_2)Cbs]^+$ and $[AC\text{-}(10\text{-}NH_2)Cbs]^+$ and results were compared to $[ACCbs]^+$, in which the corrin ring is intact.

The results of the ligand binding investigations suggested that the charge density at the metal centre is a primary discriminator for the affinity of the metal for an incoming ligand. As assessed from the Bader charges obtained from a QTAIM analysis, the cobalt metal becomes more positive and harder as C10 H is changed to NO_2 and less positive and softer on changing C10 H to NH_2. Thus, hard anions are favoured by a cobalt corrin with a hard metal centre, in $[AC\text{-}(10\text{-}NO_2)Cbs]^+$; whereas the softer metal centre in $[ACCbs]^+$ and $[AC\text{-}(10\text{-}NH_2)Cbs]^+$ heavily favours the softer anions. Results for aromatic N-donor ligands (DMAP and imidazole) showed that these ligands are less favoured by the harder metal centre in $[AC\text{-}(10\text{-}NO_2)Cbs]^+$.

We have shown that perturbing the electronic structure of the corrin by substituting the H at C10 either by NO_2 or NH_2 can result in different thermodynamic behaviour of the axial coordination site, which verifies the importance of the *cis* influence of the corrin on the chemistry of Co(III).

References on page 190

5.6 References

(1) Knapton, L.; Marques, H. M. *Dalton Trans.* **2005**, 889.

(2) Brown, K. L.; Cheng, S.; Zou, X.; Zubkowski, J. D.; Valente, E. J.; Knapton, L.; Marques, H. M. *Inorg. Chem.* **1997**, *36*, 3666.

(3) Perry, C. B.; Fernandes, M. A.; Brown, K. L.; Zou, X.; Valente, E. J.; Marques, H. M. *Eur. J. Inorg. Chem.* **2003**, 2095.

(4) Marques, H. M.; Knapton, L.; Zou, X.; Brown, K. L. *J. Chem. Soc. Dalton Trans.* **2002**, 3195.

(5) Chemaly, S. M.; Florczak, M.; Dirr, H.; Marques, H. M. *Inorg. Chem.* **2011**, *50*, 8719.

(6) Chemaly, S. M.; Brown, K. L.; Fernandes, M. A.; Munro, O. Q.; Grimmer, C.; Marques, H. M. *Inorg. Chem.* **2011**, *50*, 8700.

(7) Chemaly, S. M.; Kendall, L.; Nowakowska, M.; Pon, D.; Perry, C. B.; Marques, H. M. *Inorg. Chem.* **2013**, *52*, 1077.

(8) Nowakowska, M. MSc University of the Witswatersrand, 2014.

(9) Knapton, L. PhD, University of the Witwatersrand, 2005.

(10) Garau, G.; Geremia, S.; Marzilli, L. G.; Nardin, G.; Randaccio, L.; Tauzher, G. *Acta Cryst., Sec. B: Struct. Sci* **2003**, *59*, 51.

(11) Garau, G.; Geremia, S.; Marzilli, L. G.; Nardin, G.; Randaccio, L.; Tauzher, G. *Acta Crystallogr., Sect. B: Struct. Sci* **2003**, *59*, 51.

(12) Pratt, J. M. *The Inorganic Chemistry of Vitamin B_{12}*; Academic Press: London, 1972.

(13) Navizet, I.; Perry, C. B.; Govender, P. P.; Marques, H. M. *J. Phys. Chem. B.* **2012**, *116*, 8836.

(14) Howard, S. T.; Krygowski, T. M. *Can. J. Chem.* **1997**, *75*, 1174.

(15) O'Brien, S. E.; Popelier, P. L. *Can. J. Chem.* **1999**, *77*, 28.

(16) Vidal, I.; Melchor, S.; Alkorta, I.; Elguero, J.; Sundberg, M. R.; Dobado, J. A. *Organometallics.* **2006**, *25*, 5638.

(17) González, L.; Mó, M.; Yáñez, M.; Elguero, J. *J. Mol. Str.* **1996**, *371*, 1.

(18) Espinosa, E.; Souhassou, M.; Lachekar, H.; Lecomte, C. *Acta Cryst. B.* **1999**, *55*, 563.

(19) Bader, R. F. W.; Matta, C. F.; Cortés-Guzmán, F. *Organometallics.* **2004**, *23*.

(20) Sobczyk, L.; Grabowski, S. J.; Krygowski, T. M. *Chem. Rev.* **2005**, *105*, 3513.

(21) Grabowski, S. J. *J. Phys. Chem. A* **2000**, *105*, 5551.

(22) Bader, R. F. W.; Essén, H. *J. Chem. Phys.* **1984**, *80*, 1943.

(23) Bader, R. F. W.; Matta, C. F. *Inorg. Chem.* **2001**, *40*, 5603.

(24) Espinosa, E.; Alkorta, I.; Elguero, J.; Molins, E. *J. Chem. Phys.* **2002**, *117*, 5529.

(25) Zipp, C. F.; Michael, J. P.; Fernandes, M. A.; Mathura, S.; Perry, C. B.; Navizet, I.; Govender, P. P.; Marques, H. M. *Inorg. Chem.* **2014**, *53*, 4418.

(26) Varadwaj, P. R.; Marques, H. M. *Theor. Chem. Acc.* **2010**, *127*, 711.

(27) Varadwaj, P. R.; Cukrowski, I.; Perry, C. B.; Marques, H. M. *J. Phys. Chem. A.* **2011**, *115*, 6629.

(28) Varadwaj, P. R.; Varadwaj, A.; Marques, H. M. *J. Phys. Chem. A.* **2011**, *115*, 13180.

(29) Govender, P. P.; Navizet, I.; Perry, C. B.; Marques, H. M. *J. Phys. Chem. A.* **2013**, *117*, 3057.

CHAPTER 6

The Kinetics of the Reaction of Aquacyano-10-nitrocobester, Aquacyano-10-aminocobester and Aquacyanocobester with Cyanide

6.1 Introduction

One of the notable features of the chemistry of Co(III) in a cobalt corrin is its lability toward ligand substitution. As discussed earlier, it is believed that this lability is related to the electronic structure of corrin.[1-6] The approximate lability ratio of the metal ion toward substitution in corrin, porphyrin, cobaloxime, and tetra-ammine system is 10^9:10^6:10^4:1.[7,8] These observations suggest that labilisation of the axial ligand increases with the extent of delocalisation of the *cis* π electron system (ammine < cobaloxime < porphyrin) and inversely with the size of the macrocyclic cavity (porphyrin < corrin). It appears likely that this kinetic *cis*-effect is a consequence of the donation of electron density from the equatorial ligand to the metal, making the metal softer and imparting to it a degree of softer and more labile Co(II) character. The partially delocalised electron cloud and macrocyclic cavity size of the corrin ring are the key factors in the labilising of the central Co(III) ion. To date, several studies have been carried out to investigate the *cis*-effect of the corrin ring by modification of the structure of the corrin. A common ligand used to study the rates of ligand substitution reactions is CN^- because the reactions occur with a moderate speed and the affinity of Co(III) in corrin for CN^- is very high (**Equation 6.1**).[5,6,9]

$$[H_2O–Co–CN]^+ + CN^- \rightleftharpoons [CN–Co–CN] + H_2O \qquad (\mathbf{6.1})$$

Determining the rate constant for ligand substituting reactions of water bound to cobalt in aquacyanocobester, $[ACCbs]^+$, aquacyano-stable yellow cobester, $[ACSYCbs]^+$ and 5-seco-aquacyanocobester [5-seco-ACCbs], provided the opportunity to observe the effect of the modification of the equatorial ligand on the lability of the cobalt corrin (**Figure 5.1**, **Chapter 5**).[3,6] The kinetic results revealed that cobalt metal is softer and more labile in $[ACCbs]^+$; thus the rate constant for the reaction of $[ACCbs]^+$ with CN^- was higher ($4.8 \pm 0.3 \times 10^4\ M^{-1}s^{-1}$)[6] than [5-seco-ACCbs] ($3.4 \pm 0.2 \times 10^2\ M^{-1}s^{-1}$)[3] and $[ACSYCbs]^+$ ($1.53 \pm 0.2 \times 10^4\ M^{-1}s^{-1}$).[6] This suggests

References on page 201

that decreasing the extent of the π electron delocalisation within the corrin macrocycle and increasing the macrocyclic cavity size decreases the amount of electron density donated to the cobalt metal, hence significantly increases the inertness of the Co(III) ion. The investigation into the effect of the structure of the corrin ligand on the kinetics of the ligand substitution reaction on Co(III) is extended in this work. The kinetics of the substitution of the axially coordinated H_2O ligand by the probe ligand, CN^-, were determined for aquacyano-10-nitrocobester [AC-(10-NO_2)Cbs]$^+$, aquacyano-10-aminocobester [AC-(10-NH_2)Cbs]$^+$ and aquacyanocobester [ACCbs]$^+$ under pseudo first-order conditions using stopped-flow spectrophotometry and compared to determine the kinetic *cis*-effect of the C10 substituent on the lability of the Co–H_2O bond.

6.2 Results and Discussion

The kinetics of the substitution of H_2O in [ACCbs]$^+$, [AC-(10-NO_2)Cbs]$^+$ and [AC-(10-NH_2)Cbs]$^+$ in 50% isopropanol/buffer mixtures (0.1 M CHES, pH 9.5) were determined by stopped-flow spectrophotometry between 10 and 30 ^oC at 370, 361 and 372 nm, respectively, by mixing equal volumes of solutions of the cobester and cyanide. The final concentration of the cobester was approximately 25 μM. Cyanide solutions were freshly prepared in the same solvent system and were between 0.5 and 5 mM in cyanide (on mixing) for reactions with [ACCbs]$^+$ and [AC-(10-NH_2)Cbs]$^+$ and between 2.5 and 25 mM for reactions with [AC-(10-NO_2)Cbs]$^+$.

In all reactions, biphasic kinetics were observed because of the inevitable presence of the aquahydroxo complex which is formed from a reaction between aquacyano species in solution. The absorbance-time traces (**Figure 6.1**) were therefore fitted to **Equation 6.4**, appropriate for parallel reactions.

As was established for [ACCbs]$^+$,[5] the faster phase is due to substitution of H_2O *trans* to CN^-; it accounted for approximately 75%, 90% and 65% of the absorbance change at the monitoring wavelengths for the reaction of CN^- with [AC-(10-NH_2)Cbs]$^+$, [ACCbs]$^+$ and [AC-(10-NO_2)Cbs]$^+$, respectively. The slower phase is due to substitution of H_2O *trans* to OH^-. In **Equation 2.11**, k_f and k_s are the pseudo first-order rate constants for the faster and slower phases, respectively, A_∞ is the absorbance at the end of the reaction, $|A_0 - A_1|$ the absorbance change associated with the faster phase and $|A_1 - A_\infty|$ that associated with the slower phase.

References on page 201

$$A_\lambda = A_\infty + \left(A_0 - A_1\right)\mathrm{e}^{-k_f^{obs}t} + (A_1 - A_\infty)\mathrm{e}^{-k_s^{obs}t} \quad \textbf{(2.11)}$$

The observed pseudo first-order rate constants were corrected (**Equation 2.12**) for the effect of pH since hydroxide is inert to substitution in the cobalt corrins, where pK_{Co} is the acid dissociation constant of coordinated H_2O on Co(III) in the cobester being studied;[10-13] the [CN^-] was corrected for the acid dissociation constant of HCN since HCN reacts negligibly slowly compared to CN^- itself. [10,12]

$$k_i = k_i^{obs}\left(1+10^{\mathrm{pH}-\mathrm{p}K_{Co}}\right), \left(i = f, s\right) \quad \textbf{(2.12)}$$

References on page 201

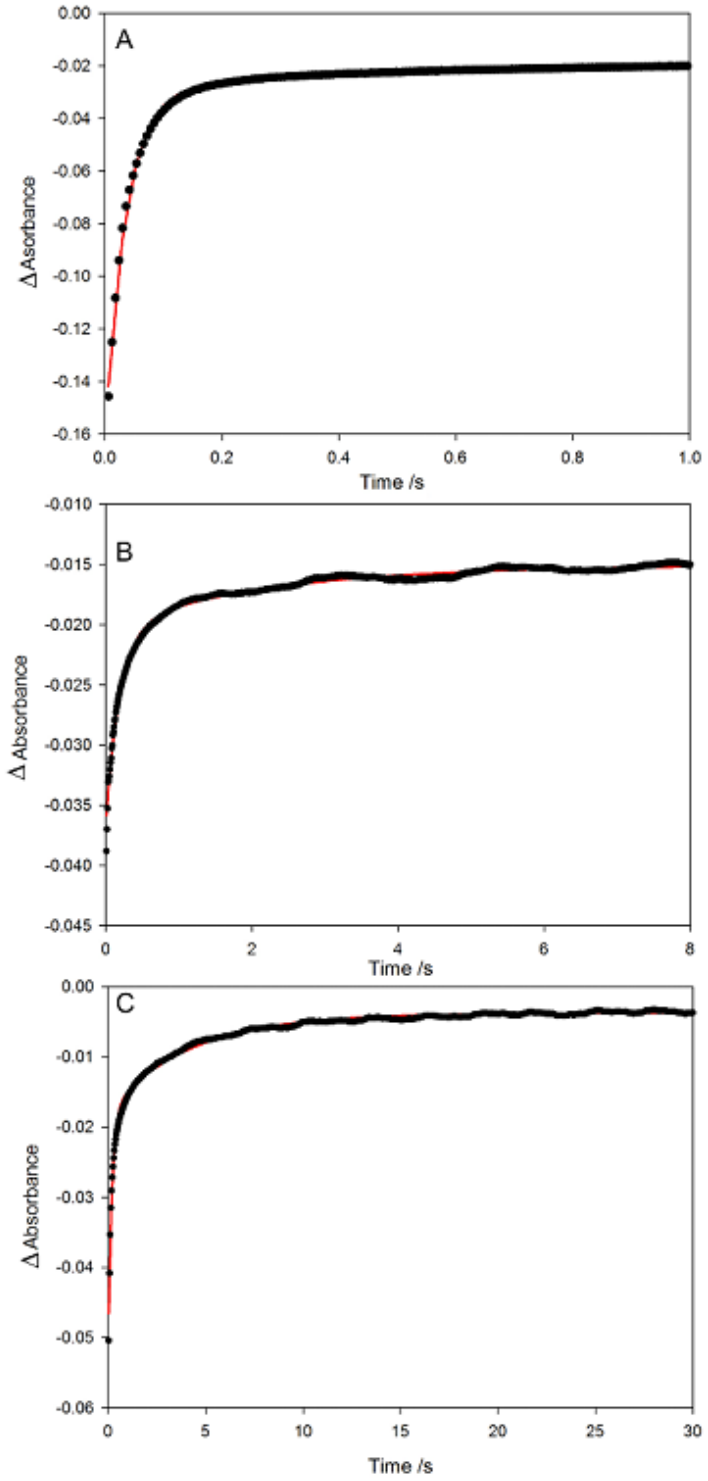


Figure 6.1 Fits of **Equation 6.4** to the absorbance-time trace of the reaction at 25 ºC of CN^- with (A) [ACCbs[$^+$, 370 nm, [CN^-] = 0.386 mM, pH 8.9; (B) [AC-(10-NO_2)Cbs]$^+$, 361 nm, [CN^-] = 6.17 mM, pH 9.4; and (C) [AC-(10-NH_2)Cbs]$^+$, 372 nm, [CN^-] = 0.204 mM, pH 9.1.

References on page 201

The second-order rate constants, k_f^{II}, were determined from weighed linear least squares plots of k_i, (i = f,s), against the effective [CN^-]. Values of $\Delta H^{\ddagger}$ and $\Delta S^{\ddagger}$ were determined from the slope and intercept, respectively, of an Eyring plot of $\ln(k^{II}h/k_BT)$ against T^{-1}, where h and k_B are the Plank and Boltzmann constants, respectively.

The kinetics data obtained for the substitution of coordinated H_2O in $[ACCbs]^+$, $[AC\text{-}(10\text{-}NO_2)Cbs]^+$ and $[AC\text{-}(10\text{-}NH_2)Cbs]^+$ are summarised in **Table 6.1**. The primary data are given in **Appendix 6.1** and examples of the results and regression analysis of the standard non-linear least squares curve fitting data can be found in **Digital Appendix D**. **Figure 6.2** shows the Eyring plots from which values of $\Delta H^{\ddagger}$ and $\Delta S^{\ddagger}$ were determined.

References on page 201

Table 6.1 Kinetic Data for the Substitution of Coordinated H_2O in the Three Cobesters with CN^-.

Temp /°C	k_f^{II} [a] /10^3 M^{-1} s^{-1}	$\Delta H_f^{\ddagger}$ /kJ mol^{-1}	$\Delta S_f^{\ddagger}$ /J K^{-1} mol^{-1}	k_f^{II}(25 °C) [b] /M^{-1} s^{-1}	k_s^{II} [a] /10^3 M^{-1} s^{-1}	$\Delta H_s^{\ddagger}$ /kJ mol^{-1}	$\Delta S_s^{\ddagger}$ /J K^{-1} mol^{-1}	k_s^{II}(25 °C) [b] /M^{-1} s^{-1}
[AC(10-NH_2)Cbs]$^+$								
10.0	12.3(3)	40(3)	-27(11)	2.4×10^4	0.53(1)	34(3)	-71(9)	1.3×10^3
18.0	19(2)				0.74(3)			
21.0	25(4)				0.88(6)			
25.0	27(3)				1.11(11)			
30.0	41(3)				0.53(4)			
[ACCbs]$^+$								
10.0	21(1)	58(3)	43(12)	7.5×10^4	5.14(8)	92(19)	150(66)	3.2×10^4
18.0	39(2)				8.2(5)			
21.0	58(3)				24(2)			
25.0	81(1)				9.7(5)			
30.0	110(3)				65(1)			
[AC(10-NO_2)Cbs]$^+$								
10.0	0.20(1)	90(3)	119(12)	1.7×10^3	0.046(2)	77(8)	53(28)	1.2×10^2
15.0	0.39(3)				0.18(1)			
18.0	0.62(4)				0.22(3)			
21.0	0.97(9)				0.40(10)			
25.0	1.62(13)				0.80(12)			
30.0	2.54(17)				1.8(2)			

[a] Corrected for the pK_a of HCN and the fraction of the inert hydroxocobester in solution (**Equation 2.12**). [b]Interpolated from the values of $\Delta H^{\ddagger}$ and $\Delta S^{\ddagger}$.

References on page 201

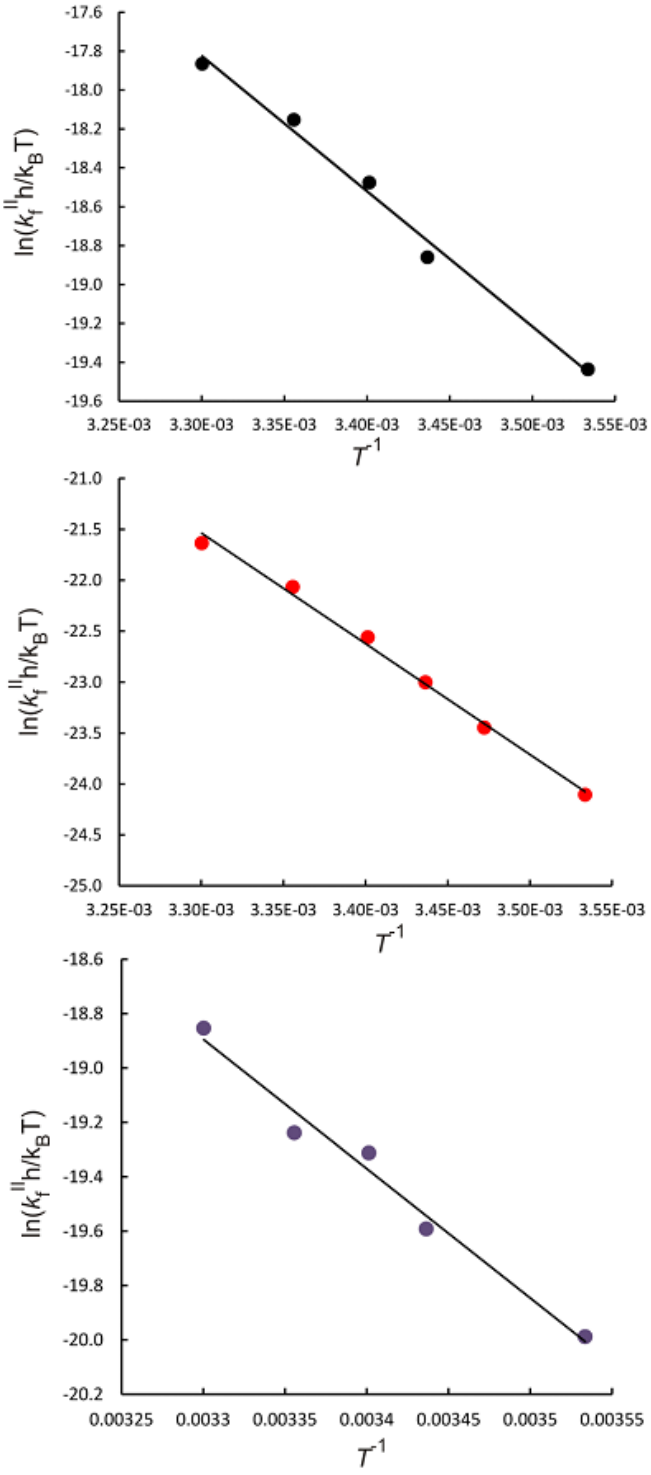


Figure 6.2 Eyring plots for the reaction of (A) (top) $[ACCbs]^+$, (middle) $[AC\text{-}(10\text{-}NO_2)Cbs]^+$ and (bottom) $[AC\text{-}(10\text{-}NH_2)Cbs]^+$ with CN^-.

References on page 201

The values of the second-order rate constants, k_f^{II}, for substitution of H_2O on Co(III) by CN^- *trans* to CN^- in the $[AC\text{-}(10\text{-}Z)Cbs]^+$ (Z = H, NH_2 and NO_2) are not very different (**Table 6.1**), and the ratio between the largest (for Z = H, $k_f^{II} = 7.5 \times 10^4\ M^{-1}s^{-1}$ at 25 °C) and the smallest (Z = NO_2, $k_f^{II} = 1.7 \times 10^3\ M^{-1}s^{-1}$ at 25 °C) is just over 40. The values for k_s^{II}, where the substitution is *trans* to OH^-, are much slower, as expected, and parallel values of k_f^{II}. In this case, the discrimination is larger, and $[aquahydroxoCbs]^+$ reacts some 250 times faster than $[aquahydroxo(10\text{-}NO_2)Cbs]^+$.

The relative insensitivity of k_f^{II} to Z is because of a compensation effect between $\Delta H^{\ddagger}$ and $\Delta S^{\ddagger}$, with smaller values of $\Delta H^{\ddagger}$, which would lead to large values of k_f^{II}, offset by larger values of $\Delta S^{\ddagger}$ (**Figure 6.3**). Indeed, if all three reactions had the same value of $\Delta S^{\ddagger}$ then k_f^{II} would vary in the approximate ratio 10^9:10^6:1 for Z = NH_2, H and NO_2, respectively. The compensation effect therefore masks the *very significant* differences in the reactivity of the metal ion towards the entering CN^- ligand.

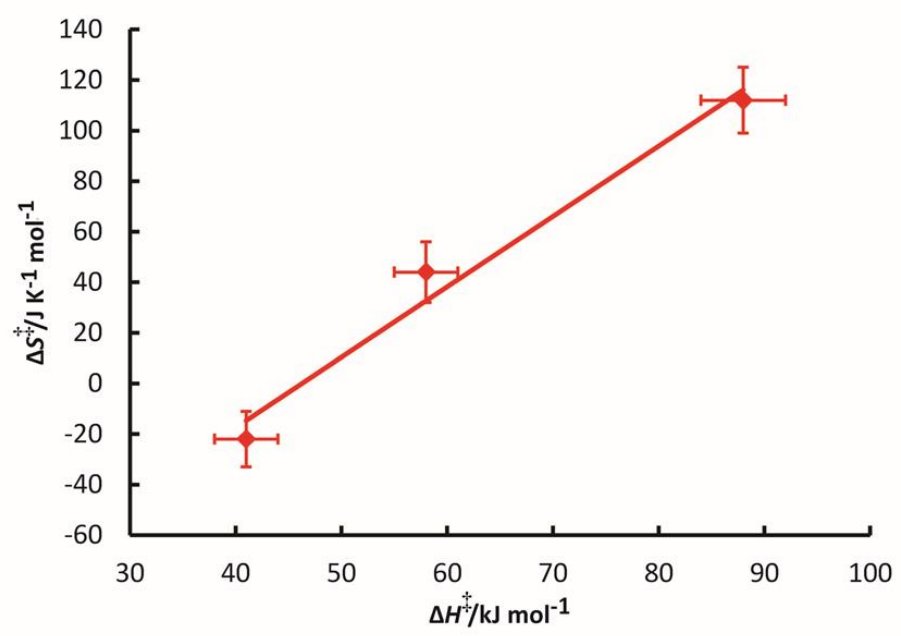


Figure 6.3 There is a compensation effect between values of $\Delta H^{\ddagger}$ and $\Delta S^{\ddagger}$ for the ligand substitution of coordinated H_2O in $[AC\text{-}(10\text{-}Z)Cbs]^+$ (Z = H, NH_2, NO_2).

References on page 201

It is well-established that the ligand substitution reactions of cobalt corrins proceed through a dissociative interchange (I_d) mechanism where there is nucleophilic participation of the entering ligand in the transition state.[10,12,14-17]

A small value of $\Delta H^{\ddagger}$ is indicative of a transition state that occurs early along the reaction coordinate, where there is substantial bond formation between the entering ligand and the metal while the bonding between the metal and the departing ligand is still significant. This will contribute to a negative value of $\Delta S^{\ddagger}$, reflecting a loss of freedom of the entering ligand which has not been wholly compensated for by the increasing freedom of the departing ligand. A late transition state, on the other hand, will have a large $\Delta H^{\ddagger}$ value because bond breaking to the departing ligand has not been significantly compensated for by bond formation to the entering ligand; this is offset by a positive value of $\Delta S^{\ddagger}$ because of a disordered transition state with significant freedom of the departing ligand and with only a small loss of freedom of the entering ligand.

The results given in **Table 6.1** are consistent with an early transition state for the reaction between CN^- and $[AC\text{-}(10\text{-}NH_2)Cbs]^+$, a somewhat later transition state between CN^- and $[ACCbs]^+$, and a much later transition state when CN^- reacts with $[AC\text{-}(10\text{-}NO_2)Cbs]^+$. This is understandable since the hardness of the metal centre increases, and its affinity for entering CN^- decreases, as the C10 substituent is changed from NH_2 to H to NO_2. This convincingly illustrates the very profound effect that altering the electronic structure of the equatorial ligand in a Co(III) macrocycle will have on the reactivity of the metal ion.

6.3 Conclusions

The kinetics study showed that the second-order rate constants, k_f^{II}, for substitution of H_2O on Co(III) by CN^- increase in the order $[AC\text{-}(10\text{-}NO_2)Cbs]^+ < [AC\text{-}(10\text{-}NH_2)Cbs]^+ < [ACCbs]^+$; they are not very different and the ratio between the largest and the smallest values of k_f^{II} is just over 40. However, this is misleading because of a compensation effect between $\Delta H^{\ddagger}$ and $\Delta S^{\ddagger}$. As values of $\Delta H^{\ddagger}$ become smaller, which causes an increase in the reaction rate, $\Delta S^{\ddagger}$ becomes less positive (or more negative), which causes a decrease in the reaction rate. Hence, comparing rate constants at any particular temperature is not very informative and the compensation effect

References on page 201

masks the *very significant* differences in the reactivity of the metal ion towards the entering CN^- ligand.

The compensation effect is attributed to the position of the transition state along the reaction coordinate, which depends on the charge density on the metal ion. An early transition state occurred for the reaction between CN^- and $[AC\text{-}(10\text{-}NH_2)Cbs]^+$ because the charge density increases on Co(III) and the converse holds for the reaction between CN^- and $[AC\text{-}(10\text{-}NO_2)Cbs]^+$. If the value of $\Delta S^{\ddagger}$ was the same for all the three cobesters, then the approximate ratio 10^9:10^6:1 for the values of k_f^{II} would be expected for Z = NH_2, H and NO_2, respectively.

The conclusion is that manipulating the electronic structure of the corrin affects the kinetics of axial ligand substitution. Therefore, the values of activation parameters ($\Delta H^{\ddagger}$ and $\Delta S^{\ddagger}$) for the three cobesters are different, when the electronic structure of corrin is disrupted either by an electron-withdrawing (NO_2) or by an electron-donating (NH_2) group.

References on page 201

6.4 References

(1) Zipp, C. F. PhD, University of the Witwatersrand, 2013.

(2) Mathura, S. PhD, University of the Witwatersrand, 2013.

(3) Nowakowska, M. MSc University of the Witswatersrand, 2014.

(4) Chemaly, S. M.; Kendall, L.; Nowakowska, M.; Pon, D.; Perry, C. B.; Marques, H. M. *Inorg. Chem.* **2013**, *52*, 1077.

(5) Chemaly, S. M.; Brown, K. L.; Fernandes, M. A.; Munro, O. Q.; Grimmer, C.; Marques, H. M. *Inorg. Chem.* **2011**, *50*, 8700.

(6) Chemaly, S. M.; Florczak, M.; Dirr, H.; Marques, H. M. *Inorg. Chem.* **2011**, *50*, 8719.

(7) Knapton, L.; Marques, H. M. *Dalton Trans.* **2005**, 889.

(8) Brown, K. L.; Cheng, S.; Zou, X.; Zubkowski, J. D.; Valente, E. J.; Knapton, L.; Marques, H. M. *Inorg. Chem.* **1997**, *36*, 3666.

(9) Baldwin, D. A.; Betterton, E. A.; Pratt, J. M. *J. Chem. Soc. Dalton Trans.* **1983**, 2217.

(10) Reenstra, W. W.; Jencks, W. P. *J. Am. Chem. Soc.* **1979**, *101*, 5780.

(11) Marques, H. M.; Marsh, J. H.; Mellor, J. R.; Munro, O. Q. *Inorg. Chim. Acta.* **1990**, *170*, 259.

(12) Marques, H. M.; Brown, K. L.; Jacobsen, W. *J. Biol. Chem.* **1988**, *263*, 12378.

(13) Marques, H. M.; Baldwin, D. A.; Pratt, J. M. *J. Inorg. Biochem.* **1987**, *29*, 77.

(14) Marques, H. M.; Munro, O. Q.; Cumming, B. M.; de Nysschen, C. *J. Chem. Soc. Dalton Trans.* **1994**, 297.

(15) Marques, H. M. *J. Chem. Soc. Dalton Trans.* **1991**, 1437.

(16) Marques, H. M. *J. Chem. Soc. Dalton Trans.* **1991**, 339.

(17) Stochel, G.; van Eldik, R. *Inorg. Chem.* **1990**, *29*, 2075.

CHAPTER 7

Conclusions and Future Work

7.1 Conclusions

The normally inert cobalt(III) ion is relatively labile in its complexes with corrin macrocycles.[1-17] This labilisation seems to be the result of a substantial *cis*-effect which causes the transfer of electron density from the corrin ring to the central cobalt metal, therefore imparting to it some Co(II)-like character. Co(II), unlike Co(III) is very labile.[4,5,16,18]

The aim of this study was to further investigate the relationship between the electronic structure of the corrin ring and the chemistry of cobalt in the corrins. Thus, a study was undertaken on C10 substituted cobalamins and cobesters, in which the electronic structure of the corrin is altered, in order to obtain a greater understanding of the *cis*-labilising effect of the corrin ring. The C10 substituted compounds studied were aqua-10-bromocobalamin $[H_2O\text{-}(10\text{-}Br)Cbl]^+$, dicyano-10-nitrocobester $[DC\text{-}(10\text{-}NO_2)Cbs]$ and dicyano-10-aminocobester $[DC\text{-}(10\text{-}NH_2)Cbs]$. As discussed in **Chapter 2**, all compounds were synthesised following minor modifications of established methods.

Before any solution chemistry investigations could be performed, the dicyanocobester species had to be converted to their aquacyano form because the coordinated water can be substituted by an exogenous ligand. Since the kinetics and thermodynamics of the substitution reactions for these compounds are pH-dependent and hydroxo species is inert to substitution,[1,2,5] the pK_a for these compounds had to be determined in the first place.

This chapter is divided in two sections for convenience and the results for cobalamins and cobesters are summarised separately.

- **$[H_2O\text{-}(10\text{-}Br)Cbl]^+$**

The pK_a of $[H_2O\text{-}(10\text{-}Br)Cbl]^+$ was determined at 25 ^oC in aqueous solution as 7.23 ± 0.03. The pK_a of aquacobalamin $[H_2OCbl]^+$ and aqua-10-chlorocobalamin $[H_2O\text{-}(10\text{-}Cl)Cbl]^+$ were also determined under the identical experimental conditions as 7.62 ± 0.01 and 7.22 ± 0.02,

References on page 207

respectively. The data indicate that as the electron-donor ability of the C10 substituent increases the value of pK_a decreases. This is consistent with Br and Cl both donating electron density to the corrin ring and consequently increasing the negative charge on the O atom of coordinated H_2O; thus the acidity of the axial H_2O ligand increases marginally, resulting in a lower pK_a. Then, the stability constants for replacement of coordinated H_2O by various anionic (N_3^-, NO_2^-, SCN^-, SO_3^{2-}) and neutral ligands (imidazole, DMAP) were determined for $[H_2O\text{-}(10\text{-Br})Cbl]^+$ as well as $[H_2O\text{-}(10\text{-Cl})Cbl]^+$ and $[H_2OCbl]^+$, in order to look at the *cis*-labilising influence in the cobalamins. The anions all have stability constants that are higher for coordination to $[H_2O\text{-}(10\text{-Br})Cbl]^+$ and $[H_2O\text{-}(10\text{-Cl})Cbl]^+$ than to $[H_2OCbl]^+$, whereas the neutral ligands have stability constants that are lower. Furthermore, for the anionic ligands we note that values of $\Delta K = \log K_{10H} - \log K_{10Br}$ roughly correlate with the spectrochemical series,[19] *viz*, $\underline{S}CN^- < N_3^- < \underline{N}CS^- < NO_2^- < SO_3^{2-}$ (although NO_2^- is usually[20] higher in the spectrochemical series than SO_3^{2-}). This is attributed to the ability of the Br atom at C10 to act as both a π electron-donor towards and, because of its electronegativity, a σ-withdrawing moiety. In addition, results from a QTAIM analysis showed that when the H atom at the C10 position is changed to Cl or Br, the positive charge on the metal atom decreases; hence the metal becomes more electron rich. This suggests that $[H_2O\text{-}(10\text{-Br})Cbl]^+$ or $[H_2O\text{-}(10\text{-Cl})Cbl]^+$ will discriminate against a neutral ligand because the metal is more electron rich and will be less capable of accepting charge donation from the axial donor. If the ligand is an anion, however, the charge donation can be accepted by delocalisation onto the C10 Cl or Br; the C10 substituent acts as a charge reservoir for the additional charge and in this regard Br and Cl are much more effective than H.

The kinetics of the substitution of N_3^- and imidazole with $[H_2O\text{-}(10\text{-Br})Cbl]^+$ were investigated to determine how perturbing the electronic structure of the corrin affects rate constants. The reaction kinetics for both ligands were found to be slower for $[H_2O\text{-}(10\text{-Br})Cbl]^+$ than $[H_2OCbl]^+$, consonant with the previous observations[21] of the reaction of N_3^- and pyridine with $[H_2O\text{-}(10\text{-Cl})Cbl]^+$ and $[H_2OCbl]^+$. The differences in rate constants are not large but are significant (**Table 4.2)**. They arise from values of $\Delta H^‡$ that are smaller for the reactions with the 10-Cl and 10-Br derivatives than for that with $[H_2OCbl]^+$, but which fail to compensate for $\Delta S^‡$ values that are much more negative. This can be related to the dissociative interchange mechanism of the ligand substitution reactions of the cobalt corrins.[21] The smaller $\Delta H^‡$ and more negative $\Delta S^‡$ values are indicative of a transition state that occurs earlier along the reaction

References on page 207

coordinate in the reactions of these ligands with the 10-Cl and 10-Br derivatives than in their reactions with $[H_2OCbl]^+$. The late transition state in $[H_2OCbl]^+$ is a consequence of the lower charge density on the metal and making it a better electrophile both towards the incoming and the departing ligand. These thermodynamic and kinetic results show that modification with the electronic structure of the corrin ring in cobalamins can influence the chemistry of the metal ion.

- **$[AC\text{-}(10\text{-}NO_2)Cbs]^+$, $[AC\text{-}(10\text{-}NH_2)Cbs]^+$ and $[ACCbs]^+$.**

The pK_a values of aquacyano-10-nitrocobester ($[AC\text{-}(10\text{-}NO_2)Cbs]^+$) and aquacyano-10-aminocobester ($[AC\text{-}(10\text{-}NH_2)Cbs]^+$), as well as aquacyanocobester ($[ACCbs]^+$), were determined at 25 ^oC in 50% isopropanol/buffer solutions as 10.2, 10.4 and 10.6, respectively. Once the pK_a values were determined, the stability constants for substitution reactions of axially coordinated H_2O by a series of anionic (N_3^-, NO_2^-, SCN^-, SO_3^{2-}, CN^-) and neutral (imidazole, methylamine, DMAP) ligands were studied. The study has shown that the anionic ligands with a softer donor atom such as SO_3^{2-} and CN^- bound preferentially to the softer cobalt atom in $[AC\text{-}(10\text{-}NH_2)Cbs]^+$, and $[ACCbs]^+$, and anionic ligands with a harder donor atom such as N_3^-, NO_2^- and SCN^- bound preferentially to the harder Co(III) centre in $[AC\text{-}(10\text{-}NO_2)Cbs]^+$. DMAP clearly has a higher affinity for $[AC\text{-}(10\text{-}NH_2)Cbs]^+$ and $[ACCbs]^+$ than for $[AC\text{-}(10\text{-}NO_2)Cbs]^+$, but there is little discrimination in the case of imidazole and $MeNH_2$. These results imply that the electron density at the metal centre is a primary discriminator for the affinity of the metal for an exogenous ligand. Anionic ligands with a hard donor atom are favoured by a cobalt corrin with a hard metal centre; but in particular, the softer metal centre in $[AC\text{-}(10\text{-}NH_2)Cbs]^+$, and $[ACCbs]^+$, heavily favours the softer anions. These observations were verified by QTAIM analysis to show that substitution of C10 by an electron-donating group, NH_2 causes the transfer of electron density to the Co(III) metal ion and makes the metal softer, while substitution of C10 by an electron-withdrawing group, NO_2 withdraws the electron density from the Co(III) metal centre and resulting in a harder metal centre.

Kinetics data for the substitution of H_2O by CN^- were obtained under pseudo first-order conditions. The results showed that the substitution reaction proceeded with biphasic kinetics. As discussed in **Chapter 6** the faster reaction corresponds to the substitution of the axially coordinated H_2O by CN^- and the slower phase corresponds to the substitution of the axially coordinated H_2O *trans* to OH^- in aquahydroxo complex by CN^-. The second-order rate constants

References on page 207

were found to be 1.7 x 10^3, 2.4 x 10^4 and 7.5 x 10^4 $M^{-1}s^{-1}$ for $[AC\text{-}(10\text{-}NO_2)Cbs]^+$, $[AC\text{-}(10\text{-}NH_2)Cbs]^+$, and $[ACCbs]^+$, in 50% isopropanol/buffer, respectively. The difference in rate of the reaction of the three cobesters was not very large, and the ratio between the largest (for $[ACCbs]^+$, k_f^{II} = 7.5 × 10^4 $M^{-1}s^{-1}$ at 25 °C) and the smallest (for $[AC\text{-}(10\text{-}NO_2)Cbs]^+$, k_f^{II} = 1.7 × 10^3 $M^{-1}s^{-1}$ at 25 °C) is just over 40, and does not to follow the electron donor properties of the C10 substituent. This is misleading, however, because of a compensation effect between $\Delta H^{\ddagger}$ and $\Delta S^{\ddagger}$. As values of $\Delta H^{\ddagger}$ become smaller, it causes an increase in the reaction rate, $\Delta S^{\ddagger}$ becomes less positive (more negative) which causes a decrease in the reaction rate. The compensation effect is attributed to the position of the transition state along the reaction coordinate; this depends on the charge density on the metal ion, which increases as the C10 substituent is changed from NO_2 to NH_2. This explains why an early transition state occurs for the reaction between CN^- and $[AC\text{-}(10\text{-}NH_2)Cbs]^+$ and a much later transition state when CN^- reacts with $[AC\text{-}(10\text{-}NO_2)Cbs]^+$. If all three reactions had the same value of $\Delta S^{\ddagger}$ then the values of the rate constant would be in the approximate ratio 10^9:10^6:1 for $[AC\text{-}(10\text{-}NH_2)Cbs]^+$, $[ACCbs]^+$ and $[AC\text{-}(10\text{-}NO_2)Cbs]^+$, respectively. The kinetic results illustrate the very profound *cis*-effect that altering the electronic structure of the corrin ring will have on the reactivity of the metal ion.

This work has provided further evidence that altering the electronic structure of the corrin in both cobalamins and cobesters can have a profound effect on the stability of Co(III) corrin complexes with axial ligands, and on the kinetics of the substitution of axial H_2O. These *cis*-effects may play a role in the labilisation of the Co− C bond in coenzyme B_{12}, and should not be overlooked when assessing the origin of the remarkable lability of this cofactor.

7.2 Future work

This study has provided evidence of the importance of *cis*-effects in the chemistry of the cobalt corrins. It has laid the foundation for an extensive study of the *cis*-influence of the C10 substituent on the lability of Co–*β* bond. In future work it is envisaged that the bromine atom at the C10 position in $[H_2O\text{-}(10\text{-}Br)Cbl]^+$ can be substituted by a range of electron-donating and electron-withdrawing substituents, probably starting with methylboronic acid (one of the simplest boronic acids). Substituting Br with an alkenyl group or some other conjugated

References on page 207

functional group would allow the conjugation of the corrin ring to be extended, which provides an opportunity to investigate the effect of extending the conjugation system.

As it is well-known that diminishing the extent of delocalisation in the corrin π-electron system and subsequent opening of the macrocyclic cavity inhibits the ability of the system to impart electron density onto the cobalt ion. Therefore, future work will devoted to the opposite approach and increasing the conjugation system. This will be achieved by synthesising another vitamin B_{12} derivative, pyrocobester,[22,23] in which the extent of the conjugation system increases while the cavity size remains intact, to determine whether increasing the electron density of the corrin ring will further increase the lability of the Co(III) ion.

All these studies should provide further insight into the *cis*-labilising effect of the corrin and its influence on the coordination chemistry of Co(III).

References on page 207

7.3 References

(1) Knapton, L. PhD, University of the Witwatersrand, 2005.

(2) Chemaly, S. M.; Florczak, M.; Dirr, H.; Marques, H. M. *Inorg. Chem.* **2011**, *50*, 8719.

(3) Marques, H. M.; Egan, T. J.; Marsh, J. H.; Mellor, J. R.; Munro, O. Q. *Inorg. Chim. Acta.* **1989**, *166*, 249.

(4) Brown, K. L.; Cheng, S.; Zou, X.; Zubkowski, J. D.; Valente, E. J.; Knapton, L.; Marques, H. M. *Inorg. Chem.* **1997**, *36*, 3666.

(5) Chemaly, S. M.; Brown, K. L.; Fernandes, M. A.; Munro, O. Q.; Grimmer, C.; Marques, H. M. *Inorg. Chem.* **2011**, *50*, 8700.

(6) Randall, W. C.; Alberty, R. A. *Biochem.* **1967**, *6*, 1520.

(7) Reenstra, W. W.; Jencks, W. P. *J. Am. Chem. Soc.* **1979**, *101*, 5780.

(8) Balt, S.; van Herk, A. M. *Transition Met. Chem.* **1983**, *8*, 152.

(9) Baldwin, D. A.; Betterton, E. A.; Pratt, J. M. *J. Chem. Soc. Dalton Trans.* **1983**, 2217.

(10) Marques, H. M.; Brown, K. L.; Jacobsen, W. *J. Biol. Chem.* **1988**, *263*, 12378.

(11) Stochel, G.; van Eldik, R.; Kunkely, H.; Vogler, A. *Inorg. Chem.* **1989**, *28*, 4314.

(12) Marques, H. M. *J. Chem. Soc. Dalton Trans.* **1991**, 339.

(13) Marques, H. M.; Bradley, J. C.; Campbell, L. A. *J. Chem. Soc. Dalton Trans.* **1992**, 2019.

(14) Hamza, M. S. A.; Zou, X.; Brown, K. L.; van Eldik, R. *Inorg. Chem* **2001**, *50*, 5440.

(15) Hamza, M. S. A.; Elawady, M. A.; Marques, H. M. *Afr. J. Chem.* **2008**, *40*, 5440.

(16) Chemaly, S. M.; Kendall, L.; Nowakowska, M.; Pon, D.; Perry, C. B.; Marques, H. M. *Inorg. Chem.* **2013**, *52*, 1077.

(17) Perry, C. B.; Marques, H. M. *S. Afr. J. Chem.* **2005**, *58*, 9.

(18) Knapton, L.; Marques, H. M. *J. Chem. Soc. Dalton Trans.* **1997**, 3827.

(19) T. Ishii, S.; Tsuboi, G.; Sakane, Y. M.; Breedlove, B. K. *Dalton Trans.* **2009**, 680.

(20) Kettle, S. F. A. *Physical Inorganic Chemistry, A Coordination Chemistry Approach*; OUP: Oxford, UK, 1998.

(21) Knapton, L.; Marques, H. M. *Dalton Trans.* **2005**, 889.

(22) Ernst, L.; Holze, G.; Inhoffen, H. H. *Liebigs. Ann. Chem.* **1981**, 198.

(23) Kräutler, B.; stepanek, R.; Holze, G. *Helv. Chim. Acta.* **1983**, *66*, 44.

Appendices for Chapter 2

2.1 Calculation for Multi-Component Buffer

For a 50.0 mL, 1 mM multi-component buffer containing 1 mM MOPS, HEPES, Tris, CHES, CAPS and 0.5 M Na_2SO_4:

For buffers: $n = C \times V$, $n = \frac{m}{M}$

For example for MOPS buffer

$n = 1 \times 10^{-3} \times 50 \times 10^{-3}$

$n = 5 \times 10^{-5}$ mol

$5 \times 10^{-5} = \frac{m}{209.26}$

$M = 0.0104$ g

Therefore, a 50.0 mL, 1.0 mM multi-component buffer requires:

0.01191g of HEPES, 0.00605 g of Tris, 0.01036 g of CHES, 0.1106 g of CAPS and 0.009762 g of MES.

For 0.5 M Na_2SO_4:

$\mu = \frac{1}{2} \sum C_i Z_i^2$

$0.5 = \frac{1}{2} ([Na^+].(1))([SO_4^{-2}].(-2)^2)$

$0.5 = \frac{1}{2} ([Na^+] + 4[SO_4^{2-}])$

Since $[Na^+] = 2\,[SO_4^{2-}]$

$0.5 = ½ (2[SO_4^{2-}] + 4[SO_4^{2-}])$

$0.5 = 3\ [SO_4^{2-}]$

$[SO_4^{2-}] = 0.1666\ M$

$n = C \times V$

$n = 0.1666 \times 50 \times 10^{-3}$

$n = 0.00833\ mol$

$n = \frac{m}{M}$

$0.00833 = m/\ 142.04$

$m = 1.1831\ g$

2.2 ESI-MS Data for $[H_2O\text{-}(10\text{-}Br)Cbl]^+$

Positive mode

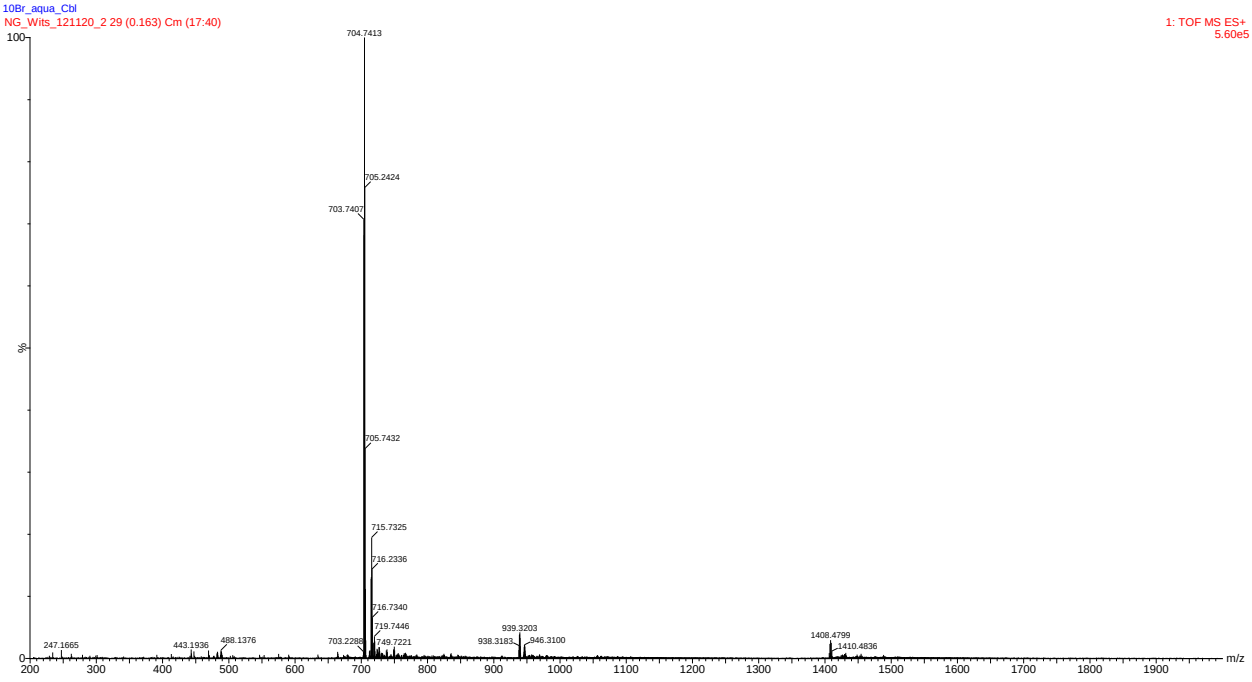


Figure 2.2.1 The positive mode of ESI-MS spectrum of $[H_2O\text{-}(10\text{-}Br)Cbl]^+$.

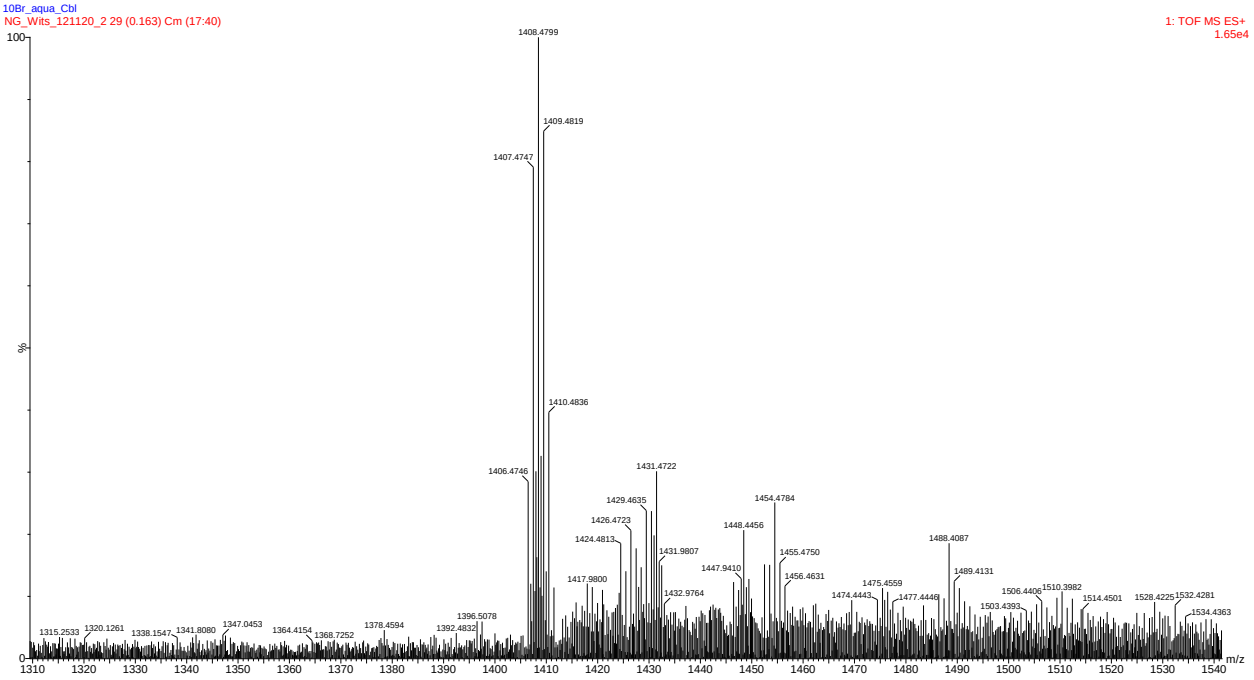


Figure 2.2.2 The positive mode ESI-MS of $[H_2O\text{-}(10\text{-}Br)Cbl]^+$ indicating the loss of the axial water ligand (1408) and also the loss of the axial water ligand with addition of a sodium ion (1431).

Negative mode

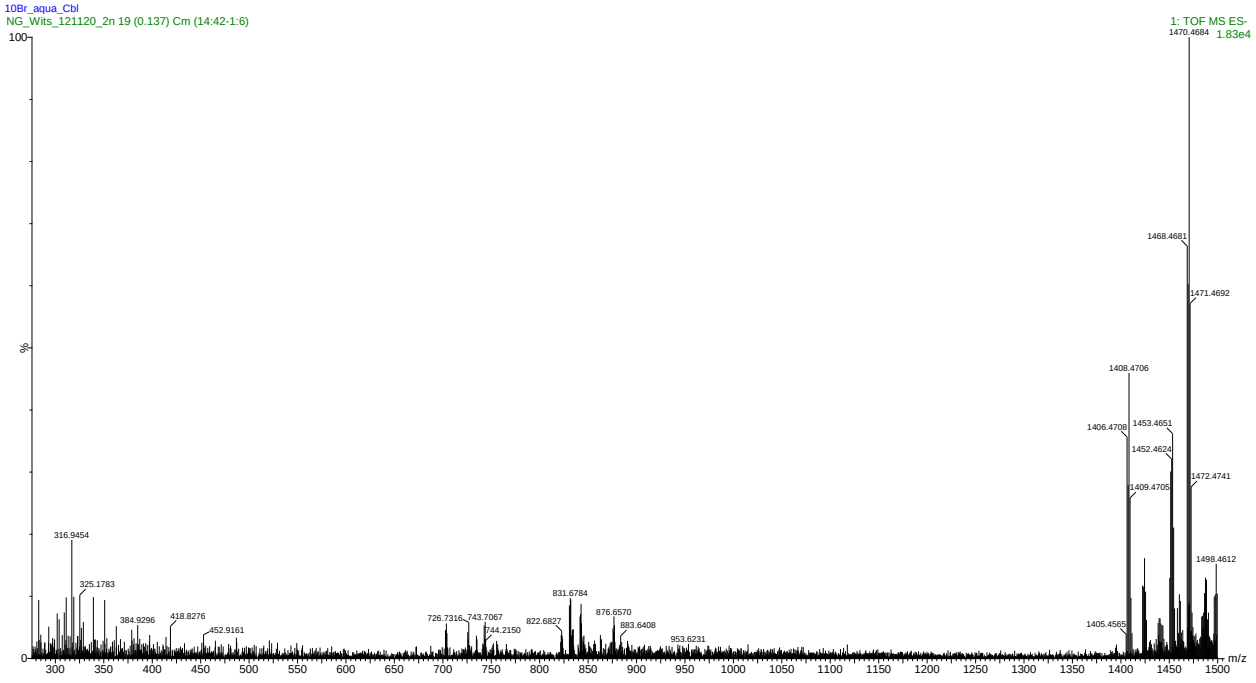


Figure 2.2.3 The negative mode ESI-MS spectrum of $[H_2O\text{-}(10\text{-}Br)Cbl]^+$.

2.3 ESI-MS Data for [DC-(10-NO_2)Cbs]

Positive mode

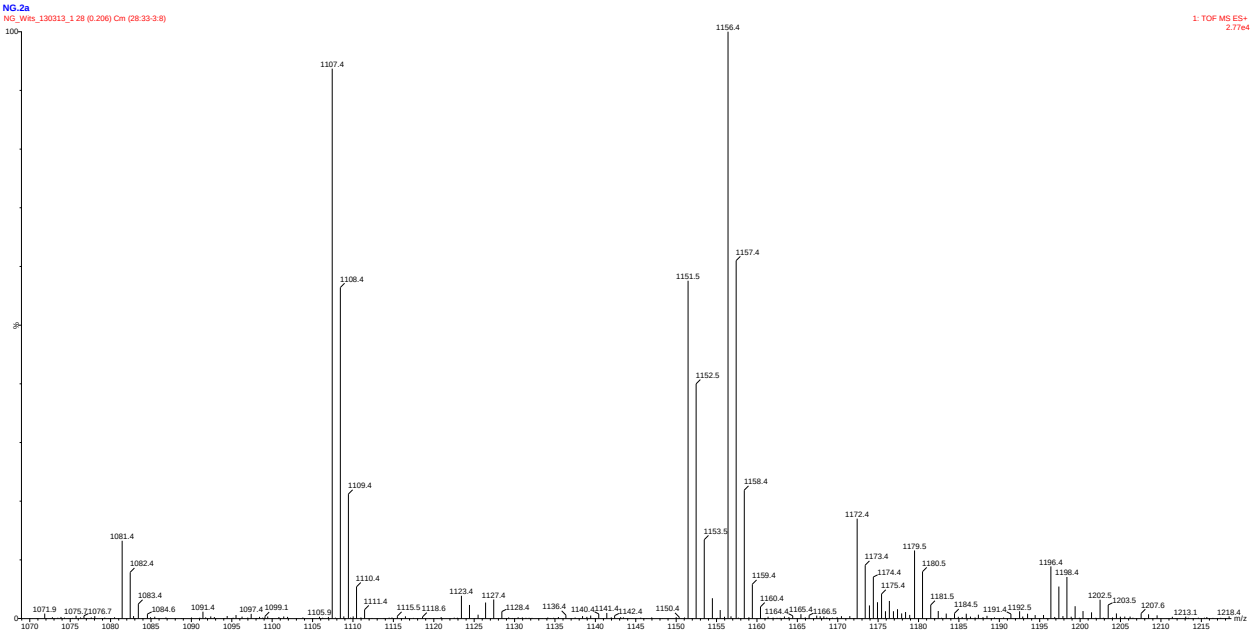


Figure 2.3.1 The positive mode ESI-MS of [DC-(10-NO_2)Cbs] indicating the loss of one axial cyanide ligand (1107) and addition of sodium ion (1156).

Negative mode

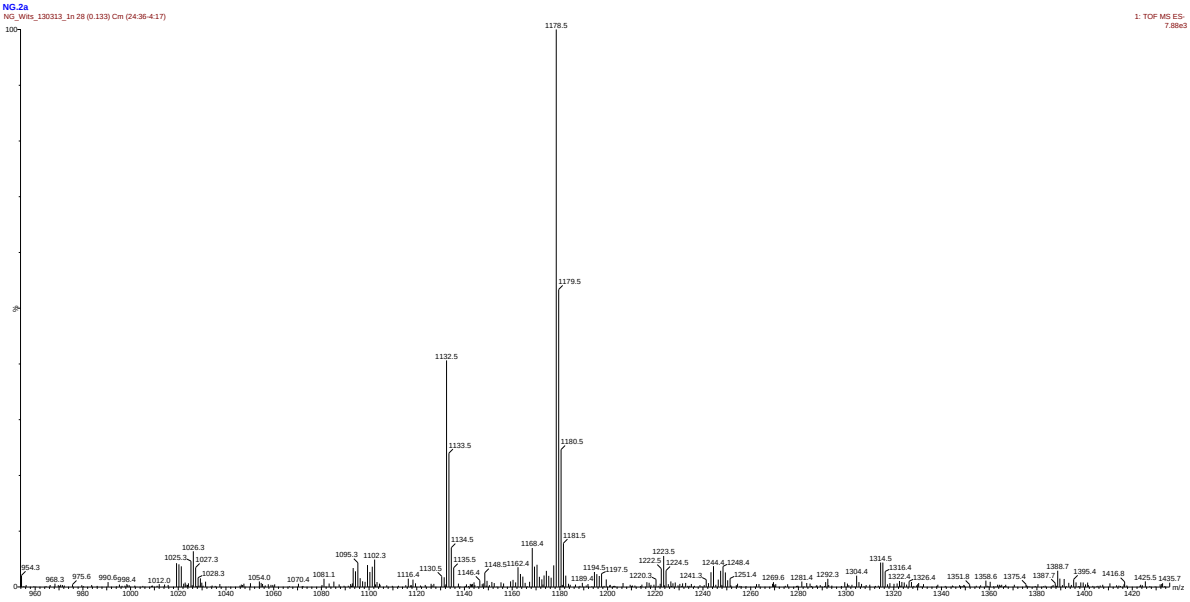


Figure 2.3.2 The negative ESI-MS spectrum of [DC-(10-NO_2)Cbs].

Positive mode

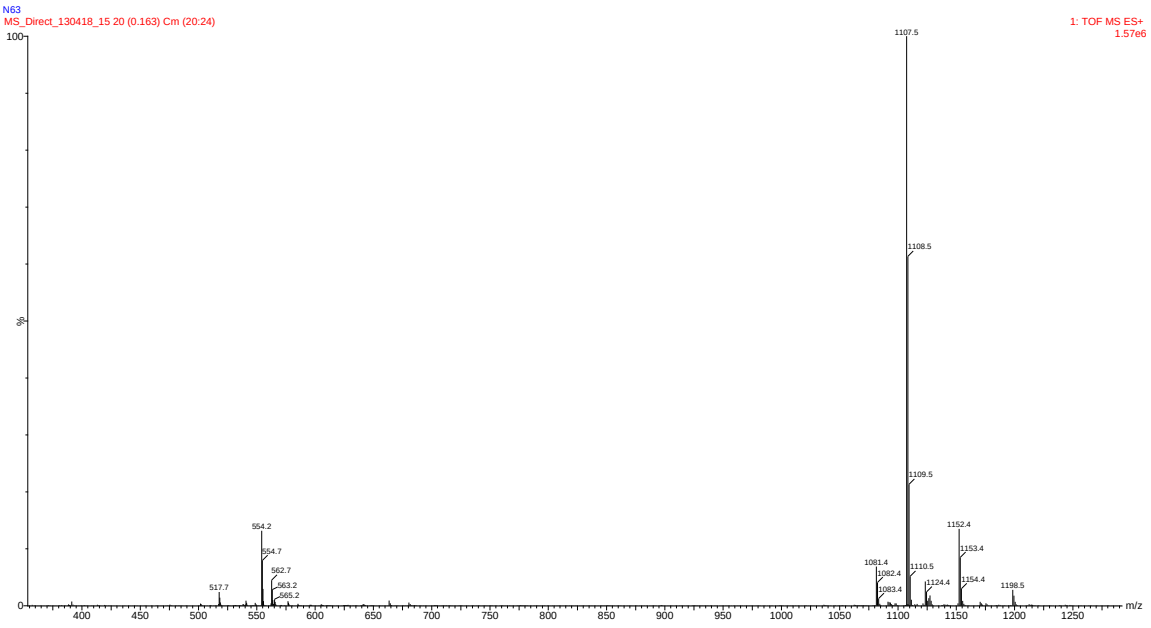


Figure 2.3.3 The positive ESI-MS of [DC-(10-NO_2)Cbs] indicating the loss of the water axial ligand (1107).

2.4 ESI-MS Data for $[AC\text{-}(10\text{-}NO_2)Cbs]^+$

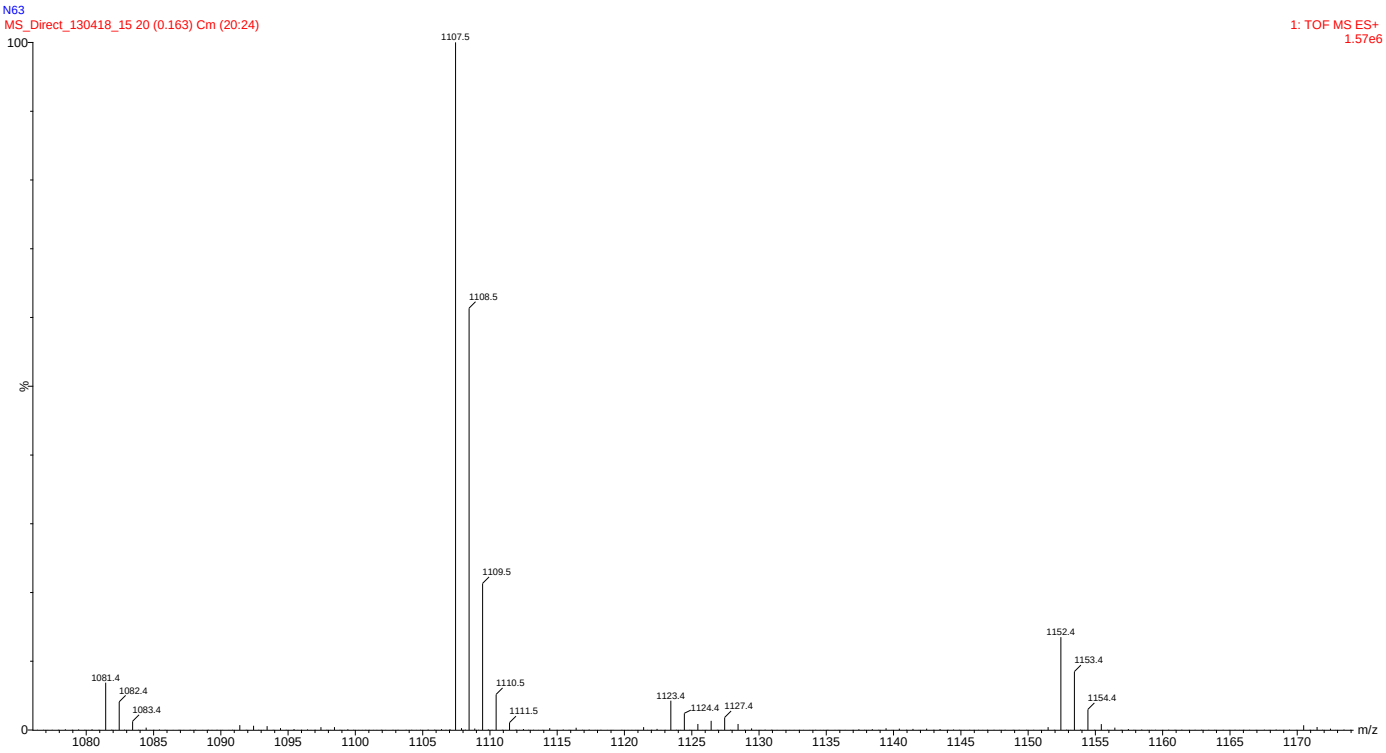


Figure 2.4.1 The positive mode ESI-MS of $[AC\text{-}(10\text{-}NO_2)Cbs]^+$ indicating the loss of an axial water ligand (1107.5).

2.5 NMR Spectra and Assignments for $[H_2O\text{-}(10\text{-}Br)Cbl]^+$ in CD_3OD

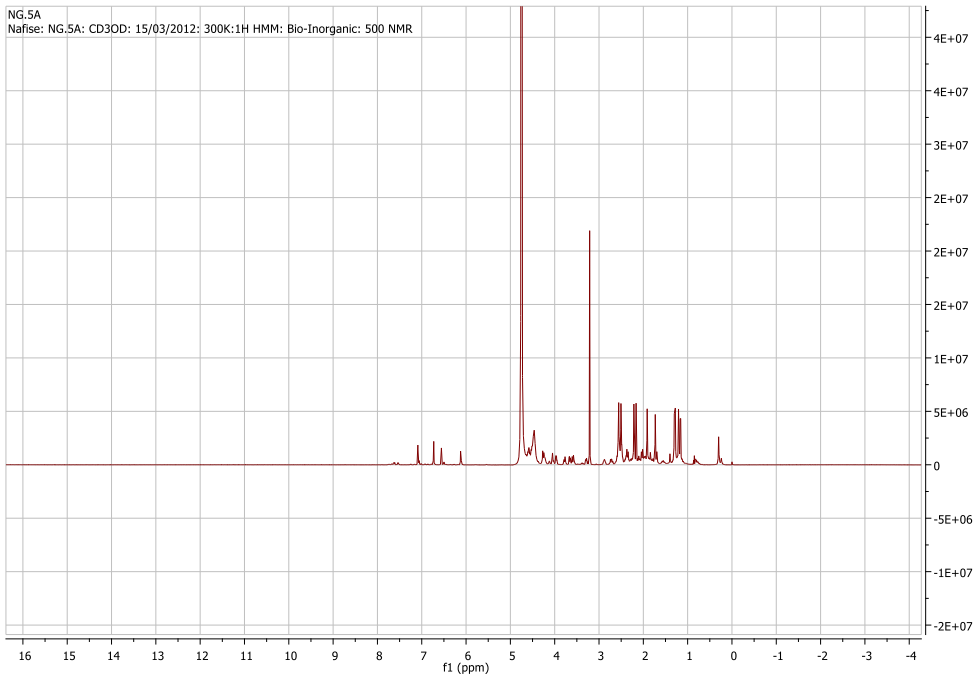


Figure 2.5.1 ^{1}H spectrum of $[H_2O\text{-}(10\text{-}Br)Cbl]^+$.

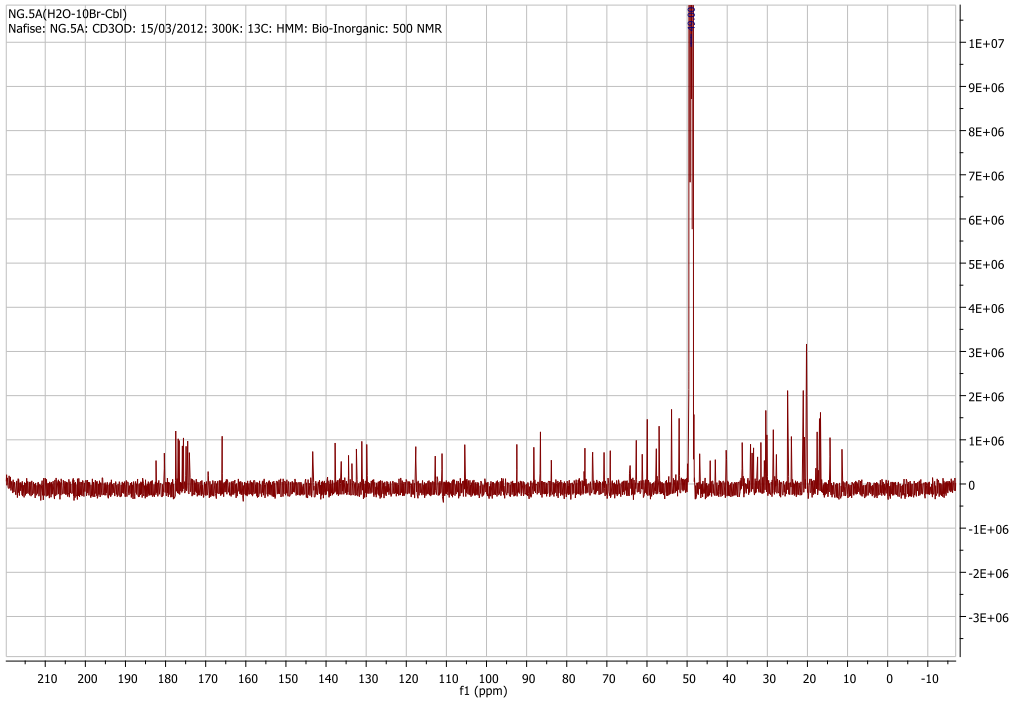


Figure 2.5.2 ^{13}C spectrum of $[H_2O\text{-}(10\text{-}Br)Cbl]^+$.

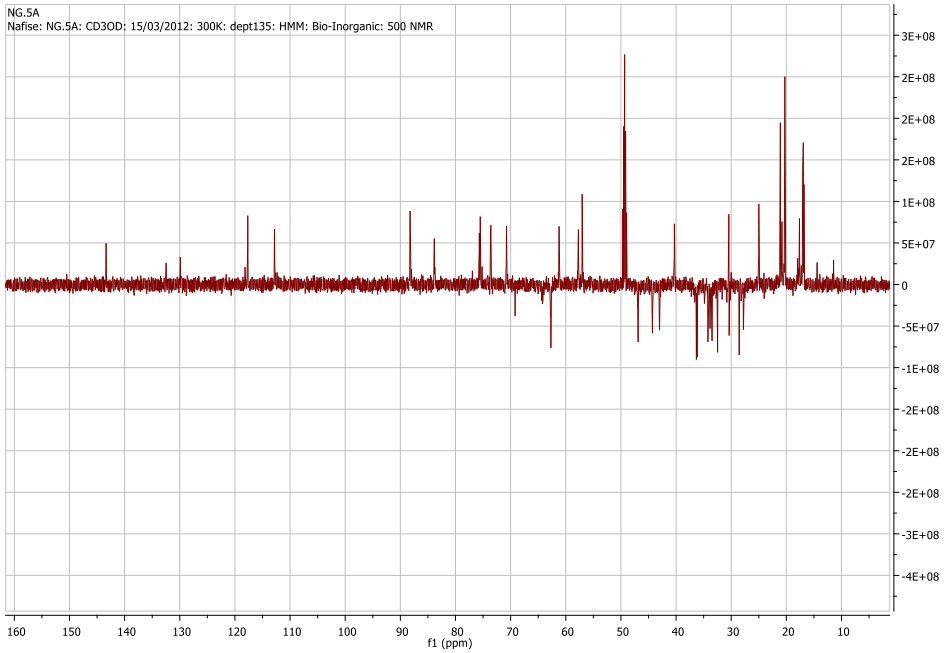


Figure 2.5.3 Dept 135 spectrum of $[H_2O\text{-}(10\text{-}Br)Cbl]^+$.

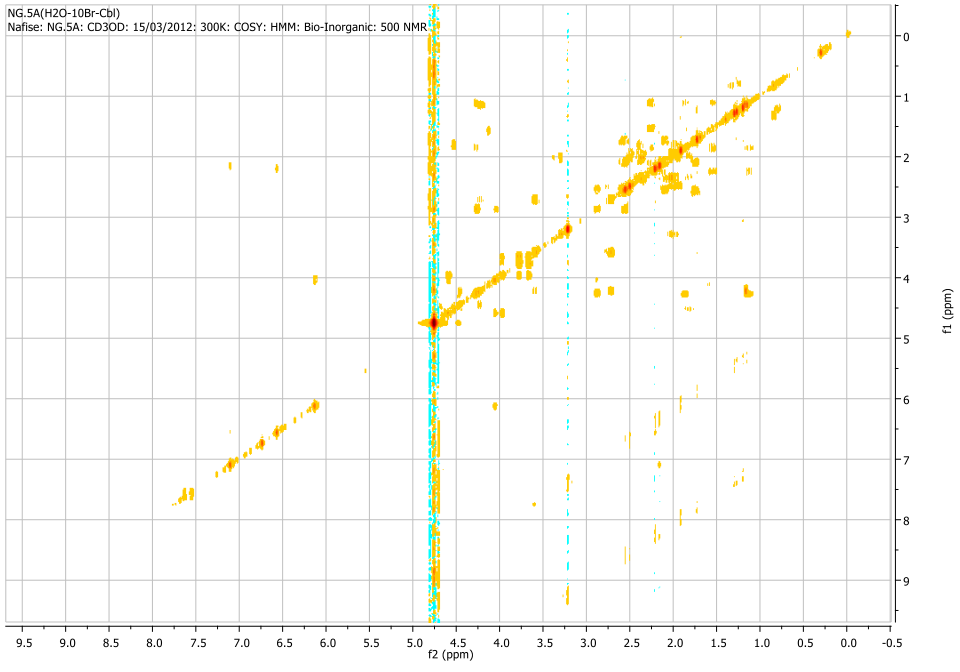


Figure 2.5.4 COSY spectrum of $[H_2O\text{-}(10\text{-}Br)Cbl]^+$.

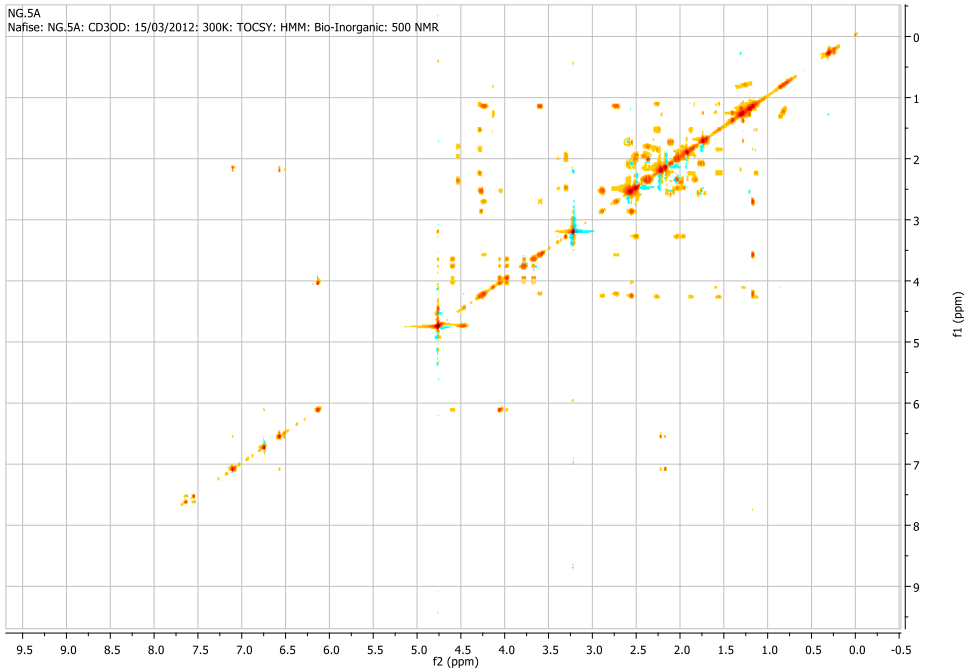


Figure 2.5.5 TOCSY spectrum of $[H_2O\text{-}(10\text{-}Br)Cbl]^+$.

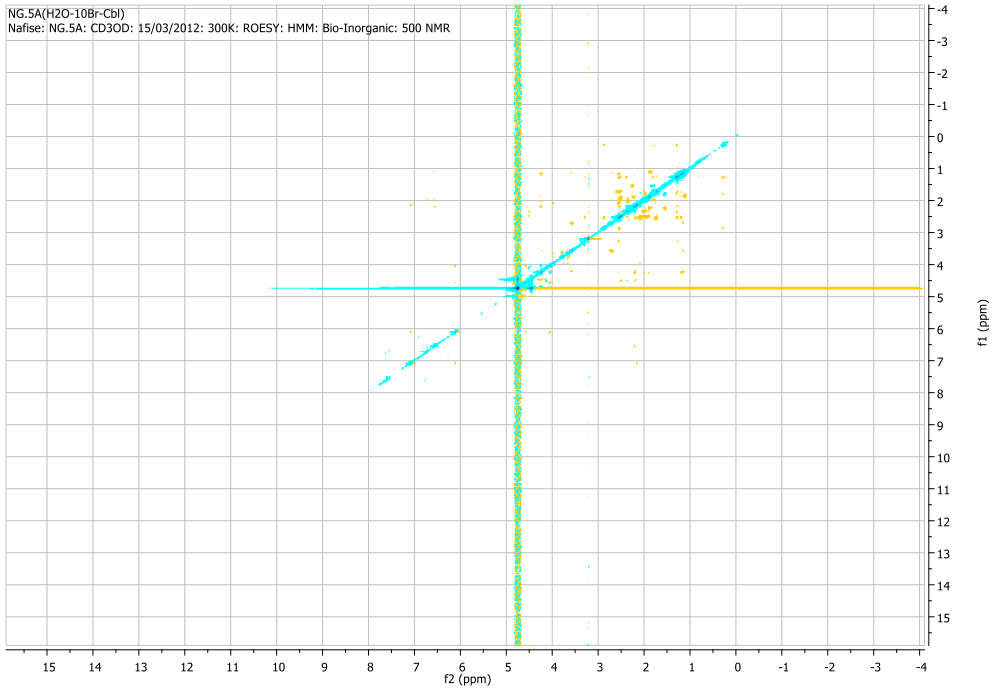


Figure 2.5.6 ROSEY spectrum of $[H_2O\text{-}(10\text{-}Br)Cbl]^+$.

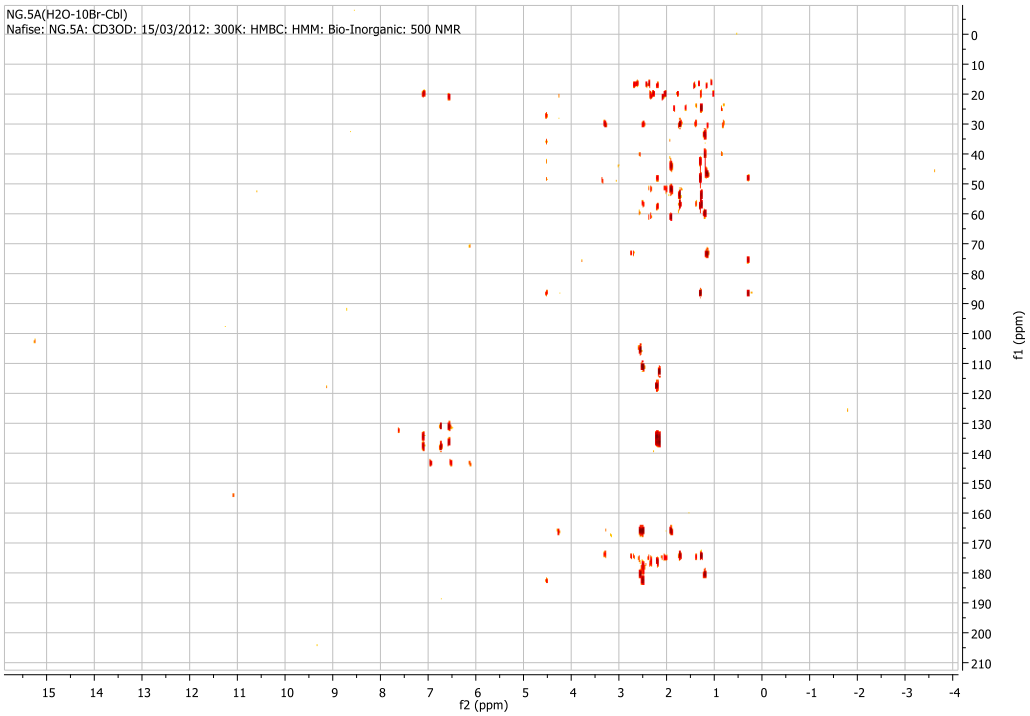


Figure 2.5.7 HMBC spectrum of $[H_2O\text{-}(10\text{-}Br)Cbl]^+$.

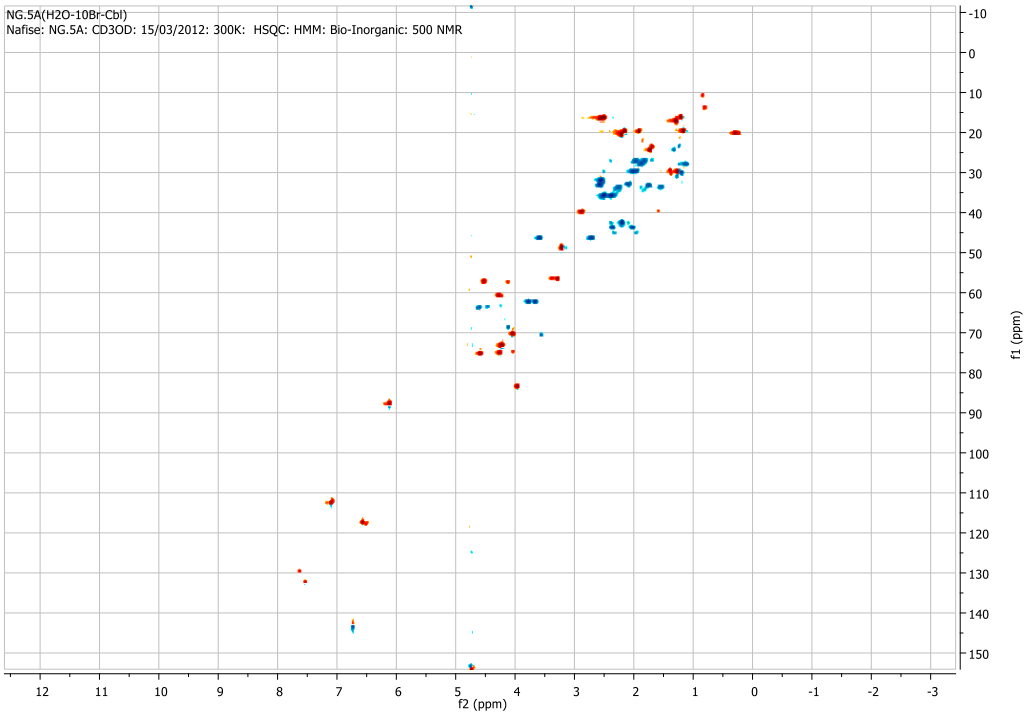


Figure 2.5.8 HSQC spectrum of $[H_2O\text{-}(10\text{-}Br)Cbl]^+$.

Table 2.5.1 Assignment of the ^{1}H resonances of $[H_2OCbl]^+$ and $[H_2O\text{-}(10\text{-}Br)Cbl]^+$ in CD_3OD, referenced to TMS.

H on atom	$[H_2OCbl]^+$ ^{1}H /ppm	$[H_2O\text{-}(10\text{-}Br)Cbl]^+$ ^{1}H /ppm	H on atom	$[H_2OCbl]^+$ ^{1}H /ppm	$[H_2O\text{-}(10\text{-}Br)Cbl]^+$ ^{1}H /ppm
C20	0.39	0.30	C53	2.54 [b]	2.56
C46	1.13	1.28	C60	2.54 [b]	2.55
C36	1.85	1.91	Pr1	2.70, 3.59	2.73, 3.60
Pr3	1.17	1.16	C18	2.92	2.88
C54	1.20	1.21	C13	3.28	3.29
C42	1.61 [a]	1.56, 2.27	C8	3.36	4.27
C25	1.34	1.30	R5	3.66, 3.80	3.66, 3.78
C55	1.73, 2.63	1.75, 2.59	R4	3.95	3.97
C41	1.06, 1.95	1.70, 1.98	R2	4.03	4.05
C48	1.78, 1.97	1.96, 2.03	Pr2	4.22	4.24
C47	1.40	1.73	C19	4.33	4.26
C30	1.86, 1.98	1.82, 1.99	C3	4.44	4.52
C37	1.99, 2.01	2.03, 2.36	R3	4.55	4.59
B11	2.15	2.16	C10	6.02	–
C56	2.11, 2.56	2.11, 2.56	R1	6.09	6.12
C26	2.15, 2.20	2.20, 2.36	B4	6.55	6.56
B10	2.20	2.21	B2	6.71	6.73
C31	2.36 [a]	2.38 [a]	B7	7.07	7.09
C35	2.48	2.50 [b]	f_H	7.75	7.75
C49	2.46	2.50 [b]			

[a] Only one resonance unambiguously observed. [b] The ^{1}H resonances of the C35 and C49 protons overlap.

Table 2.5.2 Assignment of the ^{13}C resonances of $[H_2OCbl]^+$ and $[H_2O\text{-}(10\text{-}Br)Cbl]^+$ in CD_3OD.

Atom	**$[H_2OCbl]^+$ (in CD_3OD, this work)** ^{13}C /ppm	**$[H_2OCCbl]^+$ (in D_2O[6])** ^{13}C /ppm	**$[H_2O\text{-}(10\text{-}Br)Cbl]^+$ (in CD_3OD, this work)** ^{13}C /ppm	**$[H_2O\text{-}(10\text{-}Cl)Cbl]^+$ (in 10% D_2O/90% H_2O[7])** ^{13}C /ppm
C53	16.23	18.3	17.00	18.13
C35	16.56	18.2	16.88	18.83
C54	17.00	19.5	16.75	19.03
C25	17.58	20.6	17.58	20.30
B11	20.16	22.1	20.21	21.72
C36	20.16	24.0	20.22	23.86
Pr3	20.16	22.0	20.21	21.72
C47	20.45	22.5	24.96	24.63
B10	20.88	22.8	21.04	22.54
C20	20.93	22.7	20.76	22.23
C30	27.68	29.3	27.74	29.09
C48	29.71	30.9	30.12	31.25
C41	27.38	29.3	28.51	29.85
C46	32.51	35.1	30.36	32.13
C42	32.87	34.3	34.18	33.99
C60	32.51	34.3	32.42	33.99
C55	33.62	35.5	33.80	35.14
C56	33.26	35.8	33.43	35.37
C31	36.33	37.8	36.26	38.18
C49	35.45	37.6	36.12	37.52
C18	40.16	42.5	40.26	42.27
C26	43.03	46.3	42.98	45.88
C37	44.60	48.4	44.25	48.15
Pr1	46.82	48.3	46.85	47.90
C2	48.49	50.6	48.30	49.96
C12	49.3 *a*	51.1	53.88	53.36
C7	52.80	53.8	51.99	54.20
C13	55.15	56.7	56.99	57.92
C3	57.86	60.0	57.68	59.41
C8	58.42	60.2	61.21	59.98
C17	60.04	62.0	59.93	61.39

Atom	$[H_2OCbl]^+$ (in CD_3OD, this work) ^{13}C /ppm	$[H_2OCCbl]^+$ (in D_2O[6]) ^{13}C /ppm	$[H_2O$-(10-Br)$Cbl]^+$ (in CD_3OD, this work) ^{13}C /ppm	$[H_2O$-(10-Cl)$Cbl]^+$ (in 10% D_2O/90% H_2O[7]) ^{13}C /ppm
R 5	62.58	63.3	62.68	62.92
R 2	70.56	71.6	70.70	71.32
Pr2	73.59	75.7	73.56	75.51
R 3	75.14	75.8	75.63	75.56
C19	75.43	78.0	75.47	77.33
R 4	83.78	85.1	83.83	84.80
C1	86.60	87.9	86.57	87.58
R 1	88.12	90.3	88.12	89.91
C10	94.91	97.7	105.42	106.84
C15	104.33	107.1	105.41	107.75
C5	109.09	110.8	111.11	112.15
B7	112.62	114.8	112.79	114.42
B4	117.69	118.4	117.63	118.35
B6	135.91	138.8	134.40	138.44
B9	135.90	139.0	137.74	138.76
B5	130.97	136.7	136.21	136.26
B8	137.74	132.1	137.75	131.94
B2	143.64	144.4	143.33	143.95
C6	165.50	167.1	165.89	166.25
C14	166.19	168.8	165.92	168.18
C38	*b*	178.5	174.88	177.27
C43	*b*	179.8	*a*	179.55
C11	177.75	181.8	174.00	177.75
C27	*b*	178.8	174.89	178.51
C32	*b*	180.6	177.49	180.27
C57	*b*	177.5	177.40	177.08
C16	180.73	184.1	180.31	182.51
C61	*b*	178.5	180.30	178.18
C9	175.13	177.5	180.32	176.74
C50	*b*	180.9	182.36	180.53
C4	182.28	184.3	182.37	183.27

a C12 was observed , under the MeOD peak (~49.3). *b* Cannot be reliably assigned, all fall in a narrow range of between 174 to 178 ppm.

Hereunder follows a brief description of the assignment procedure for $[H_2O\text{-}(10\text{-}Br)Cbl]^+$. A similar procedure was followed for the assignment of the spectrum of $[H_2OCbl]^+$.

The aromatic region of the ^1H NMR spectrum (6 – 7.8 ppm vs. TMS), showed four significant signals which were assigned to R1, B2, B4 and B7 protons at 6.12, 6.73, 6.56 and 7.09 ppm, respectively. Since the 6.12 ppm ^1H signal is a doublet it can be assigned to R1; R2 (4.05 ppm) could then be assigned from the COSY spectrum. The resonance at 4.05 ppm shows strong coupling to the resonances at 6.12 and 4.59 ppm in the COSY spectrum; hence the resonance at 4.59 ppm is due to the R3 proton. This resonance is strongly coupled to that at 3.97 ppm (R4), and this in turn is coupled to the resonances at 3.66 and 3.78 ppm, which must be due to the diastereotopic protons of R5. The TOCSY spectrum shows the B7 protons (7.09 ppm) coupling to those on B11 at 2.16 ppm, and those on B4 (6.56 ppm) coupling to those on B10 at 2.21 ppm. The HMBC spectrum shows the coupling of the B7 protons (7.09 ppm) to carbon B6 and B8 at 134.40 and 137.75, respectively and also the coupling of B4 (6.56 ppm) to B5 and B9 at 136.21 and 137.74 ppm, respectively.

The most upfield ^1H signal at 0.30 ppm is due to H20.[1-5] The HMBC spectrum shows H20 coupling to C1, C2 and C19 at 86.57, 48.30 and 75.47 ppm, respectively. The ROSEY spectrum also shows the through-space coupling between H20 (0.30 ppm) and H25 at 1.30 ppm. The TOCSY spectrum shows H25 (1.30 ppm) coupling to the diastereotopic protons H26 at 2.20 and 2.36 ppm. The ROSEY spectrum shows the through space coupling between H26 and H3 (4.52 ppm). The TOCSY spectrum shows a range of couplings between H3, H30 and H31 at 4.52, 1.82 and 2.38 ppm, respectively. The HMBC spectrum shows a coupling between H3 and C4 at 4.52 and 182.37 ppm, respectively.

The COSY spectrum shows couplings between H19, H18 and H60 at 4.26, 2.88 and 2.55 ppm, respectively. The TOCSY spectrum shows long range coupling between H18, H55 and H60 at 2.88, 2.59 and 2.55 ppm, respectively. The COSY spectrum shows coupling between H55 and H56 at 2.59 and 2.11 ppm, respectively. The HMBC spectrum shows coupling between H55 (2.59 ppm) and C17 (59.93 ppm), and between C17 and H54 (1.21 ppm).

To start assigning the eastern half of the molecule, the ROSEY spectrum was used to assign H35; it shows a through-space interaction with H3 (4.52 ppm) at 2.50 ppm. The H37, H36 and H8

signals were assigned by finding the through-space interactions between them and H35 (2.50 ppm). The diastereotopic H37 protons have signals at 2.03 and 2.36 ppm; H36 resonates at 1.91 ppm, and H8 at 4.27 ppm. The HMBC spectrum shows coupling between H35 (2.50 pm) and C5 (111.09 ppm) and C6 (165.80 ppm). The COSY spectrum shows that the H8 resonance at 4.27 ppm couples to the signals at 1.70 and 1.78 ppm which correspond to the diastereotopic protons H41; H41 shows a strong coupling to the resonance at 2.27 ppm which is due to H42.

The ^{13}C assignment of C10 is usually made using an HSQC spectrum; this was not applicable in this case as there is no H on C10. The assignment of the resonance (at 105.42 ppm) was therefore made by default as this was the only unassigned carbon signal in the general region where C10 occurs in cobalamins.

The HMBC spectrum of H53 (2.56 ppm) shows long range coupling to three carbon signals at 105.41, 165.92 and 180.31 ppm which correspond to C15, C14 and C16, respectively. The ROSEY spectrum shows through-space coupling between B10 (2.21 ppm) and H49 (2.50 ppm). The CSOSY spectrum shows coupling between H49 (2.50 ppm) and diastereotopic H48 (1.96 and 2.03 ppm). H48 couples with H13 (3.29 ppm). The ROSEY spectrum shows through-space coupling between H13 and H46 (1.28 pm); H46 couples with H47 (1.73 ppm).

A doublet peak at 2.73 ppm was assigned to the Pr1 protons. The COSY spectrum shows that the H(Pr1) resonance at 2.73 ppm couples to the signals at 4.24 and 7.75 ppm which corresponds to H(Pr2) and f_H, respectively. H(Pr2) shows a coupling to the signal at 1.16 ppm which is due to H(Pr3).

The HMBC spectrum of H8 (4.27 ppm) shows long range coupling to two carbon signals at 51.99 and 180.32 ppm which correspond to C7 and C9, respectively. The amide carbonyl signals of C38, C32, C27, C61, C57, C50 were assigned by finding their coupling with H37, H31, H26, H60, H56 and H49, respectively in the HMBC spectrum.

2.6 NMR Spectra and Assignments for [DC-(10-NO_2)Cbs] in $CDCl_3$

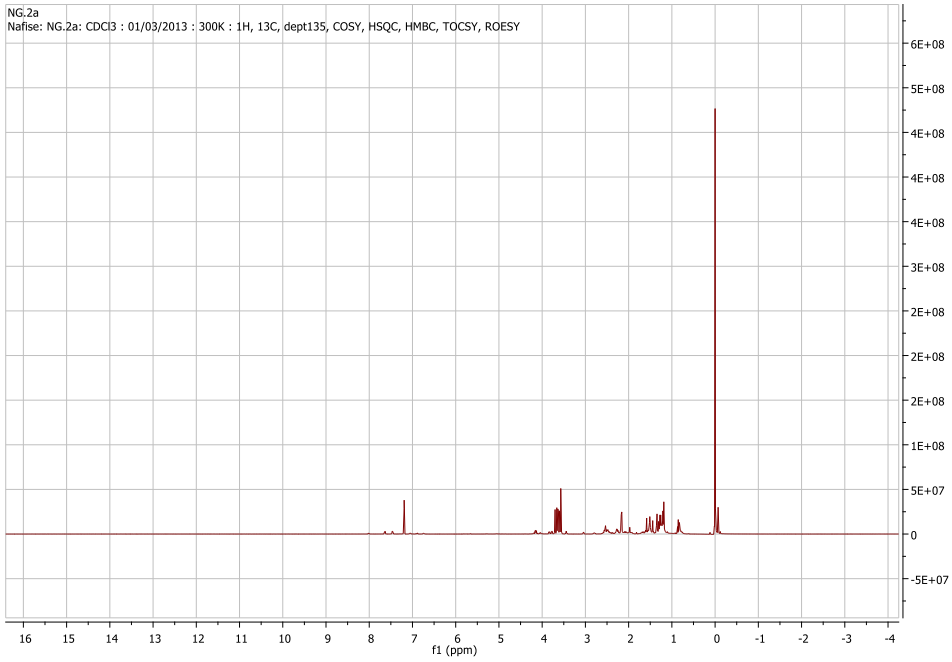


Figure 2.6.1 ^{1}H spectrum of [DC-(10-NO_2)Cbs].

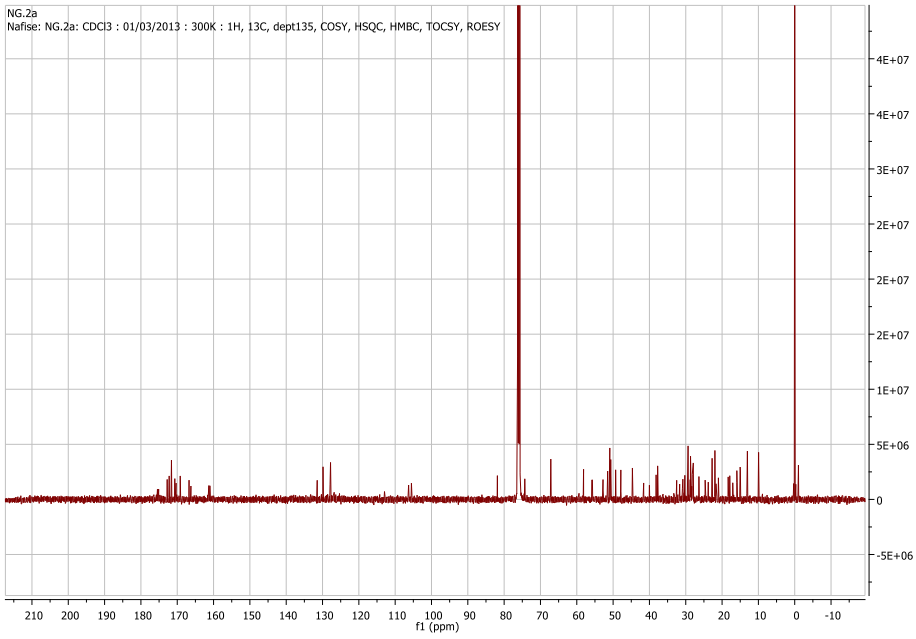


Figure 2.6.2 ^{13}C Spectrum of [DC-(10-NO_2)Cbs].

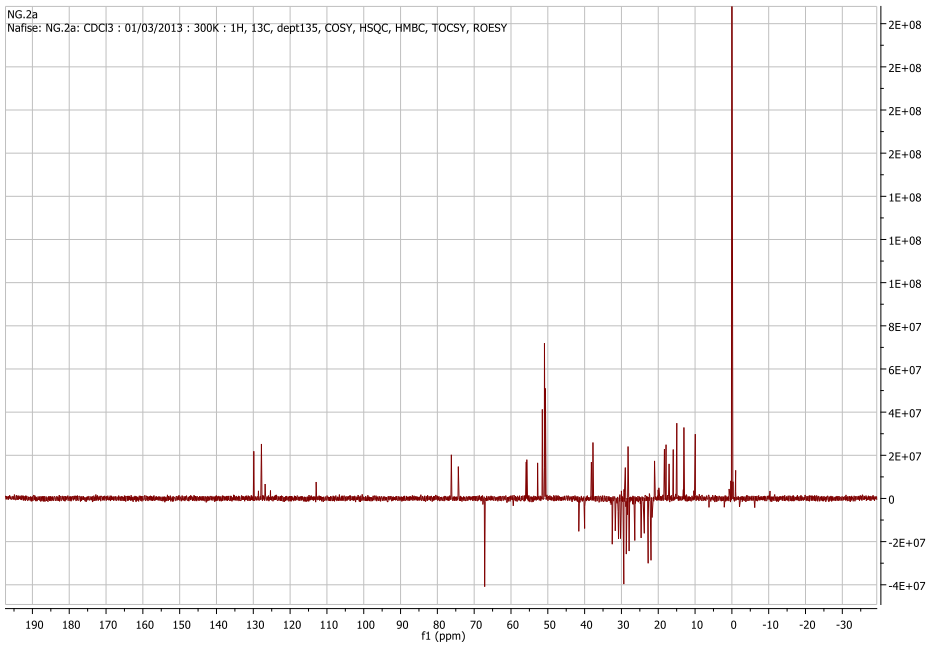


Figure 2.6.3 Dept 135 spectrum of [DC-(10-NO_2)Cbs].

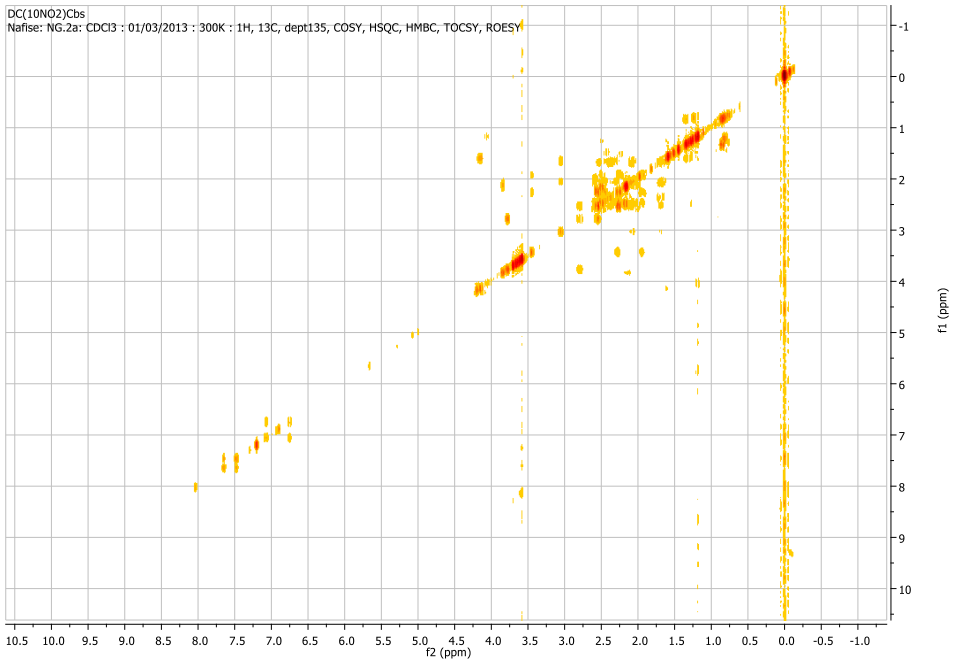


Figure 2.6.4 COSY spectrum of [DC-(10-NO_2)Cbs].

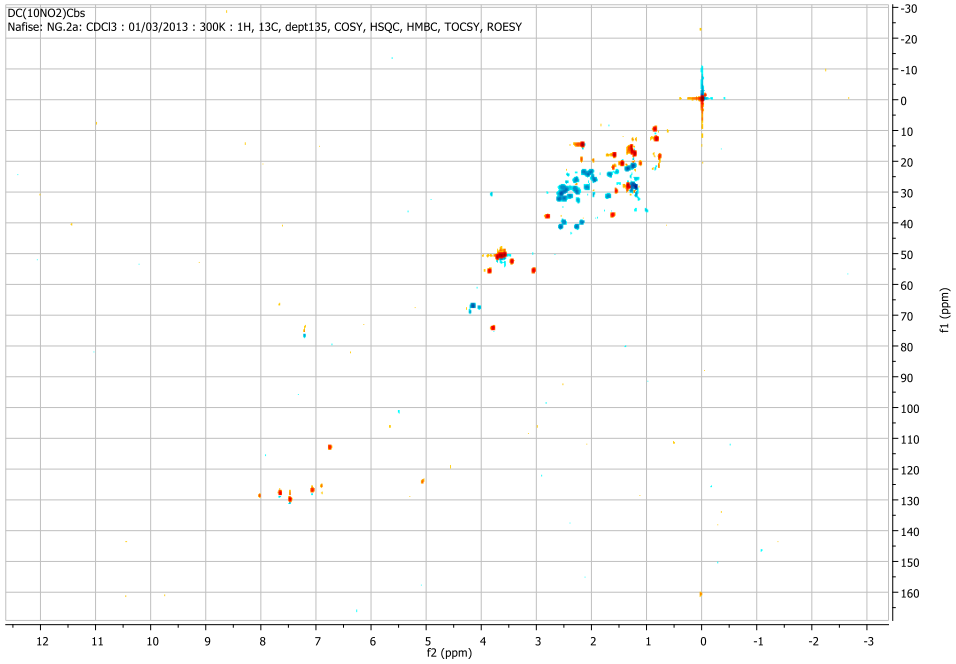


Figure 2.6.5 HSQC spectrum of [DC-(10-NO_2)Cbs].

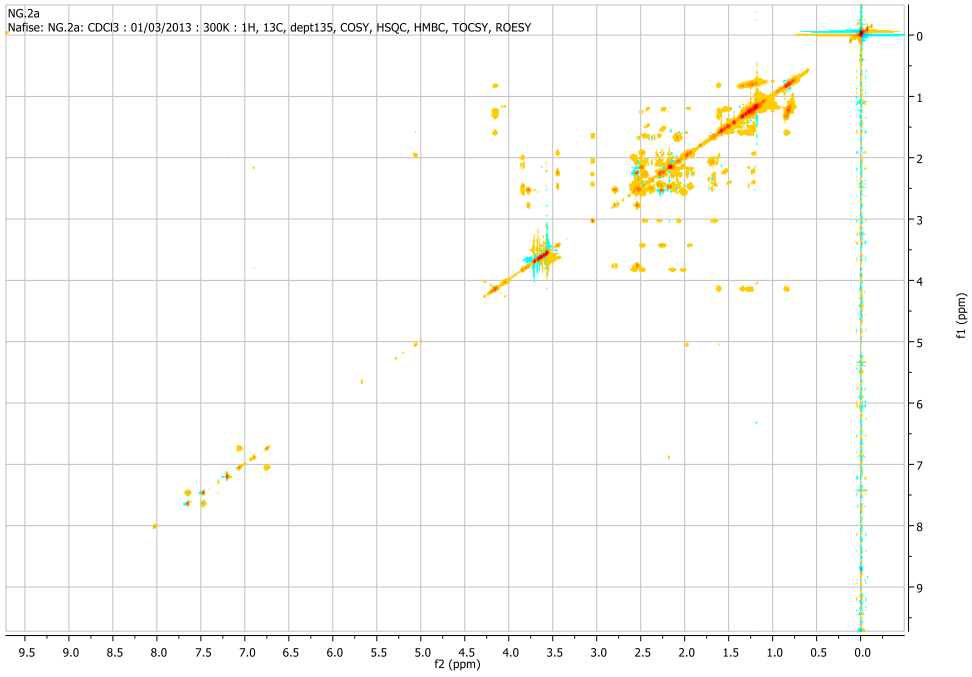


Figure 2.6.6 TOCSY spectrum of [DC-(10-NO_2)Cbs].

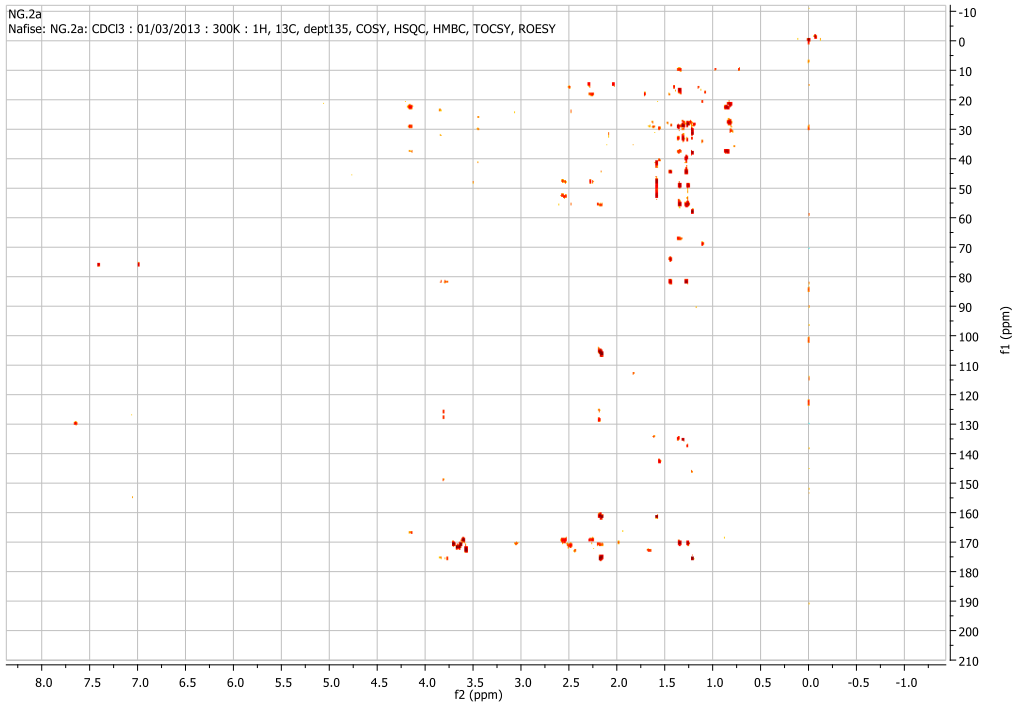


Figure 2.6.7 HMBC spectrum of [DC-(10-NO_2)Cbs].

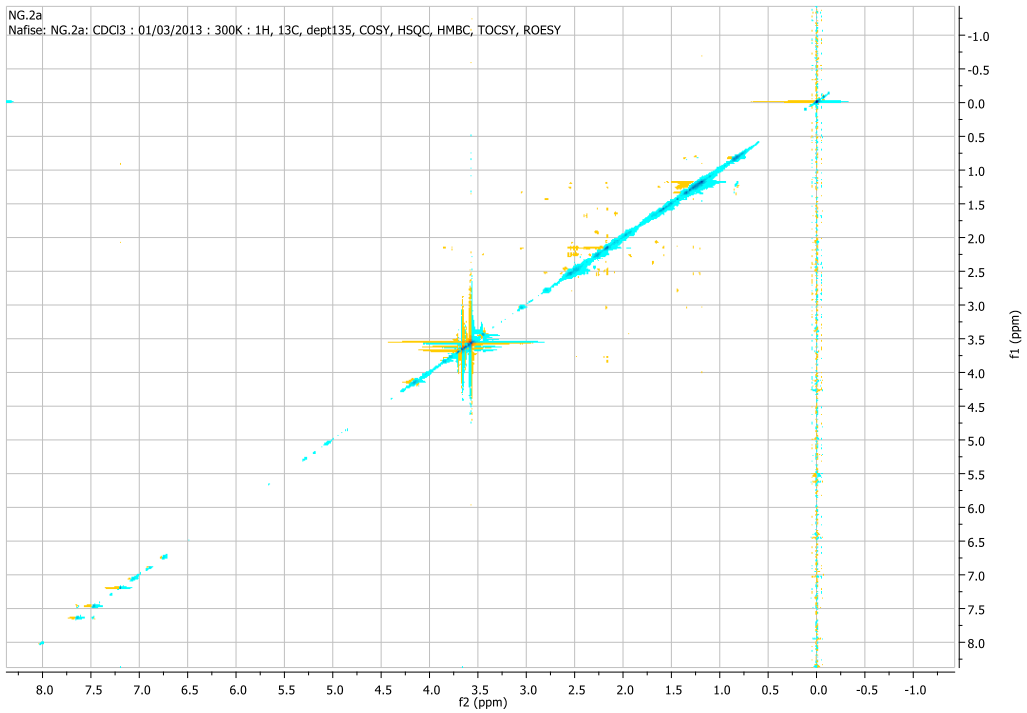


Figure 2.6.8 ROSEY spectrum of [DC-(10-NO_2)Cbs].

Table 2.6.1 Assignment of the ^{1}H resonances of [DCCbs] and [DC-(10-NO_2)Cbs] in $CDCl_3$, referenced to TMS.

H on atom	[DCCbs] [1] ^{1}H /ppm	[DC-(10-NO_2)Cbs] ^{1}H /ppm	H on atom	[DCCbs][1] ^{1}H /ppm	[DC-(10-NO_2)Cbs] ^{1}H /ppm
C20	1.52	1.45	C53	2.24	2.17
C46	1.21	1.34	C60	2.62	2.54
C36	1.57	1.58	C18	2.83	2.8
C54	1.27	1.21	C13	3.03	3.04
C42	2.49, 2.38	2.26, 2.5	C8	3.45	3.44
C25	1.52	1.28	C19	3.80	3.78
C55	1.74, 2.44	1.7, 2.38	C3	3.82	3.84
C41	1.75, 2.13	1.95, 2.29	C10	5.59	–
C48	2.08, 1.83	1.68, 2.08			
C47	1.38	1.26			
C30	2.22, 2.06	2.02, 2.14			
C37	2.71, 2.41	2.27, 2.56			
C56	2.20, 2.56	2.09, 2.51			
C26	2.28, 2.60	2.18, 2.49			
C31	2.53, 2.64	2.49, 2.57			
C35	2.19	2.16			
C49	2.28, 2.54	2.3, 2.45			

Table 2.6.2 Assignment of the ^{13}C resonances of [DCCbs] and [DC-(10-NO_2)Cbs] in $CDCl_3$.

Atom	**[DCCbs][2] (in $CDCl_3$,) ^{13}C /ppm**	**[DCCbs][3] (in $CDCl_3$) ^{13}C /ppm**	**[DC-(10-NO_2)Cbs] (in $CDCl_3$, this work) ^{13}C /ppm**
C53	15.27	15.28	14.91 or 15.02 [b]
C35	15.88	15.90	14.97 or 15.02 [b]
C54	18.48	18.48	17.91
C25	16.96	17.97	15.93
C36	19.28	19.26	18.32
C47	19.86	19.84	17.08
C20	22.08	22.07	21.04
C30	25.04	24.99	23.80
C48	25.77	25.72	24.66
C41	26.50	26.49	26.38
C46	31.14	31.15	28.21
C42	31.24	31.15	30.26
C60	31.83	31.82	30.80
C55	32.66	32.65	31.68
C56	29.77	29.74	28.96
C31	33.81	33.81	32.51
C49	30.84	30.81	29.37
C18	39.33	39.35	38.16
C26	41.22	41.24	40.02
C37	42.36	42.20	41.59
C2	45.76	45.76	44.69
C12	47.07	47.10	49.30
C7	48.67	48.71	47.87
C13	53.73	53.72	55.70
C3	56.68	56.73	55.86
C8	54.22	54.25	52.77
C17	58.37	58.42	58.13
C19	74.85	74.87	74.32
C1	82.59	82.64	81.86
C10	91.24	91.27	124 [c]
C15	102.20	102.30	105.54

Atom	**[DCCbs]^2 (in $CDCl_3$,) ^{13}C /ppm**	**[DCCbs]^3 (in $CDCl_3$) ^{13}C /ppm**	**[DC-(10-NO_2)Cbs] (in $CDCl_3$, this work) ^{13}C /ppm**
C5	103.61	103.74	106.30
C6	163.61	163.66	161.30
C14	163.53	163.57	161.02
C38	171.01	171.06	169.18
C43	173.49	173.57	*a*
C11	176.23	176.34	170.32
C27	171.93	172.01	*a*
C32	172.92	172.99	*a*
C57	172.7	172.99	*a*
C16	175.61	175.80	175.44
C61	171.73	171.82	*a*
C9	171.47	171.58	166.23
C50	173.85	173.91	*a*
C4	175.27	175.46	106.30

a signals could not be reliably assigned. [b] can not be differentiated from HSQC. [c] predicted chemical shift for C10.

2.7 Crystallographic Data

Table 2.7.1 Crystallographic data for bis(aqua–(10-bromo)cobalamin) hydrogen phosphate pentatriacontahydrate and azido–(10-bromo)cobalamin di(sodium azide) triacetone solvate pentahydrate.

CCDC Deposition Code	CCDC-1057492	CCDC-1057493
Empirical formula	$(C_{62}\ H_{89}\ Br\ Co\ N_{13}\ O_{15}\ P)_2$, HPO_4, $35(H_2O)$	$C_{62}\ H_{95}\ Br\ Co\ N_{16}\ O_{19}\ P$, $2(NaN_3)$, $3(C_3H_6O)$, $5(H_2O)$
Formula weight	3578.07	1932.70
Temperature	173(2) K	173(2) K
Wavelength	1.54178 Å	0.71073 Å
Crystal system	Triclinic	Orthorhombic
Space group	P_1	$P2_12_12_1$
Unit cell dimensions	a = 12.0184(4) Å α = 89.348(2)°.	a = 15.3745(4) Å
	b = 14.8684(5) Å β = 80.785(2)°.	b = 23.4023(6) Å
	c = 25.7024(8) Å γ = 85.911(2)°.	c = 25.3443(7) Å
Volume	4522.1(3) $Å^3$	9118.8(4) $Å^3$
Z	1	4
Density (calculated)	1.314 Mg m^{-3}	1.408 Mg m^{-3}
Absorption coefficient	2.981 mm^{-1}	0.739 mm^{-1}
F(000)	1895	4072
Crystal size	0.10 × 0.10 × 0.05 mm^3	0.60 × 0.07 × 0.05 mm^3
Theta range for data collection	2.98 to 49.39°	1.55 to 25.00°.
Index ranges	$-11 \le h \le 11$, $-14 \le k \le 13$, $-24 \le l \le 24$	$-15 \le h \le 18$, $-27 \le k \le 27$, $-30 \le l \le 30$
Reflections collected	36423	62372
Independent reflections	15262 [R(int) = 0.0611]	16040 [R(int) = 0.2016]

Completeness to theta	49.39º, 91.8%	26.00°, 100.0 %
Absorption correction	Semi-empirical from equivalents	Semi-empirical from equivalents
Refinement method	Full-matrix least-squares on F^2	Full-matrix least-squares on F^2
Data / restraints / parameters	15262 / 199 / 2001	16040 / 0 / 1115
Goodness-of-fit on F^2	1.113	0.938
Final R indices [$I > 2\sigma(I)$]	R_1 = 0.0928, wR_2 = 0.2395	R_1 = 0.0636, wR_2 = 0.0929
R indices (all data)	R_1 = 0.1055, wR_2 = 0.2529	R_1 = 0.1976, wR_2 = 0.1232
Absolute structure parameter	-0.016(5)	-0.010(10)
Largest diff. peak and hole	0.699 and -0.568 e.Å^{-3}	0.752 and -0.654 e Å^{-3}

Table 2.7.2 Selected bond lengths (Å) and bond angles (deg) in bis(aqua–(10-bromo)cobalamin) hydrogen phosphate pentatriacontahydrate.

Bond Lengths	
C(1A)-N(1A)	1.491(13)
C(1A)-C(20A)	1.509(15)
C(1A)-C(19A)	1.544(15)
C(1A)-C(2A)	1.566(16)
C(2A)-C(21A)	1.512(19)
C(2A)-C(3A)	1.535(17)
C(2A)-C(22A)	1.560(18)
C(3A)-C(4A)	1.448(16)
C(3A)-C(24A)	1.562(16)
C(4A)-N(1A)	1.275(13)
C(4A)-C(5A)	1.502(17)
C(5A)-C(6A)	1.363(17)
C(5A)-C(27A)	1.585(18)
C(6A)-N(2A)	1.364(15)
C(6A)-C(7A)	1.515(17)
C(7A)-C(8A)	1.53(2)
C(7A)-C(28A)	1.54(2)
C(7A)-C(29A)	1.561(17)
C(8A)-C(9A)	1.533(18)
C(8A)-C(31A)	1.581(19)
C(9A)-N(2A)	1.351(15)
C(9A)-C(10A)	1.380(17)
C(10A)-C(11A)	1.393(17)
C(10A)-Br(1A)	1.887(11)
C(11A)-N(3A)	1.372(14)
C(11A)-C(12A)	1.538(18)
C(12A)-C(34A)	1.53(2)
C(12A)-C(35A)	1.564(19)
C(12A)-C(13A)	1.573(19)
C(13A)-C(14A)	1.485(15)
C(13A)-C(36A)	1.554(19)
C(14A)-N(3A)	1.341(14)
C(14A)-C(15A)	1.392(16)
C(15A)-C(16A)	1.412(15)
C(15A)-C(39A)	1.539(16)
C(16A)-N(4A)	1.302(12)
C(16A)-C(17A)	1.535(15)
C(17A)-C(40A)	1.533(15)
C(17A)-C(18A)	1.568(16)
C(17A)-C(43A)	1.569(15)
C(18A)-C(41A)	1.518(15)
C(18A)-C(19A)	1.530(15)
C(19A)-N(4A)	1.500(13)
C(22A)-C(23A)	1.517(9)
C(23A)-O(8A)	1.236(5)
C(23A)-N(8A)	1.321(5)
C(24A)-C(25A)	1.503(17)
C(25A)-C(26A)	1.514(9)
C(26A)-O(9A)	1.240(5)
C(26A)-N(9A)	1.322(5)
C(29A)-C(30A)	1.519(9)
C(30A)-O(10A)	1.237(5)
C(30A)-N(10A)	1.320(5)
C(31A)-C(32A)	1.56(2)
C(32A)-C(33A)	1.522(9)
C(33A)-O(11A)	1.236(5)
C(33A)-N(11A)	1.318(5)
C(36A)-C(37A)	1.60(2)
C(37A)-C(38A)	1.518(9)
C(38A)-O(12A)	1.240(5)
C(38A)-N(12A)	1.318(5)
C(41A)-C(42A)	1.517(8)
C(42A)-O(13A)	1.239(5)
C(42A)-N(13A)	1.317(5)
C(43A)-C(44A)	1.517(15)
C(44A)-C(45A)	1.501(17)
C(45A)-O(14A)	1.211(15)
C(45A)-N(7A)	1.319(16)
C(46A)-N(7A)	1.440(17)
C(46A)-C(47A)	1.50(2)
C(47A)-O(3A)	1.414(17)
C(47A)-C(48A)	1.58(2)
C(49A)-O(4A)	1.409(14)
C(49A)-C(50A)	1.485(16)

C(49A)-C(52A)	1.520(18)	C(4B)-C(5B)	1.410(19)
C(50A)-O(5A)	1.410(13)	C(5B)-C(6B)	1.368(19)
C(50A)-C(51A)	1.532(17)	C(5B)-C(27B)	1.51(2)
C(51A)-O(6A)	1.391(14)	C(6B)-N(2B)	1.427(17)
C(51A)-N(6A)	1.463(14)	C(6B)-C(7B)	1.513(19)
C(52A)-C(53A)	1.47(2)	C(7B)-C(8B)	1.45(2)
C(52A)-O(6A)	1.475(17)	C(7B)-C(29B)	1.541(18)
C(53A)-O(7A)	1.47(3)	C(7B)-C(28B)	1.62(2)
C(54A)-N(5A)	1.330(13)	C(8B)-C(9B)	1.509(19)
C(54A)-N(6A)	1.369(13)	C(8B)-C(31B)	1.569(18)
C(55A)-N(5A)	1.373(13)	C(9B)-N(2B)	1.287(16)
C(55A)-C(60A)	1.387(15)	C(9B)-C(10B)	1.35(2)
C(55A)-C(56A)	1.389(15)	C(10B)-C(11B)	1.45(2)
C(56A)-C(57A)	1.392(17)	C(10B)-Br(1B)	1.917(12)
C(57A)-C(58A)	1.41(2)	C(11B)-N(3B)	1.342(15)
C(57A)-C(61A)	1.50(2)	C(11B)-C(12B)	1.544(19)
C(58A)-C(59A)	1.32(2)	C(12B)-C(13B)	1.452(19)
C(58A)-C(62A)	1.62(2)	C(12B)-C(34B)	1.55(2)
C(59A)-C(60A)	1.336(16)	C(12B)-C(35B)	1.65(2)
C(60A)-N(6A)	1.414(14)	C(13B)-C(36B)	1.49(2)
Co(1A)-N(1A)	1.894(9)	C(13B)-C(14B)	1.515(18)
Co(1A)-N(4A)	1.902(8)	C(14B)-C(15B)	1.353(18)
Co(1A)-N(3A)	1.912(9)	C(14B)-N(3B)	1.425(15)
Co(1A)-N(2A)	1.922(9)	C(15B)-C(16B)	1.455(19)
Co(1A)-O(15A)	1.933(7)	C(15B)-C(39B)	1.499(19)
Co(1A)-N(5A)	1.975(8)	C(16B)-N(4B)	1.276(14)
O(1A)-P(1A)	1.507(10)	C(16B)-C(17B)	1.531(16)
O(2A)-P(1A)	1.481(11)	C(17B)-C(18B)	1.493(17)
O(3A)-P(1A)	1.571(10)	C(17B)-C(43B)	1.530(16)
O(4A)-P(1A)	1.607(8)	C(17B)-C(40B)	1.541(15)
C(1B)-C(20B)	1.519(17)	C(18B)-C(41B)	1.486(17)
C(1B)-N(1B)	1.524(15)	C(18B)-C(19B)	1.548(16)
C(1B)-C(19B)	1.538(17)	C(19B)-N(4B)	1.470(15)
C(1B)-C(2B)	1.564(18)	C(22B)-C(23B)	1.536(14)
C(2B)-C(22B)	1.528(19)	C(23B)-O(8B)	1.236(5)
C(2B)-C(21B)	1.55(2)	C(23B)-N(8B)	1.321(5)
C(2B)-C(3B)	1.558(19)	C(24B)-C(25B)	1.53(3)
C(3B)-C(4B)	1.508(19)	C(25B)-C(26B)	1.524(9)
C(3B)-C(24B)	1.54(2)	C(26B)-O(9B)	1.233(5)
C(4B)-N(1B)	1.280(15)	C(26B)-N(9B)	1.319(5)

C(29B)-C(30B)	1.503(9)	C(58B)-C(59B)	1.34(2)
C(30B)-O(10B)	1.244(5)	C(58B)-C(62B)	1.50(2)
C(30B)-N(10B)	1.322(5)	C(59B)-C(60B)	1.373(18)
C(31B)-C(32B)	1.51(2)	C(60B)-N(6B)	1.385(15)
C(32B)-C(33B)	1.517(9)	Co(1B)-N(3B)	1.905(10)
C(33B)-O(11B)	1.241(5)	Co(1B)-N(4B)	1.908(9)
C(33B)-N(11B)	1.318(5)	Co(1B)-N(1B)	1.916(10)
C(36B)-C(37B)	1.53(3)	Co(1B)-O(15B)	1.943(8)
C(37B)-C(38B)	1.522(10)	Co(1B)-N(2B)	1.944(9)
C(38B)-O(12B)	1.238(5)	Co(1B)-N(5B)	1.962(9)
C(38B)-N(12B)	1.319(5)	O(1B)-P(1B)	1.535(17)
C(41B)-C(42B)	1.524(9)	O(2B)-P(1B)	1.40(2)
C(42B)-O(13B)	1.236(5)	O(3B)-P(1B)	1.586(10)
C(42B)-N(13B)	1.320(5)	O(4B)-P(1B)	1.582(9)
C(43B)-C(44B)	1.501(16)	O(1P)-P(1P)	1.63(2)
C(44B)-C(45B)	1.486(19)	O(2P)-P(1P)	1.50(2)
C(45B)-O(14B)	1.278(17)	O(3P)-P(1P)	1.55(2)
C(45B)-N(7B)	1.309(18)	O(4P)-P(1P)	1.438(19)
C(46B)-C(47B)	1.45(2)		
C(46B)-N(7B)	1.463(18)	**Bond Angles**	
C(47B)-O(3B)	1.397(17)		
C(47B)-C(48B)	1.57(2)	N(1A)-C(1A)-C(20A)	110.5(8)
C(49B)-O(4B)	1.449(14)	N(1A)-C(1A)-C(19A)	101.8(8)
C(49B)-C(52B)	1.498(18)	C(20A)-C(1A)-C(19A)	109.9(9)
C(49B)-C(50B)	1.511(18)	N(1A)-C(1A)-C(2A)	101.3(8)
C(50B)-O(5B)	1.425(14)	C(20A)-C(1A)-C(2A)	114.5(8)
C(50B)-C(51B)	1.481(17)	C(19A)-C(1A)-C(2A)	117.6(8)
C(51B)-O(6B)	1.383(15)	C(21A)-C(2A)-C(3A)	114.2(10)
C(51B)-N(6B)	1.506(15)	C(21A)-C(2A)-C(22A)	110.1(11)
C(52B)-O(6B)	1.465(14)	C(3A)-C(2A)-C(22A)	104.3(9)
C(52B)-C(53B)	1.52(2)	C(21A)-C(2A)-C(1A)	114.3(10)
C(53B)-O(7B)	1.32(2)	C(3A)-C(2A)-C(1A)	102.9(9)
C(54B)-N(6B)	1.293(13)	C(22A)-C(2A)-C(1A)	110.5(8)
C(54B)-N(5B)	1.360(13)	C(4A)-C(3A)-C(2A)	101.4(9)
C(55B)-C(60B)	1.371(15)	C(4A)-C(3A)-C(24A)	109.4(10)
C(55B)-C(56B)	1.392(18)	C(2A)-C(3A)-C(24A)	116.6(9)
C(55B)-N(5B)	1.429(14)	N(1A)-C(4A)-C(3A)	114.7(10)
C(56B)-C(57B)	1.388(19)	N(1A)-C(4A)-C(5A)	120.3(11)
C(57B)-C(58B)	1.36(2)	C(3A)-C(4A)-C(5A)	125.0(11)
C(57B)-C(61B)	1.54(2)	C(6A)-C(5A)-C(4A)	124.6(10)

C(6A)-C(5A)-C(27A)	123.6(11)	C(15A)-C(16A)-C(17A)	129.0(10)
C(4A)-C(5A)-C(27A)	111.8(12)	C(40A)-C(17A)-C(16A)	110.2(8)
C(5A)-C(6A)-N(2A)	122.6(10)	C(40A)-C(17A)-C(18A)	112.3(9)
C(5A)-C(6A)-C(7A)	127.2(11)	C(16A)-C(17A)-C(18A)	101.1(7)
N(2A)-C(6A)-C(7A)	110.2(11)	C(40A)-C(17A)-C(43A)	108.2(8)
C(6A)-C(7A)-C(8A)	100.9(9)	C(16A)-C(17A)-C(43A)	115.3(8)
C(6A)-C(7A)-C(28A)	118.3(13)	C(18A)-C(17A)-C(43A)	109.7(8)
C(8A)-C(7A)-C(28A)	112.4(10)	C(41A)-C(18A)-C(19A)	113.0(8)
C(6A)-C(7A)-C(29A)	108.8(9)	C(41A)-C(18A)-C(17A)	116.3(9)
C(8A)-C(7A)-C(29A)	109.4(11)	C(19A)-C(18A)-C(17A)	101.5(8)
C(28A)-C(7A)-C(29A)	106.8(10)	N(4A)-C(19A)-C(18A)	99.9(8)
C(7A)-C(8A)-C(9A)	101.9(9)	N(4A)-C(19A)-C(1A)	107.4(8)
C(7A)-C(8A)-C(31A)	114.0(14)	C(18A)-C(19A)-C(1A)	122.0(8)
C(9A)-C(8A)-C(31A)	106.0(9)	C(23A)-C(22A)-C(2A)	117.2(12)
N(2A)-C(9A)-C(10A)	126.6(11)	O(8A)-C(23A)-N(8A)	122.0(7)
N(2A)-C(9A)-C(8A)	108.0(13)	O(8A)-C(23A)-C(22A)	121.3(6)
C(10A)-C(9A)-C(8A)	125.4(12)	N(8A)-C(23A)-C(22A)	116.6(5)
C(9A)-C(10A)-C(11A)	125.3(10)	C(25A)-C(24A)-C(3A)	115.1(10)
C(9A)-C(10A)-Br(1A)	113.3(9)	C(24A)-C(25A)-C(26A)	111.9(8)
C(11A)-C(10A)-Br(1A)	121.0(10)	O(9A)-C(26A)-N(9A)	122.0(7)
N(3A)-C(11A)-C(10A)	122.7(10)	O(9A)-C(26A)-C(25A)	120.9(5)
N(3A)-C(11A)-C(12A)	110.4(10)	N(9A)-C(26A)-C(25A)	117.1(5)
C(10A)-C(11A)-C(12A)	126.2(11)	C(30A)-C(29A)-C(7A)	118.1(10)
C(34A)-C(12A)-C(11A)	120.0(13)	O(10A)-C(30A)-N(10A)	122.4(7)
C(34A)-C(12A)-C(35A)	106.4(12)	O(10A)-C(30A)-C(29A)	120.8(5)
C(11A)-C(12A)-C(35A)	103.2(11)	N(10A)-C(30A)-C(29A)	116.8(5)
C(34A)-C(12A)-C(13A)	115.6(12)	C(32A)-C(31A)-C(8A)	116.6(11)
C(11A)-C(12A)-C(13A)	101.7(9)	C(33A)-C(32A)-C(31A)	108.7(14)
C(35A)-C(12A)-C(13A)	109.0(11)	O(11A)-C(33A)-N(11A)	122.6(8)
C(14A)-C(13A)-C(36A)	107.7(10)	O(11A)-C(33A)-C(32A)	120.4(6)
C(14A)-C(13A)-C(12A)	100.8(10)	N(11A)-C(33A)-C(32A)	117.0(5)
C(36A)-C(13A)-C(12A)	112.9(10)	C(13A)-C(36A)-C(37A)	112.5(12)
N(3A)-C(14A)-C(15A)	126.0(9)	C(38A)-C(37A)-C(36A)	110.1(12)
N(3A)-C(14A)-C(13A)	115.3(10)	O(12A)-C(38A)-N(12A)	122.3(8)
C(15A)-C(14A)-C(13A)	118.7(10)	O(12A)-C(38A)-C(37A)	120.7(6)
C(14A)-C(15A)-C(16A)	123.5(10)	N(12A)-C(38A)-C(37A)	117.0(5)
C(14A)-C(15A)-C(39A)	118.8(11)	C(42A)-C(41A)-C(18A)	111.9(8)
C(16A)-C(15A)-C(39A)	117.7(11)	O(13A)-C(42A)-N(13A)	122.5(7)
N(4A)-C(16A)-C(15A)	121.9(10)	O(13A)-C(42A)-C(41A)	120.6(5)
N(4A)-C(16A)-C(17A)	109.1(9)	N(13A)-C(42A)-C(41A)	116.7(5)

C(44A)-C(43A)-C(17A)	116.7(8)	N(1A)-Co(1A)-N(2A)	91.3(4)
C(45A)-C(44A)-C(43A)	111.8(9)	N(4A)-Co(1A)-N(2A)	171.3(4)
O(14A)-C(45A)-N(7A)	122.9(12)	N(3A)-Co(1A)-N(2A)	94.8(4)
O(14A)-C(45A)-C(44A)	120.2(12)	N(1A)-Co(1A)-O(15A)	88.7(3)
N(7A)-C(45A)-C(44A)	116.9(13)	N(4A)-Co(1A)-O(15A)	87.5(3)
N(7A)-C(46A)-C(47A)	113.1(11)	N(3A)-Co(1A)-O(15A)	91.8(3)
O(3A)-C(47A)-C(46A)	110.9(15)	N(2A)-Co(1A)-O(15A)	86.5(3)
O(3A)-C(47A)-C(48A)	108.2(13)	N(1A)-Co(1A)-N(5A)	91.5(3)
C(46A)-C(47A)-C(48A)	109.8(15)	N(4A)-Co(1A)-N(5A)	95.9(3)
O(4A)-C(49A)-C(50A)	113.3(10)	N(3A)-Co(1A)-N(5A)	88.3(3)
O(4A)-C(49A)-C(52A)	108.1(10)	N(2A)-Co(1A)-N(5A)	90.1(3)
C(50A)-C(49A)-C(52A)	105.1(9)	O(15A)-Co(1A)-N(5A)	176.6(3)
O(5A)-C(50A)-C(49A)	110.7(9)	C(4A)-N(1A)-C(1A)	111.3(9)
O(5A)-C(50A)-C(51A)	107.0(8)	C(4A)-N(1A)-Co(1A)	129.9(8)
C(49A)-C(50A)-C(51A)	100.1(10)	C(1A)-N(1A)-Co(1A)	118.1(7)
O(6A)-C(51A)-N(6A)	106.3(9)	C(9A)-N(2A)-C(6A)	111.2(10)
O(6A)-C(51A)-C(50A)	107.2(8)	C(9A)-N(2A)-Co(1A)	122.8(8)
N(6A)-C(51A)-C(50A)	112.6(10)	C(6A)-N(2A)-Co(1A)	125.5(8)
C(53A)-C(52A)-O(6A)	109.0(14)	C(14A)-N(3A)-C(11A)	108.6(9)
C(53A)-C(52A)-C(49A)	120.4(12)	C(14A)-N(3A)-Co(1A)	125.8(7)
O(6A)-C(52A)-C(49A)	103.2(10)	C(11A)-N(3A)-Co(1A)	125.6(8)
O(7A)-C(53A)-C(52A)	110.1(15)	C(16A)-N(4A)-C(19A)	113.0(8)
N(5A)-C(54A)-N(6A)	110.4(9)	C(16A)-N(4A)-Co(1A)	131.0(7)
N(5A)-C(55A)-C(60A)	111.5(9)	C(19A)-N(4A)-Co(1A)	115.1(6)
N(5A)-C(55A)-C(56A)	131.3(9)	C(54A)-N(5A)-C(55A)	106.3(8)
C(60A)-C(55A)-C(56A)	117.2(9)	C(54A)-N(5A)-Co(1A)	121.2(7)
C(55A)-C(56A)-C(57A)	120.4(10)	C(55A)-N(5A)-Co(1A)	132.4(7)
C(56A)-C(57A)-C(58A)	116.6(12)	C(54A)-N(6A)-C(60A)	108.4(8)
C(56A)-C(57A)-C(61A)	118.5(11)	C(54A)-N(6A)-C(51A)	126.6(9)
C(58A)-C(57A)-C(61A)	124.7(12)	C(60A)-N(6A)-C(51A)	123.3(9)
C(59A)-C(58A)-C(57A)	124.1(12)	C(45A)-N(7A)-C(46A)	122.4(12)
C(59A)-C(58A)-C(62A)	121.3(14)	C(47A)-O(3A)-P(1A)	123.1(11)
C(57A)-C(58A)-C(62A)	114.6(14)	C(49A)-O(4A)-P(1A)	121.4(7)
C(58A)-C(59A)-C(60A)	117.5(11)	C(51A)-O(6A)-C(52A)	110.1(8)
C(59A)-C(60A)-C(55A)	124.2(11)	O(2A)-P(1A)-O(1A)	116.8(6)
C(59A)-C(60A)-N(6A)	132.6(11)	O(2A)-P(1A)-O(3A)	113.6(6)
C(55A)-C(60A)-N(6A)	103.2(9)	O(1A)-P(1A)-O(3A)	106.2(6)
N(1A)-Co(1A)-N(4A)	82.3(4)	O(2A)-P(1A)-O(4A)	110.7(6)
N(1A)-Co(1A)-N(3A)	173.9(4)	O(1A)-P(1A)-O(4A)	110.0(5)
N(4A)-Co(1A)-N(3A)	91.7(4)	O(3A)-P(1A)-O(4A)	97.8(4)

C(20B)-C(1B)-N(1B)	109.6(9)	N(3B)-C(11B)-C(12B)	109.4(11)
C(20B)-C(1B)-C(19B)	110.9(10)	C(10B)-C(11B)-C(12B)	129.7(12)
N(1B)-C(1B)-C(19B)	102.4(8)	C(13B)-C(12B)-C(11B)	101.8(10)
C(20B)-C(1B)-C(2B)	115.1(10)	C(13B)-C(12B)-C(34B)	110.0(14)
N(1B)-C(1B)-C(2B)	100.6(9)	C(11B)-C(12B)-C(34B)	120.3(15)
C(19B)-C(1B)-C(2B)	116.7(10)	C(13B)-C(12B)-C(35B)	111.6(13)
C(22B)-C(2B)-C(21B)	110.2(11)	C(11B)-C(12B)-C(35B)	102.6(12)
C(22B)-C(2B)-C(3B)	107.3(11)	C(34B)-C(12B)-C(35B)	110.1(15)
C(21B)-C(2B)-C(3B)	113.4(11)	C(12B)-C(13B)-C(36B)	118.8(14)
C(22B)-C(2B)-C(1B)	113.0(10)	C(12B)-C(13B)-C(14B)	104.7(11)
C(21B)-C(2B)-C(1B)	110.2(11)	C(36B)-C(13B)-C(14B)	108.7(12)
C(3B)-C(2B)-C(1B)	102.6(10)	C(15B)-C(14B)-N(3B)	126.9(11)
C(4B)-C(3B)-C(24B)	109.6(12)	C(15B)-C(14B)-C(13B)	126.2(12)
C(4B)-C(3B)-C(2B)	102.5(10)	N(3B)-C(14B)-C(13B)	106.8(10)
C(24B)-C(3B)-C(2B)	119.5(14)	C(14B)-C(15B)-C(16B)	123.1(11)
N(1B)-C(4B)-C(5B)	125.8(12)	C(14B)-C(15B)-C(39B)	119.4(13)
N(1B)-C(4B)-C(3B)	110.4(11)	C(16B)-C(15B)-C(39B)	117.4(13)
C(5B)-C(4B)-C(3B)	123.7(12)	N(4B)-C(16B)-C(15B)	121.5(11)
C(6B)-C(5B)-C(4B)	122.7(12)	N(4B)-C(16B)-C(17B)	111.9(11)
C(6B)-C(5B)-C(27B)	119.1(13)	C(15B)-C(16B)-C(17B)	126.2(12)
C(4B)-C(5B)-C(27B)	118.2(14)	C(18B)-C(17B)-C(43B)	111.6(9)
C(5B)-C(6B)-N(2B)	124.4(11)	C(18B)-C(17B)-C(16B)	100.2(9)
C(5B)-C(6B)-C(7B)	131.7(12)	C(43B)-C(17B)-C(16B)	115.9(10)
N(2B)-C(6B)-C(7B)	103.8(13)	C(18B)-C(17B)-C(40B)	113.5(10)
C(8B)-C(7B)-C(6B)	104.3(11)	C(43B)-C(17B)-C(40B)	108.3(9)
C(8B)-C(7B)-C(29B)	112.8(13)	C(16B)-C(17B)-C(40B)	107.2(9)
C(6B)-C(7B)-C(29B)	109.1(9)	C(41B)-C(18B)-C(17B)	118.7(10)
C(8B)-C(7B)-C(28B)	111.0(11)	C(41B)-C(18B)-C(19B)	113.6(10)
C(6B)-C(7B)-C(28B)	113.3(12)	C(17B)-C(18B)-C(19B)	103.6(8)
C(29B)-C(7B)-C(28B)	106.4(10)	N(4B)-C(19B)-C(1B)	108.0(9)
C(7B)-C(8B)-C(9B)	101.8(12)	N(4B)-C(19B)-C(18B)	100.6(9)
C(7B)-C(8B)-C(31B)	114.6(13)	C(1B)-C(19B)-C(18B)	122.4(9)
C(9B)-C(8B)-C(31B)	108.8(11)	C(2B)-C(22B)-C(23B)	119.4(15)
N(2B)-C(9B)-C(10B)	126.5(12)	O(8B)-C(23B)-N(8B)	122.1(7)
N(2B)-C(9B)-C(8B)	108.9(14)	O(8B)-C(23B)-C(22B)	119.6(9)
C(10B)-C(9B)-C(8B)	124.3(14)	N(8B)-C(23B)-C(22B)	115.9(9)
C(9B)-C(10B)-C(11B)	126.8(11)	C(25B)-C(24B)-C(3B)	112.5(16)
C(9B)-C(10B)-Br(1B)	116.5(11)	C(26B)-C(25B)-C(24B)	106.7(14)
C(11B)-C(10B)-Br(1B)	116.3(12)	O(9B)-C(26B)-N(9B)	122.7(8)
N(3B)-C(11B)-C(10B)	120.4(12)	O(9B)-C(26B)-C(25B)	120.7(6)

N(9B)-C(26B)-C(25B)	116.7(5)	C(60B)-C(55B)-C(56B)	120.4(11)
C(30B)-C(29B)-C(7B)	115.5(10)	C(60B)-C(55B)-N(5B)	108.3(10)
O(10B)-C(30B)-N(10B)	121.2(7)	C(56B)-C(55B)-N(5B)	131.3(11)
O(10B)-C(30B)-C(29B)	121.1(5)	C(57B)-C(56B)-C(55B)	115.9(12)
N(10B)-C(30B)-C(29B)	117.7(5)	C(58B)-C(57B)-C(56B)	124.1(14)
C(32B)-C(31B)-C(8B)	118.6(13)	C(58B)-C(57B)-C(61B)	117.0(12)
C(31B)-C(32B)-C(33B)	113.9(11)	C(56B)-C(57B)-C(61B)	118.6(13)
O(11B)-C(33B)-N(11B)	122.5(7)	C(59B)-C(58B)-C(57B)	118.1(12)
O(11B)-C(33B)-C(32B)	120.5(6)	C(59B)-C(58B)-C(62B)	118.6(16)
N(11B)-C(33B)-C(32B)	116.9(5)	C(57B)-C(58B)-C(62B)	122.2(14)
O(12B)-C(38B)-N(12B)	122.5(8)	C(58B)-C(59B)-C(60B)	121.1(13)
O(12B)-C(38B)-C(37B)	120.7(6)	C(55B)-C(60B)-C(59B)	120.4(12)
N(12B)-C(38B)-C(37B)	116.9(5)	C(55B)-C(60B)-N(6B)	105.5(9)
C(18B)-C(41B)-C(42B)	113.0(9)	C(59B)-C(60B)-N(6B)	134.0(12)
O(13B)-C(42B)-N(13B)	122.8(7)	N(3B)-Co(1B)-N(4B)	92.1(4)
O(13B)-C(42B)-C(41B)	120.1(5)	N(3B)-Co(1B)-N(1B)	174.8(4)
N(13B)-C(42B)-C(41B)	116.5(5)	N(4B)-Co(1B)-N(1B)	82.8(4)
C(44B)-C(43B)-C(17B)	116.9(9)	N(3B)-Co(1B)-O(15B)	92.9(4)
C(45B)-C(44B)-C(43B)	111.9(10)	N(4B)-Co(1B)-O(15B)	88.1(3)
O(14B)-C(45B)-N(7B)	122.2(13)	N(1B)-Co(1B)-O(15B)	87.8(4)
O(14B)-C(45B)-C(44B)	118.3(15)	N(3B)-Co(1B)-N(2B)	94.3(5)
N(7B)-C(45B)-C(44B)	119.5(13)	N(4B)-Co(1B)-N(2B)	171.0(5)
C(47B)-C(46B)-N(7B)	114.3(10)	N(1B)-Co(1B)-N(2B)	90.8(5)
O(3B)-C(47B)-C(46B)	109.8(13)	O(15B)-Co(1B)-N(2B)	85.3(3)
O(3B)-C(47B)-C(48B)	108.9(11)	N(3B)-Co(1B)-N(5B)	87.3(4)
C(46B)-C(47B)-C(48B)	111.1(11)	N(4B)-Co(1B)-N(5B)	94.9(3)
O(4B)-C(49B)-C(52B)	110.5(9)	N(1B)-Co(1B)-N(5B)	92.3(4)
O(4B)-C(49B)-C(50B)	111.4(11)	O(15B)-Co(1B)-N(5B)	177.0(3)
C(52B)-C(49B)-C(50B)	103.5(9)	N(2B)-Co(1B)-N(5B)	91.7(3)
O(5B)-C(50B)-C(51B)	107.5(8)	C(4B)-N(1B)-C(1B)	114.3(10)
O(5B)-C(50B)-C(49B)	111.4(9)	C(4B)-N(1B)-Co(1B)	128.5(9)
C(51B)-C(50B)-C(49B)	100.0(10)	C(1B)-N(1B)-Co(1B)	116.1(7)
O(6B)-C(51B)-C(50B)	109.2(9)	C(9B)-N(2B)-C(6B)	112.4(11)
O(6B)-C(51B)-N(6B)	105.8(9)	C(9B)-N(2B)-Co(1B)	123.7(9)
C(50B)-C(51B)-N(6B)	113.1(10)	C(6B)-N(2B)-Co(1B)	123.7(9)
O(6B)-C(52B)-C(49B)	104.0(9)	C(11B)-N(3B)-C(14B)	109.6(10)
O(6B)-C(52B)-C(53B)	110.3(12)	C(11B)-N(3B)-Co(1B)	126.6(8)
C(49B)-C(52B)-C(53B)	120.3(12)	C(14B)-N(3B)-Co(1B)	123.8(8)
O(7B)-C(53B)-C(52B)	109.3(16)	C(16B)-N(4B)-C(19B)	111.4(9)
N(6B)-C(54B)-N(5B)	111.3(9)	C(16B)-N(4B)-Co(1B)	132.7(8)

C(19B)-N(4B)-Co(1B)	115.1(7)	O(2B)-P(1B)-O(4B)	110.4(11)
C(54B)-N(5B)-C(55B)	104.4(9)	O(1B)-P(1B)-O(4B)	107.6(8)
C(54B)-N(5B)-Co(1B)	124.5(7)	O(2B)-P(1B)-O(3B)	117.2(10)
C(55B)-N(5B)-Co(1B)	131.0(8)	O(1B)-P(1B)-O(3B)	102.7(8)
C(54B)-N(6B)-C(60B)	110.4(9)	O(4B)-P(1B)-O(3B)	100.1(5)
C(54B)-N(6B)-C(51B)	123.0(10)	O(4P)-P(1P)-O(2P)	103(2)
C(60B)-N(6B)-C(51B)	125.1(9)	O(4P)-P(1P)-O(3P)	108.9(13)
C(45B)-N(7B)-C(46B)	123.7(12)	O(2P)-P(1P)-O(3P)	112.9(19)
C(47B)-O(3B)-P(1B)	122.2(10)	O(4P)-P(1P)-O(1P)	109.4(13)
C(49B)-O(4B)-P(1B)	119.4(7)	O(2P)-P(1P)-O(1P)	112(2)
C(51B)-O(6B)-C(52B)	108.8(9)	O(3P)-P(1P)-O(1P)	110(2)
O(2B)-P(1B)-O(1B)	117.2(14)		

Table 2.7.3 Selected bond lengths (Å) and bond angles (deg) in azido-(10-bromo)cobalamin di(sodium azide) triacetone solvate pentahydrate.

Bond lengths	
C(1)-N(1)	1.495(7)
C(1)-C(19)	1.536(9)
C(1)-C(20)	1.537(9)
C(1)-C(2)	1.583(9)
C(2)-C(21)	1.511(9)
C(2)-C(3)	1.549(8)
C(2)-C(22)	1.555(9)
C(3)-C(4)	1.525(9)
C(3)-C(24)	1.537(9)
C(4)-N(1)	1.303(7)
C(4)-C(5)	1.410(8)
C(5)-C(6)	1.370(9)
C(5)-C(27)	1.530(9)
C(6)-N(2)	1.391(8)
C(6)-C(7)	1.523(8)
C(7)-C(30)	1.546(8)
C(7)-C(28)	1.570(9)
C(7)-C(8)	1.578(9)
C(8)-C(9)	1.508(9)
C(8)-C(31)	1.525(9)
C(9)-C(10)	1.371(9)
C(9)-N(2)	1.372(8)
C(10)-C(11)	1.414(9)
C(10)-Br(1)	1.899(6)
C(11)-N(3)	1.331(7)
C(11)-C(12)	1.524(9)
C(12)-C(34)	1.526(9)
C(12)-C(13)	1.539(9)
C(12)-C(35)	1.562(10)
C(13)-C(36)	1.538(10)
C(13)-C(14)	1.548(9)
C(14)-C(15)	1.345(8)
C(14)-N(3)	1.408(8)
C(15)-C(16)	1.445(9)
C(15)-C(39)	1.510(9)
C(16)-N(4)	1.305(8)
C(16)-C(17)	1.541(8)
C(17)-C(43)	1.522(9)
C(17)-C(40)	1.543(9)
C(17)-C(18)	1.548(9)
C(18)-C(19)	1.519(8)
C(18)-C(41)	1.548(9)
C(19)-N(4)	1.463(8)
C(22)-C(23)	1.525(10)
C(23)-O(1)	1.228(9)
C(23)-N(5)	1.327(9)
C(24)-C(25)	1.527(9)
C(25)-C(26)	1.535(10)
C(26)-O(2)	1.250(8)
C(26)-N(6)	1.310(9)
C(28)-C(29)	1.513(9)
C(29)-O(3)	1.224(9)
C(29)-N(7)	1.319(9)
C(31)-C(32)	1.513(9)
C(32)-C(33)	1.509(10)
C(33)-O(4)	1.226(9)
C(33)-N(8)	1.342(10)
C(36)-C(37)	1.550(10)
C(37)-C(38)	1.537(10)
C(38)-O(5)	1.215(9)
C(38)-N(9)	1.336(10)
C(41)-C(42)	1.530(10)
C(42)-O(6)	1.246(9)
C(42)-N(10)	1.318(8)
C(43)-C(44)	1.519(9)
C(44)-C(45)	1.508(9)
C(45)-O(7)	1.246(9)
C(45)-N(11)	1.334(9)
C(46)-N(11)	1.463(8)
C(46)-C(47)	1.503(9)
C(47)-O(8)	1.455(8)
C(47)-C(48)	1.512(9)
C(49)-O(11)	1.401(7)

C(49)-C(50)	1.520(9)	O(2W)-Na(1)	2.482(7)
C(49)-C(52)	1.520(9)	O(3W)-Na(2)	2.564(6)
C(50)-O(12)	1.392(7)	O(4W)-Na(2)	2.699(6)
C(50)-C(51)	1.531(9)	O(5W)-Na(2)	2.438(6)
C(51)-O(13)	1.412(8)	Na(1)-O(3)#3	2.451(7)
C(51)-N(12)	1.475(8)	Na(2)-O(6)#4	2.250(6)
C(52)-O(13)	1.440(8)	C(1A)-O(1A)	1.265(11)
C(52)-C(53)	1.536(10)	C(1A)-C(2A)	1.435(14)
C(53)-O(14)	1.396(9)	C(1A)-C(3A)	1.540(15)
C(54)-N(13)	1.307(8)	C(4A)-O(2A)	1.253(13)
C(54)-N(12)	1.338(8)	C(4A)-C(5A)	1.472(17)
C(55)-C(60)	1.366(9)	C(4A)-C(6A)	1.490(17)
C(55)-C(56)	1.373(9)	C(7A)-C(8A)	1.476(15)
C(56)-C(57)	1.455(10)	C(8A)-O(3A)	1.241(12)
C(56)-C(61)	1.511(9)	C(8A)-C(9A)	1.465(15)
C(57)-C(58)	1.356(10)	N(4A)-N(5A)	0.973(9)
C(57)-C(62)	1.505(10)	N(5A)-N(6A)	1.242(11)
C(58)-C(59)	1.392(9)	N(7A)-N(9A)	1.177(11)
C(59)-N(12)	1.375(8)	N(7A)-N(8A)	1.249(12)
C(59)-C(60)	1.405(9)		
C(60)-N(13)	1.427(8)	**Bond angles**	
N(1)-Co(1)	1.914(5)	N(1)-C(1)-C(19)	102.6(5)
N(1A)-N(2A)	1.136(8)	N(1)-C(1)-C(20)	110.4(6)
N(1A)-Co(1)	1.942(6)	C(19)-C(1)-C(20)	109.9(6)
N(2)-Co(1)	1.897(5)	N(1)-C(1)-C(2)	101.0(5)
N(2A)-N(3A)	1.177(9)	C(19)-C(1)-C(2)	118.4(6)
N(3)-Co(1)	1.936(5)	C(20)-C(1)-C(2)	113.4(6)
N(4)-Co(1)	1.886(5)	C(21)-C(2)-C(3)	112.9(6)
N(13)-Co(1)	1.974(6)	C(21)-C(2)-C(22)	109.4(6)
O(3)-Na(1)#1	2.451(7)	C(3)-C(2)-C(22)	107.6(6)
O(5)-Na(1)	2.566(6)	C(21)-C(2)-C(1)	115.6(6)
O(6)-Na(2)#2	2.250(6)	C(3)-C(2)-C(1)	101.5(5)
O(7)-Na(1)	2.378(6)	C(22)-C(2)-C(1)	109.3(6)
O(8)-P(1)	1.562(5)	C(4)-C(3)-C(24)	114.1(6)
O(9)-P(1)	1.496(6)	C(4)-C(3)-C(2)	102.6(5)
O(9)-Na(2)	2.378(6)	C(24)-C(3)-C(2)	115.6(6)
O(10)-P(1)	1.483(5)	N(1)-C(4)-C(5)	124.8(6)
O(11)-P(1)	1.599(5)	N(1)-C(4)-C(3)	108.9(5)
O(14)-Na(2)	2.407(6)	C(5)-C(4)-C(3)	126.3(6)
O(1W)-Na(1)	2.464(7)	C(6)-C(5)-C(4)	122.3(6)

C(6)-C(5)-C(27)	119.0(6)	C(15)-C(16)-C(17)	126.3(6)
C(4)-C(5)-C(27)	118.4(6)	C(43)-C(17)-C(16)	117.2(6)
C(5)-C(6)-N(2)	124.1(6)	C(43)-C(17)-C(40)	109.5(6)
C(5)-C(6)-C(7)	127.0(7)	C(16)-C(17)-C(40)	106.5(6)
N(2)-C(6)-C(7)	108.7(6)	C(43)-C(17)-C(18)	111.5(6)
C(6)-C(7)-C(30)	118.0(6)	C(16)-C(17)-C(18)	99.5(5)
C(6)-C(7)-C(28)	106.3(5)	C(40)-C(17)-C(18)	112.3(6)
C(30)-C(7)-C(28)	110.9(6)	C(19)-C(18)-C(41)	114.4(6)
C(6)-C(7)-C(8)	99.9(6)	C(19)-C(18)-C(17)	102.4(5)
C(30)-C(7)-C(8)	111.6(5)	C(41)-C(18)-C(17)	115.5(6)
C(28)-C(7)-C(8)	109.5(6)	N(4)-C(19)-C(18)	103.2(5)
C(9)-C(8)-C(31)	113.4(6)	N(4)-C(19)-C(1)	107.6(5)
C(9)-C(8)-C(7)	99.1(5)	C(18)-C(19)-C(1)	120.9(6)
C(31)-C(8)-C(7)	112.1(6)	C(23)-C(22)-C(2)	115.7(7)
C(10)-C(9)-N(2)	124.8(6)	O(1)-C(23)-N(5)	121.4(8)
C(10)-C(9)-C(8)	125.7(6)	O(1)-C(23)-C(22)	123.7(7)
N(2)-C(9)-C(8)	109.3(6)	N(5)-C(23)-C(22)	114.8(8)
C(9)-C(10)-C(11)	126.8(6)	C(25)-C(24)-C(3)	116.2(6)
C(9)-C(10)-Br(1)	114.6(5)	C(24)-C(25)-C(26)	112.4(6)
C(11)-C(10)-Br(1)	118.1(5)	O(2)-C(26)-N(6)	124.4(8)
N(3)-C(11)-C(10)	122.0(7)	O(2)-C(26)-C(25)	121.5(7)
N(3)-C(11)-C(12)	110.0(6)	N(6)-C(26)-C(25)	114.2(7)
C(10)-C(11)-C(12)	127.5(6)	C(29)-C(28)-C(7)	112.8(6)
C(11)-C(12)-C(34)	122.6(6)	O(3)-C(29)-N(7)	123.2(8)
C(11)-C(12)-C(13)	100.4(6)	O(3)-C(29)-C(28)	121.8(8)
C(34)-C(12)-C(13)	111.7(6)	N(7)-C(29)-C(28)	115.1(8)
C(11)-C(12)-C(35)	105.8(6)	C(32)-C(31)-C(8)	115.3(6)
C(34)-C(12)-C(35)	107.5(6)	C(33)-C(32)-C(31)	111.6(7)
C(13)-C(12)-C(35)	107.8(6)	O(4)-C(33)-N(8)	122.0(9)
C(36)-C(13)-C(12)	114.6(6)	O(4)-C(33)-C(32)	122.3(8)
C(36)-C(13)-C(14)	106.8(6)	N(8)-C(33)-C(32)	115.6(8)
C(12)-C(13)-C(14)	102.3(5)	C(13)-C(36)-C(37)	117.3(7)
C(15)-C(14)-N(3)	130.4(6)	C(38)-C(37)-C(36)	110.4(7)
C(15)-C(14)-C(13)	123.3(6)	O(5)-C(38)-N(9)	124.2(8)
N(3)-C(14)-C(13)	106.1(5)	O(5)-C(38)-C(37)	121.1(9)
C(14)-C(15)-C(16)	120.9(6)	N(9)-C(38)-C(37)	114.8(8)
C(14)-C(15)-C(39)	119.0(6)	C(42)-C(41)-C(18)	112.2(6)
C(16)-C(15)-C(39)	120.1(5)	O(6)-C(42)-N(10)	123.8(7)
N(4)-C(16)-C(15)	121.3(5)	O(6)-C(42)-C(41)	121.4(7)
N(4)-C(16)-C(17)	112.3(6)	N(10)-C(42)-C(41)	114.8(7)

C(44)-C(43)-C(17)	115.6(6)	C(9)-N(2)-C(6)	109.5(6)
C(45)-C(44)-C(43)	110.9(6)	C(9)-N(2)-Co(1)	123.8(5)
O(7)-C(45)-C(44)	120.6(7)	C(6)-N(2)-Co(1)	125.5(4)
N(11)-C(45)-C(44)	116.3(8)	N(1A)-N(2A)-N(3A)	177.5(9)
N(11)-C(46)-C(47)	113.3(6)	C(11)-N(3)-C(14)	111.9(6)
O(8)-C(47)-C(46)	107.3(6)	C(11)-N(3)-Co(1)	126.2(5)
O(8)-C(47)-C(48)	106.7(6)	C(14)-N(3)-Co(1)	121.8(4)
C(46)-C(47)-C(48)	109.4(6)	C(16)-N(4)-C(19)	109.5(5)
O(11)-C(49)-C(50)	113.8(6)	C(16)-N(4)-Co(1)	133.4(5)
O(11)-C(49)-C(52)	110.6(6)	C(19)-N(4)-Co(1)	114.9(4)
C(50)-C(49)-C(52)	102.6(6)	C(45)-N(11)-C(46)	122.0(7)
O(12)-C(50)-C(49)	111.7(6)	C(54)-N(12)-C(59)	106.5(6)
O(12)-C(50)-C(51)	109.8(6)	C(54)-N(12)-C(51)	125.3(6)
C(49)-C(50)-C(51)	100.0(5)	C(59)-N(12)-C(51)	126.8(7)
O(13)-C(51)-N(12)	108.5(6)	C(54)-N(13)-C(60)	103.9(6)
O(13)-C(51)-C(50)	107.9(6)	C(54)-N(13)-Co(1)	123.6(5)
N(12)-C(51)-C(50)	110.6(6)	C(60)-N(13)-Co(1)	132.4(5)
O(13)-C(52)-C(49)	105.0(5)	C(29)-O(3)-Na(1)#1	160.4(6)
O(13)-C(52)-C(53)	108.9(6)	C(38)-O(5)-Na(1)	149.5(6)
C(49)-C(52)-C(53)	113.0(6)	C(42)-O(6)-Na(2)#2	150.1(5)
O(14)-C(53)-C(52)	111.6(7)	C(45)-O(7)-Na(1)	171.3(5)
N(13)-C(54)-N(12)	115.1(7)	C(47)-O(8)-P(1)	120.5(4)
C(60)-C(55)-C(56)	120.7(7)	P(1)-O(9)-Na(2)	148.3(3)
C(55)-C(56)-C(57)	119.1(7)	C(49)-O(11)-P(1)	118.0(4)
C(55)-C(56)-C(61)	121.1(7)	C(51)-O(13)-C(52)	109.4(5)
C(57)-C(56)-C(61)	119.8(7)	C(53)-O(14)-Na(2)	122.8(5)
C(58)-C(57)-C(56)	120.5(8)	O(10)-P(1)-O(9)	116.5(3)
C(58)-C(57)-C(62)	120.9(8)	O(10)-P(1)-O(8)	107.2(3)
C(56)-C(57)-C(62)	118.5(7)	O(9)-P(1)-O(8)	113.2(3)
C(57)-C(58)-C(59)	118.3(8)	O(10)-P(1)-O(11)	109.1(3)
N(12)-C(59)-C(58)	131.5(7)	O(9)-P(1)-O(11)	108.4(3)
N(12)-C(59)-C(60)	106.5(7)	O(8)-P(1)-O(11)	101.3(3)
C(58)-C(59)-C(60)	122.0(7)	N(4)-Co(1)-N(2)	172.2(2)
C(55)-C(60)-C(59)	119.3(7)	N(4)-Co(1)-N(1)	82.6(2)
C(55)-C(60)-N(13)	132.7(7)	N(2)-Co(1)-N(1)	90.7(2)
C(59)-C(60)-N(13)	107.9(6)	N(4)-Co(1)-N(3)	91.7(2)
C(4)-N(1)-C(1)	114.6(6)	N(2)-Co(1)-N(3)	95.0(2)
C(4)-N(1)-Co(1)	127.8(4)	N(1)-Co(1)-N(3)	174.2(2)
C(1)-N(1)-Co(1)	116.6(4)	N(4)-Co(1)-N(1A)	91.1(3)
N(2A)-N(1A)-Co(1)	119.3(6)	N(2)-Co(1)-N(1A)	84.8(3)

N(1)-Co(1)-N(1A)	88.4(3)
N(3)-Co(1)-N(1A)	91.0(2)
N(4)-Co(1)-N(13)	94.1(2)
N(2)-Co(1)-N(13)	90.1(2)
N(1)-Co(1)-N(13)	92.7(2)
N(3)-Co(1)-N(13)	88.5(2)
N(1A)-Co(1)-N(13)	174.8(2)
O(7)-Na(1)-O(3)#3	103.5(2)
O(7)-Na(1)-O(1W)	100.6(2)
O(3)#3-Na(1)-O(1W)	92.2(2)
O(7)-Na(1)-O(2W)	118.1(2)
O(3)#3-Na(1)-O(2W)	84.3(2)
O(1W)-Na(1)-O(2W)	140.9(2)
O(7)-Na(1)-O(5)	100.3(2)
O(3)#3-Na(1)-O(5)	156.1(2)
O(1W)-Na(1)-O(5)	82.0(2)
O(2W)-Na(1)-O(5)	85.69(19)
O(6)#4-Na(2)-O(9)	104.7(2)
O(6)#4-Na(2)-O(14)	156.6(2)
O(9)-Na(2)-O(14)	92.4(2)
O(6)#4-Na(2)-O(5W)	92.2(2)
O(9)-Na(2)-O(5W)	139.7(2)
O(14)-Na(2)-O(5W)	84.5(2)
O(6)#4-Na(2)-O(3W)	82.8(2)
O(9)-Na(2)-O(3W)	105.4(2)
O(14)-Na(2)-O(3W)	77.3(2)
O(5W)-Na(2)-O(3W)	112.9(2)
O(6)#4-Na(2)-O(4W)	96.9(2)
O(9)-Na(2)-O(4W)	63.07(19)
O(14)-Na(2)-O(4W)	105.1(2)
O(5W)-Na(2)-O(4W)	78.98(19)
O(3W)-Na(2)-O(4W)	168.1(2)
O(1A)-C(1A)-C(2A)	127.6(13)
O(1A)-C(1A)-C(3A)	121.1(13)
C(2A)-C(1A)-C(3A)	111.1(11)
O(2A)-C(4A)-C(5A)	116.5(15)
O(2A)-C(4A)-C(6A)	125.4(16)
C(5A)-C(4A)-C(6A)	117.9(14)
O(3A)-C(8A)-C(9A)	121.4(14)
O(3A)-C(8A)-C(7A)	119.4(13)
C(9A)-C(8A)-C(7A)	118.9(13)

Symmetry transformations used to generate equivalent atoms:

#1 -x+1,y+1/2,-z+3/2 #2 x-1/2,-y+1/2,-z+1 #3 -x+1,y-1/2,-z+3/2

#4 x+1/2,-y+1/2,-z+1

2.8 Derivation of Equations for the Determination of Stability Constants

The binding isotherm of a system with log $K < 4$

An equilibrium exists between the chromophore (M) and free ligand in solution:

$$M + L \rightleftharpoons ML$$

The equilibrium constant can be defined as:

$$K = \frac{[ML]}{[M][L]}$$

From Beer's law (where b is the path length of the cell) the initial and final absorbances can be defined:

$$A_0 = \varepsilon_M b[M]_0$$
$$A_1 = \varepsilon_{ML} b[ML]_1$$

At any point during the titration:

$$A = \varepsilon_M b[M] + \varepsilon_{ML} b[ML]$$
$$[M]_0 = [M] + [ML]$$
$$[ML]_1 = [M]_0 = [M] + [ML]$$
$$\therefore A = \varepsilon_M b([M]_0 - [ML]) + \varepsilon_{ML} b[ML]$$
$$A = \varepsilon_M b[M]_0 - \varepsilon_M b[ML] + \varepsilon_{ML} b[ML]$$
$$A - \varepsilon_M b[M]_0 = [ML](\varepsilon_M b + \varepsilon_{ML} b)$$
$$\therefore [ML] = \frac{A - \varepsilon_M b[M]_0}{\varepsilon_{ML} b - \varepsilon_M b}$$
$$[ML] = \frac{A - A_0}{\varepsilon_{ML} b - \varepsilon_M b}$$

Equation 2.8.1

Similarly

$$A = \varepsilon_M b[M] + \varepsilon_{ML} b[ML]$$
$$A = \varepsilon_M b[M] + \varepsilon_{ML} b([ML]_1 - [M])$$
$$A = \varepsilon_M b[M] + \varepsilon_{ML} b[ML]_1 - \varepsilon_{ML} b[M]$$
$$A - \varepsilon_M b[M]_1 = [M](\varepsilon_M b - \varepsilon_{ML} b)$$

$$\therefore [M] = \frac{A - \varepsilon_M b[M]_1}{\varepsilon_M b - \varepsilon_{ML} b}$$
$$[M] = \frac{A - A_1}{\varepsilon_M b - \varepsilon_{ML} b}$$

Considering the equilibrium constant

$$K = \frac{[ML]}{[M][L]}$$

Substituting in **Equation 2.7.1** and **2.3**:

$$K = \frac{A - A_0}{\varepsilon_{ML} b - \varepsilon_M b} \cdot \frac{1}{L} \cdot \frac{\varepsilon_M b - \varepsilon_{ML} b}{A - A_1}$$
$$K = \frac{A - A_0}{\varepsilon_{ML} b - \varepsilon_M b} \cdot \frac{1}{L} \cdot \frac{\varepsilon_{ML} b - \varepsilon_M b}{A_1 - A}$$
$$K = \frac{A - A_0}{A_1 - A} \cdot \frac{1}{L}$$
$$K[L] = \frac{A - A_0}{A_1 - A}$$
$$\therefore K[L] = \frac{A_0 - A}{A - A_1}$$

Equation 2.7.2

Assuming that $[L]_0 \approx [L]$ and K is small:

$$K[L] = \frac{A_0 - A}{A - A_1}$$

$$A_0 - A = K[L](A - A_1)$$

$$A_0 - A = K[L]A - K[L]A_1$$

$$K[L]A + A = K[L]A_1 + A_0$$

$$A(K[L] + 1) = K[L]A_1 + A_0$$

$$\therefore A = \frac{A_0 + A_1 K[L]}{1 + K[L]}$$

Equation 2.7.3

The binding isotherm of a system when log $K > 4$

If K is large $[L]_{free} \neq [L]_T$. An expression for $[L]_{free}$ can be derived.

$$[L]_{free} = [L]_T - [ML]$$

$$[ML] = [M]_T - [M]$$

$$[M]_T = [ML] + [M]$$

From the equilibrium constant:

$$[M]_T = [ML] + \frac{[ML]}{K[L]_{free}}$$

$$[M]_T = [ML]\left(1 + \frac{1}{K[L]_{free}}\right)$$

$$[M]_T = [ML]\left(\frac{1 + K[L]_{free}}{K[L]_{free}}\right)$$

$$\therefore [ML] = \frac{[M]_T K[L]_{free}}{1 + K[L]_{free}}$$

$$\therefore [L]_{free} = [L]_T - \frac{[M]_T K[L]_{free}}{1 + K[L]_{free}}$$

$$\therefore [L]_{free}(1 + K[L]_{free}) = [L]_T(1 + K[L]_{free}) - [M]_T K[L]_{free}$$

$$[L]_{free} + K[L]_{free}^{\,2} = [L]_T + K[L]_T[L]_{free} - [M]_T K[L]_{free}$$

$$K[L]_{free}^{\,2} + (1 + [M]_T K - [L]_T K)[L]_{free} - [L]_T = 0$$

This has the form:

$$a_1[L]_{free}{}^2 + a_2[L]_{free} + a_3 = 0$$

where $a_1 = K$; $a_2 = 1 + [M]_T K - [L]_T K$ and $a_3 = -[L]_T$

$$\therefore [L]_{free} = \frac{-a_2 \pm \sqrt{a_2{}^2 - 4a_1 a_3}}{2a_1}$$

$$[L]_{free} > 0$$

$$\therefore [L]_{free} = \frac{-a_2 + \sqrt{a_2{}^2 - 4a_1 a_3}}{2a_1}$$

Substituted in **Equation 2.7.3**

$$A = \frac{A_0 + A_1 K[L]_{free}}{1 + K[L]_{free}}$$

Equation 2.7.4

2.9 Derivation of Equations for the Correction of *K* Taking Free Ligand and Metal into Account

An equilibrium between the chromophore (M) and free ligand in solution:

$$M + L_T \rightleftharpoons ML$$

The equilibrium constant can be defined as:

$$K = \frac{[ML]}{[M][L]}$$

An equilibrium also exists for the ligand:

$$LH \rightleftharpoons L + H^+$$

Assume L and not LH binds to M

$$K_{aL} = \frac{[L][H^+]}{[LH]}$$

$$[L_T] = [L] + [LH]$$

$$[L_T] = [L] + \frac{[L][H^+]}{K_{aL}}$$

$$[L_T] = [L]\left(1 + \frac{[H^+]}{K_{aL}}\right)$$

$$[L] = \frac{[L_T]}{1 + \frac{[H^+]}{K_{aL}}}$$

$$\therefore\ [L] = \frac{[L_T]}{1 + 10^{pK_a - pH}}$$

Equation 2.8.1

Thus the fraction of available ligand is given by:

$$\frac{1}{1 + 10^{pK_a - pH}}$$

In addition to the equilibrium between protonated and deprotonated ligand, there existsan equilibrium between the aqua and hydroxo form of the metal as follows:

$$\text{M-H}_2\text{O} \rightleftharpoons \text{M-OH} + \text{H}^+$$

The equilibrium constant can be defined as:

$$K_{aM} = \frac{[\text{M-OH}][H^+]}{[\text{M-H}_2\text{O}]}$$

M-H_2O and not M-OH is able to undergo ligand substitution reactions as follows:

$$\text{M-H}_2\text{O} + \text{L} \rightleftharpoons \text{M-L} + \text{H}_2\text{O}$$

$$K = \frac{[\text{ML}]}{[\text{M-H}_2\text{O}][\text{L}]}$$

Thus:

$$K = \frac{[\mathrm{ML}]}{[\mathrm{M}_T][\mathrm{L}]}$$

$$[M_T] = [\mathrm{M\text{-}H_2O}] + [\mathrm{M\text{-}OH}]$$

$$[M_T] = [\mathrm{M\text{-}H_2O}] + \frac{K_{aM}[\mathrm{M\text{-}H_2O}]}{[H^+]}$$

$$[M_T] = [\mathrm{M\text{-}H_2O}]\left(1 + \frac{K_{aM}}{[H^+]}\right)$$

$$[\mathrm{M\text{-}H_2O}] = \frac{[M_T]}{1 + \frac{K_{aM}}{[H^+]}}$$

$$\therefore [\mathrm{M\text{-}H_2O}] = \frac{[M_T]}{1 + 10^{pH - pK_{aM}}}$$

Equation 2.8.2

Thus the fraction of available chromophore is given by:

$$\frac{1}{1 + 10^{pH - pK_{aM}}}$$

From the equilibrium between the chromophore and ligand we have:

$$\mathrm{M} + \mathrm{L}_T \rightleftharpoons \mathrm{ML}$$

Taking the free ligand (**Equation 2.8.1**) and free chromophore (**Equation 2.8.2**) into account:

$$K = \frac{[ML]}{[M][L]}$$

$$K = \frac{[ML]}{[M][L]}(1 + 10^{pK_a - pH})(1 + 10^{pH - pK_{aM}})$$

Thus:

$$K = K_{obs}(1 + 10^{pK_a - pH})(1 + 10^{pH - pK_{aM}})$$

Equation 2.8.3

Appendices for Chapter 3

3.1 Spectroscopic Changes for Binding of Anionic and Neutral Ligands to [H_2O-(10-Z)Cbl]$^+$

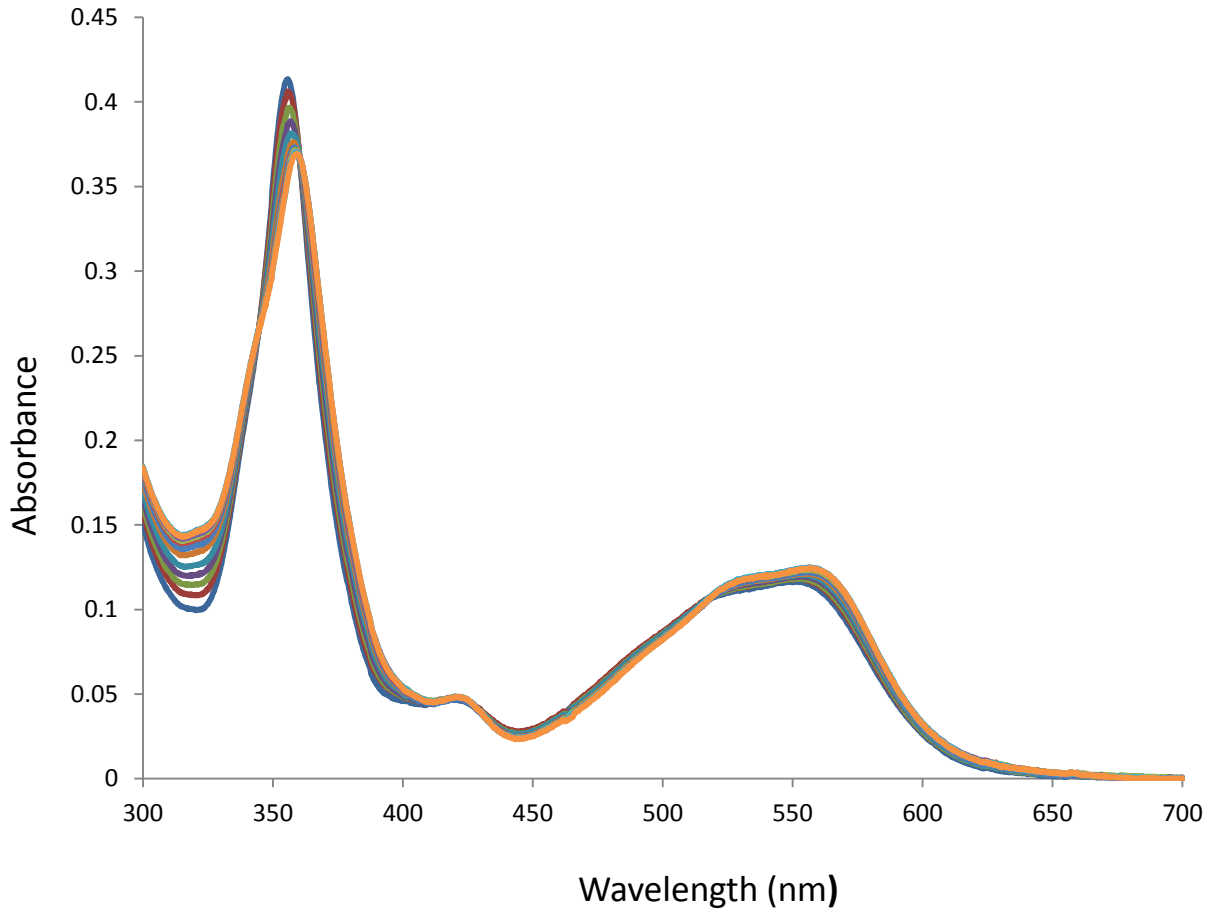


Figure 3.1.1 The absorbance changes observed for the binding of NO_2^- to [H_2O-(10-Br)Cbl]$^+$.

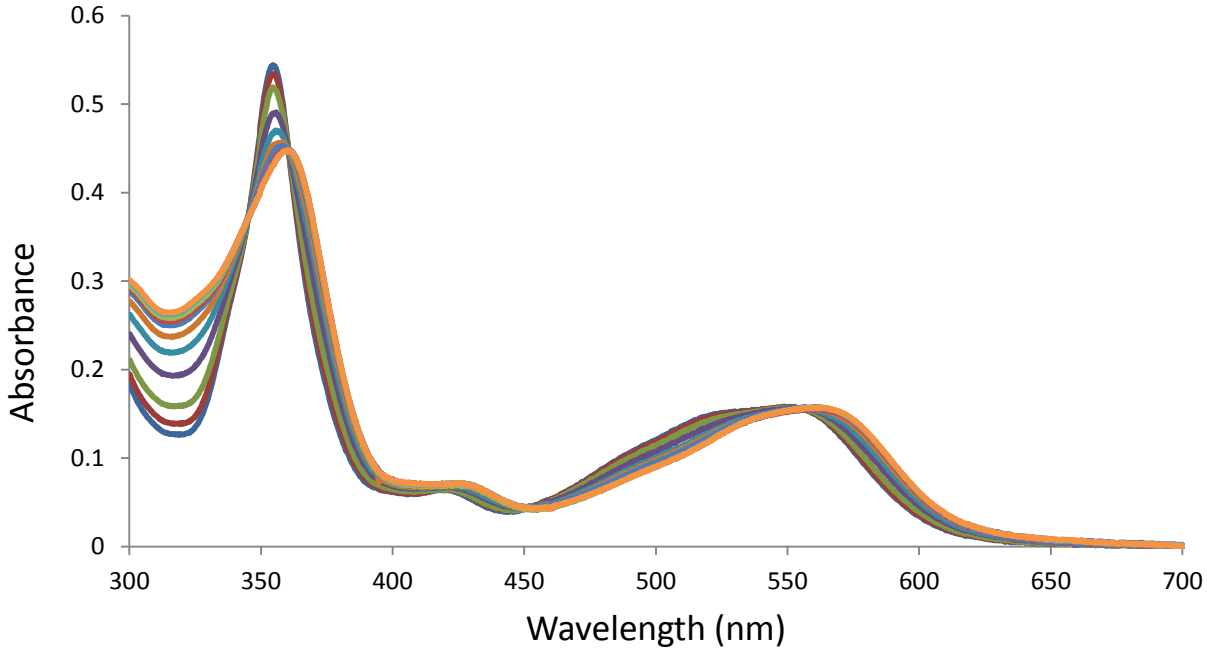


Figure 3.1.2 The absorbance changes observed for the binding of N_3^- to $[H_2O\text{-}(10\text{-}Cl)Cbl]^+$.

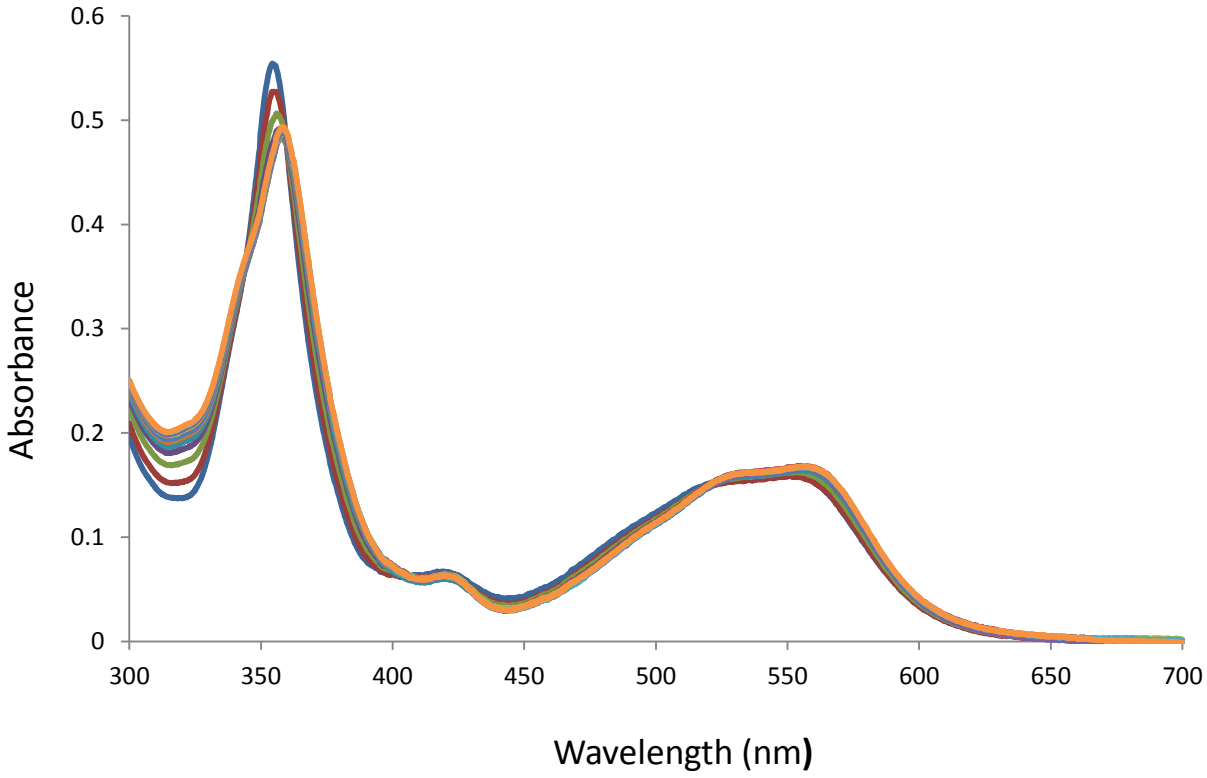


Figure 3.1.3 The absorbance changes observed for the binding of NO_2^- to $[H_2O\text{-}(10\text{-}Cl)Cbl]^+$.

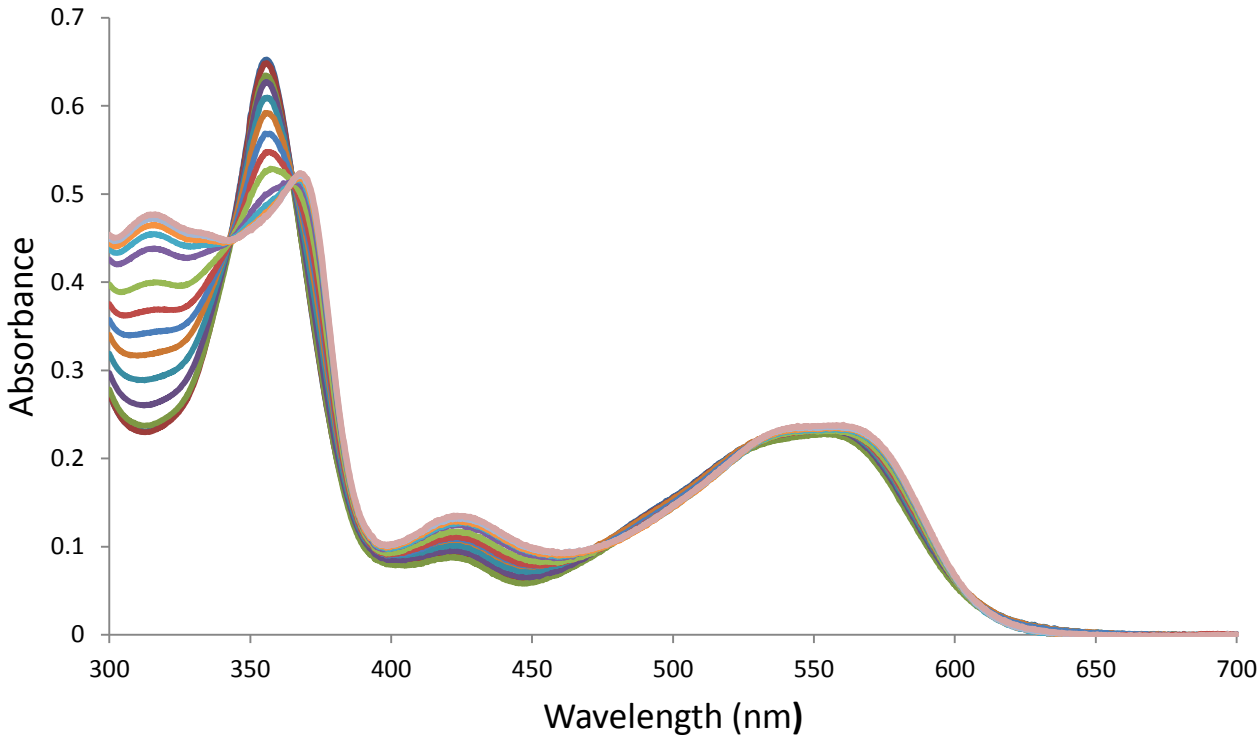


Figure 3.1.4 The absorbance changes observed for the binding of SO_3^{2-} to $[H_2O\text{-}(10\text{-}Cl)Cbl]^+$.

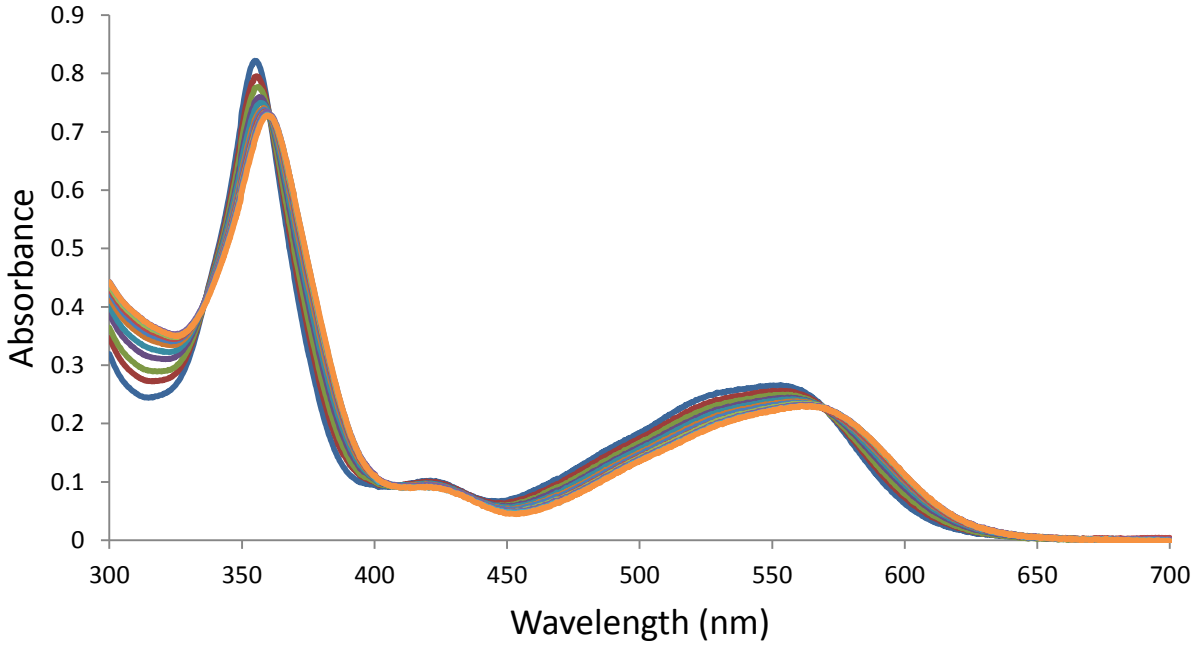


Figure 3.1.5 The absorbance changes observed for the binding of SCN^- to $[H_2O\text{-}(10\text{-}Cl)Cbl]^+$.

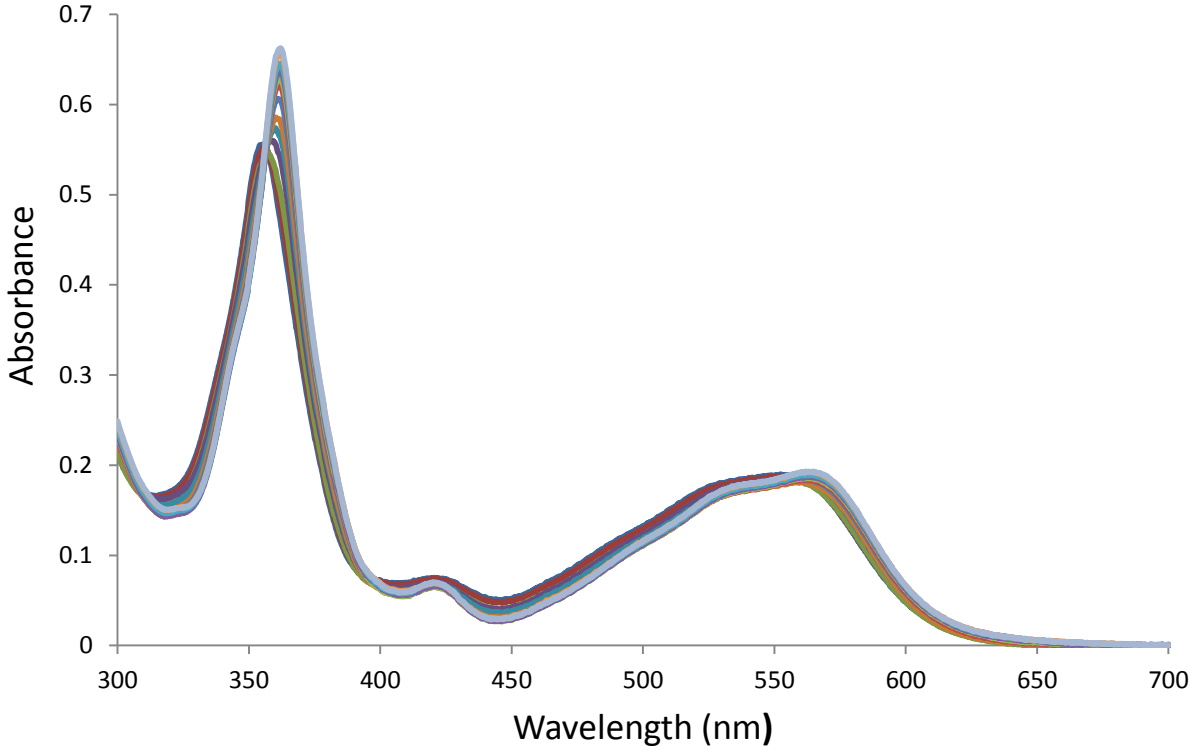


Figure 3.1.6 The absorbance changes observed for the binding of imidazole to $[H_2O\text{-}(10\text{-}Cl)Cbl]^+$.

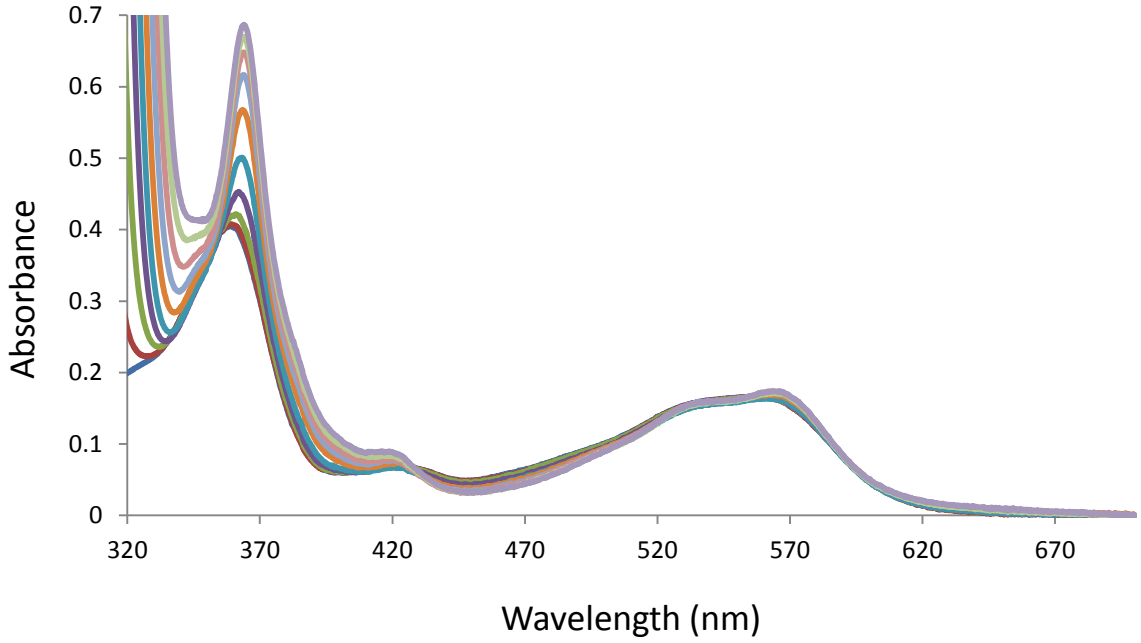


Figure 3.1.7 The absorbance changes observed for the binding of DMAP to $[H_2O\text{-}(10\text{-}Cl)Cbl]^+$.

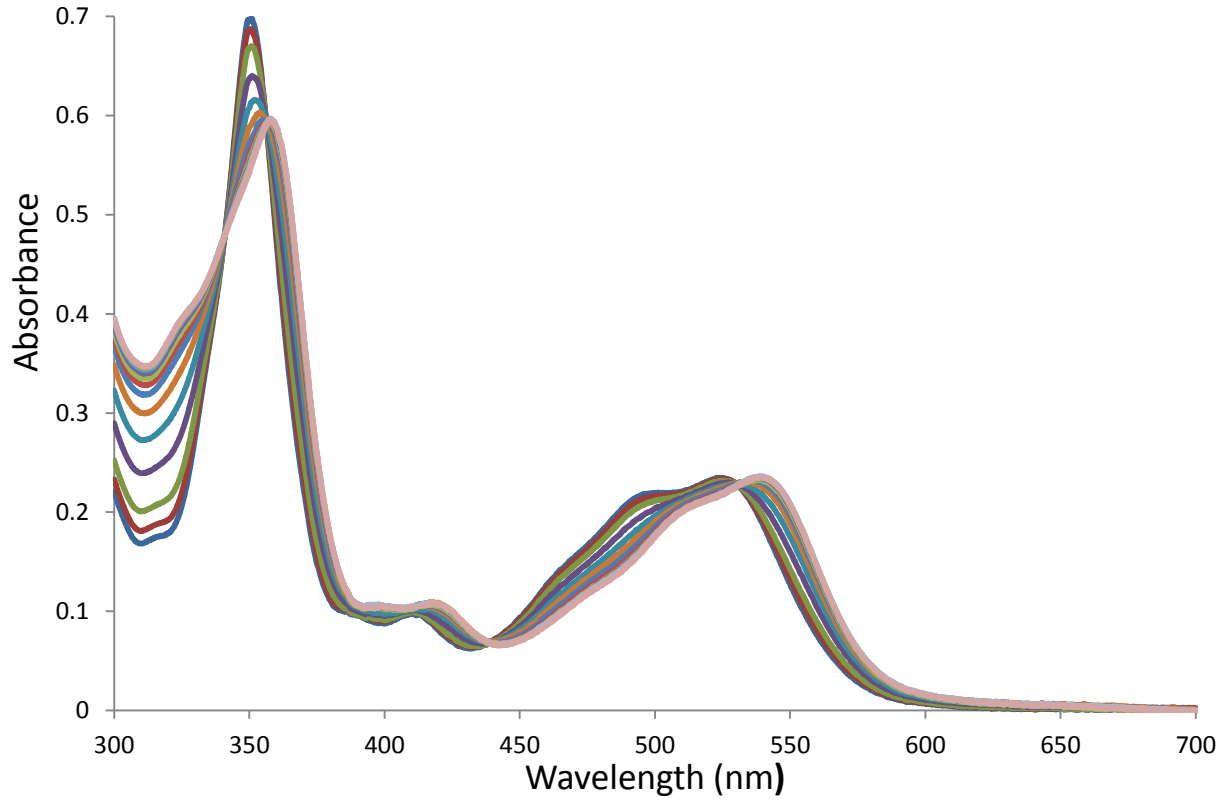


Figure 3.1.8 The absorbance changes observed for the binding of N_3^- to $[H_2OCbl]^+$.

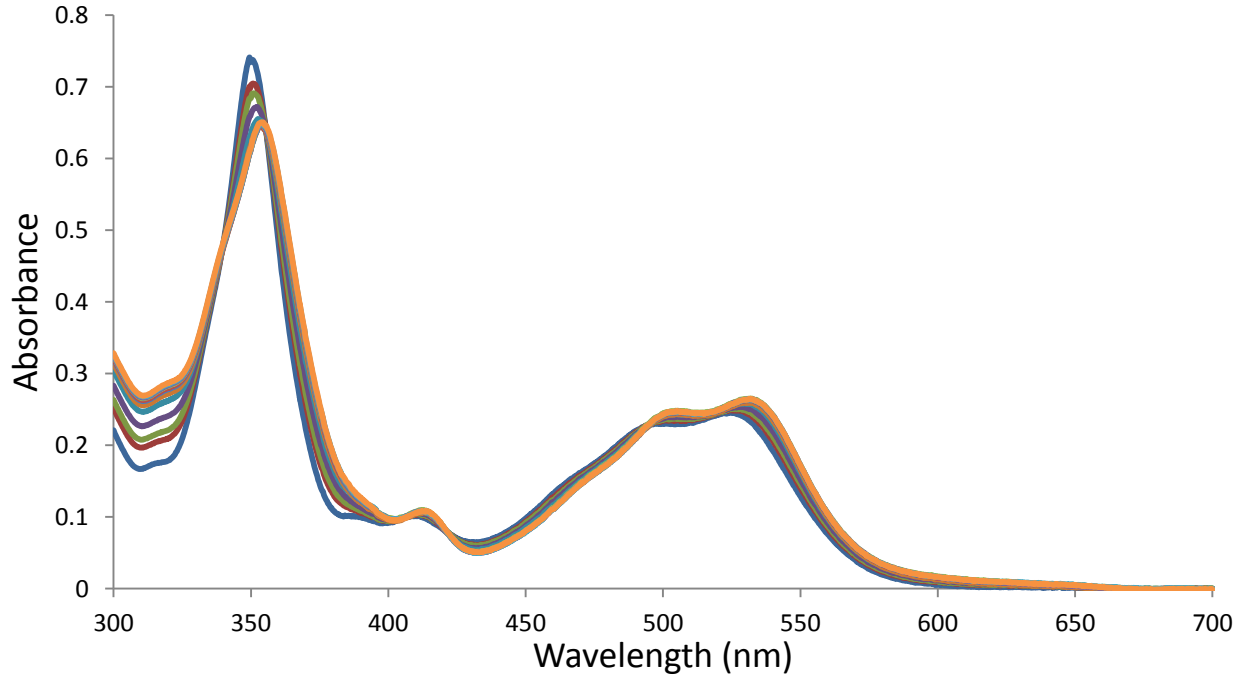


Figure 3.1.9 The absorbance changes observed for the binding of NO_2^- to $[H_2OCbl]^+$.

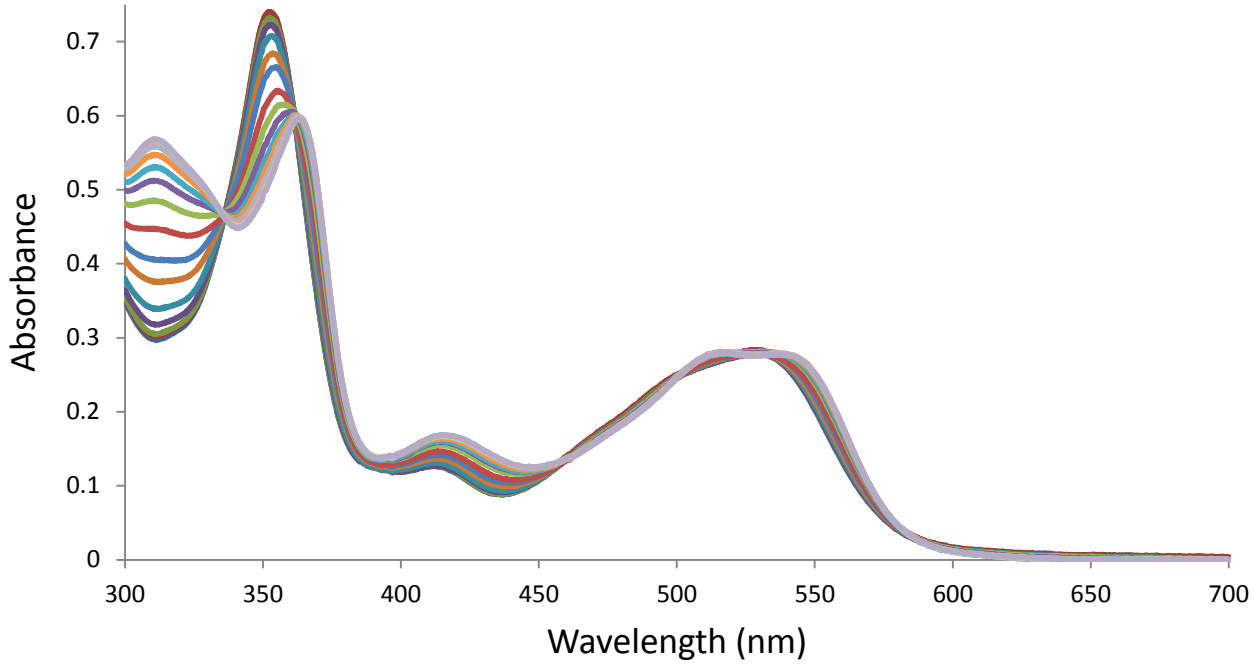


Figure 3.1.10 The absorbance changes observed for the binding of SO_3^{2-} to $[H_2OCbl]^+$.

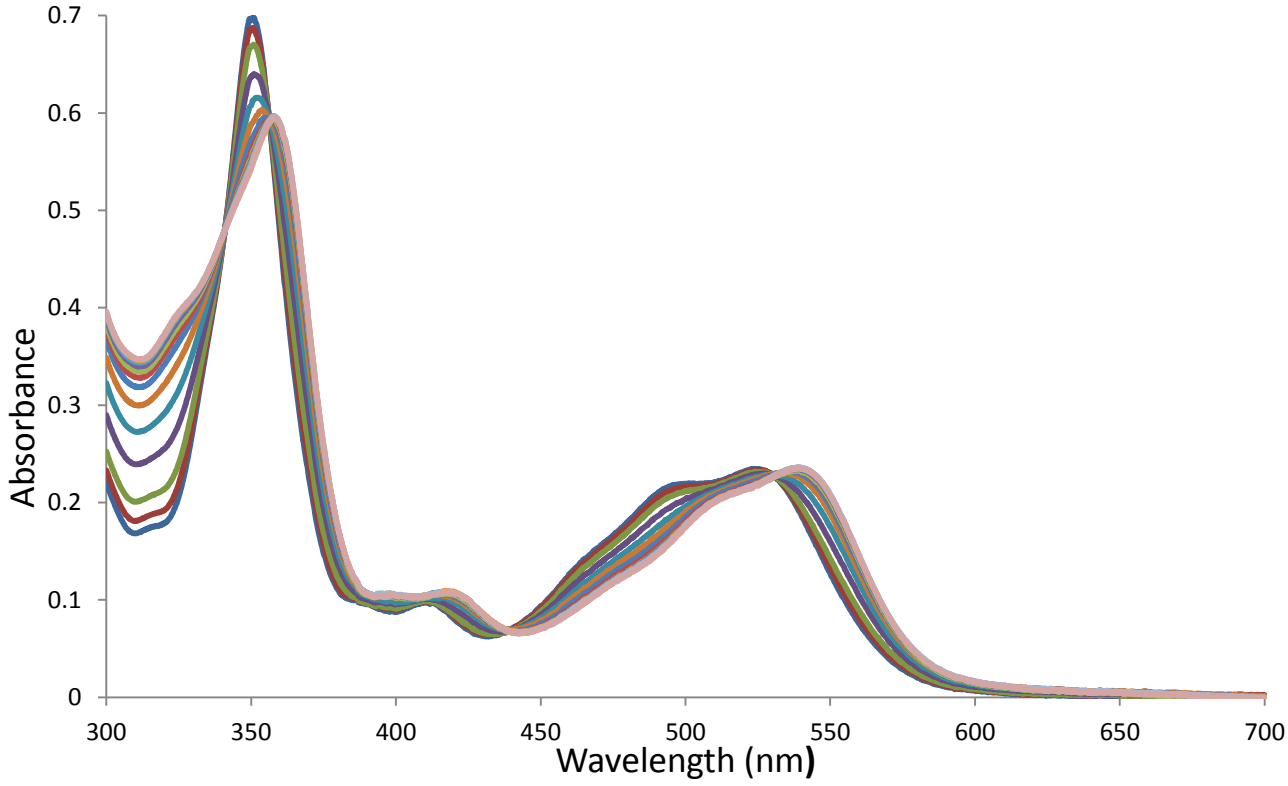


Figure 3.1.11 The absorbance changes observed for the binding of SCN^- to $[H_2OCbl]^+$.

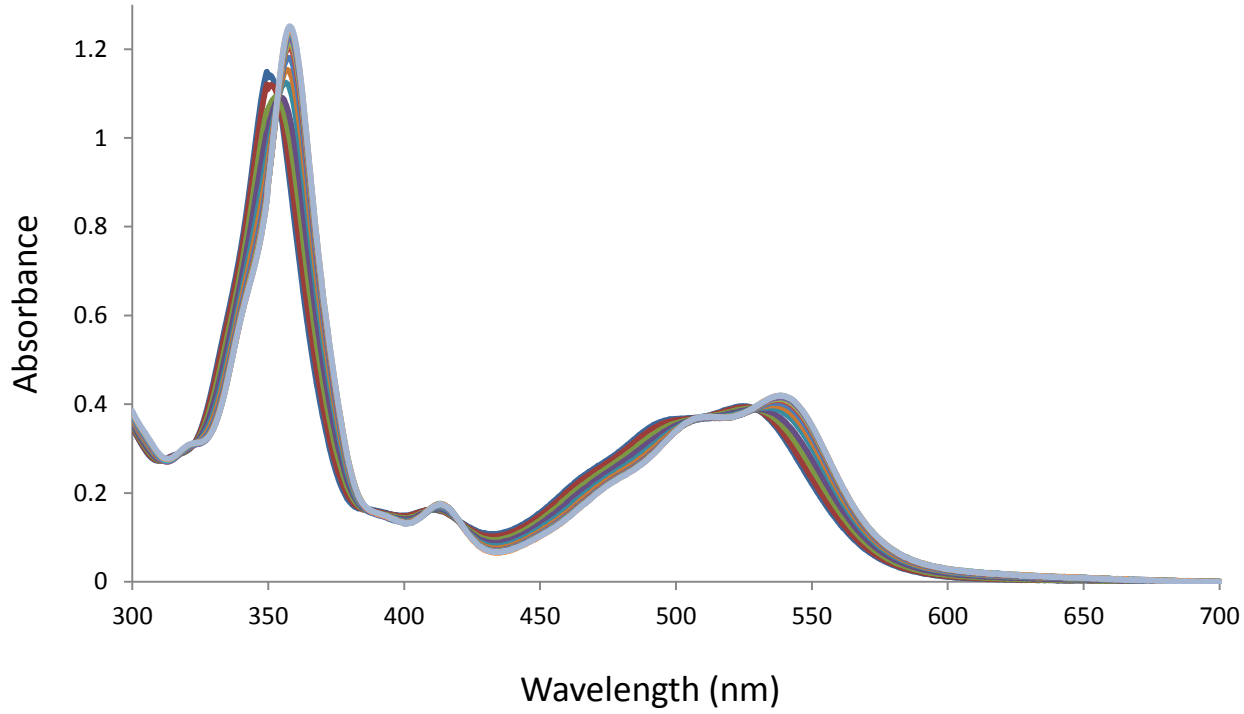


Figure 3.1.12 The absorbance changes observed for the binding of imidazole to $[H_2OCbl]^+$.

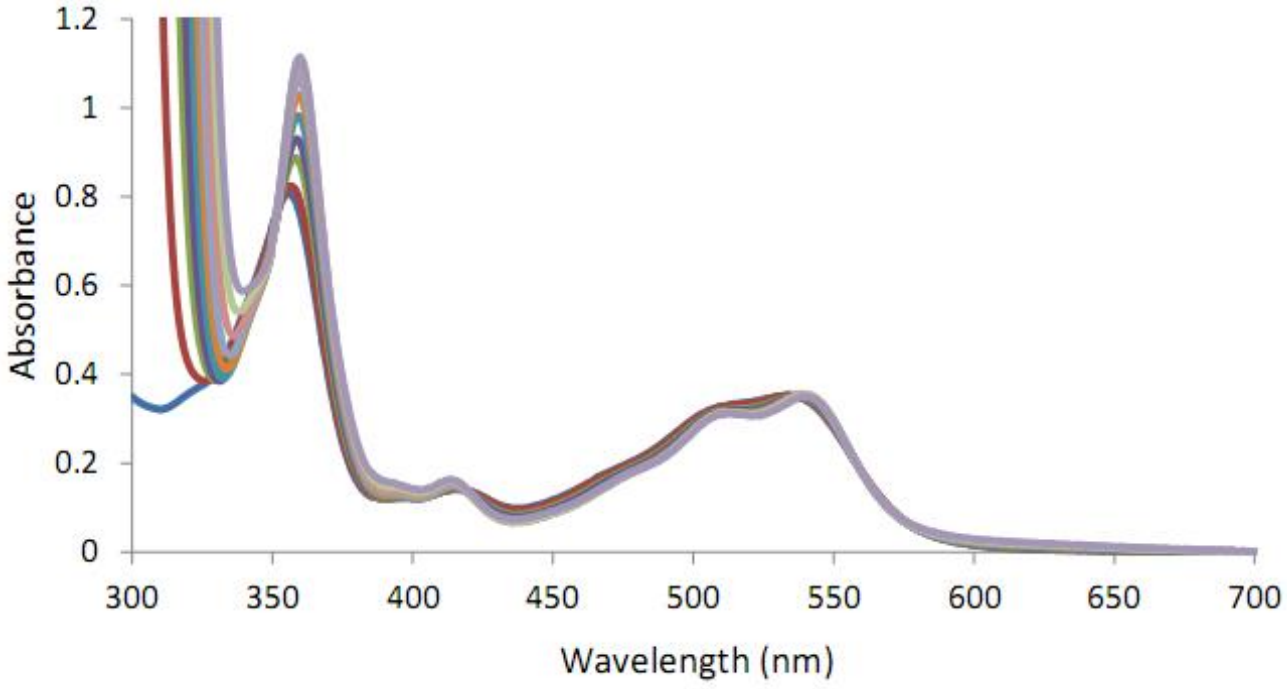


Figure 3.1.13 The absorbance changes observed for the binding of imidazole to $[H_2OCbl]^+$.

Appendices for Chapter 4

4.1 Primary Kinetic Data for the Reaction of N_3^- and Imidazole with $[H_2O\text{-}(10\text{-}Br)Cbl]^+$

Table 4.1.1 Primary kinetic data for the reaction of N_3^- and $[H_2O\text{-}(10\text{-}Br)Cbl]^+$ in aqueous solution (pH 6, MES buffer, $\mu = 0.50$ M, Na_2SO_4).

Temp /°C	$[N_3^-]$ / M	k_I /s^{-1}	std err /s^{-1}	k_{II} /$M^{-1}s^{-1}$	std err /$M^{-1}s^{-1}$	k_r /s–1	std err /s^{-1}
10.0	4.197E-05	6.74E-03	4.73E-05				
	6.269E-05	8.53E-03	1.15E-04				
	8.329E-05	1.10E-02	6.09E-05				
	1.036E-04	1.33E-02	7.46E-05				
	1.238E-04	1.56E-02	9.45E-05	108	3	2.1E-03	2.0E-04
15.0	3.237E-05	7.55E-03	6.27E-05				
	6.397E-05	1.15E-02	4.25E-05				
	6.462E-05	1.25E-02	8.50E-05				
	8.468E-05	1.46E-02	7.22E-05				
	1.054E-04	1.84E-02	6.36E-05				
	1.260E-04	1.94E-02	1.48E-04	138	10	3.1E-03	8.0E-04
17.5	4.140E-05	1.35E-02	6.30E-05				
	6.182E-05	1.80E-02	5.09E-05				
	8.214E-05	2.31E-02	7.18E-05				
	1.023E-04	2.35E-02	6.90E-05				
	1.222E-04	2.85E-02	1.79E-04	176	24	6.9E-03	1.9E-03
20.0	2.092E-05	1.43E-02	1.18E-04				
	3.157E-05	1.74E-02	8.85E-05				
	4.184E-05	1.99E-02	1.26E-04				
	6.235E-05	2.57E-02	1.28E-04				
	8.279E-05	3.17E-02	2.34E-04	277	5	8.5E-03	2.4E-04
25.0	8.313E-05	4.65E-02	9.07E-04				
	6.257E-05	3.88E-02	2.91E-04				
	4.181E-05	3.10E-02	2.28E-04				
	3.143E-05	2.74E-02	2.75E-04				
	2.091E-05	2.52E-02	1.82E-04	339	19	1.7E-02	8.5E-04
30.0	2.089E-05	3.89E-02	6.36E-04				

	2.747E-05	4.15E-02	6.62E-04				
	3.172E-05	4.55E-02	4.95E-04				
	3.872E-05	4.81E-02	3.12E-04	530	63	2.8E-02	2.0E-03
35.0	2.143E-05	6.04E-02	1.45E-03				
	3.151E-05	6.77E-02	1.36E-03				
	3.803E-05	7.18E-02	1.50E-03				
	4.238E-05	6.97E-02	1.70E-03				
	5.261E-05	8.35E-02	1.54E-03	685	122	4.5E-02	4.7E-03

Table 4.1.2 Primary kinetic data for the reaction of imidazole and $[H_2O\text{-}(10\text{-}Br)Cbl]^+$ in aqueous solution (pH 7, MOPS buffer, $\mu = 0.50$ M, Na_2SO_4).

Temp /°C	**[Im] / M**	k_I **/s^{-1}**	**std err /s^{-1}**	k_{II} **/M^{-1}s^{-1}**	**std err /M^{-1}s^{-1}**	k_r **/s–1**	**std err /s^{-1}**
15.0	1.59E-03	4.44E-03	5.17E-05				
	3.92E-03	9.52E-03	7.19E-05				
	7.68E-03	2.10E-02	6.80E-05				
	1.13E-02	2.59E-02	1.13E-04				
	1.48E-02	3.97E-02	2.48E-04	2.5	0.2	0.0004	0.0014
20.0	1.59E-03	8.08E-03	3.27E-05				
	3.92E-03	1.95E-02	8.42E-05				
	7.68E-03	3.52E-02	2.47E-04				
	1.13E-02	5.48E-02	3.55E-04				
	1.48E-02	6.84E-02	7.58E-04	4.6	0.1	8.0E-04	5.0E-04
25.0	6.21E-04	5.15E-03	3.07E-04				
	1.64E-03	1.19E-02	2.59E-03				
	2.59E-03	1.37E-02	6.19E-03				
	3.41E-03	1.82E-02	1.18E-02				
	3.50E-03	2.70E-02	7.42E-03				
	6.50E-03	3.88E-02	3.86E-03	5.8	0.7	1.5E-03	2.6E-03
30.0	7.76E-04	1.23E-02	5.20E-04				
	1.92E-03	2.71E-02	2.81E-03				
	3.75E-03	4.76E-02	7.71E-03				
	5.53E-03	7.05E-02	1.50E-02				
	7.21E-03	8.72E-02	2.61E-02	11.7	0.3	4.0E-03	1.1E-03
35.0	7.95E-04	2.09E-02	1.50E-04				
	1.97E-03	4.54E-02	2.13E-03				
	3.84E-03	7.37E-02	9.26E-03				
	5.62E-03	1.03E-01	2.57E-02	16.6	0.7	9.8E-03	2.5E-03

Appendices for Chapter 6

6.1 Primary kinetic data for the reaction of CN^- with $[AC\text{-}(10\text{-}NO_2)Cbs]^+$, $[AC\text{-}(10\text{-}NH_2)Cbs]^+$ and $[ACCbs]^+$ in 50% isoprpanol

Table 6.1.1 Primary kinetic data for the reaction of CN^- and $[AC\text{-}(10\text{-}NO_2)Cbs]^+$ in 50% isoprpanol (pH 9.5, CHES buffer).

$[AC(10NH_2)Cbs]^+$																	
Temp	**$[CN^-]$ [a]**	**k_f^{obs}**	**k_s^{obs}**	**$(A_0\text{-}A_1)$ [b]**	**$k_f^{II\prime}$ [c]**	**pH [e]**	**Fract aqua**	**k_f^{II} [d]**	**$\Delta H_f^{\ddagger}$**	**$\Delta S_f^{\ddagger}$**	**k_f^{II}(25 °C) [e]**	**k_s^{II}**	**Fract aqua**	**k_s^{II} [d]**	**$\Delta H_s^{\ddagger}$**	**$\Delta S_s^{\ddagger}$**	**k_s^{II}(25 °C) [e]**
/°C	**/10^{-4} M**	**/s^{-1}**	**/s^{-1}**	**(%)**	**/10^4 M^{-1} s^{-1}**	**pH**	**Fraction AC-Cbs**	**/10^4 M^{-1} s^{-1}**	**/kJ mol^{-1}**	**/J K^{-1} mol^{-1}**	**/M^{-1} s^{-1}**	**/10^2 M^{-1} s^{-1}**	**Fraction AH-Cbs**	**/10^4 M^{-1} s^{-1}**	**/kJ mol^{-1}**	**/J K^{-1} mol^{-1}**	**/M^{-1} s^{-1}**
10	1.809	2.21(3)	0.090(1)	78.1(1)	1.21(3)	9.36	0.99	1.23(3)	40(3)	-27(11)	2.97×10^4	5.31(12)	0.29	0.18(12)	34(3)	-71(9)	1.1×10^3
	3.618	4.38(11)	0.166(4)	79.3(1)													
	7.235	8.3(7)	0.320(14)	79.5(9)													
	1.085	13.8(4)	0.549(15)	79.0(9)													
	14.47	17.9(4)	0.754(12)	78.0(5)													
	18.09	21.2(1.0)	0.95(2)	77.1(6)													
18	1.948	3.08(4)	0.135(1)	72.4(3)	1.83(19)	9.19	0.97	1.9(2)				7.4(3)	0.28	2.7(3)			
	3.896	4.9(4)	0.225(11)	74.3(6)													
	7.790	9.8(8)	0.45(3)	74.7(7)													
	11.69	18.0(8)	0.79(2)	75.4(8)													
	15.58	27(3)	1.18(10)	74.5(1.1)													
	19.48	42(7)	1.47(7)	74.3(9)													
21	0.9943	2.89(10)	0.129(2)	70.4(4)	2.4(3)	9.13	0.97	2.5(4)				8.8(6)	0.28	3.2(6)			
	1.989	4.8(1)	0.201(3)	72.5(4)													
	3.978	9.1(2)	0.370(10)	75.1(4)													
	7.954	12.8(1)	0.534(14)	75.9(9)													
	11.93	33(3)	1.27(1)	76.3(9)													
	15.91	36(3)	1.32(4)	76.0(4)													
	19.89	53(4)	1.86(6)	76.4(7)													
25	1.021	3.31(2)	0.139(4)	69.8(8)	2.6(3)	9.04	0.96	2.7(3)				11(1)	0.27	4.1(1)			
	2.042	4.9(5)	0.219(14)	71.4(9)													
	4.083	9.8(8)	0.404(12)	74.2(2)													
	8.165	13.9(7)	0.63(3)	73.6(7)													
	1.225	37(2)	1.50(3)	75.6(9)													
	16.33	37(8)	1.5(2)	74.9(7)													
	20.42	60(10)	2.2(2)	75.7(1.0)													
30	1.043	3.3(4)	0.177(7)	69(2)	3.85(12)	8.93	0.94	4.1(3)				15(2)	0.27	5.6(2)			
	5.040	9.8(3)	0.262(8)	66.8(7)													

[AC(10NH$_2$)Cbs]$^+$

Temp /ºC	[CN$^-$] ^{a} /10^{-4} M	k_f^{obs} /s^{-1}	k_s^{obs} /s^{-1}	(A_0-A_1) ^{b} (%)	$k_f^{II\prime}$ ^{c} /10^4 M^{-1} s^{-1}	pH ^{e} pH	Fract aqua Fraction AC-Cbs	k_f^{II} ^{d} /10^4 M^{-1} s^{-1}	$\Delta H_f^{\ddagger}$ /kJ mol^{-1}	$\Delta S_f^{\ddagger}$ /J K^{-1} mol^{-1}	k_f^{II}(25 ºC) ^{e} /M^{-1} s^{-1}	k_s^{II} /10^2 M^{-1}s^{-1}	Fract aqua Fraction AH-Cbs	k_s^{II} ^{d} /10^4 M^{-1} s^{-1}	$\Delta H_s^{\ddagger}$ /kJ mol^{-1}	$\Delta S_s^{\ddagger}$ /J K^{-1} mol^{-1}	k_s^{II}(25 ºC) ^{e} /M^{-1} s^{-1}
	10.08	38.8(6)	0.37(2)	70.4(4)													
	20.16	75(2)	0.75(8)	72.2(1.4)													
	30.24	110(5)	1.7(2)	75.4(1.0)													
	40.31	153(6)	2.2(3)	74(2)													

Table 6.1.2 Primary kinetic data for the reaction of CN^- and $[AC\text{-}(10\text{-}NO_2)Cbs]^+$ in 50% isoprpanol (pH 9.5, CHES buffer).

$[AC(10\text{-}NO_2)Cbs]^+$																	
Temp	**$[CN^-]$ [a]**	**k_f^{obs}**	**k_s^{obs}**	**$(A_0\text{-}A_1)$ [b]**	**k_f^{II}′ [c]**	**pH [e]**	**Fract aqua**	**k_f^{II} [d]**	**$\Delta H_f^{\ddagger}$**	**$\Delta S_f^{\ddagger}$**	**k_f^{II}(25 °C) [e]**	**k_s^{II}**	**Fract aqua**	**k_s^{II} [d]**	**$\Delta H_s^{\ddagger}$**	**$\Delta S_s^{\ddagger}$**	**k_s^{II}(25 °C) [e]**
/°C	**/10^{-3} M**	**/s^{-1}**	**/s^{-1}**	**(%)**	**/10^2 M^{-1} s^{-1}**		**Fraction AC-Cbs**	**/10^2 M^{-1} s^{-1}**	**/kJ mol^{-1}**	**/J K^{-1} mol^{-1}**	**/M^{-1} s^{-1}**	**/10^1 M^{-1} s^{-1}**	**Fraction AH-Cbs**	**/10^2 M^{-1} s^{-1}**	**/kJ mol^{-1}**	**/J K^{-1} mol^{-1}**	**/M^{-1} s^{-1}**
10.0	1.544	0.46(1)	0.048(2)	57.6(5)	1.87(10)	9.80	0.94	2.00(13)	90(3)	119(12)	1.50×10^3	2.00(22)	0.44	0.46(3)	77(8)	53(28)	1.3×10^2
	2.316	0.61(1)	0.061(1)	58.6(5)													
	3.088	0.85(3)	0.087(3)	57.4(2)													
	6.176	1.45(4)	0.16(5)	58.1(4)													
	9.264	1.8(2)	0.163(5)	66(1)													
	12.35	2.4(2)	0.236(8)	65(1)													
	15.44	3.2(3)	0.37(2)	62(1)													
15.0	1.54	0.65(4)	0.064(3)	47(1)	3.59(23)	9.67	0.91	3.93(3)				5.9(3)	0.32	1.82(3)			
	2.30	1.2(3)	0.12(2)	53(3)													
	3.07	1.5(2)	0.15(1)	50(1)													
	6.14	2.8(4)	0.25(1)	58(2)													
	9.22	3.3(7)	0.32(2)	60(1)													
	12.29	4.0(4)	0.41(3)	62(3)													
	15.36	5(1)	0.54(7)	63(3)													
18.0	1.551	1.1(1)	0.108(4)	52.6(7)	5.56(29)	9.60	0.90	6.2(4)				5.9(3)	0.26	2.24(3)			
	2.327	1.35(9)	0.122(2)	55(1)													
	3.103	1.59(9)	0.15(1(	57(2)													
	6.205	3.4(2)	0.33(2)	61(2)													
	9.308	5.0(8)	0.50(4)	59(4)													
	12.41	6(2)	0.73(11)	60.3(7)													
	15.51	9(2)	1.0(2)	58(6)													
21.0	1.551	1.5(2)	0.15(5)	76(3)	8.56(59)	9.52	0.88	9.7(9)				8.6(1.1)	0.22	4(1)			
	2.327	2.4(2)	0.28(2)	76(2)													
	3.103	2.8(4)	0.28(5)	77(2)													
	6.205	4.9(7)	0.31(20)	82(2)													
	9.308	7.1(5)	0.60(8)	83(1)													
	12.41	9(1)	1.1(2)	80(4)													

[AC(10-NO_2)Cbs]$^+$																
Temp	**[CN^-] [a]**	**k_f^{obs}**	**k_s^{obs}**	**(A_0-A_1) [b]**	**$k_f^{II\prime}$ [c]**	**pH [e]**	**Fract aqua**	**k_f^{II} [d]**	**$\Delta H_f^{\ddagger}$**	**$\Delta S_f^{\ddagger}$**	**k_f^{II}(25 °C) [e]**	**k_s^{II}**	**Fract aqua**	**k_s^{II} [d]**	**$\Delta H_s^{\ddagger}$**	**$\Delta S_s^{\ddagger}$**	**k_s^{II}(25 °C) [e]**
/°C	**/10^{-3} M**	**/s^{-1}**	**/s^{-1}**	**(%)**	**/10^2 M^{-1} s^{-1}**		**Fraction AC-Cbs**	**/10^2 M^{-1} s^{-1}**	**/kJ mol^{-1}**	**/J K^{-1} mol^{-1}**	**/M^{-1} s^{-1}**	**/10^1 M^{-1} s^{-1}**	**Fraction AH-Cbs**	**/10^2 M^{-1} s^{-1}**	**/kJ mol^{-1}**	**/J K^{-1} mol^{-1}**	**/M^{-1} s^{-1}**
	15.51	14.1(9)	1.5(3)	80(4)													
25.0	1.543	1.9(2)	0.165(4)	69.3(7)	13.8(9)	9.41	0.85	16.2(1.3)				13.3(1.2)	0.17	8(1)			
	2.315	2.47(2)	0.24(4)	72(2)													
	3.086	4.3(3)	0.37(3)	67(1)													
	6.172	6(1)	0.56(15)	70(4)													
	9.258	9(2)	0.9(2)	74(3)													
	12.34	15.4(8)	1.5(2)	69(5)													
	15.43	23(2)	2.3(5)	62(3)													
30.0	1.538	2.6(3)	0.198(9)	64(1)	20.8(1.1)	9.28	0.82	25.4(1.7)				21(2)	0.12	18(2)			
	2.306	3.2(4)	0.27(3)	65(2)													
	3.075	6(1)	0.5(1)	63(5)													
	6.151	10(3)	0.8(3)	69(5)													
	9.226	14(4)	1.4(7)	69(4)													
	12.30	23(4)	2.0(6)	67(5)													
	15.38	31(8)	3.4(7)	68(4)													

Table 6.1.3 Primary kinetic data for the reaction of CN^- and $[ACCbs]^+$ in 50% isoprpanol (pH 9.5, CHES buffer).

[ACCbs]$^+$																
Temp	**[CN$^-$] [a]**	**k_f^{obs}**	**k_s^{obs}**	**(A_0-A_1) [b]**	**k_f^{II} [c]**	**pH [e]**	**Fract aqua**	**k_f^{II} [d]**	**$\Delta H_f^{\ddagger}$**	**$\Delta S_f^{\ddagger}$**	**k_f^{II}(25 °C) [e]**	**k_s^{II}**	**Fract aqua**	**k_s^{II} [d]**	**$\Delta H_s^{\ddagger}$**	**$\Delta S_s^{\ddagger}$**	**k_s^{II}(25 °C) [e]**
/°C	**/10^{-4} M**	**/s**	**/s**	**(%)**	**/10^4 M^{-1} s^{-1}**		**Fraction AC-Cbs**	**/10^4 M^{-1} s^{-1}**	**/kJ mol^{-1}**	**/J K^{-1} mol^{-1}**	**/M^{-1} s^{-1}**	**/10^3M^{-1}s^{-1}**	**Fraction AH-Cbs**	**/10^4 M^{-1} s^{-1}**	**/kJ mol^{-1}**	**/J K^{-1} mol^{-1}**	**/M^{-1} s^{-1}**
10.0	1.890	4.20(5)	0.52(3)	85.3(4)	2.12(11)	9.39	0.99	2.13(12)	58(3)	44(12)	7.75×10^4	2.36(8)	0.46	0.51(8)	92(19)	150(66)	3.3×10^4
	3.780	8.70(19)	0.91(2)	88.4(1)													
	7.558	18.3(4)	1.9(2)	89(1)													
	11.34	27.6(6)	2.5(3)	90.1(8)													
	15.12	35(3)	3.3(4)	90(1)													
	18.90	39.5(6)	4.4(2)	89.4(4)													
18.0	1.920	11.63)	3.2(1)	67(2)	3.85(21)	9.18	0.98	3.91(22)				2.41(48)	0.29	0.82(5)			
	3.841	17.3(3)	2.3(3)	87.2(8)													
	7.680	35(2)	4.3(6)	89(1)													
	11.52	56(4)	6.0(5)	90.0(4)													
	15.36	60(5)	5.4(8)	91(1)													
	19.20	76(2)	6.9(1.1)	92.2(9)													
21.0	0.9735	5.3(1)	0.66(4)	83.5(4)	5.69(25)	9.10	0.98	5.80(26)				6(2)	0.25	2.4(9)			
	1.947	10.3(3)	1.3(2)	85(1)													
	3.895	20.(7)	2.0(2)	88.9(8)													
	7.788	42(3)	3.4(3)	90.5(8)													
	11.68	73(2)	10(3)	87(3)													
25.0	0.9790	5.71(9)	0.102(3)	91.3(1)	7.93(12)	9.00	0.98	8.11(12)				*f*					
	1.958	11.8(9)	0.5(3)	69(1)													
	3.917	27(1)	1.5(2)	93.2(8)													
	7.831	61(4)	3.4(8)	94.0(8)													
	11.75	90(4)	3.8(9)	95.7(6)													
30.0	0.9599	7.79(9)	0.169(3)	90.4(1)	10.7(3)	8.87	0.97	11.0(3)				9(1)	0.14	6.5(8)			
	1.920	18.92(8)	0.86(1)	92.1(3)													
	3.840	40(1)	1.37(3)	94.4(3)													